Mechanical behaviour of copper at high strain rates

MECHANICAL BEHAVIOUR OF COPPER AT HIGH STRAIN RATES

by

A.G. Walker, B.Sc., M.Sc.

A Doctoral Thesis

Submitted in partial fulfilment of the requirements
for the award of
Doctor of Philosophy of Loughborough University of Technology

September 1987

"All men are like grass,
and all their glory is like the flowers of the field;
the grass withers and the flowers fall,
but the word of the Lord stands for ever."

1 Peter 1: 24-25

dedicated to MO

ACKNOWLEDGEMENTS

The author wishes to express his thanks to Dr. D.J. Parry and Mr. H.R. Stewardson of the Department of Physics, Loughborough University, Mr. P.N. Jones and Dr. R.M. Bateman of R.A.R.D.E., Fort Halstead, Mrs. J. Darrant and all others who with their advice, assistance and encouragement have enabled this work to be completed.

ABSTRACT

The primary objectives of this research were to determine the macroscopic properties of polycrystalline OFHC copper for various grain sizes over a wide range of strain rates and temperatures, and to relate the properties to the fundamental microscopic mechanisms which control the deformation characteristics of the material.

Compressive and tensile tests were performed at strain rates from $10^{-3}s^{-1}$ to more than 6 x $10^{3}s^{-1}$, and at temperatures from 20°C to 600°C. Five grain sizes were investigated, from 20μm to 240μm. Dynamic behaviour was observed with a modified split Hopkinson pressure bar (SHPB) system which produced constant strain rates in compression and tension. Many alterations and precautionary measures were required to guarantee reliable dynamic tensile tests. Considerable improvements were made to the data acquisition, analysis and presentation capabilities of the SHPB system. A new method of calibrating the system was developed in which the impact velocity of the projectile was measured by an opto-electronic device. Quasi-static behaviour was ascertained using an Instron test machine. Microstructural changes produced by the mechanical tests were determined by metallographic examinations.

At strain rates upto $10^{3}s^{-1}$ the copper showed a low strain rate sensitivity and the results were consistent with a thermally activated deformation mechanism. The strain rate sensitivity increased sharply above $10^{3}s^{-1}$ and there was an excellent correlation with a model based on the simultaneous influences of thermal activation and viscous drag. The Hall-Petch relation between stress and grain size, usually applied to quasi-static behaviour, was shown to be valid for dynamic deformation in certain cases. In dynamic tensile tests fracture occurred at about $1300s^{-1}$ due to multiple loading and it was possible to estimate the fracture strain from the SHPB records. The elongation at fracture was always slightly greater in dynamic tests than in quasi-static tests.

CONTENTS

PAGE

CHAPTER 3 HIGH STRAIN RATE COMPRESSIVE TESTING TECHNIQUE

CHAPTER 4 HIGH STRAIN RATE TENSILE TESTING TECHNIQUE

CHAPTER 1

INTRODUCTION

1.1 Mechanical Properties of Materials

The objectives of mechanical tests are generally two-fold.

(a) to measure the macroscopic properties of materials to determine their suitability for various engineering structures, according to the envisaged environmental conditions; and

(b) to yield further information about the fundamental microscopic mechanisms which control the deformation characteristics of materials when subjected to different macroscopic mechanical variables.

This research project is concerned with the investigation of both (a) and (b) as related to the properties of copper at high rates of strain.

1.1.1 Elastic Deformation

When a stress, defined as force per unit area, is applied to a material, the latter is deformed and the change in length of the material, in the direction of the force, divided by its original length is defined as the resultant strain.

i.e. Axial Stress (σ) = Force (F)/Area (A) (1.1)

and Axial Strain (ε) = Change in Length (ΔL) /Original Length (L) (1.2)

The portion OY in Figure 1.1 of the typical stress versus strain curve for a metallic solid, describes the elastic deformation of the material. In this region there is a linear relation between stress and strain, and when the applied stress is removed the strain also returns to zero. Point Y is the elastic limit and the corresponding stress is called the yield stress of the material. The gradient of OY is known as the elastic modulus or Young's modulus.

1.1.2 Plastic or Permanent Deformation

For metals the strain at the elastic limit is very small, typically of the order of 0.001 (alternatively expressed as 0.1%). If the stress is increased beyond the elastic limit then the strain increases much more rapidly and the material is said to flow plastically. In this region, defined by YC in Figure 1.1, the material is permanently deformed. Upon removal of the stress from point A, the strain only recovers to ε_B, resulting in a permanent deformation. If the material is loaded again it will closely follow the straight line BA, remaining elastic up to A, consequently achieving a higher yield stress. This process of increasing the yield stress is known as strain hardening or work hardening.

1.1.3 Effects on Stress-Strain Relation of Other Mechanical and Physical Variables

The precise relation between stress and strain is dependent on the value of other mechanical and physical parameters such as deformation history, temperature, grain size and

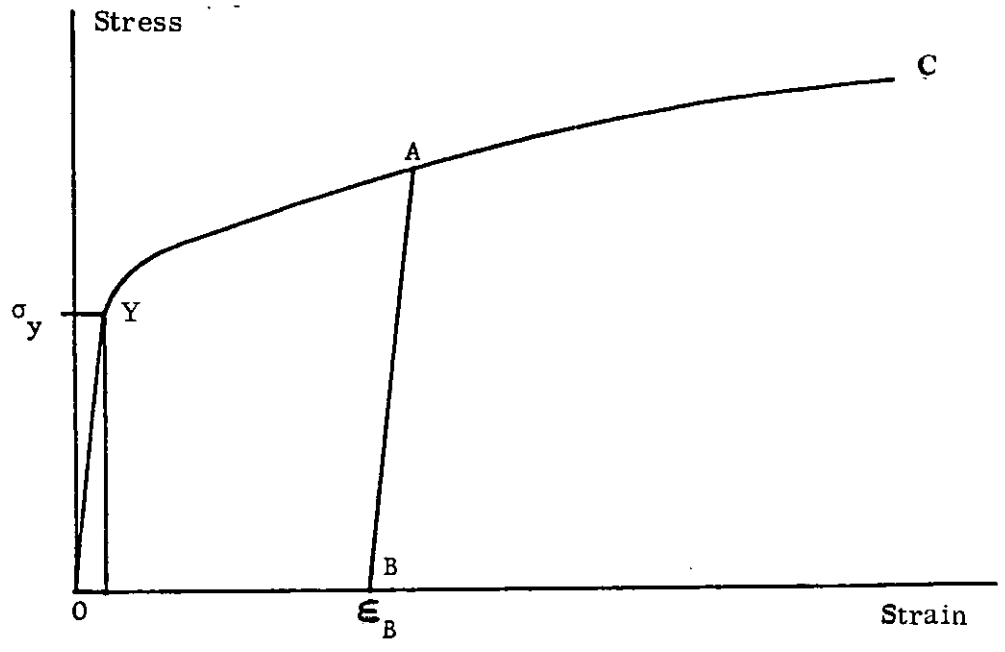

Figure 1.1 Typical Stress Against Strain Curve

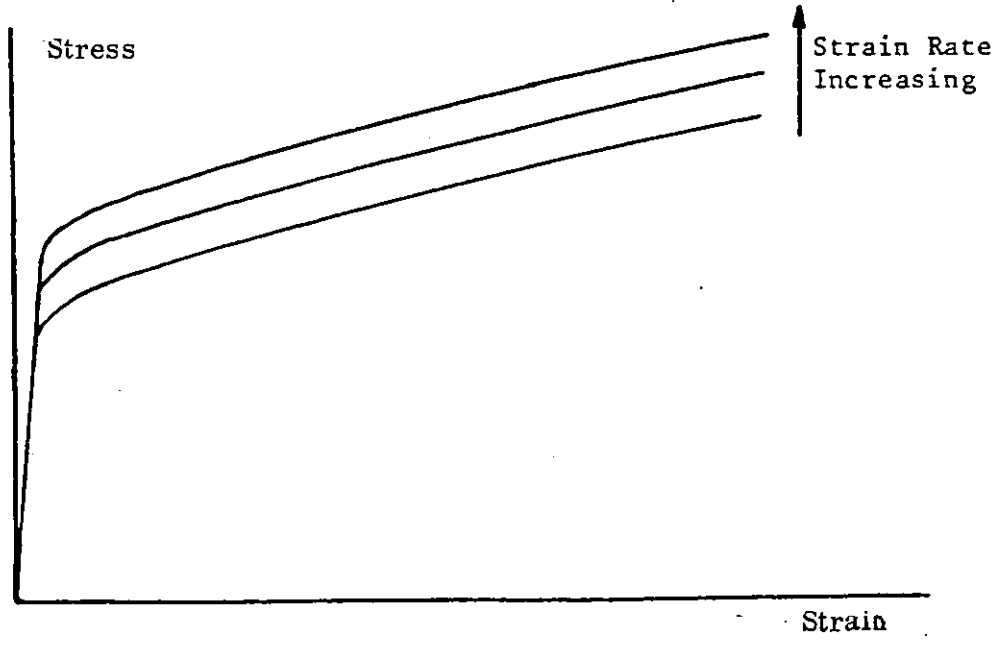

Figure 1.2 Effect of Increasing Strain Rate

strain rate. The effects of the last three variables on the stress-strain relation of polycrystalline copper are all evaluated in some detail in this dissertation.

1.2 Strain Rate

Strain rate, or rate of change of strain ($d\varepsilon/dt$), has been measured over at least 17 orders of magnitude, i.e. from $10^{-12}s^{-1}$ to more than $10^{5}s^{-1}$ in mechanical tests and naturally occurring events. These strain rate variations can be sub-divided and classified according to Table 1.1. The different classifications serve to separate differences in the type of test or manner of load application rather than to imply regions of change in the basic mechanisms of deformation.

Strain rate can have a significant effect on the mechanical behaviour of a material (Figure 1.2 shows a typical trend for metallic materials) and consequently its influence on oxygen-free high conductivity (OFHC) copper is of principal concern in this thesis, particularly at high rates of strain, i.e. $>10^{2}s^{-1}$.

1.3 High Strain Rate Phenomena

Examples of high strain rate phenomena include impacts, explosions and metal forming of various types. In all of these cases the materials involved are permanently deformed in very short periods of time; typically less than a

Table 1.1

Classification of Mechanical Tests

according to Strain Rate

Strain Rate Classification	Strain Rate (s^{-1})	Usual Method of Loading	Dynamic Consideration in Testing
Creep	$< 10^{-5}$	Constant Load or Stress Machine	Strain vs. Time or Creep Rate Recorded
Quasi-Static	10^{-5}-10^{-1}	Hydraulic or Screw Machine	Constant Strain Rate Test
Intermediate Strain Rate	10^{-1}-10^{2}	Pneumatic or Mechanical Machine	Mechanical Resonance in Specimen and Machine
Bar Impact	10^{2}-10^{4}	Mechanical or Explosive Loading	Elastic-Plastic Wave Propagation
High Velocity Plate Impact	$> 10^{4}$	Explosively Driven Plate Impact	Shock Wave Propagation

millisecond. Of the processes classed as metal forming, forging takes place at strain rates of the order of $10^3 s^{-1}$, metal cutting at 10^3-$10^5 s^{-1}$ and wire drawing at up to $2 \times 10^5 s^{-1}$. The detonation of explosives can cause strain rates of $10^5 s^{-1}$ or more in adjacent structures.

1.4 Stress Wave Propagation

At low or intermediate strain rates, where the time between the application of a force to a body and the setting up of equilibrium within the body is short compared with the times in which the observations are made, the whole of the body can be considered to be accelerated into motion at the same instant. This is the viewpoint taken by rigid dynamics.

At high strain rates, however, where forces are only applied for very short periods of time, the effects on the body must be considered in terms of the propagation of stress waves through the body, with two separated points on the body being accelerated at different times.

Since stress wave propagation in solids has been treated at length by several authors, e.g. KOLSKY (1963) and JOHNSON (1972), it suffices to consider only some of the salient features from their publications.

1.4.1 Elastic Wave Propagation in Unbounded Isotropic Solids

In extended isotropic solids, two types of elastic stress

wave may be propagated. These are dilatational waves and distortional waves. The particle motion in a plane dilatational wave is along the direction of propagation, whilst in a plane distortional wave it is perpendicular to the direction of propagation.

The velocity of the dilatational wave

$$c_1 = [\ (k + \tfrac{4}{3}\mu\ )/\rho\ ]^{1/2} \qquad (1.3)$$

The velocity of the distortional wave

$$c_2 = (\mu/\rho)^{1/2} \qquad (1.4)$$

where ρ is the density of the solid, k its bulk modulus and μ its rigidity modulus.

1.4.2 Elastic Wave Propagation in Cylindrical Bars

This particular case of elastic wave propagation in a bounded solid medium has been chosen because of the use of the Hopkinson bar technique by the author, which is based on wave propagation along solid cylinders. The technique is described in Chapters 3 and 4.

The elementary theory of the propagation of elastic disturbances along a cylindrical bar predicts that longitudinal, torsional and flexural (or bending) waves will travel with the following velocities:

Longitudinal velocity $c_o = (E/\rho)^{1/2}$ (1.5)

Torsional velocity $c_t = (\mu/\rho)^{1/2}$ (1.6)

Flexural velocity $c_f = 2\pi a \cdot c_o/\lambda$ (1.7)

where E = Young's modulus

a = radius of bar

and λ = wavelength

Hence the elementary theory of the propagation of elastic disturbances along a cylindrical bar predicts that dispersion, i.e. variation of wave velocity according to frequency content, will occur with flexural pulses, whilst longitudinal and torsional waves will be propagated without change in form.

However, POCHHAMMER (1876) and CHREE (1889) independently derived more exact equations to describe the propagation of infinite sinusoidal waves in circular bars. The Pochhammer - Chree theory shows that the velocity of propagation of longitudinal sinusoidal waves depends on their wavelength, and it is only when torsional waves are travelling in their fundamental mode that dispersion is absent. This theory also indicates that for all three types of waves the elementary theory applies only when the wavelength is large compared with the radius of the bar.

1.4.3 Propagation of an Elastic Pulse in a Solid Cylinder

In the split Hopkinson pressure bar technique, to be described later, a longitudinal elastic pulse is propagated towards the test specimen. In 1948, DAVIES treated the case of the propagation of an elastic stress pulse in terms of the exact Pochhammer - Chree theory. He showed that a longitudinal pulse whose original length is comparable with the radius will become distorted as it travels along the

bar, and the main pulse will be followed by a train of oscillations of high frequency. In addition, any sharp changes in gradient will be rounded off, and constant amplitude parts of the pulse will become oscillatory curves.

1.5 The History of High Strain Rate Studies and the Types of Dynamic Test Machines Employed

There are several excellent reviews and books on the history of impact tests and the machines used (e.g. BITANS and WHITTON (1972), GOLDSMITH (1960), HARDING (1980), ELLWOOD (1983)), the details of which would be superfluous to repeat in this dissertation. Some of the highlights from these reviews, however, are as follows.

The earliest reported tests were carried out by J.HOPKINSON (1872), who performed experiments on iron wires by loading them with dropping weights.

The earliest rotary-type impact machine on record, where the kinetic energy of a flywheel was used to break the specimen, was that of GUILLERY (1906) where strain rates of the order of $200s^{-1}$ were achieved.

OROWAN (1950) was the first to use a compression machine known as a 'cam plastometer' which was capable of imparting constant true rates of strain. It consisted of two platens between which a specimen was compressed when one of the platens was driven by a logarithmically shaped cam, while the other platen remained fixed to the machine frame via a

dynamometer.

Charpy and Izod notched-bar impact tests, which can achieve strain rates up to about $200s^{-1}$, are now regularly used, but suffer from the severe disadvantage of being purely comparative tests and are not able to yield fundamental information concerning the behaviour of the material.

Finally, the most commonly used, fully instrumented test machine, since its development in the late 1940's is the split Hopkinson pressure bar apparatus. This apparatus has been configured in a variety of ways to produce stress, strain and strain rate data in compression, tension and torsion at strain rates up to $5 \times 10^4 s^{-1}$. The validity of the data above about $10^4 s^{-1}$, however, is questionable.

In Chapters 3 and 4, the stages of development of this apparatus, for compressive and tensile tests, are reported.

1.6 The Relevance of Oxygen-Free High Conductivity (OFHC) Polycrystalline Copper in the Current Investigation

The test material, OFHC polycrystalline copper, was chosen because of its relevance to the interests of the Ammunition Materials Section of the Royal Armaments Research and Development Establishment, from which the author was a recipient of a Collaborating Award for Science and Engineering. The Establishment is developing high-explosive anti-tank shaped charge warheads. Figure 1.3 is a schematic view of an anti-tank guided weapon containing a shaped charge warhead.

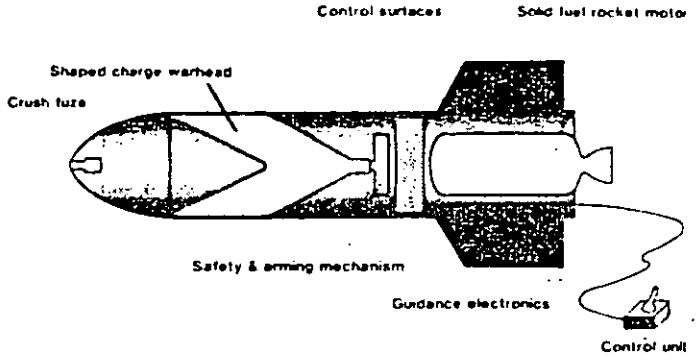

Figure 1.3 A schematic view of an anti-tank guided weapon

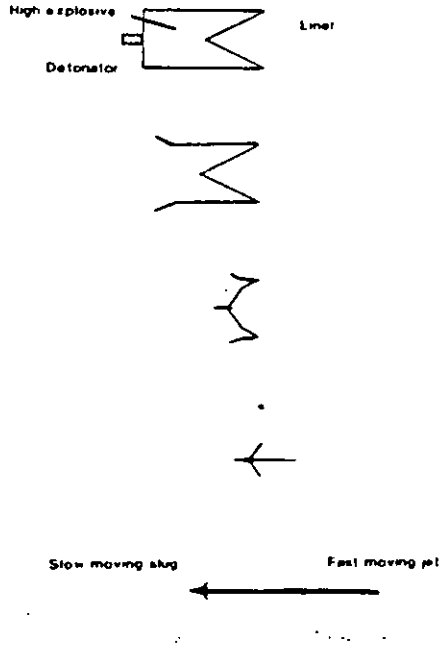

Figure 1.4 The mechanism of shaped charge collapse

1.6.1 Shaped Charge Warheads

If an explosive charge with a symmetrical cavity is placed against a solid surface, with the cavity nearest the surface, then the hole produced by this charge is deeper than with a plain charge. The precise shape of the cavity has an important influence on the depth and width of the hole and is the subject of much research. Now, if the cavity is lined with metal, then the hole can be very deep indeed.

The action of the detonation is to progressively collapse the liner on to the axis of the cavity which, for the purposes of the attack of armour, is usually conical. By correct selection of the cone angle, liner thickness and material, it is possible for the metal, now moving at high velocity, to emerge as a molten jet. The laws of the conservation of energy and momentum dictate that some of the material moves much slower. As a result, a number of molten jets are soon formed, with a solid plug bringing up the rear. The sequence of events during the collapse of the shaped charge can be seen in Figure 1.4.

Consideration of the forces involved, and treating the liner as a fluid, lead to the conclusion, confirmed many times by experiment, that the fastest parts of the jet are travelling at typically $7km.s^{-1}$. This extremely high velocity causes such high pressures in impact with, for example, a steel target that the target material is forced aside. The highest velocity jet penetrates the target first. The succeeding jets bore holes of smaller diameter

than the higher energy leading jet. Consequently, a tapered hole penetrates the target. Finally, the low velocity solid slug lodges in the cavity formed by the jets.

Traditionally, the shaped charge liners were made of steel. Improvements in the performance of the liner is being sought through the use of other materials. Consequently, RARDE wish to investigate the high strain rate properties of copper. Both the compressive and tensile properties of copper are essential to the further development of the shaped charge technique.

1.7 Objectives of the Current Investigation

The principal objective of the current investigation was to determine the mechanical properties of polycrystalline copper in compression and in tension over a wide range of strain rates, strains, temperatures and grain sizes using a Split Hopkinson Pressure Bar (SHPB) system.

A review of previous literature on the dynamic mechanical properties of copper has revealed that most workers have investigated only the room temperature compressive behaviour for polycrystalline copper of unknown grain size. Very few have undertaken tensile tests at high strain rates and only one paper has reported the effects of grain size variation. Consequently, the current research attempts to produce a more complete characterisation of the mechanical behaviour of copper.

In addition to the main research programme, secondary objectives were to enhance the laboratory´s data acquisition, analysis and presentation capabilities and to design an opto-electronic device, which, by measuring the impact velocity of the projectile, could accurately calibrate the SHPB system.

CHAPTER 2

LITERATURE REVIEW OF THE BEHAVIOUR OF COPPER AT HIGH RATES OF STRAIN

2.1 Introduction

In recent years, research into the mechanical behaviour of materials at high rates of strain has increased significantly due to improved testing techniques. This literature review contains a summary of experimental and theoretical investigations of the properties of copper at strain rates in excess of one hundred per second.

Copper specimens have been tested in compression, torsion and tension at rates of strain up to $6 \times 10^4 s^{-1}$ and at temperatures ranging from $-200^{\circ}C$ to $900^{\circ}C$. The results from these three test modes are presented in sections 2.2, 2.3 and 2.4, respectively. Section 2.5 outlines various theories which have been proposed to explain these results. Section 2.6 summarises the conclusions of the research performed on the high strain rate behaviour of copper over the past two decades.

2.2 Compressive Tests

2.2.1 Experimental Techniques

(a) Test Machines

By far the most common test machine for compressing a copper specimen at high rates of strain is the split Hopkinson pressure bar (SHPB), in which a small cylindrical

specimen is inserted between the adjacent ends of two steel bars and a large stress rapidly applied to one of the bars. The conventional apparatus and the theory of its operation are described in detail in Chapter 3.

The SHPB was used by LINDHOLM (1964), KUMAR and KUMBLE (1969), EDINGTON (1969), WATSON and RIPPERGER (1969), KISHIDA and SENDA (1972), GLENN and BRADLEY (1973), LINDHOLM (1978), SHIOIRI et al (1978), STELLY and DORMEVAL (1978), BHUSHAN and JAHSMAN (1978), and FOLLANSBEE et al (1984).

They achieved maximum strain rates of:

$1.6 \times 10^3 s^{-1}$, $2 \times 10^3 s^{-1}$, $1.2 \times 10^3 s^{-1}$, $10^3 s^{-1}$,
$1.1 \times 10^3 s^{-1}$, $9.5 \times 10^2 s^{-1}$, $6.4 \times 10^4 s^{-1}$,
$2.5 \times 10^4 s^{-1}$, $8 \times 10^3 s^{-1}$, $>10^3 s^{-1}$ and $3 \times 10^4 s^{-1}$,

respectively. In all cases the specimens were deformed under conditions of uniaxial stress, which resulted in triaxial strain. Additionally, Bhushan and Jahsman, monitored the behaviour of copper under conditions of uniaxial strain. This was achieved by constraining the radial expansion of the test specimen with a close fitting collar.

HAWKYARD et al (1968) used the impact of a projectile on to a rigid anvil. This yielded an upper strain rate of $5 \times 10^3 s^{-1}$. SAMANTA (1969) devised a test involving an instrumented drop hammer which resulted in strain rates up to $6 \times 10^2 s^{-1}$. DOWLING et al (1970) employed a vertical

testing machine in which a punch bar impacted directly on to the test specimen, the resulting stress pulse being transmitted to a lower die tube. This enabled them to attain a maximum strain rate of the order of $10^4 s^{-1}$. Finally, WULF (1974), and HASHMI and HAQUE (1986) operated a modified Hopkinson bar, where again the incident, or loading, bar was discarded and the projectile struck the specimen directly. They achieved strain rate maxima of 5 x $10^4 s^{-1}$ and 3.3 x $10^4 s^{-1}$, respectively.

The dimensions of the test machines are frequently omitted from published papers but from the data available the diameters of the pressure bars vary from 10 to 20mm. Notable exceptions were: Lindholm's SHPB of 1978, in which miniature bars 4.7mm in diameter and 300mm in length were used; Follansbee et al's SHPB of 1984, in which diameters of 9.5mm, 6.3mm and 4.7mm were used at strain rates of 10^3-$10^4 s^{-1}$, 2 x $10^4 s^{-1}$ and 3 x $10^4 s^{-1}$, respectively; and Bhushan and Jahsman's SHPB of 1978, where the bars were 0.91m long and 38mm in diameter.

(b) Data Acquisition Techniques

In most cases the incident, reflected and transmitted pulses, were measured by means of resistance strain gauges mounted on the pressure bars and displayed, after amplification, on a dual beam oscilloscope as strain versus time records.

Watson and Ripperger (1969) extended the measuring technique used by KARNES and RIPPERGER (1966), and CHALUPNIK and RIPPERGER (1966). They measured the load and

strain simultaneously in the specimen while the specimen was inside a high temperature environment. Karnes and Chalupnik had previously performed their tests at room temperature. During the plastic straining of the specimen, the average stress over its cross-section was measured by quartz crystals at either end of it. Surface strain was measured by a strain gauge attached to the specimen. It was stated by the authors that this technique does not require any assumptions of any uniformity of stress, strain and strain rate over the entire length of the specimen.

Strain measurements were performed by Wulf (1974) using a co-axial capacitor from which the position of the back face of the projectile could be measured, following deformation of the specimen, and hence the specimen strain calculated.

Kishida and Senda (1972) determined the stress in the specimen by analyzing the wave propagation along the input bar.

In the compressive tests performed by Lindholm (1964 and 1978) the measured reflected pulse was integrated so that the oscilloscope displayed stress v. strain directly, rather than strain v. time.

2.2.2 Test Specimens

(a) Dimensions

With the exception of the single crystals of parallelepiped cross-section tested by Stelly and Dormeval (1978), all specimens were cylindrical and usually with diameters

similar to the pressure bars. Shiori et al (1978) showed that any mis-match of cross-sectional areas between the pressure bars and the specimen is not important. Various length (ℓ) to diameter (d) ratios have been selected and these ratios can be approximately grouped into the following categories:

(I) $\ell/d < 0.5$

This ratio was favoured by Lindholm (1964), Samanta (1969), Glenn and Bradley (1973), Edington (1969), and Bhushan and Jahsman (1978). The reasons given for choosing this ratio were:

(i) to minimise lateral inertia effects
(ii) to maintain a constant stress level over the length of the specimen.

In the current investigation a ratio of 0.433 was chosen. The theoretical justification for this ratio is given in Section 3.4.

(II) $0.5 < \ell/d < 2$

These dimensions have been used by Hawkyard et al (1968), Kumar and Kumble (1969), Edington (1969), Wulf (1974), Lindholm (1978), Shioiri et al (1978), Stelly and Dormeval (1978), Follansbee et al (1984), and Hashmi and Haque (1986). In this group a compromise has been reached between the previous group and an attempt to minimise the end surface friction which is larger for smaller ℓ : d ratios.

(III) $\ell/d > 2$

When long specimens were used, wave propagation effects had to be considered. Long specimens were used by Hawkyard et al (1968), Watson and Ripperger (1969), and Kishida and Senda (1972).

(b) Composition

Exact chemical analyses of the compressive specimens were not specified except in the case of Watson and Ripperger (1968) whose polycrystalline Bridgeport copper contained the following impurities in parts per million (ppm):

S (40), Si (50), Pb (10) and Mg (trace)

Oxygen-free high conductivity (OFHC) copper was used by Kumar and Kumble (1969), Glenn and Bradley (1973), Wulf (1974), Shioiri et al (1978), Bhushan and Jahsman (1978), and Hashmi and Haque (1986). Samanta (1969) and Lindholm (1978) used 99.9% pure copper; the latter used commercially pure copper in 1964. Hawkward et al (1968) tested high conductivity B.S. 1432 copper and in 1984, Follansbee et al used high conductivity electrolytic copper.

Single crystals of 99.999% pure copper were employed by Edington (1969), and Stelly and Dormeval (1978).

(c) Annealing

After machining most specimens were annealed in vacuum before being strained. A wide range of annealing temperatures have been employed. Most used temperatures between 530^{o}C and 650^{o}C. Lindholm (1964) chose the lowest

annealing temperature of 343°C and Stelly and Dormeval (1978) the highest of 1000°C. Annealing times ranged from 20 mins to 24 hours.

A full list of all quoted annealing temperatures and times, and exact specimen dimensions and chemical compositions appears in WALKER (1982).

(d) Grain Size

Grain sizes were rarely declared in compressive test papers. The exceptions were (with dimensions in microns):

Dowling et al (1970)	-	37
Glenn and Bradley (1973)	-	47
Lindholm (1978)	-	800
Follansbee et al (1984)	-	37

2.2.3 Results

(a) Room Temperature Tests

Lindholm (1964) (strain rate, $\dot{\varepsilon} \leqslant 1.6 \times 10^{3} s^{-1}$) recorded maximum stresses and strains of 310 MPa and 0.22, respectively. He observed that stress increases with strain rate for a given strain, especially at high strains (Figure 2.1). Copper is less rate sensitive than other face centred cubic (FCC) metals such as aluminium and lead. He also proposed that a thermally activated mechanism was predominant over the strain rate range tested, due probably to the intersection of glide and forest dislocations.

Stress and strain rate were related by the equation:

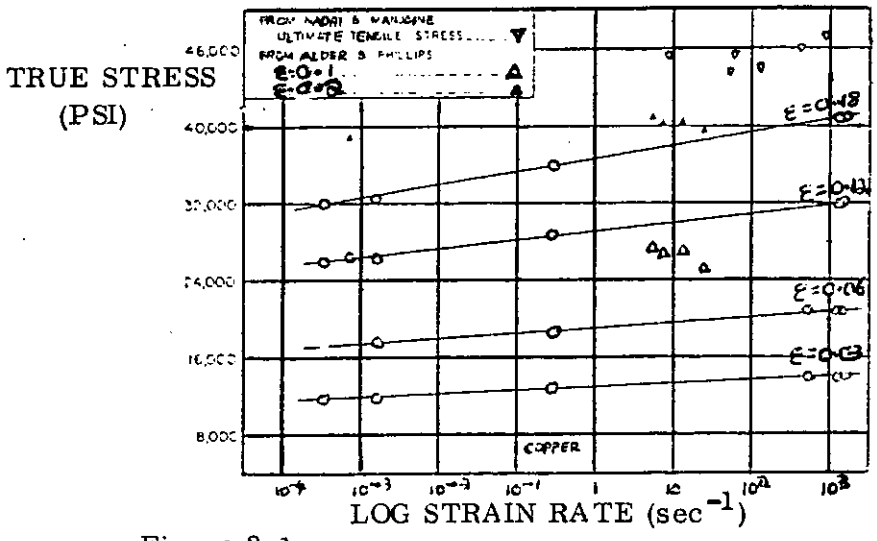

Figure 2.1 Flow stress as a function of strain rate for copper.
(Lindholm, 1964)

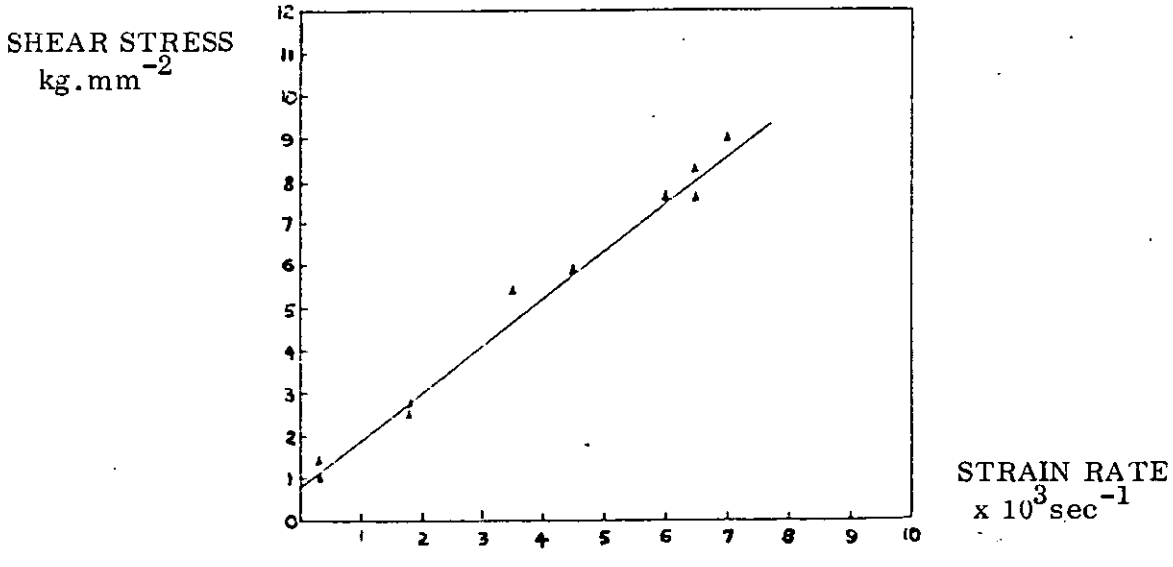

Figure 2.2 The resolved shear 0·1% proof stress versus strain rate
(Edington, 1969)

Flow stress $\sigma = \sigma_o(\varepsilon) + \sigma_1(\varepsilon) \log \dot{\varepsilon}$ (2.1)

where $\sigma_o(\varepsilon)$ is the stress-strain relation at unit strain rate

and $\sigma_1(\varepsilon)$ is a function of strain

The results of Edington (1969) ($\dot{\varepsilon} \leqslant 9 \times 10^3 s^{-1}$), who tested single crystals, showed that, although copper is strain rate insensitive below $10^3 s^{-1}$, it is extremely strain rate sensitive above this figure, (Figure 2.2). He used long specimens and thus concluded that previously reported high strain rate behaviour is real and not just associated with short specimens. He deduced that at high strain rates, stress is a linear function of strain rate and phonon viscosity is the rate controlling process. However, the number of mobile dislocations is almost constant at all strain rates despite the flow stress at high strain rates being phonon viscosity controlled.

Dowling et al's (1970) ($\dot{\varepsilon} \leqslant 10^4 s^{-1}$) tests resulted in strains up to 25% and stresses up to 180MPa. They found that at high strain rates yield stress drops appeared which became larger as the strain rate increased. The following relation for copper at high strain rates was derived:

$$\partial\tau/\partial \ln \dot{\gamma} = \tau \qquad (2.2)$$

where τ = flow stress, $\dot{\gamma}$ = shear strain rate and $\partial\tau/\partial \ln \dot{\gamma}$ is the rate sensitivity.

The authors found that copper is very strain rate

sensitive, the sensitivity being greater than 6.9MPa at very high strain rates. They deduced that the yield drops were a direct consequence of the increased rate sensitivity at these strain rates. They also found that there is a rapid increase in flow stress above $10^3 s^{-1}$ and at strain rates > $5 \times 10^3 s^{-1}$ there is a linear relation between yield stress and strain rate (Figure 2.3).

Kishida and Senda (1972) ($\dot{\varepsilon} \leqslant 1.1 \times 10^3 s^{-1}$) also discovered stress drops, especially at strain rates of 600 and $800 s^{-1}$ (Figure 2.4). They formulated a constitutive equation:

$$\dot{\sigma} = E\dot{\varepsilon} - g(\sigma - f(\varepsilon)) \qquad (2.3)$$

where the 2nd term on the right hand side represents the time rate of stress relaxation, $\sigma = f(\varepsilon)$ being the static stress-strain relation.

Glenn and Bradley (1973) ($\dot{\varepsilon} \leqslant 9 \times 10^2 s^{-1}$) deduced that the non-dynamic contribution to strain rate sensitivity was about 60% of the total flow stress increase when the specimen was strained. Also, the dynamic flow stress at $500 s^{-1}$ was 25% higher than the quasi-static flow stress over the strain range 0.08 to 0.2. Hardness measurements yielded results showing more strain hardening to occur during dynamic tests than static tests.

Wulf (1974) ($\dot{\varepsilon} \leqslant 5 \times 10^4 s^{-1}$) produced true strains up to 1.0 and true stresses up to about 700MPa. The results showed an initial linear increase of flow stress with

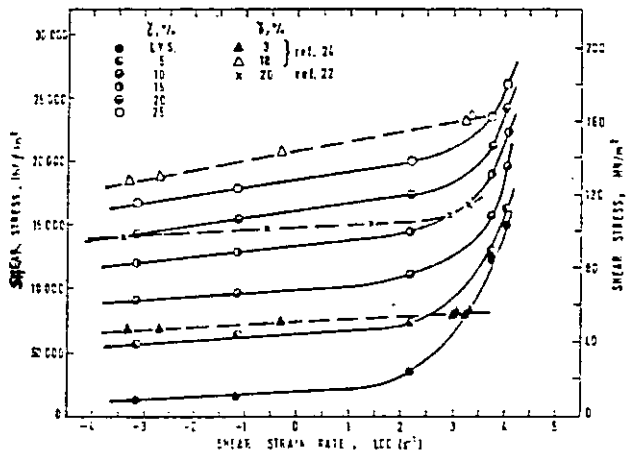

Figure 2.3 *Strain-rate-sensitivity of copper.* (Dowling et al, 1970)

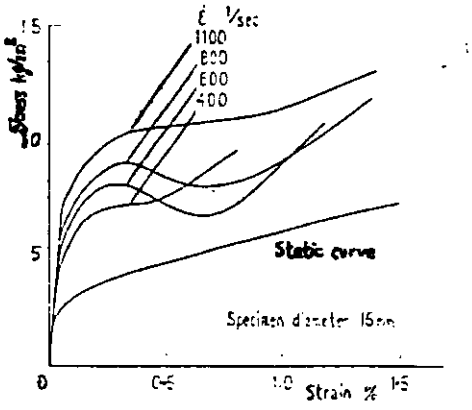

Figure 2.4 Stress-strain curves of annealed copper (Kishida and Senda, 1972)

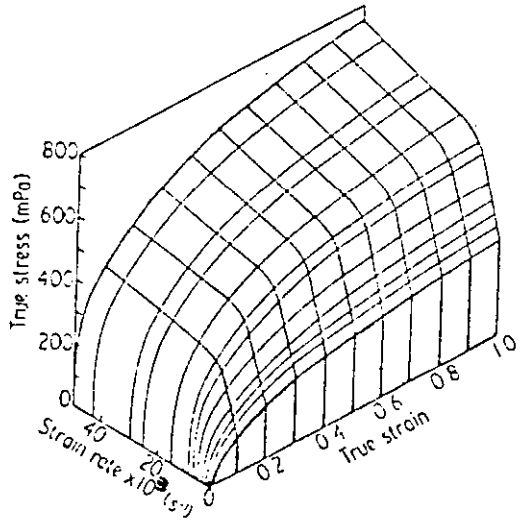

Figure 2.5 True stress versus true strain versus strain rate for annealed OFHC copper (Wulf, 1974)

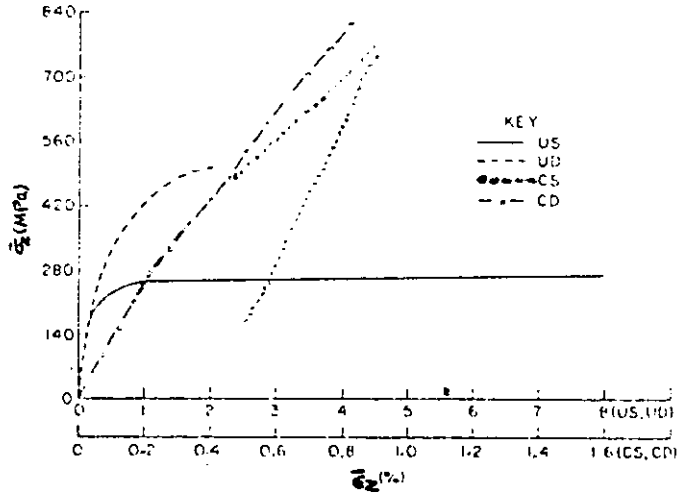

Figure 2.6 Axial stress-strain curves for oxygen-free copper (Bhushan and Jahsman, 1978)

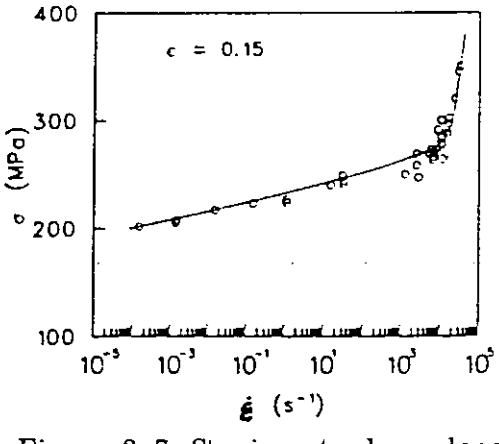

Figure 2.7 Strain rate dependence of the flow stress of copper (Follansbee et al, 1984)

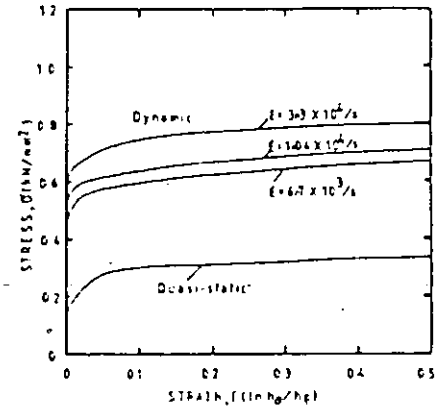

Figure 2.8 Dynamic stress-strain curves for copper (Hashmi and Haque, 1986)

strain at $\dot{\varepsilon} > 10^3 s^{-1}$ (Figure 2.5).

He suggested that the stress required to give dislocation velocities needed for the high strain rates was sufficient for dislocations to glide past short range barriers without the aid of thermal fluctuations.

The following equation was presented which relates strain rate ($\dot{\varepsilon}$) to the flow stress (σ):

$$\dot{\varepsilon} = \frac{(3)^{1/2} \rho_m b^2 \ (\sigma - \sigma^*)}{B} \qquad (2.4)$$

where ρ_m = mobile dislocation density (m^{-2})

B = damping coefficient (Pa.s)

b = Burgers vector (m)

σ^* = internal back stress (Pa)

He calculated the value of ρ_m to be $10^{11}\ m^{-2}$.

Stelly and Dormeval (1978) ($\dot{\varepsilon} \leqslant 8 \times 10^3 s^{-1}$) once again confirmed that two fields are evident, i.e. below $10^3 s^{-1}$ stress varies very little but at greater strain rates there is a sharp rise in stress and a linear relation between stress and strain rate for each strain level. It was also found that although the strain rate sensitivity of copper is very low in the lower region, it increases to between 16 and 30 MPa in the higher region (c.f. strain rate sensitivity was measured at more than 6.9 MPa by Dowling et al (1970)).

The linear relation between shear flow stress (τ) and the

shear strain rate ($\dot{\gamma}$) was expressed in the form:

$$\tau = \tau_B + \alpha \dot{\gamma} \qquad (2.5)$$

where $\alpha = B / \rho_m b^2 = 4.5 \times 10^3 Pa.s$

and τ_B is the stress required to overcome the forest dislocation barriers to dislocation motion. (N.B. τ_B is the same parameter as internal back stress σ^*, used by Wulf (1974)). They calculated ρ_m to be between 4 x $10^{10} m^{-2}$ and 3 x $10^{11} m^{-2}$, in agreement with Wulf.

Bhushan and Jahsman (1978) ($\dot{\varepsilon} > 10^3 s^{-1}$) compared low and high strain rate tests on confined and unconfined specimens. In the former case the specimen is prevented from expanding radially as it contracts longitudinally by being surrounded by a close fitting steel collar. The specimen is then effectively tested under conditions of uniaxial strain rather than the more conventional uniaxial stress, which occurs when the specimen is unconfined. Figure 2.6 compares the quasi-static unconfined (US), dynamic unconfined (UD), quasi-static confined (CS) and dynamic confined (CD) test results. It can be seen that the strain rate sensitivity is greater when the specimen is subjected to uniaxial stress than when subjected to uniaxial strain.

Follansbee et al (1984) ($\dot{\varepsilon} \lesssim 3 \times 10^4 s^{-1}$) showed that the strain rate sensitivity increases rapidly when the strain rate exceeds about $10^4 s^{-1}$ and in this high strain rate regime there is a linear relation between stress and strain rate according to:

$$\sigma = \sigma_b + \beta \dot{\varepsilon} \qquad (2.6)$$

σ_b and β are constants, which Follansbee et al define as a threshold stress ($\hat{\sigma}$) and $M^2B/b^2\rho_m$, respectively, where M is the average Taylor orientation factor, B the drag coefficient, b the Burgers vector and ρ_m the mobile dislocation density (Figure 2.7).

Hashmi and Haque (1986) ($\dot{\varepsilon} \leqslant 3.3 \times 10^4 s^{-1}$) tested specimens up to a strain of 50% and concluded that copper is strongly strain rate sensitive, this sensitivity decreasing with increase in strain (Figure 2.8). No correction is necessary for inertial effects because inertia is more or less cancelled out by the stress diminishing effect caused by the localised temperature rise during deformation. This temperature rise was quoted as 20K at $3.3 \times 10^4 s^{-1}$ over a strain of 10%. A correction for friction being estimated at 0.08 over strains of about 10%-40% at room temperature.

(b) Tests at Various Temperatures

Hawkyard et al (1968) employed a single strain rate of approximately $5 \times 10^3 s^{-1}$ and varied the temperature of the specimen from 20°C to 600°C. They achieved strains as high as 0.9, the stress reducing from 280MPa at 20°C to 40 MPa at 600°C for this maximum strain. Their graphs of dynamic stress/static stress versus homologous temperature (T_H) show a sharp rise at $T_H > 0.5$ (Figure 2.9), where homologous temperature is testing temperature (K) divided by the melting point of copper (K).

Samanta (1969) ($\dot{\varepsilon} \leqslant 600 s^{-1}$) varied the test temperature from 450°C to 900°C and found that copper strain hardens considerably up to 600°C but above this temperature

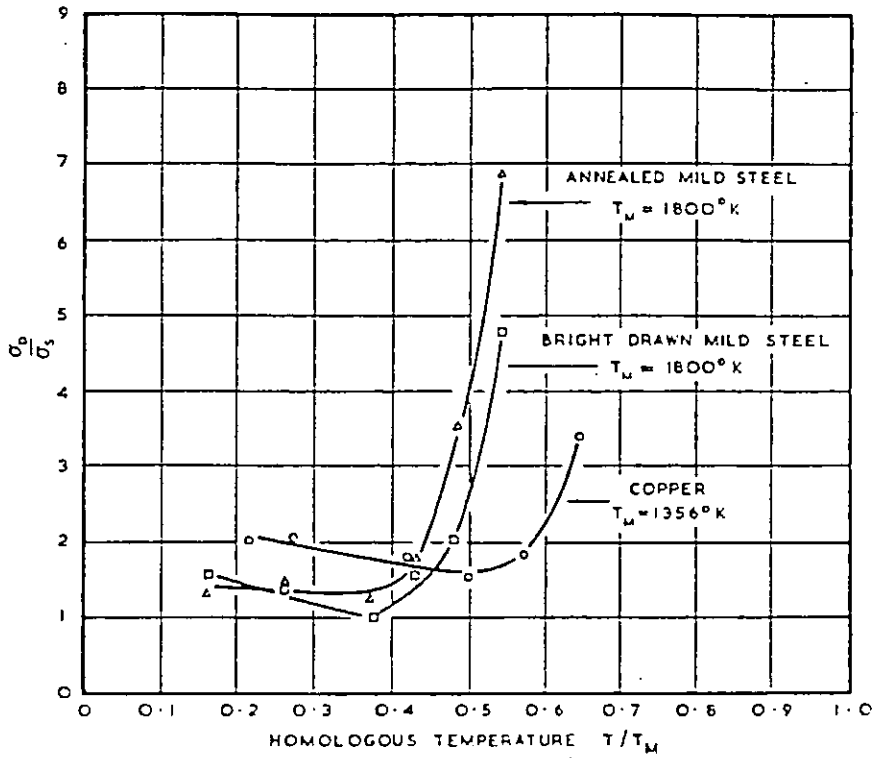

Figure 2.9 Variation of dynamic/static mean yield stress ratios with homologous temperature (T/T_m) (Hawkyard et al, 1968)

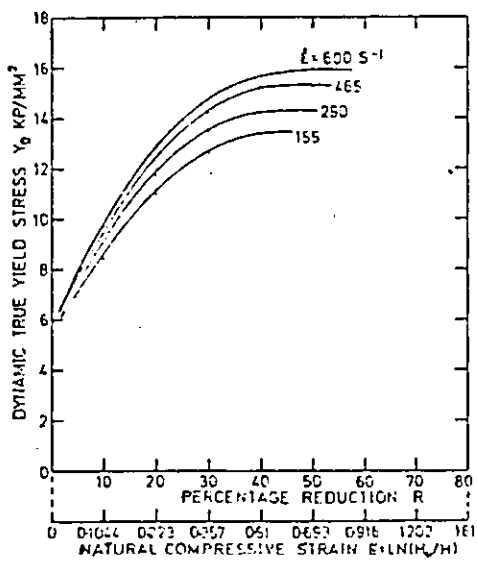

Figure 2.10 Dynamic true yield stress versus natural compressive strain at 750°C (Samanta, 1969)

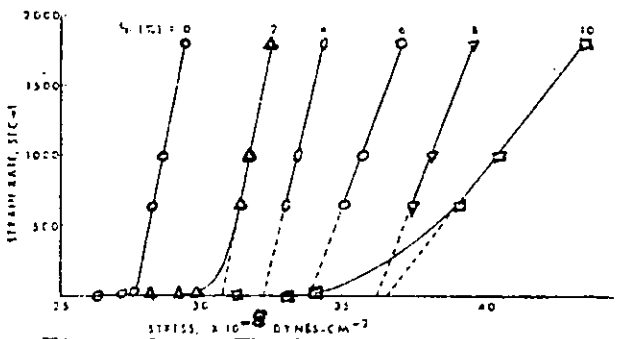

Figure 2.11 The linear dependence of flow stress on strain rate at high strain rates for OFHC copper at 300°K (Kumar and Kumble, 1969)

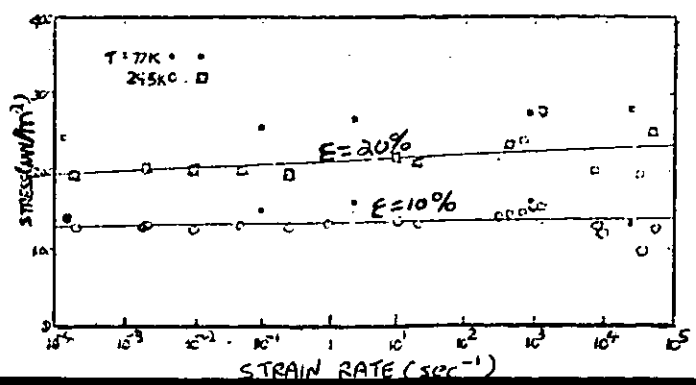

Figure 2.12 Flow stress for 99.999% copper (Lindholm, 1978)

recrystallisation predominates over strain hardening. Above 600°C, dynamic yield stress (Y_D), strain rate ($\dot{\varepsilon}$) and temperature (Θ) can be related by:

$$Y_D = \alpha \beta^{\Theta} \dot{\varepsilon}^{(\gamma\Theta - \lambda)} \qquad (2.7)$$

where α, β, γ and λ are strain-dependent constants, (see Figure 2.10 for an example of a stress-strain curve at 750°C). Hence for the strain rates tested a simple thermally activated mechanism predominates. It was also found that rate sensitivity increased with increases in temperature and strain.

Kumar and Kumble (1969) ($\dot{\varepsilon} \lesssim 2 \times 10^3 s^{-1}$) carried out their observations at room temperature (Figure 2.11), 147°C and 317°C. The pressure bars were only brought near the test specimen at firing time to minimise reflections due to thermal gradients. Below $10^3 s^{-1}$ mobile dislocations are thermally activated over the forest dislocation barriers and above this figure, dislocation motion is viscous drag limited.

$$\text{i.e. } \tau = \tau_B + \alpha \dot{\gamma} \qquad (2.8)$$

ρ_m is independent of strain rate and also strain, up to 6%.

Watson and Ripperger (1969) ($\dot{\varepsilon} \lesssim 10^3 s^{-1}$) applied a temperature range of 25°C to 440°C. They concluded that copper was strain rate sensitive, the sensitivity increasing with increased temperature, and the strain rate

effect was a material property, not a radial-inertia effect.

Lindholm (1978) applied by far the widest range of strain rates and temperatures to his test specimens. He achieved strain rates up to $6 \times 10^4 s^{-1}$ and a temperature variation from -196^oC to 22^oC (Figure 2.12). Despite the large variations he failed to detect any mode change, i.e. no transition from a thermally activated region to a viscous damping region. There was no sharp rise in flow stress at $10^3 s^{-1}$ as reported by other authors. He also found that copper has lower strain rate and temperature sensitivities than aluminium, which he subjected to the same tests. Reducing the test temperature of copper from 22^oC to -196^oC increased the stress less than 20% over the entire strain-rate range.

Shioiri et al (1978) ($\dot{\varepsilon} \leqslant 2.5 \times 10^4 s^{-1}$) carried out their investigations at temperatures of 20^oC, 300^oC and 500^oC. (Figure 2.13). An abrupt change in the strain rate sensitivity occurred at a strain rate of $10^4 s^{-1}$ at all temperatures. Taking into account time lags due to lateral inertia, local temperature rises in the pressure bars and a time lag which was inversely proportional to the velocity of the projectile, they discovered the following relation between stress, strain and strain rate:

$$\sigma = K(\dot{\varepsilon})(\varepsilon)^{0.5} \qquad (2.9)$$

where $K(\dot{\varepsilon})$ is a function of the nominal strain rate. Their results also showed that a mismatch between the

cross-sectional areas of the bars and the specimens is not important.

(c) Incremental and Decremental Strain Rate Tests

These tests have become increasingly popular recently especially in torsional dynamic tests (see section 2.3). Incremental tests involve initially straining the specimen quasi-statically (strain rate $\sim 10^{-4}s^{-1}$) and then suddenly imposing a high strain rate. Decremental tests operate in the reverse order.

Stelly and Dormeval (1978) are the only workers to use the procedures in compression tests. However, they did not suddenly change the strain rate after the initial part of the experiment but removed the stress from the specimen before applying the incremental/decremental strain rate. They used single crystals with parallelepiped cross-sections which were strained in the < 112 > direction and had faces of (111) and (110) types. The dynamic strain rates were $2 \times 10^{3}s^{-1}$ and $8 \times 10^{3}s^{-1}$. The incremental tests yielded stress-strain curves which were generally between the static and dynamic curves and showed no tendency to reach the purely dynamic curve, i.e. no 'fading memory' effect was observed as frequently observed when polycrystalline copper is strained in torsion. The decremental stress-strain curves were situated near the static curve.

2.3 Torsional Tests

Torsional tests have been increasingly used in recent

years. The advantages over compressive tests, e.g. errors due to lateral inertia, have been frequently quoted in the literature.

2.3.1 Experimental Techiques

(a) Test Machines

Three types of dynamic testing machines are most commonly employed for straining materials in torsion. These are:-

(i) Rotary Flywheel
(ii) Hydraulic Torsional Actuator
(iii) Torsional Split Hopkinson Pressure Bar

The last of these has been used most often for testing copper in torsion at high rates of strain. It was employed by YEW and RICHARDSON (1969), CAMPBELL and DOWLING (1970), ELEICHE and CAMPBELL (1974), CLYENS and CAMPBELL (1974), SENSENY et al (1975), LIPKIN et al (1978) and SENSENY et al (1978).

The maximum shear strain rates ($\dot{\gamma}$) achieved in these experiments were $5 \times 10^2 s^{-1}$, $90 s^{-1}$, $9 \times 10^2 s^{-1}$, $2.7 \times 10^3 s^{-1}$, $2 \times 10^3 s^{-1}$, $1.2 \times 10^3 s^{-1}$ and $3 \times 10^2 s^{-1}$, respectively.

A rotary flywheel was designed for torsional tests by BITANS and WHITTON (1970-71); a similar device being used by STURGES et al (1979). The former achieved shear strain rates of $10^3 s^{-1}$ and the latter $1.4 \times 10^3 s^{-1}$.

A new improved hydraulic torsional actuator, was recently developed by LINDHOLM et al (1980). This enabled them to attain a maximum strain rate of $330s^{-1}$.

Short rise times and long pulse durations are important factors in high strain rate tests. Rise times of 30 μs, 25 μs and 10 μs were reported by Campbell and Dowling, Eleiche and Campbell, and Senseny et al (1975), respectively. Clyens and Campbell achieved a rise time of 25 μs on a short-base SHPB and 12 μs on a long-base SHPB. Pulse durations of 1040 μs, 550 μs and 490 μs were quoted by Eleiche and Campbell, Clyens and Campbell, and Senseny et al (1978), respectively.

(b) Data Acquisition Techniques

The techniques for measuring and recording the data from the torsional SHPB tests were basically the same as those in operation in the compressive SHPB tests.

A dynamometer of the resistance strain gauge type measured the flywheel torque in Bitans and Whitton's experiment. The angle of twist was recorded by a photoelectric device. The outputs from both devices were fed via a pre-amplifier for display on an oscilloscope. Analysis of the two traces yielded values of shear stress (τ), shear strain (γ) and shear strain rate ($\dot{\gamma}$).

Sturges et al used similar transducers to measure the relevant parameters.

In Lindholm et al's method rotary capacitance and load

transducers recorded the angle of twist and torque, respectively. An analogue-to-digital converter, in the form of a transient recorder, recorded their results for future display and analysis.

Eleiche and Campbell also digitised their results. The analysis being performed with the aid of an ICL 1906A computer.

2.3.2 Test Specimens

(a) Dimensions

In all cases the test specimens were hollow cylinders. Unlike the compressive specimens, there was no fixed relation between specimen length and diameter. The lengths varied from 1.27mm to 900mm and the outside diameters from 12.7mm to 38.1mm.

(b) Composition

Eleiche and Campbell, Campbell and Dowling, Clyens and Campbell, and Bitans and Whitton, quoted the exact composition of the specimens employed, as determined by chemical or spectrographic analysis. However, most authors stated a more general description, e.g. OFHC copper. No single crystals of copper have been tested in torsion.

(c) Annealing

Annealing temperatures varied from 350^{o}C to 700^{o}C and annealing times from 1 to 2 hrs, with the exception of Campbell and Dowling, who annealed their specimens for 20 hrs.

Senseny et al (1978) and Bitans and Whitton annealed their specimens in an argon atmosphere and a salt bath, respectively. All the others preferred a vacuum.

Walker (1982) lists all the quoted specimen dimensions, chemical compositions, annealing temperatures and times.

(d) Grain Size

The average grain size in microns was quoted in 5 papers. These were:

Eleiche and Campbell	(1974)	- 53
Lipkin et al	(1978)	- 80
Clyens and Campbell	(1974)	- 30
Senseny et al	(1978)	- 35
Lindholm et al	(1980)	- 25-35

2.3.3 Results

(a) Room Temperature Tests

The work of Bitans and Whitton ($\dot{\gamma} \leqslant 10^3 s^{-1}$) yielded the rather surprising result that the stress (at a given strain) DECREASES with increase in strain rate (Figure 2.14). This contradicts all other high strain rate tests on copper. In addition, the gradients of the initial portion of their stress-strain curves decreased with increasing strain rate in an almost systematic fashion. At increased rates of strain there was a marked increase in ductility, especially at strain rates of $25s^{-1}$ and above.

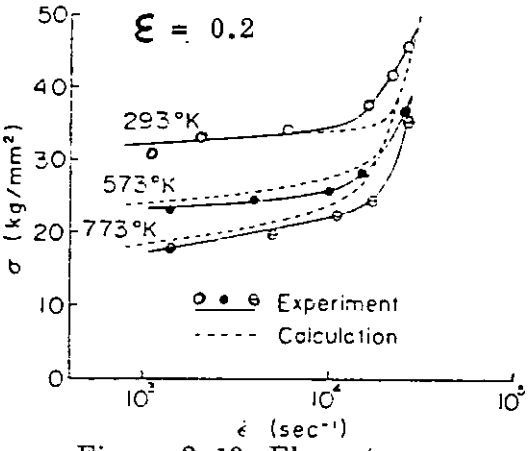

Figure 2.13 Flow stress versus strain rate
(Shioiri et al, 1978)

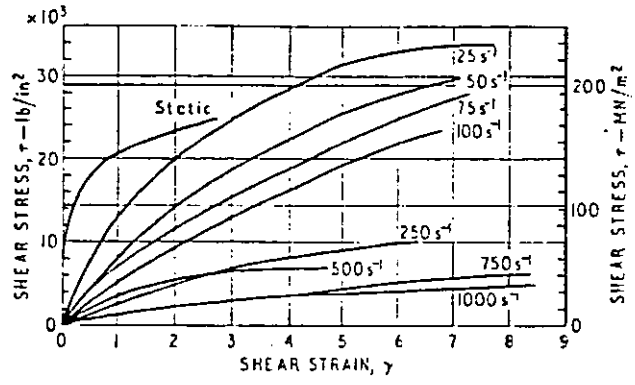

Figure 2.14 - curves for copper at = 25-1000s^{-1}
(Bitans and Whitton, 1970-71)

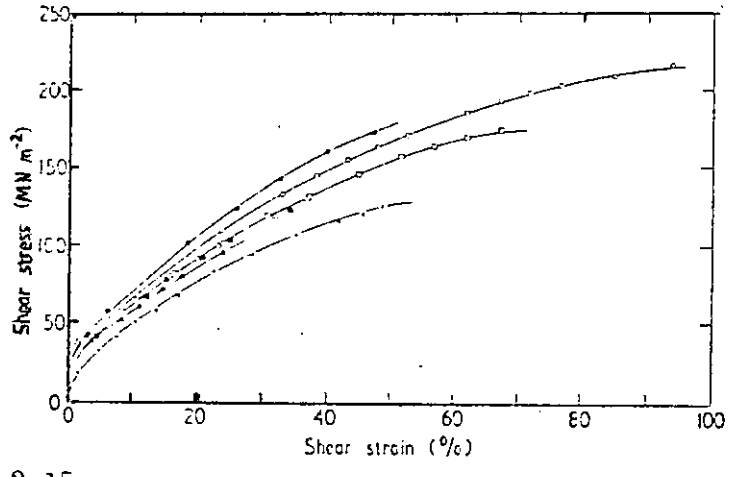

Figure 2.15 Shear stress–strain curves for OFHC copper. Tests in short-base machine (rise time 25 μs): ● 2700 s^{-1}; ■ 1900 s^{-1}; ▲ 1100 s^{-1}. Tests in long-base machine (rise time 12 μs): ○ 2500 s^{-1}; □ 1200 s^{-1}; △ 750 s^{-1}; +, test at 0·004 s^{-1} in screw-driven machine.
(Clyens and Campbell, 1974)

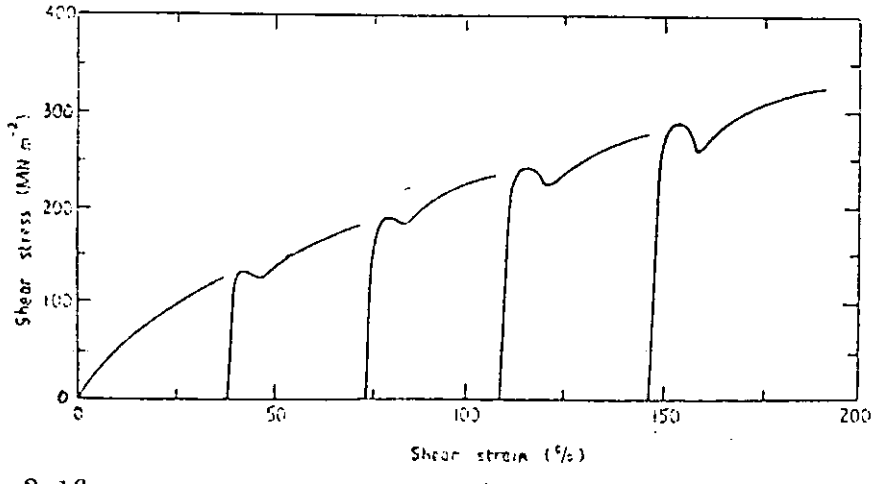

Figure 2.16 Shear stress–strain curves for OFHC copper specimen subjected to repeated dynamic loading (mean strain rate, 1900 s^{-1}).
(Clyens and Campbell, 1974)

They suggested that a sudden application of shear strain could generate adiabatic shear bands in the metal being deformed. The heat generated by the plastic work in the bands of intense shear would soften the material so that shearing deformation would occur in these bands in preference to surrounding material. Hence the larger the shear strain rate, the larger the number of shear bands and the lower the stress for a given strain. Many workers have discussed their findings, most disagreeing with their results and offering explanations for possible errors in their work.

Clyens and Campbell ($\dot{\gamma} \leq 2.7 \times 10^3 s^{-1}$) performed tests with a conventional short-base SHPB (2.6m) and a newly designed long base SHPB (4.6m). The larger machine resulted in a shorter pulse rise time and a longer pulse duration. In addition the total strain was increased (Figure 2.15). Their results showed little difference in response between the two machines, there being no evidence of a decrease in flow stress due to a reduction in rise time from 25 μs to 12 μs. Bitans and Whitton suggested that with rise times as short as 12 μs, adiabatic shear bands would form allowing plastic flow at greatly reduced stresses.

Clyens and Campbell found a positive rate sensitivity which increased with strain and is large at high strain rates. They also detected yield drops for repeated dynamic loading, similar to those reported by HARDING (1971) (see Tensile tests - section 2.4), but of smaller magnitude (Figure 2.16).

Sturges et al ($\dot{\gamma} \leqslant 1400s^{-1}$) reported a modest increase of flow stress with increase in strain rate. At high pressures, larger strains were achieved before failure of the specimens, but the flow stresses were approximately the same.

Lindholm et al ($\dot{\gamma} \leqslant 330s^{-1}$) presented evidence of positive strain hardening and strain rate effect up to $10s^{-1}$, followed by strain hardening decreasing with a load drop occurring at about $\gamma = 5$ (Figure 2.17). Subsequent metallographic examination showed that severe strain localisation occurred in the specimens, i.e. localised adiabatic shear bands associated with the instability of the stress-strain behaviour. This was explained by thermal softening overcoming strain hardening.

(b) Incremental/Decremental Tests at Room Temperature

Yew and Richardson ($\dot{\gamma} \lesssim 500s^{-1}$) performed high strain rate tests on both stress-free and pre-stressed specimens. The former tests demonstrated that a fast moving elastic pulse runs ahead of a slower moving plastic pulse. Also these tests suggested that copper is strain rate INSENSITIVE at $500s^{-1}$. The incremental tests showed that low level strains travel at higher velocities than high level strains, i.e. evidence for strain rate sensitivity. In addition, the dynamic stress-strain curve deviated from the quasi-static curve. Hence they concluded that copper is strain rate SENSITIVE.

Campbell and Dowling ($\dot{\gamma} \lesssim 90s^{-1}$) justified their use of dynamic incremental shear loading by stating that other

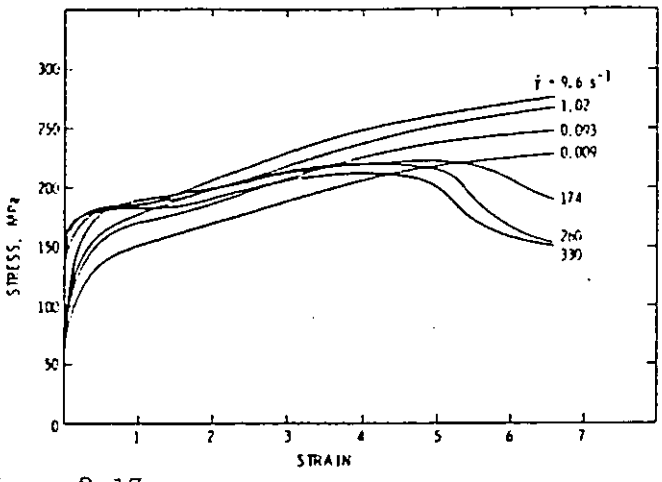

Figure 2.17 Shear stress-strain curves for OFHC copper
(Lindholm et al, 1980)

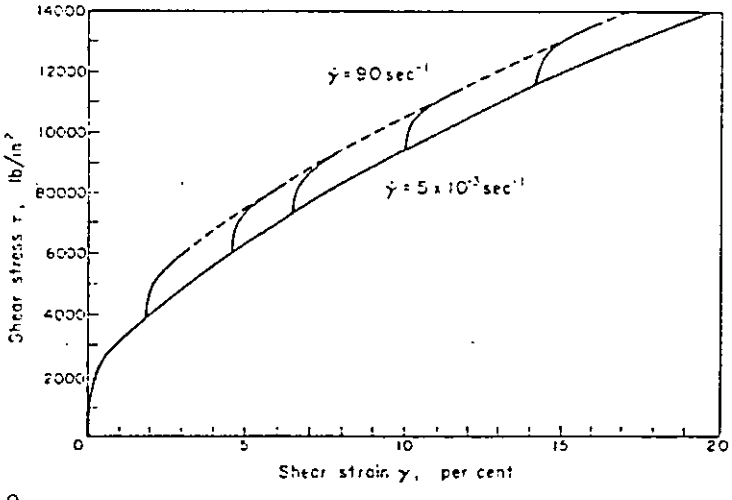

Figure 2.18 Incremental stress-strain curves from tests on short specimens of copper.
(Campbell and Dowling, 1970)

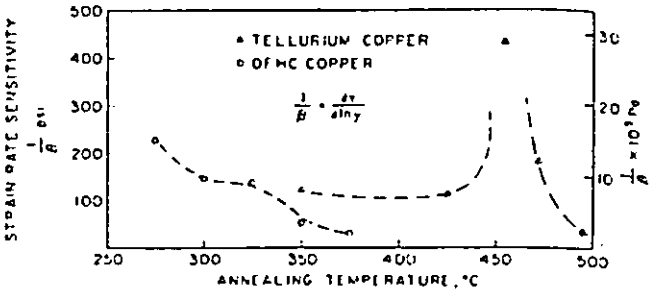

Figure 2.19 Strain-rate sensitivity plotted against annealing temperature for both OFHC copper and tellurium copper; in both cases the low strain-rate stress level is compared with the stress level obtained from constant high strain rate deformation.
(Senseny et al, 1975)

workers have shown that experiments in which test materials are not pre-strained give little indication of the rate dependence of the material. They found that the incremental wave travelled at approximately the same velocity as the elastic wave and a small reduction in wave speed resulted from an increase in the pre-strain. The initial slope of the incremental stress-strain curve was about the same as the shear modulus of copper. The mean rate sensitivity in the strain rate range $5 \times 10^{-3} s^{-1}$ to $90 s^{-1}$ did not vary significantly with pre-strain. This differed from constant strain rate tests and hence flow stress must depend on strain rate history as well as the current values of stress and strain rate (Figure 2.18).

In 1975, Senseny et al ($\dot{\gamma} \lesssim 2 \times 10^{3} s^{-1}$) investigated the influence of annealing temperature on the strain rate sensitivity of copper in torsion. They included tellurium copper in their experiments as well as the usual OFHC copper. The strain rate sensitivity was found to decrease with increasing annealing temperature except for a sharp rise in the strain rate sensitivity at the recrystallisation temperature of tellurium copper (Figure 2.19). They also confirmed the general conclusion that strain rate sensitivity is positive in all cases.

Lipkin et al ($\dot{\gamma} \lesssim 1.2 \times 10^{3} s^{-1}$) criticised the analysis of rate-jump tests because it assumed that the microstructure remained constant during the deformation. However, when the strain rate is increased suddenly the increase in flow stress may generate new dislocations. As a result, in their current paper the results of dynamic strain rate

REDUCTION tests are published.

They performed two experiments. In the first, the specimen was annealed at 450°C and the initial plastic strain rate was constant at $1200s^{-1}$ for 175 μs, then reduced to $180s^{-1}$, and then increased again. When the strain rate was falling, the flow stress continued to rise although there was a reduction in this increase for approximately 100 μs when was decreasing from $900s^{-1}$ to $180s^{-1}$ and back up to $400s^{-1}$. In fact, the stress was almost constant when $\dot{\gamma} \leq 400s^{-1}$ (Figure 2.20).

In the second experiment, where the specimen is annealed at 400°C, the initial plastic strain rate was $850s^{-1}$. After 190 us this was reduced to $175s^{-1}$, the reduction being completed after 45 μs (Figure 2.21). There were two main differences from experiment one, namely the strain rate minimum remained constant for almost 200 μs and a small transient in the strain rate appeared after about 300 μs.

Although the two specimens showed no difference in grain size, the one annealed at the lower temperature was more stiff and the initial portion of the transmitted stress v. time curve exhibited an elastic-plastic transition which was not present for the other specimen. They concluded that the fall in stress could be caused by microstructural rearrangement such as that associated with the formation of dislocation cell walls, the rearrangement depending on the dynamic recovery from a thermodynamically unstable structure produced by a particular thermo- mechanical history.

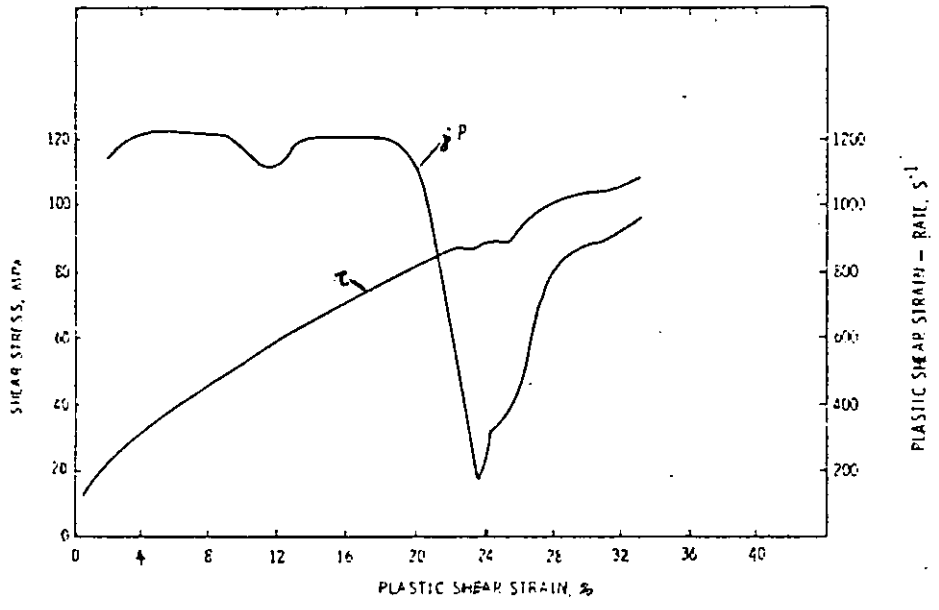

Figure 2.20 Reduced records for experiment I. τ and $\dot{\gamma}P$ vs γP (Lipkin et al, 1978)

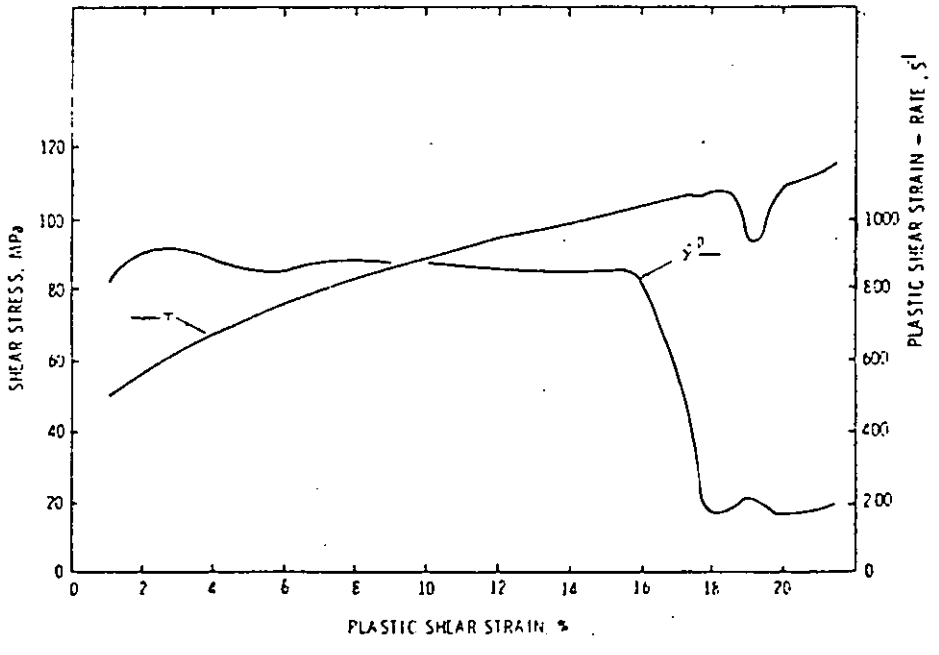

Figure 2.21 Reduced records for experiment II. τ and $\dot{\gamma}P$ vs γP (Lipkin et al, 1978)

(c) Incremental Tests at Various Temperatures

Eleiche and Campbell performed incremental tests at temperatures of 24, 200 and 400°C (Figure 2.22) and at three static strains of 0.1, 0.25 and 0.5. The strain rate was increased from $3 \times 10^{-3} s^{-1}$ to $900 s^{-1}$. Each incremental curve showed a small initial elastic response which was more marked at higher values of pre-strain. Strain hardening always followed the initial response, the rate of which decreased more rapidly with large pre-strain. Hence with the smaller values of pre-strain, the specimens have less 'memory' of their previous strain-rate history, i.e. they have a quicker recovery and transition to the exclusively dynamic stress-strain curve. This contradicts the effect found in aluminium by FRANTZ and DUFFY (1972). Eleiche and Campbell also found that, for a given pre-strain, the post-jump strain required for a given percentage recovery of stress was only slightly affected by the testing temperature.

In constant strain rate tests they stated that strain-hardening increased with increase in strain rate or decrease in temperature over the whole deformation range and, in common with all other workers, except Bitans and Whitton, a positive strain rate sensitivity was observed.

Senseny et al (1978) tested the behaviour of copper at shear strain rates varying from $2 \times 10^{-4} s^{-1}$ to $300 s^{-1}$ and temperatures ranging from -196°C to + 250°C. The increment in $\dot{\gamma}$ produced a sharp rise in flow stress ($\Delta \tau_s$) followed by a more gradual increase. The flow stress immediately after the strain rate increment is less than

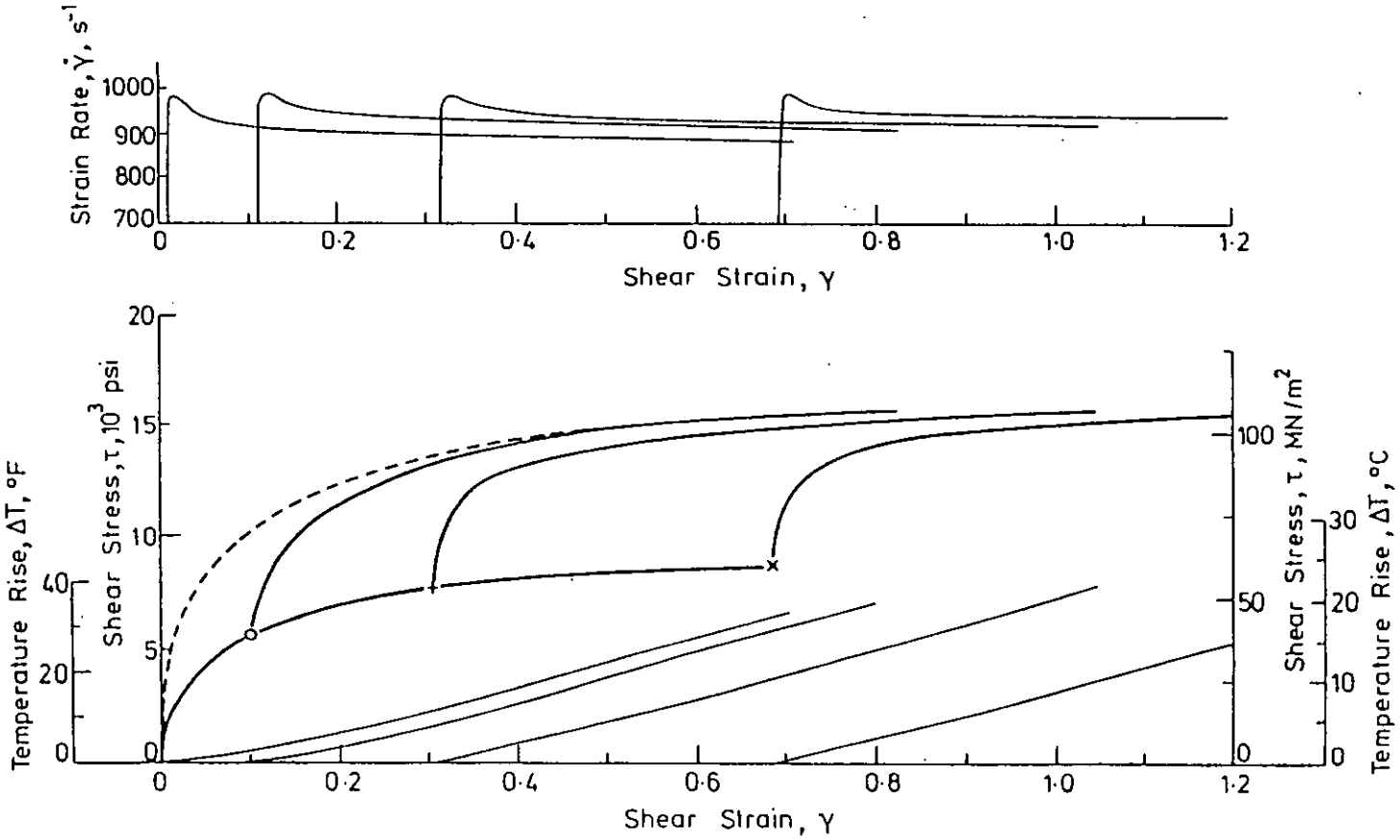

Figure 2.22 Incremental strain-rate test-results for copper at 400°C at 0.103, 0.308 and 0.688 pre-strain.

(Eleiche and Campbell, 1974)

that produced by a purely dynamic strain rate at the same strain, by an amount $\Delta\tau_h$. Hence, $\Delta\tau_h$ represents the influence of history on the stress-strain curve. Both $\Delta\tau_s$ and $\Delta\tau_h$ increase with increases in strain at all temperatures. The difference in gradients between the initial slope produced by the strain increment and the more gradual slope that followed it, was less pronounced at higher temperatures. There was a definite 'fading memory effect' at all temperatures. The slope of the τ/γ curve immediately following the increment in the strain rate was close to the elastic slope (Figure 2.23).

2.4 Tensile Tests

Compared with the number of high strain rate tests performed on copper in compression and in torsion there is a distinct paucity of tensile experiments on this material.

2.4.1 Experimental Techniques

(a) Test Machines

Harding (1971) operated a modified SHPB which produced a tensile incident stress pulse of duration 50 μs and magnitude 275 MPa by means of a rapidly induced magnetic force. This produced a mean strain rate of more than $10^3 s^{-1}$. Using an unspecified test machine, OHMORI et al (1968) subjected copper to tensile stresses at strain rates up to $160 s^{-1}$. DORMEVAL and STELLY (1976, 1979) performed tensile tests at strain rates of approximately $5 \times 10^2 s^{-1}$ in 1976 and at rates up to $1.2 \times 10^3 s^{-1}$ in 1979. In both cases they used a specially built machine known as Arbalete (Cross-Bow).

This consisted of two parallel guide-rails, between which moved a projectile propelled by rubber bands. The projectile impact speed ranged from 3 to 40ms^{-1}. The specimen, positioned between the rails, was fixed at one end (the end closer to the projectile) to a long rod acting as a dynomometer, and at the other end to a moving head which was hit by the projectile.

The same machine was used by REGAZZONI et al (1981), and REGAZZONI and MONTHEILLET (1984) to achieve a maximum strain rate of 3 x $10^3 s^{-1}$ in both cases.

Experiments using an exploding wire or exploding cylinder technique have been used by FYFE and RAJENDRAN (1979) and BAUER and BLESS (1979). All achieved strain rates of at least $10^4 s^{-1}$.

In the former paper, thin walled cylindrical specimens were dynamically loaded by an exploding wire system. Two or more 15 μF capacitors, each charged to 20kV to provide energy storage of 3KJ per capacitor were discharged through copper wire 10cm long and 0.84mm in diameter. Water was used as a coupling mechanism between the wire and the specimen.

Bauer and Bless employed two types of explosive loadings to provide strain rates at failure of 1 x $10^4 s^{-1}$ and 2.5 x $10^4 s^{-1}$. In the same paper these authors also described tensile tests using the SHPB. This apparatus was capable of testing materials in tension at strain rates up to approximately $10^3 s^{-1}$. A 'dog bone' shaped specimen was

screwed into the adjacent ends of the incident and transmitter bar. A co-axial collar surrounded the specimen to protect it from the compressive pulse. When impacted by the projectile, the elastic compressive wave travels down the incident bar through the collar and into the transmitter bar. The wave is reflected as a tensile wave at the far end of the transmitter bar and then elongates the specimen as the collar interface cannot support tensile stresses.

(b) Data Acquisition Techniques

The usual data acquisition methods were employed to provide results from the Hopkinson bar and exploding wire tests.

An alternative strain measuring technique using a high speed streak camera was used by Dormeval and Stelly to determine local changes in length along the specimen. A line network was drawn on its gauge length and from the distance between adjoining lines at successive times, the evolution of the deformation in each section of the specimen was determined.

2.4.2 Test Specimens

The dimensions, composition, annealing temperatures and times are listed, where available, in Walker (1982). The quoted grain sizes in microns were:

Harding (1971)	- 143
Dormeval and Stelly (1979)	- 90,130 & 300
Regazzoni et al (1981)	- 25
Regazzoni and Montheillet (1984)	- 25

2.4.3 Results

(a) Room Temperature Tests

Dormeval and Stelly (1976), who carried out their tests on single crystals at maximum strain rates of $500s^{-1}$, detected four zones in their stress-time curve:

(i) a stress peak between 40 and 100 μs,
(ii) after relaxation the stress rose again, but more slowly,
(iii) another stress maximum reached, followed by an even slower rise in stress,
(iv) and the stress then decreased until rupture occurred

Below 10^2s^{-1}, the stress remained constant with increase in strain rate but there was a rapid rise above this rate. As with their compressive tests of 1978 on single crystals there was no fading memory effect. However, the stress was always greater in the dynamic tests than for the corresponding value of strain in the static tests. This was not always true in the compressive tests.

In 1979, the same two workers investigated the influence of grain size, as well as strain rate, on high purity polycrystalline copper. Grain sizes of 90, 130 and 300 μm diameter were used. They applied three strain rates to their specimens, 350, 700 and $1000s^{-1}$ (Figure 2.24). They observed that their high strain rate data was compatible with the Petch relation for strains up to about 5%, i.e. stress is inversely proportional to the square root of the

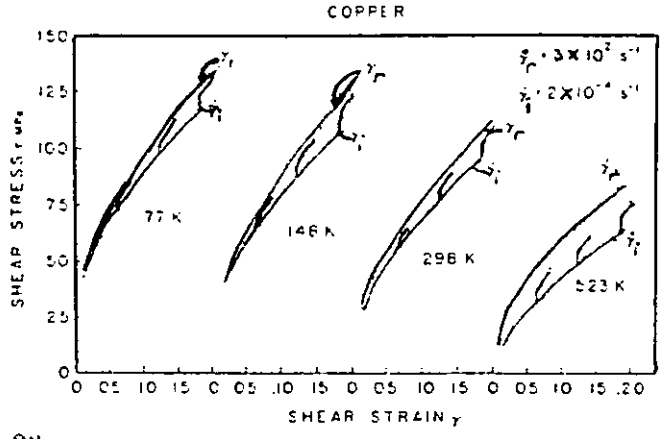

Figure 2.23 Stress-strain curves from incremental and constant strain rate tests for OFHC copper

(Senseny et al, 1978)

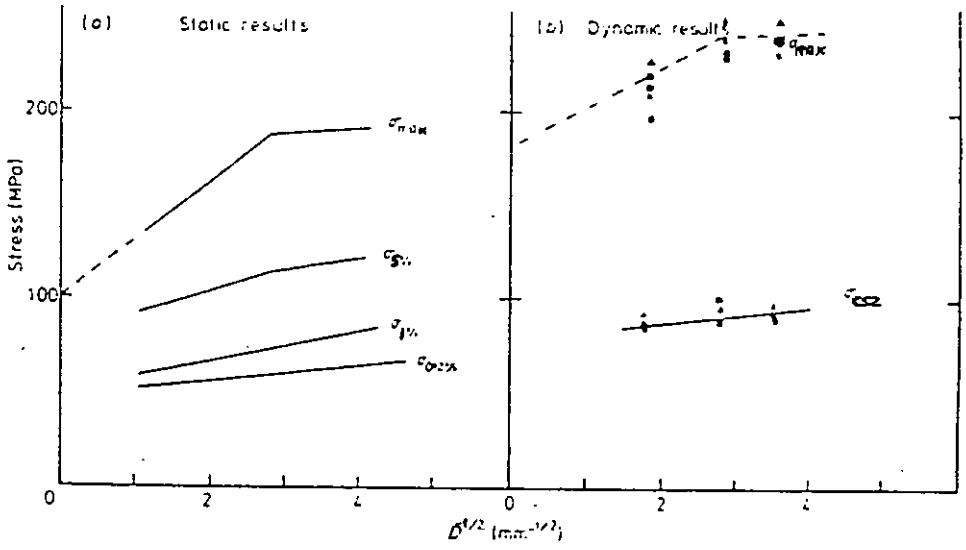

Figure 2.24 Influence of grain size on flow stresses. $\dot{\epsilon} = 350$, ■ 700, ▲ 1000 s^{-1}.
(Dormeval and Stelly, 1979)

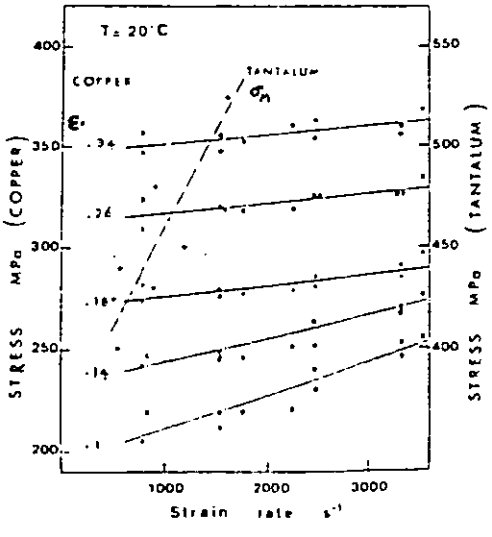

Figure 2.25 Stress/strain rate relationships for copper and tantalum in the high strain rate range.
(Regazzoni and Montheillet, 1984)

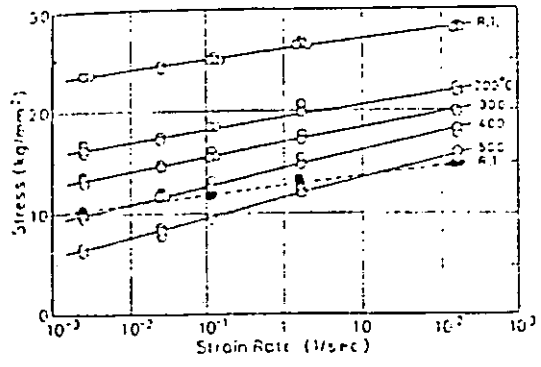

Figure 2.26 Tensile Strength (Solid Lines) and Flow Stress at Strain of 2.6ϵ_0 (Dotted Line) as a function of Strain Rate.
(Ohmori et al, 1968)

initial grain size, i.e. $\sigma = \sigma_o + KD^{-1/2}$ (2.10)

This relation had been previously shown to be valid for materials tested at quasi-static strain rates. For strain rates larger than $300s^{-1}$ they derived the following constitutive equation:

$$\sigma = \sigma_o + \alpha\dot{\varepsilon} \tag{2.11}$$

where σ_o and α are constants, ($\alpha \sim 4\text{-}8 \times 10^3 Pa.S$)

Fyfe and Rajendran followed their dynamic tests by subjecting their specimens to quasi-static strain rates up to fracture and the following features were observed:

(i) in a purely dynamic test the hoop strain at failure exceeded that obtained by static testing only,

(ii) high strain rate loading very significantly inhibited the onset of plastic instability,

(iii) the strain at failure was significantly lower than that resulting from a purely static test

The results and conclusions from the exploding cylinder tests of Bauer and Bless were:

(i) failure occurred by longitudinal fracture,

(ii) fragment size is proportional to strain rate,

(iii) more than 200 fragments resulted from the $2.5 \times 10^4 s^{-1}$ tests, but less than 10 from the $1 \times 10^4 s^{-1}$ tests,

(iv) in all cases fracture began on the

outside of the tube,

(v) an average ultimate strain of at least 1.1 resulted with a strain rate of $2.5 \times 10^4 s^{-1}$,

(vi) at strain rates greater than $10^3 s^{-1}$, flow stress is increased, resulting in more even distributions of strains,

(vii) increases in the ultimate strain were attributed to strain hardening and strain rate hardening and the effects of applied triaxial stresses.

Regazzoni and Montheillet concluded that, at high strain rates, their results were consistent with a transition regime where the deformation is controlled simultaneously by thermal activation and viscous drag. This contrasts with the conclusions of most other workers in which the former deformation mechanism dominates up to about $10^3 s^{-1}$ and the latter at higher rates of strain. Regazzoni and Montheillet also determined that there is a linear stress-strain rate relation at high strain rates (Figure 2.25) and ductility increases rapidly with strain rate above $10^3 s^{-1}$.

(b) Tests at Various Temperatures

Temperatures ranging from $20^{\circ}C$ to $550^{\circ}C$ were applied in the dynamic tensile tests of Ohmori et al. These produced a linear reduction of area with increase in temperature for a given high strain rate. The specimens were most brittle at $350^{\circ}C$ at all strain rates but there was no abnormal variation in tensile strength corresponding to brittleness

at this temperature. A linear decrease of tensile strength with increasing temperature was reported. The flow stress at a small strain and at room temperature was found to have the same strain rate sensitivity as that for the flow stress at the tensile strength at the same temperature (Figure 2.26).

Harding studied the yield behaviour of pure polycrystalline copper under repeated tensile impact loading. The strain rate imposed was greater than $10^3 s^{-1}$ and repeated at intervals of 1-2 minutes with ambient temperatures of 15°C, -78°C and -196°C. After each impact there was a drop in stress at the yield point and this yield drop increased with the number of impacts and magnitude of strain. Figures 2.27 shows the results of his tests at -196°C.

Regazzoni et al performed their experiments on two types of OFHC copper at temperatures of 20°C and 500°C. Their results are indicated in Figure 2.28. The two coppers, labelled CuC1 and CuC2 had identical overall purity (99.99%) and differed only by their Bi, Pb and S content which was slightly higher in CuC2. For both coppers and at both temperatures the variation of maximum stress (σ_M) with strain rate ($\dot{\varepsilon}$) was consistent with two strain rate regimes intersecting at about $10^3 s^{-1}$. The strain rate sensitivity, which was positive in both regimes, was much greater above $10^3 s^{-1}$. Also in this high strain rate regime, a linear stress-strain rate relation was again evident. At the lower temperature, the ductility (e_R) varied in a similar fashion to σ_M and once more the results indicated evidence of two strain rate regimes. At

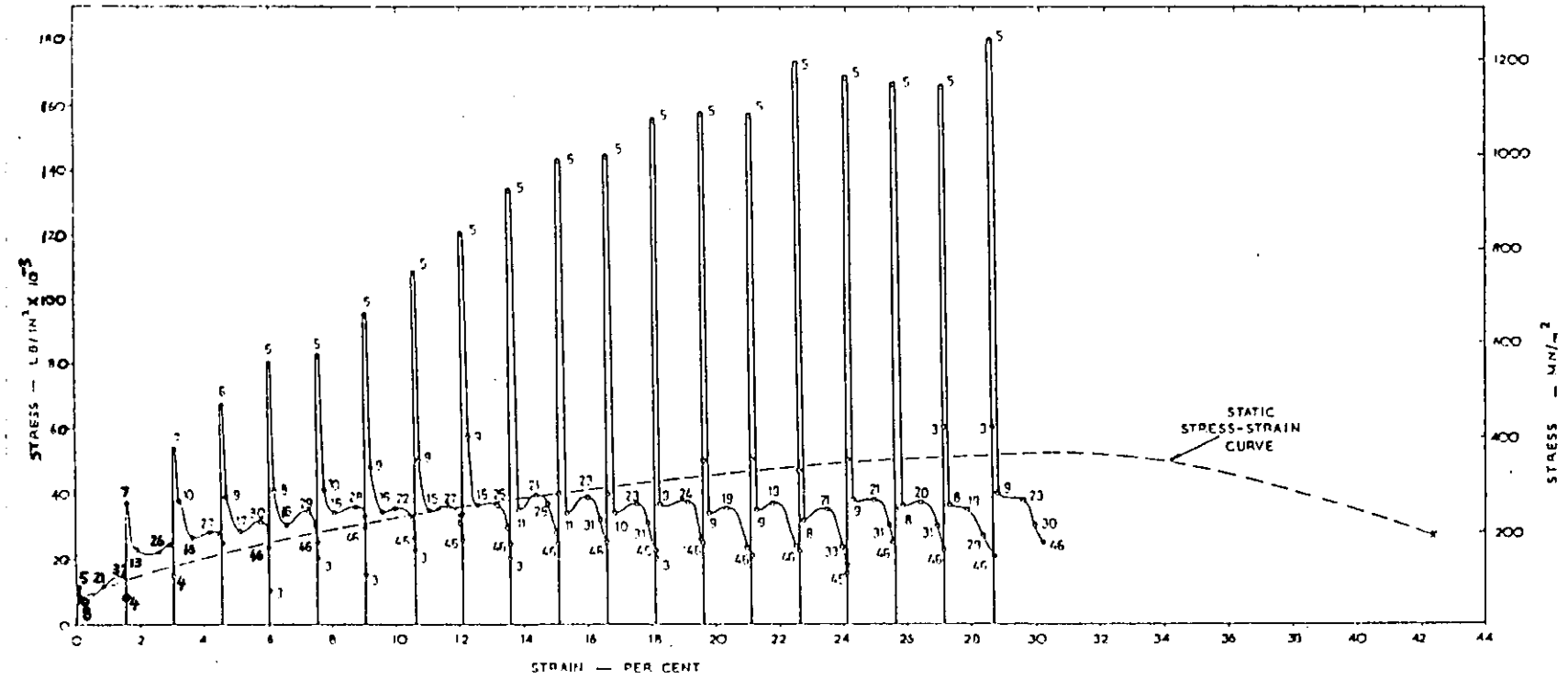

Figure 2.27 Stress strain curves for repeated impacts at 77°K (20 impacts on one specimen). (Harding, 1971)

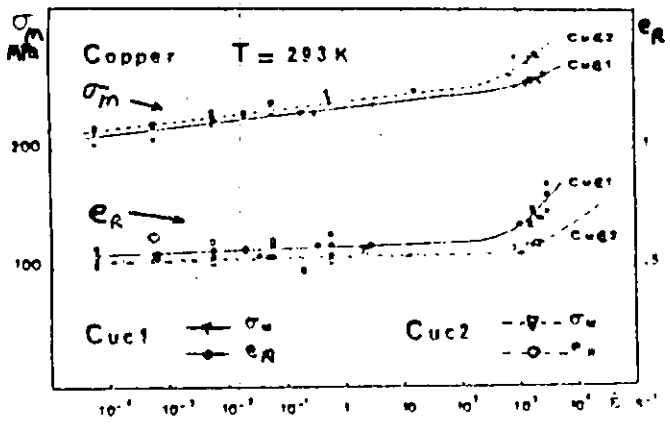

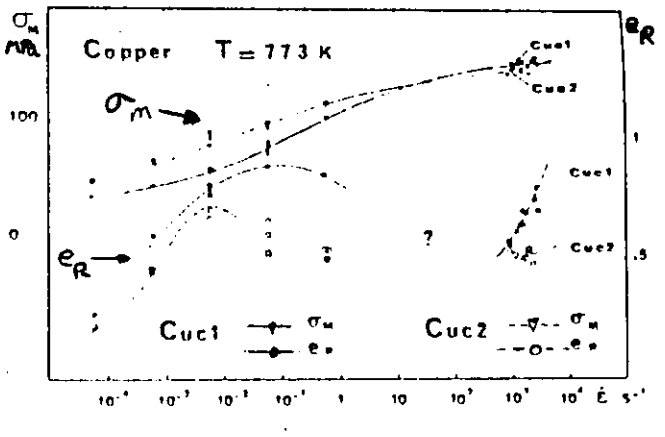

Figure 2.28 Maximum stress (σ_M) and ductility (e_R) vs. strain rate (Bonnezzi et al., 1981)

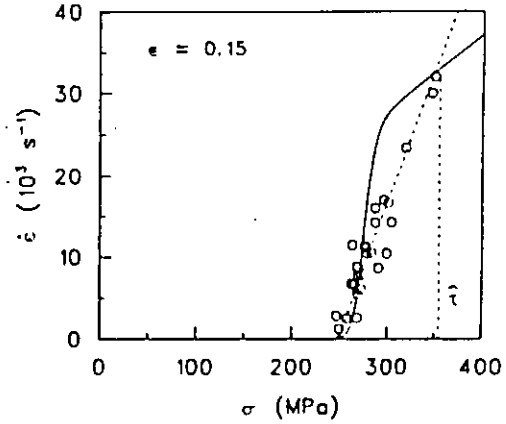

Figure 2.29 Comparison of the model with the experimental results. (Follansbee et al., 1984)

the higher temperature, however, the variation of e_R with was much more complex. At high strain rates, transgranular ductile failure was observed from the fracture surface. This was also the case of low strain rates when the two types of copper were tested at room temperature. However, for quasi-static deformation at 500°C, brittle intergranular fracture occurred.

2.5 Theoretical Analyses

This section includes a review of the microstructural analyses and the constitutive equations proposed in purely theoretical papers. It also covers the theory developed from experimental work which has not been treated in the earlier sections. A glossary of terms, most of which are peculiar to dislocation dynamics, is presented in Table 2.1.

KUMAR and KUMBLE (1969) state that the typical behaviour of metals subjected to increasing temperatures and strain rates can be divided into 4 regions:-

(i) thermally activated region,
(ii) athermal region, where the yield stress is independent of strain rate and temperature,
(iii) diffusion controlled region - temperature > $0.5T_m$ (T_m = melting temperature of copper (1357 K),
(iv) viscous damping region.

The flow stress τ for copper can be represented by the equation

Table 2.1

Glossary of Dislocation Dynamics Terms

BEND	-	the curvature of dislocation lines, i.e. the shape of the boundary between displaced and undisplaced regions.
DISLOCATION DAMPING OR DRAG COEFFICIENT (B)	-	the viscous drag force/the dislocation velocity (units: Pa.s).
FOREST DISLOCATION DENSITY (ρ_f)	-	the number of forest dislocations per unit area. Forest dislocations are localised obstacles or barriers to dislocation motion (units: m^{-2}).
IMMOBILISATION RATE	-	rate at which dislocations are immobilised due to interactions between the dislocations.
INTERNAL BACK STRESS (σ_B or σ^*)	-	stress required to overcome the forest dislocation barriers to dislocation motion.
JOGS AND KINKS	-	sharp bends in the dislocation lines with radii as small as one atomic radius. Kinks are associated with local offsets lying in the glide plane of the dislocation. Jogs are associated with offsets perpendicular to the glide plane.
MOBILE DISLOCATION DENSITY (ρ_m)	-	the number of dislocations per unit area which are mobile (units: m^{-2})
MULTIPLICATION RATE	-	The rate at which new dislocations are generated during plastic flow.
MULTIPOLES	-	grouping of dislocation lines that lie parallel to one another.
NODE	-	point of intersection of dislocation lines.
STRAIGHT DISLOCATION	-	straight line dislocations of which the edge and screw dislocations are special cases.

$$\tau = \tau_A + \tau^* + \tau_D \qquad (2.12)$$

where τ_A is the athermal component of stress, τ^* is the thermally activated component of stress, and τ_D is the stress attributed to phonon damping. At low strain rates in the thermally activated region

$$\tau \approx \tau^* \qquad (2.13)$$

When the strain rate is high, τ_D predominates. If the applied stress is high enough to overcome the barriers to dislocation motion at 0K then

$$\tau = \tau_B + \tau_D \qquad (2.14)$$

where

$$\tau_B = \tau_A + \tau^*_o$$
$$\tau_D = B.\ v/b$$

and hence, combining these equations with those which were derived in previous papers to describe the behaviour of metals in general:-

The average velocity of a dislocation damped by phonons between thermally activated events is

$$v = \frac{AL^{-1}}{(\nu)^{-1} \exp(U/kT) + ABL^{-1}/(\tau - \tau_B)b} \qquad (2.15)$$

and the strain rate is given by $\dot{\gamma} = \rho_m bv$ (2.16)

where A = area swept out per successful thermal activation (m^2)

L = average length of the dislocation segments (m)

ν = vibration frequency (Hz)

U = activation energy (J)

k = Boltzmann's constant (JK^{-1})

T = absolute temperature (K)

B = dislocation drag coefficient (Pa.s)

b = Burgers vector (m)

ρ_m = mobile dislocation density (m^{-2})

Finally they stated that the strain rate change exponent m' ($= \partial \ln \dot{\gamma} / \partial \ln \tau$) for copper at the yield strain is 150 at $10^{-3} s^{-1}$ and increases with increasing strain rate, approaching 1 in the viscous damping region.

KUMAR (1970) examined the relation between ρ_m and strain, strain rate and temperature. It has been experimentally observed for copper that flow stress

$$\tau = \tau_B + (B/\rho_m b^2)\dot{\gamma} \qquad (2.17)$$

(at high strain rates)

In single crystals of copper, ρ_m increases with the forest dislocation density (ρ_f) but the reverse is true for polycrystalline copper. Now the dislocation structure of a crystal can be described in terms of straight dislocations, bends, jogs, kinks, nodes and multipoles, which are present at any given strain. The multiplication rate is a function of kink concentration and ρ_f. As straining proceeds the concentration and capture cross-section of multipoles increase, leading to an increased rate of immobilisation.

When a mobile dislocation passes a given area of a glide plane it either generates new dislocations by collision with forest dislocations and impurities or is immobilised by collision with other mobile dislocations or multipole clusters.

Hence $\dot{\rho}_m = M v \rho_m \rho_f^{\theta} - I v \rho_m \rho_f^{\phi}$ (2.18)

where M = multiplication rate constant

I = immobilisation rate constant

θ and ϕ are constants representing the variation of the multiplication and immobilisation clusters with ρ_f, respectively.

Integrating and substituting values for ρ_m and ρ_f led Kumar to the conclusion that in single crystals the concentration of muliplication clusters increases more rapidly than that of the immobilisation clusters when ρ_f is increased by straining. The reverse is true for polycrystalline specimens.

Harding (1971) proposed the following to explain the mechanisms involved in the variation of yield drop with strain rate. A condition previously derived for strain rate sensitivity was

$$\text{strain rate sensitivity } \frac{\partial \tau}{\partial (\ln \dot{\gamma})} > \frac{G \rho_m}{C} \qquad (2.19)$$

where G = shear modulus

C = rate at which the total dislocation density decreases.

For copper, a large majority of defects generated during

the deformation are vacancies (not impurity atoms) and interaction between a moving dislocation and a supersaturation of vacancies results in the formation of jogs. Once jogged, a dislocation cannot regain its original easy gliding condition by a simple unpinning process. The consequent reduction in ρ_m should be sufficient to satisfy the inequality (2.19) and in view of the strong stress-dependence of the dislocation velocity in copper, result in a small yield drop by the dislocation multiplication process.

KLEPACZKO (1975) drew the following conclusions from an analysis of data and results from previous work. The contribution of the thermally activated component of stress to the total strain rate effect at constant strain rates is overestimated in the literature. Strain rate and temperature history effects play a very important role in the plastic behaviour of polycrystalline FCC metals. A dynamic recovery and a dislocation annihilation process are responsible for these effects. A description of strain rate and temperature history effects is possible by a coupling of two relationships. One of these is the relationship resulting from the thermally activated process which is currently dominating, while the second is of an evolutionary type. An evolutionary relationship describes the changes in structure during the course of plastic deformation.

Included in Lindholm (1978) was the description of the thermal activation and viscous drag regions.

(a) Thermal Activation Region

Resistance to dislocation motion is caused by the interaction with short range barriers whose intrinsic free energy is comparable to kT. Therefore the barriers are overcome by random thermal fluctuations.

$$\dot{\gamma} = \dot{\gamma}_o \exp\left[-v^*(\tau_o - \tau)/kT\right] \qquad (2.20)$$

where $\dot{\gamma}_o$, τ_o and v^* are constants. Hence stress increases with decrease in temperature and increase in dislocation velocity or strain rate.

(b) Viscous Drag Region

If the applied stress exceeds τ_o, the dislocations may overcome all local barriers without assistance of the available thermal energy.

$$\text{Flow stress } \tau = \frac{B}{b} v = \frac{B}{\rho b^2} \dot{\gamma} = \alpha \dot{\gamma} \qquad (2.21)$$

B and α are such that viscous drag becomes rate controlling only at very high strain rates.

CAMPBELL et al (1977) found that in torsional incremental strain rate tests from rate 1 to rate 2 after prestrain to $\gamma = \alpha$ the stress increase above the low-rate curve depended upon the strain increment $\gamma - \alpha$ but not upon the prestrain α and fitted a curve of the form

$$\tau = f_1(\gamma) + f_2(\gamma, \dot{\gamma}_1) + f_2(\gamma - \alpha, \dot{\gamma}_2) - f_2(\gamma - \alpha, \dot{\gamma}_1) \qquad (2.22)$$

The particular forms used for the two functions were

$$f_1(\gamma) = A\gamma^n \quad \text{and} \quad f_2(\gamma,\dot{\gamma}) = mA\gamma^n \ln[1 + (\dot{\gamma}/B)] \tag{2.23}$$

where A and B are constants.

The low-rate curve is represented by the first two terms on the right side of equation (2.22), while the last two terms give the stress increment above what would have been the continued low-rate curve. As a possible generalisation, equation (2.24) was proposed.

$$\tau = f_1(\gamma) + f_2[\gamma,\eta(o)] + \int_o^{\gamma} f_2^{*}[\gamma-\alpha,\eta(\alpha)]\,\eta'(\alpha)\,d\alpha \tag{2.24}$$

for arbritrary path $\dot{\gamma} = \eta(\alpha)$, where f_2^{*} means $\partial f_2(\gamma,\dot{\gamma})/\partial\dot{\gamma}$ with the partial derivative evaluated for the two values of the argument shown in square brackets. LIPKIN et al (1978) found that equation (2.24) was not consistent with the results of their decremental strain rate tests.

As stated in section 2.2.3, Follansbee et al (1984) produced results which were typical of previous investigations, i.e. a relatively mild strain rate sensitivity at low strain rates followed by a dramatic rise in sensitivity, accompanied by a linear stress-strain rate relation, at high strain rates. This linear relation has previously been used as evidence in favour of phonon or viscous drag being the dominant deformation controlling mechanism at high rates of strain. In this paper, however, the increased strain rate sensitivity is re-examined in

terms of a transition regime in which both thermal activation and phonon drag are significant.

The threshold stress ($\hat{\sigma}$) is the minimum stress necessary for a dislocation to overcome without the aid of thermal agitation the resistance of a barrier that the dislocation encounters as it moves along its glide plane. Above $\hat{\sigma}$, therefore, the deformation is controlled solely by the phonon drag mechanism. The current authors, however, discovered that the increased rate sensitivity commenced below the threshold stress and, hence, both deformation mechanisms are simultaneously active. In addition, their theoretical model indicated that an inflexion in the stress-strain rate curve should result between 0.85 $\hat{\sigma}$ and $\hat{\sigma}$. This is the solid line in Figure 2.29, which is defined by the constitutive equation:

$$\dot{\varepsilon} = \frac{\hat{\dot{\varepsilon}}\,\sigma/\hat{\sigma}}{1 + \psi(\sigma/\hat{\sigma})\exp(\Delta G/kT)} \qquad (2.25)$$

where $\hat{\dot{\varepsilon}} = \dfrac{b^2 \rho_m \hat{\sigma}}{M^2 B}$

and is the strain rate at which the transition is complete,

$$\psi = \frac{\nu_o^{-1} b\hat{\sigma}}{MB\lambda_2} \quad \text{and} \quad \Delta G = F_o[1-(\sigma/\hat{\sigma})^{1/2}]^{3/2}$$

M, B, b and ρ_m were defined in section 2.2.3. ν_o is the attempt frequency, λ_2 is the distance between barriers, k is Boltzmann's constant, T is the absolute temperature and F_o/kT is a dimensionless quantity which can be related to

the strain rate sensitivity parameter m, where

$$m = \frac{\partial \ln \dot{\varepsilon}}{\partial \ln \sigma} \quad \text{at constant T.}$$

KLEPACZKO and CHIEM (1986) demonstrated that there are two kinds of rate sensitivities for FCC metals, including copper, i.e. the instantaneous rate sensitivity and the rate sensitivity of strain hardening. The former is the rate sensitivity at constant structure. The latter is the rate sensitivity of the flow stress owing to the rate sensitive strain hardening. This rate sensitivity increases substantially as a function of strain or stress.

2.6 Summary

Many tests have been performed on copper over a wide range of strain rates and temperatures. A variety of testing techniques have been employed. There is, however, still a scarcity of tensile high strain rate data and the effects of grain size differences are virtually ignored.

In summary, the main features of the dynamic tests on copper during the previous two decades were:

2.6.1 Strain Rate Sensitivity

This was asserted to be positive by all except Bitans and Whitton (1970-71). Most declared copper to have a low strain rate sensitivity below about $10^3 s^{-1}$, followed by a sharp rise in flow stress leading to a high strain rate

sensitivity above $10^3 s^{-1}$. This suggested a transition from a thermally activated rate controlling regime to a viscous drag mechanism. A transitional strain rate of $10^4 s^{-1}$ was recorded by Shioiri et al (1978) and Follansbee et al (1984). Dormeval and Stelly (1976) who tested single crystals in tension, reported the mode change at the comparatively low strain rate of $10^2 s^{-1}$. Lindholm (1964, 1978) found no sharp rise in flow stress despite conducting tests between $10^{-4} s^{-1}$ and $10^5 s^{-1}$.

In the higher strain rate region, many investigations, including Lindholm (1964, 1978), Kumar and Kumble (1969), Dowling et al (1970), Stelly and Dormeval (1978), Regazzoni and Montheillet (1984), and Follansbee et al (1984), discovered that there was a linear relation between stress and strain rate for a particular strain level.

Ten publications indicated how strain rate sensitivity varied with strain. Seven of these showed it to be an increasing function of strain, two a decreasing function (Regazzoni and Montheillet (1984), and Hashmi and Haque (1986)), and in one, Kishida and Senda (1972) there was little or no variation.

2.6.2 Thermal Activation and Viscous Damping Regions

Of the authors who reported a sudden increase of flow stress at high rates of strain, all, except Regazzoni and Montheillet (1984), and Follansbee et al (1984), agreed that this behaviour was a consequence of the change in rate controlling mechanism from thermal activation, at the lower

strain rates, to viscous or phonon damping at the higher rates. In the two papers of 1984, the increased strain rate sensitivity of copper at high rates of strain was reported to be consistent with a regime where the deformation is controlled simultaneously by thermal activation and viscous drag.

2.6.3 Temperature Effects

Samanta (1968) reported that copper strain hardens up to $600^{o}C$ above which recrystallisation predominates. He also found that strain rate sensitivity increased with increases in temperature and strain. Watson and Ripperger (1969) found that strain rate sensitivity increased with temperature. Ohmori et al (1968) detected that copper was most brittle at 350^{oC}, at high rates of strain, and there was a linear decrease of tensile stress with increase in temperature. Senseny et al (1978) showed that strain rate sensitivity decreased with increasing annealing temperature. The above authors only applied strain rates up to $300s^{-1}$.

Stelly and Dormeval (1978) who annealed their specimens at the comparatively high temperature of $1000^{o}C$ (which suggests a large grain size) and then discovered that copper's strain rate sensitivity was very low at strain rates less than $10^{3}s^{-1}$. Lindholm (1978), who also tested specimens with a large grain size also produced results which indicated a low strain rate sensitivity for copper.

2.6.4 Strain Rate History Effects

Senseny et al (1978) observed the 'fading memory effect' at all temperatures. Eleiche and Campbell (1974) also detected this effect, smaller pre-strains producing less memory, however. The above incremental tests were performed with polycrystalline copper. Similar tests on single copper crystals by Stelly and Dormeval (1976 and 1978) failed to produce the fading memory effect.

2.6.5 Yield Stress Drops

Reductions in stress when straining specimens beyond their yield points at high strain rates were detected by Dowling et al (1970), Kishida and Senda (1972), Clyens and Campbell (1974), Harding (1971), and Lindholm et al (1980). Dowling et al observed the yield drops to increase with strain rate. Harding found that they increased in magnitude with the number of impacts and also with increase in strain level.

2.6.6 Miscellaneous

Bitans and Whitton (1970-71) and Lindholm et al (1980) both reported evidence of localised adiabatic shear bands resulting in thermal softening when high strain rates are rapidly applied. Dormeval and Stelly (1979) investigated the relation between flow stress and grain size at high rates of strain and discovered that the Petch relation (previously found to be valid at quasi-static strain rates) could still be applied so long as only small strains were

involved.

Kumar (1970) discovered two opposing mechanical properties in single crystal and polycrystalline copper. In the former, the mobile dislocation density (ρ_m) increased with increases in the forest dislocation density ρ_f. The reverse is true of the latter.

CHAPTER 3

HIGH STRAIN RATE COMPRESSIVE TESTING TECHNIQUE

3.1 The Hopkinson Pressure Bar

- from Hopkinson to Kolsky

Bertram HOPKINSON (1914) was one of the first investigators of the propagation of stress pulses in solids in a laboratory. His apparatus, the Hopkinson pressure bar, is an application of the theory of stress propagation of elastic pulses in a cylindrical bar where the length of the pulse is great compared with the radius of the bar. The cylindrical steel bar was suspended by threads in a horizontal position so that it could swing in a vertical plane. A short cylindrical pellet or time-piece was wrung on to one end of the bar and a transient pressure applied to the other end. The time-piece, which was made of the same steel as the pressure bar and had the same diameter, was loosely attached to the latter by either magnetic attraction or a smear of grease. One means of applying a transient pressure to the bar was by firing a bullet at its free end. A compressive elastic pulse then travels down the bar and through the joint between the bar and the time-piece without change in form. At the free end of the time-piece it is reflected as a pulse of tension. As soon as a tensile stress is built up across the joint between bar and time-piece, the latter will fly off with the momentum trapped in it. In Hopkinson's experiments, this momentum was measured by capturing the time-piece in a ballistic pendulum. When the time-piece is less than half of the length of the pulse, the time-piece will separate

from the bar before the reflection is completed; the momentum remaining in the bar could be determined from the amplitude of swing of the bar. If the length of the time-piece is gradually increased a point is reached at which the whole of the transient pulse is contained in the time-piece. This is indicated by the bar remaining stationary after the time-piece flies off. This situation arises when exactly half the pulse has been reflected from the free end of the time-piece. Hence the pulse length can be determined. However, it is not possible to determine the exact relation between pressure and time, but only the maximum value of pressure.

R.M. DAVIES (1948) devised a pressure bar in which the measurements were made electrically and which gave a continuous record of the longitudinal displacement produced by the pressure pulse at the free end of the bar. The displacement was measured by using the bar as the earthed conductor of a parallel-plate capacitor. The isolated conductor consisted of a metal plate held in a frame attached close to the free end. When the pressure or stress pulse reached the free end of the bar, the small movement of the earthed side of the capacitor caused a change in capacity, the resulting change in potential being monitored with an oscilloscope. Displacement time records were obtained in this way, and he demonstrated the existence of the so-called Pochhammer - Chree oscillations on the top of the pulse and showed the effects of dispersion of the component frequencies of the pulse, which manifests itself as an increased pulse length. Davies also used cylindrical condensers, in which an isolated metal

tube was held with its axis parallel to the axis of the bar which permitted the radial and longitudinal displacements of the bar surface to be measured.

An adaptation of the Davies bar was used by KOLSKY in 1949 to measure the dynamic mechanical properties of materials. The specimen, which was in the form of a thin disc, was placed between the flat faces of two cylindrical steel bars. The transient pressure was applied by firing a detonator at the end of one of the bars and the displacement of the free end of the other bar was measured, as with Davies, with a parallel-plate capacitor. From this the pressure on the specimen could be calculated. A cylindrical capacitor, fitted around the bar between the detonator and specimen, was used to measure the amplitude of the pressure pulse arriving at the specimen. From this the deformation of the specimen could be deduced. This method, alternatively known as the Kolsky Bar or Split Hopkinson Pressure Bar, is very similar to that used in the current investigation.

3.2 Description of the Split Hopkinson Pressure Bar (SHPB) Apparatus and Technique

A short cylindrical specimen (4.33mm long and 10mm in diameter) is sandwiched between two pressure bars (Figure 3.1) and is loaded by a single elastic pulse travelling through the system. The pressure bars are used both to apply the load to the specimen and as transducers to measure the displacements and applied loads at the faces of the specimen in contact with the bars.

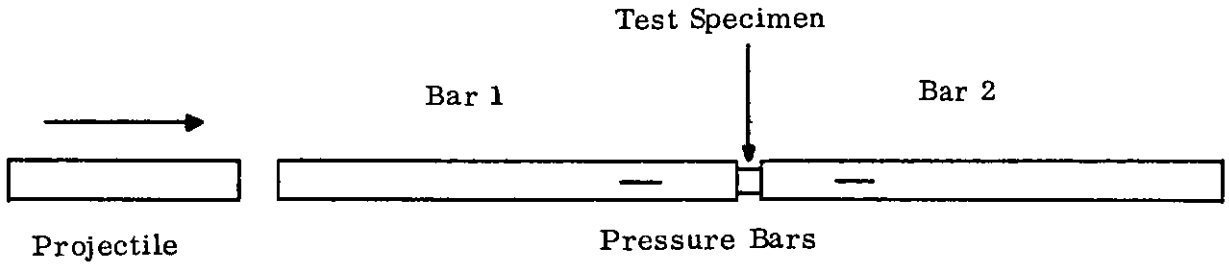

Figure 3.1 Basic arrangement of the SHPB apparatus

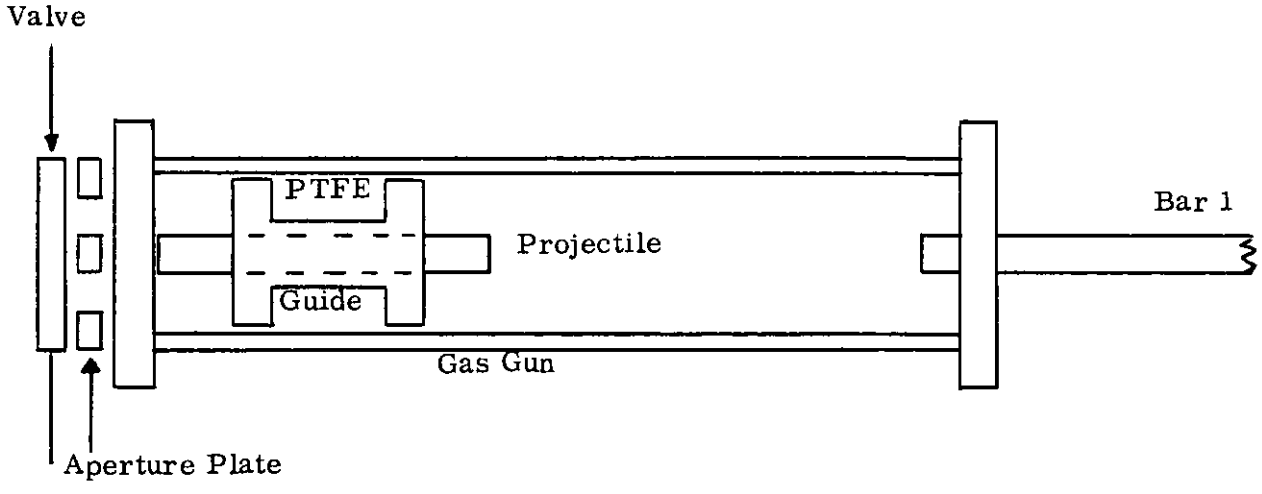

Figure 3.2 Gas gun containing projectile in position prior to "firing" gun

In the current experiments, the loading pulse is initiated by axial impact from a third bar, the projectile. This is accelerated to impact velocity within a steel gas gun (Figure 3.2). The projectile is mounted axially in a 'cotton reel' shaped PTFE guide (Figure 3.3) and firing is achieved by admitting atmospheric air into the previously evacuated gas gun by means of a hand-operated sliding valve. The impact generates two compressive pulses of equal amplitude, one of which travels along the loading bar (bar 1) and the other in the reverse direction along the projectile. Bar 1 is unloaded after the compressive pulse, reflected as a tensile wave from the free end of the projectile, returns to the impact face. The pulse in the loading bar is thus twice the length of the projectile bar if the wave velocity in the projectile is equal to that in the loading bar.

The amplitude of the loading pulse is directly proportional to the impact velocity, which is controlled by the hole size in the aperture plate (Figure 3.3) adjacent to the gas gun sliding valve. The stress applied to bar 1 is:

$$\underset{\sim}{\sigma} = \frac{v}{(\rho_1 c_1)^{-1} + (\rho_2 c_2)^{-1}} \qquad (3.1)$$

where v is the projectile velocity,

ρ_1 and ρ_2 are the densities of the projectile and pressure bars respectively,

c_1 and c_2 are the plane longitudinal wave velocities in the projectile and pressure bars respectively.

The magnitude of the loading pulse is arranged to be less

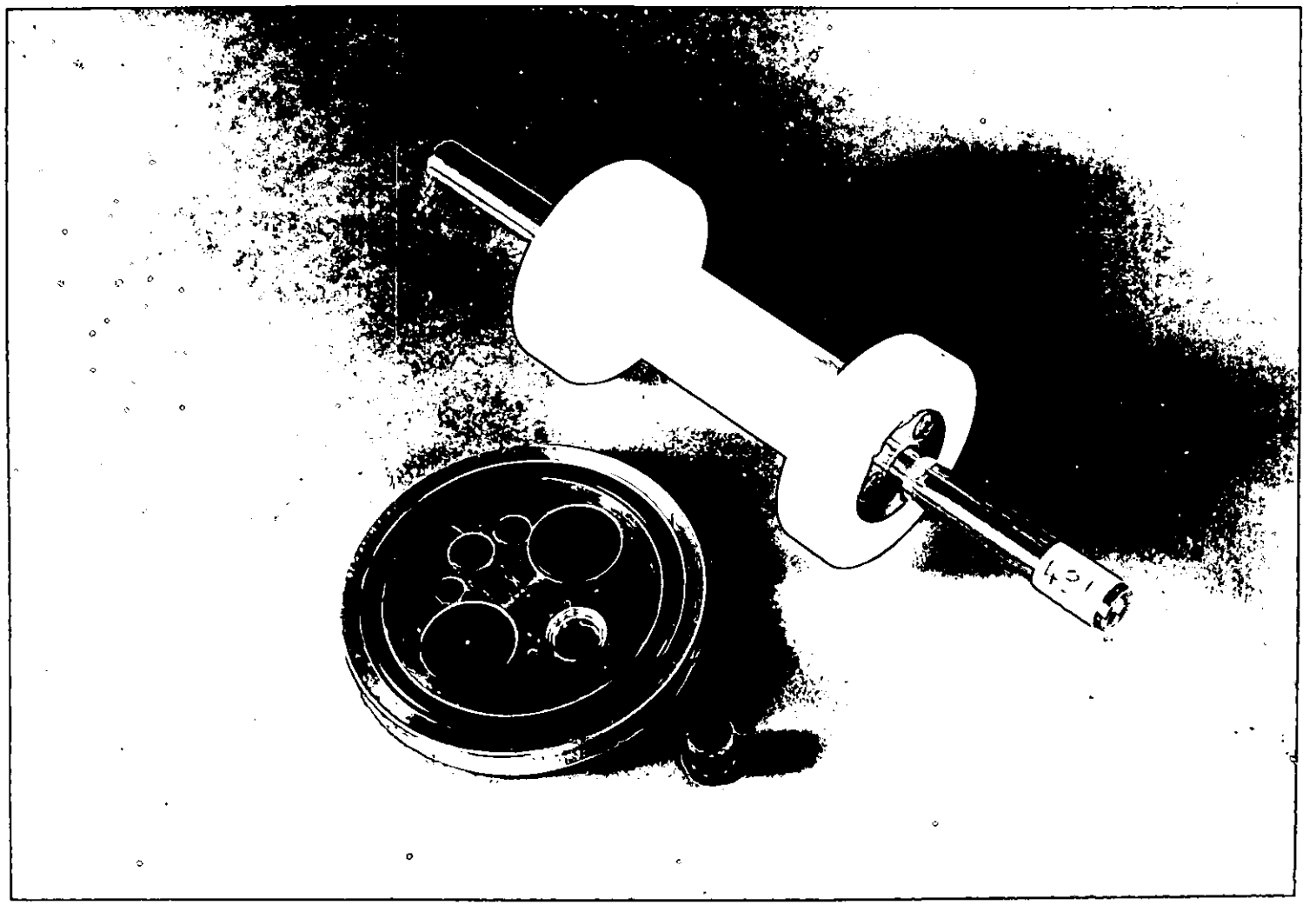

Figure 3.3. Projectile (upper right) and aperture plate with one hole unplugged.

than the elastic limit of the pressure bars, so that the latter are not damaged and only an elastic pulse is propagated along the bars.

When the compressive loading pulse in bar 1 reaches the specimen a portion of the pulse is reflected from the interface, and the rest is transmitted through the specimen to bar 2. The relative magnitudes of these incident, reflected and transmitted pulses depend on the mechanical properties of the specimen. The three pulses are recorded by resistance strain gauges (see section 3.2.4), SG1 and SG2, mounted on the radial surfaces of the pressure bars, as indicated in Figure 3.1. Numerous internal reflections occur in the short specimen during the duration of the loading pulse since the latter is very long compared with the wave transit time in the specimen. Because of the numerous internal reflections, the stress distribution in the specimen very rapidly becomes smoothed out and the stresses on the end faces of the specimen are then identical.

The location of the strain gauges is important so that continuous records can be obtained of each pulse without interference from reflections. Figure 3.10 is a typical example of strain vs. time records from an SHPB test which has been photographed from a cathode ray oscilloscope screen.

The upper trace indicates the compressive incident pulse followed by the tensile reflected pulse both of which are present in bar 1. The lower trace shows the compressive

transmitted pulse recorded in bar 2. The position of SG1 was 40cm from the test specimen. This distance was chosen so that the incident and reflected pulses are completely separated on the upper trace. In the test recorded in Figure 3.10, SG2 was also separated from the specimen by a distance of 40cm. Hopkinson Bar theory assumes that there is negligible attenuation of the elastic waves in the pressure bars. However, in practice, attenuation is finite and increases with pulse amplitude. Hence, in order to more accurately record the amplitude of the pulse transmitted into bar 2, in many tests SG2 was only 10cm from the specimen.

The overall arrangement and dimensions of the mechanical components of the SHPB system are shown schematically in Figure 3.5. The purpose of the momentum bar on the right hand side of the diagram is to remove the transmitted pulse from bar 2. Without the momentum bar, the transmitted pulse would be reflected as a tensile pulse at the free end of bar 2 and would travel repeatedly back and forth along this bar, alternating between a compressive and a tensile pulse. The net effect would be to accelerate bar 2 away from bar 1 and the specimen, with damage to the system a possible consequence, as well as being a hazard to personnel.

The transmitted pulse travels, without change of shape from bar 2 to the momentum bar, the diameter and the material composition of the latter being identical to that of the former. The momentum bar functions in the same way as Hopkinson's time-piece, so that provided the former is at

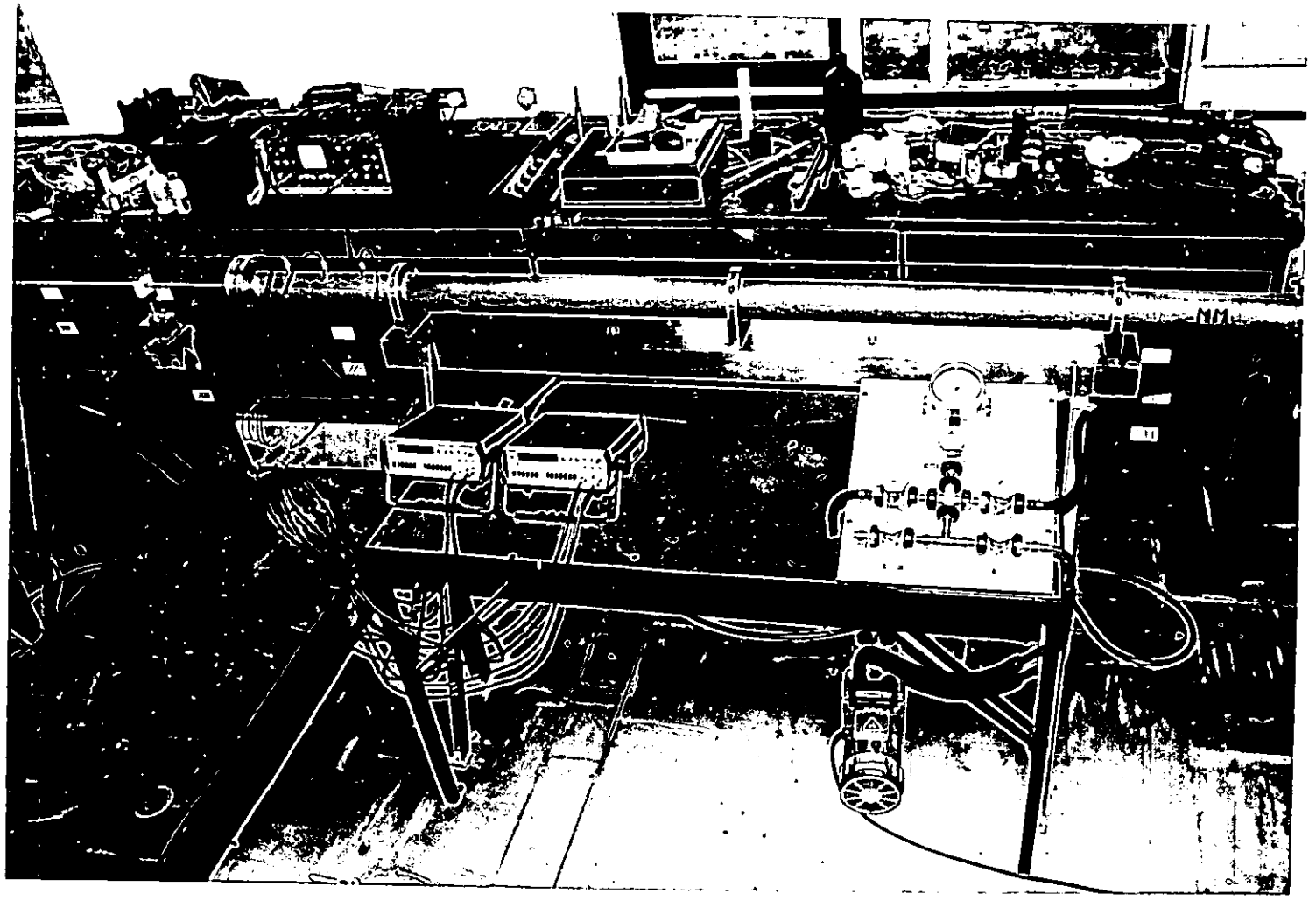

Figure 3.4. Gas gun, valve operating system, rotary pump, opto-electronic device and counter timer.

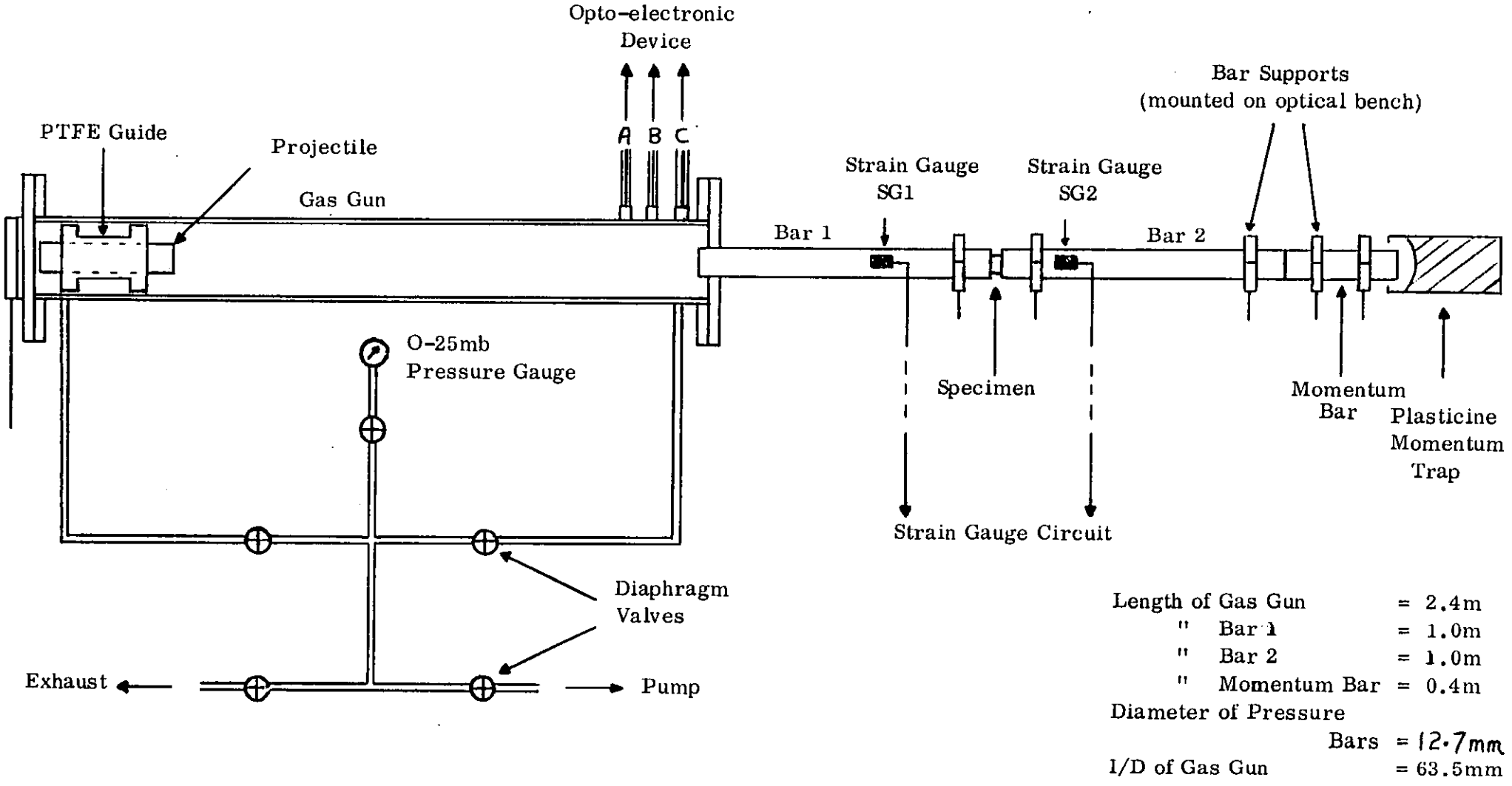

Figure 3.5 Overall arrangement of the Split Hopkinson Pressure Bar System

least half the pulse length the entire momentum of the impact will be removed from the SHPB system. The momentum bar then flies away from bar 2 and is caught in a plasticine trap as shown in figure 3.5.

A photograph of the entire SHPB system is included in Figure 3.6. The gas gun is on the right, and the pressure bars and data acquisition/processing system on the left.

3.2.1 Gas Gun

A photograph of the gas gun tube, which is made from 321 stainless steel and has a polished internal bore, and the vacuum valve system appears in Figure 3.4. The gas gun is evacuated by a rotary type vacuum pump, the minimum pressure being less than 1 Torr, with the projectile in contact with the aperture plate as shown in Figure 3.5. By rapidly removing the hand-operated sliding valve from the opening to the gas gun, the projectile is accelerated towards the end of bar 1 which extends by a few centimetres into the gas gun. The aperture plate (Figure 3.3) contains 7 circular holes, their diameters being 2, 4, 6, 8, 12, 20 and 20mm, all except the smallest hole can be closed, to prevent air passing through them, by nylon plugs. A wide range of impact velocities can be achieved by varying the aperture area by removing different combinations of the plugs. Calibration curves of impact velocity vs. aperture area and pressure bar strain vs. aperture area appear in Chapter 8 (Figures 8.4 and 8.5, respectively) and the method of measuring the impact velocity in Chapter 6.

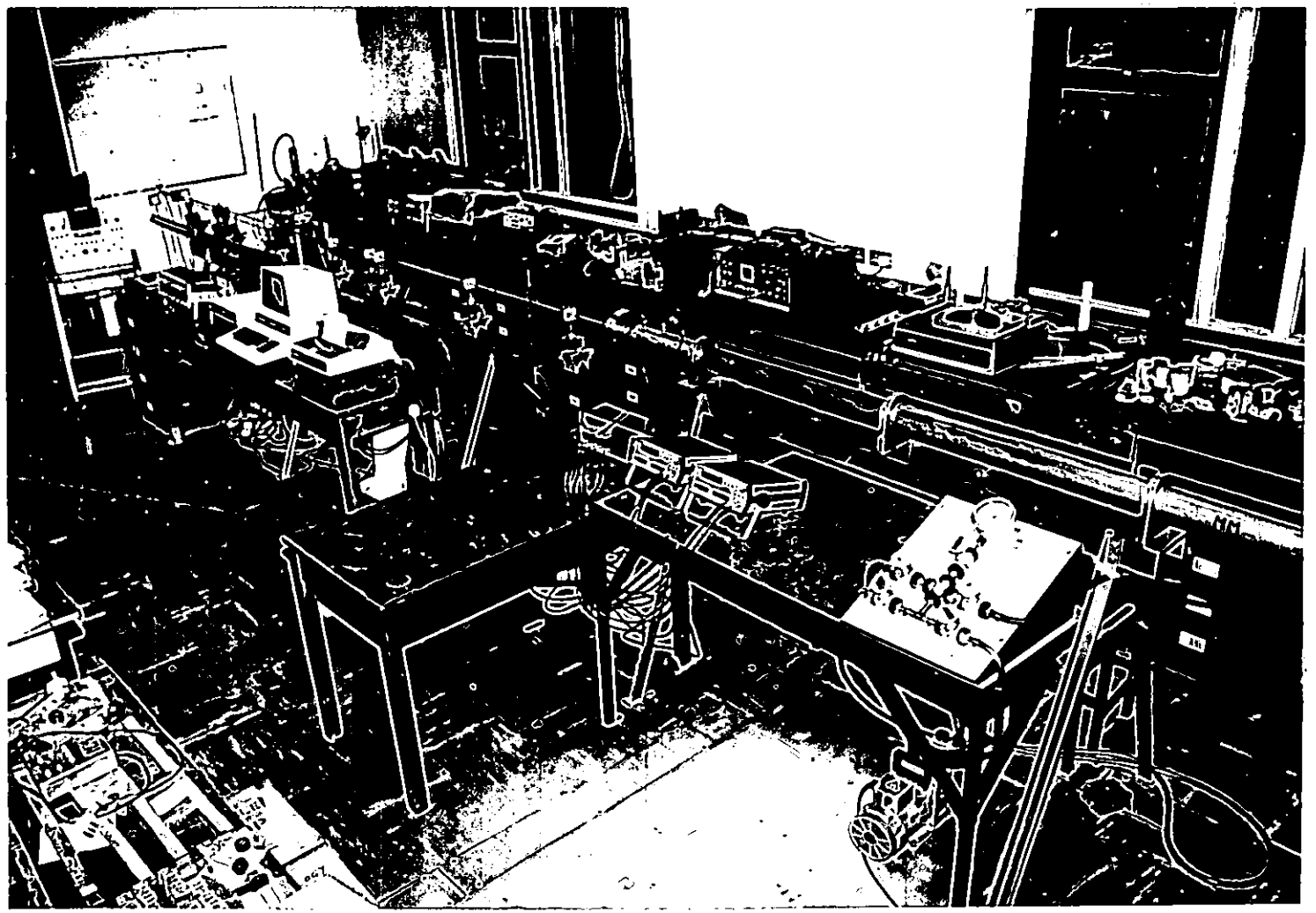

Figure 3.6. Entire SHPB system showing the pressure bars and data acquisition/analysis system on the left and the gas gun and opto-electronic device etc on the right.

The vacuum valve system consists of 5 diaphram valves and a pressure gauge which are interconnected by brass pipes. Connections to both ends of the gas gun and to the vacuum pump are achieved by thick-walled rubber tubing. The functions of the vacuum valve system are:

(a) to initiate the pumping at the aperture plate end of the gas gun, which ensures that the projectile remains in contact with the former until the gun is 'fired'. Evacuation is then performed from both ends of the gun.

(b) to enable the projectile to be returned to the open end of the gas gun subsequent to a test. This is achieved by re-evacuating the tube and then gradually admitting air to the impact end of the gun which slowly returns the projectile in a controlled fashion.

(c) to protect the pressure gauge from the sudden increase in pressure during a test by closing its adjacent valve prior to testing.

A vacuum seal is formed at the entry point of the pressure bar into the gas gun by 'O' rings which are positioned either side of the outer flange. Similarly the sliding valve plate at the open end of the gas gun contacts a large 'O' ring on its adjacent flange; the pressure differential across the plate holding it in position.

3.2.2 Projectile

The projectile (see Figure 3.3) consists of a length of rod of identical diameter to that of the pressure bars which is housed inside a 'cotton-reel' shaped PTFE guide. The external diameter of the flanges on the PTFE guide are such as to form a sliding fit inside the gas gun. A sloppy fit must be avoided because when the projectile is being accelerated down the tube by the atmospheric air, some of the latter will overtake the projectile, passing between the inner wall of the tube and the flanges of the PTFE guide, and will retard its motion.

A flexible coupling between the PTFE guide and the projectile rod is achieved by 'O' rings positioned at either end of the guide, so that when the projectile bar impacts with the pressure bar the guide continues to slide forwards and only the momentum of the rod is transferred to the pressure bar.

The length of rod used throughout the current investigation was 25cm, and so the pulse length was 50cm. The rod was prepared from either maraging steel, 431 stainless steel or duralumin, and so, as can be seen from equation (3.1), the stress applied to the loading bar could be altered by using different density projectile bars as well as by varying the impact velocity. At the maximum impact velocity of approximately $35ms^{-1}$, a maraging steel projectile was used (together with maraging steel pressure bars) because of its higher yield stress.

3.2.3 Mechanical Supports for the Pressure Bars

The horizontally aligned pressure bars are directly supported by nylon blocks in which a 'V' section has been removed from the top surface (see Figure 3.7). The nylon blocks are, in turn, mounted on commercial optical bench stands which have screw driven mechanisms, allowing each pressure bar to be moved in two mutually perpendicular directions, i.e. vertically or in the horizontal direction at right angles to the bar's longitudinal axis. In addition the stands can be moved along the optical bench in order to accommodate pressure bars of different lengths. To permit the bars to be lightly clamped in position, a further nylon block is placed on top of the bar, at each optical bench stand position; the clamping being achieved with bolts and using nuts as illustrated.

The supports for the optical bench and the gas gun are mechanically isolated from each other, apart from the 'O' rings which grip the loading bar inside the gas gun. Consequently no mechanical disturbance should be propagated from the gas gun to the pressure bars during the passage of the projectile down the bore of the gas gun tube, thus preventing the recording system from being activated too soon.

The current SHPB system has a maximum total bar length capacity of approximately 4 metres.

Since the optical bench stands were not designed to withstand large impulses each is reinforced by a 'U' shaped

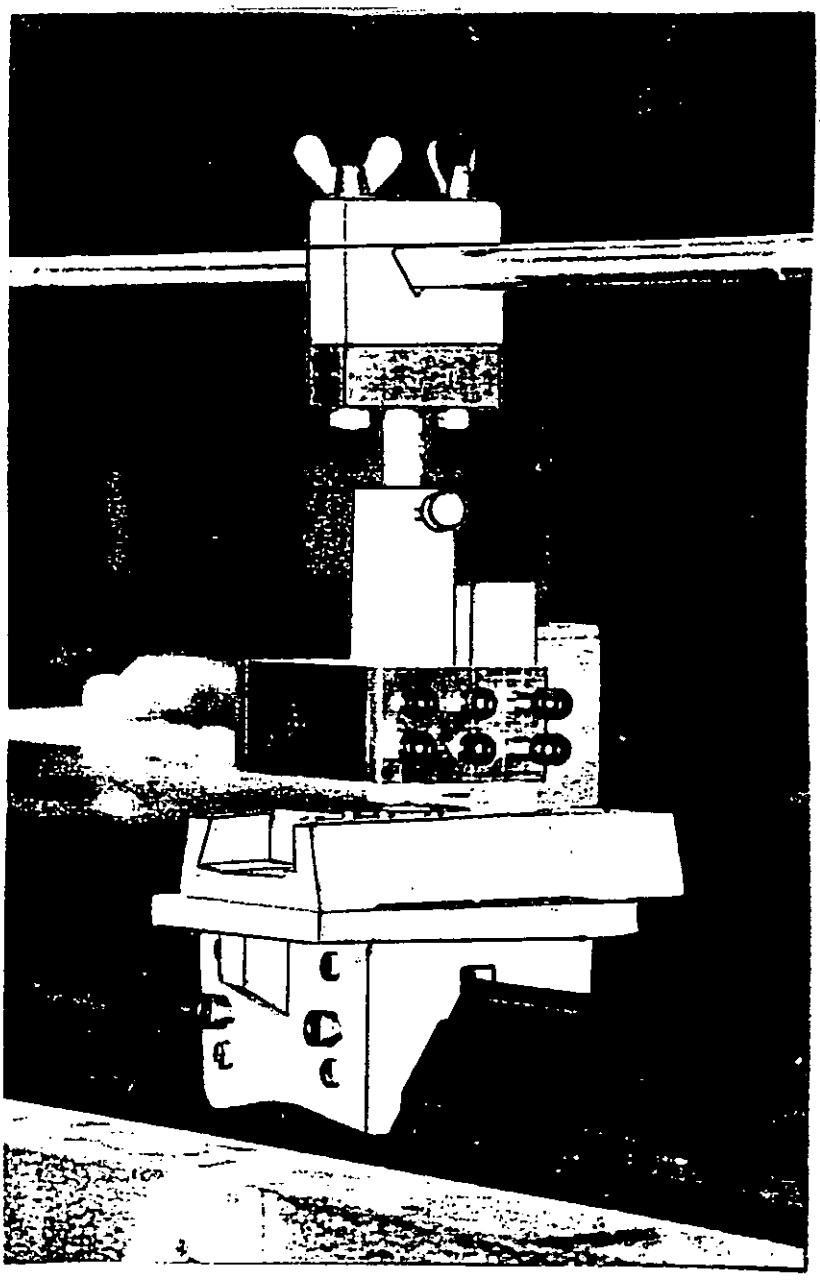

Figure 3.7 One of the mechanical supports for the pressure bars

steel clamp which prevents the vertical slide mechanism from opening up during impact and causing pressure bar misalignment.

Prior to testing, the faces of the ends of the pressure bars and the momentum bar are brought together and the bars' alignments are checked in the vertical and horizontal planes and also along their longitudinal axes. This is accomplished by a visual inspection of the bar interfaces using a light source which is placed immediately behind each interface in the direction of observation. By inspecting the interface in vertical and horizontal directions any misalignment can be discerned and then corrected.

When the compressive specimen is inserted between the end faces of bars 1 and 2, these three components are gently held together by means of the force exerted by elastic bands taped to each bar and then looped around the nearest bench stand so that the former are in tension. This prevents any vertical motion of the specimen prior to impact. The force exerted by the elastic bands on the specimen is far too small to affect the results. Complete contact between each bar end face and the adjacent specimen face is ascertained by the aforementioned visual inspection technique. Lubricant, in the form of engine oil, is applied to both faces of the specimen to reduce frictional effects during the lateral expansion of the specimen.

3.2.4 Strain Gauges

Each strain gauge consists of continuous strips of metal foil mounted on a plastic backing, (see Figure 3.8) and operates on the principle that as the gauge is compressed or stretched by a pressure pulse then its electric resistance is decreased or increased, respectively. The gauges used on the pressure bars have a gauge length of 6mm and so, assuming a wave velocity in the steel bars of approximately $6\text{mm}.\mu\text{s}^{-1}$, their temporal resolution is 1 μs. The relation between the change in resistance (dR_s) in a gauge and the strain (ε) is given by:

$$\varepsilon = \frac{1}{F} \frac{dR_s}{R_s}$$

where R_s is the quiescent resistance of the gauge, which is approximately 120 ohms. F is the gauge factor, which for the gauges used in this investigation (Tokyo Sokki Kenkyso Co. Ltd. Type FLA-6-17), is 2.11. The gauges exhibit a linear resistance/strain relation up to 1-2% in compression and up to 5-6% in tension, at which point either the backing adhesive (cyano-acrylate, type CN-2) or the resistive foil fails.

In practice, four strain gauges are affixed to the pressure bars and not just two. The gauges are mounted as diametrically opposed pairs at the aforementioned longitudinal positions SG1 and SG2. Each pair is wired in series so that:

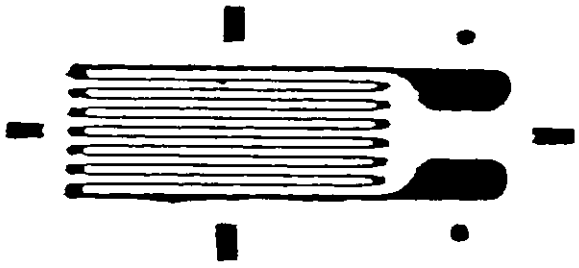

Figure 3.8 Configuration of electrical resistance strain gauge

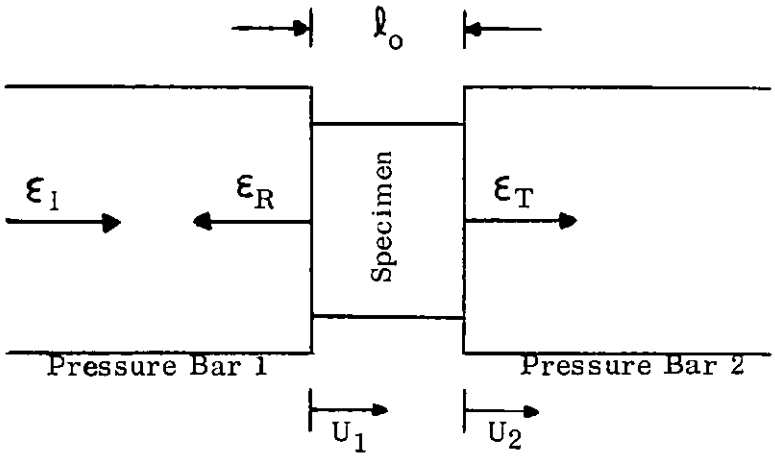

Figure 3.9 Enlarged view of specimen and ends of pressure bars, showing strain pulses and displacements of ends of bars.

(a) the output from a longitudinal wave will be double,

(b) the effects of a flexural or bending wave, occasionally generated by the projectile impact due to the misalignment of the projectile with bar 1, are cancelled out.

3.3 Theory of SHPB Technique

Having recorded the incident, reflected and transmitted strain pulses (denoted ε_I, ε_R and ε_T, respectively) the following theory can be applied, in which it is assumed that a plane stress wave is being propagated.

From the one-dimensional theory of elastic wave propagation

$$u = c_o \int_o^t \varepsilon \, dt' \tag{3.2}$$

where u is displacement at time t, c_o is the elastic wave velocity, and ε is strain. The displacement u_1 of the face of bar 1 (see Figure 3.9) is the result of both the incident strain pulse ε_I travelling in the positive x direction and the reflected strain pulse ε_R travelling in the negative x direction.

Hence:

$$u_1 = c_o \int_o^t \varepsilon_I dt' + (-c_o) \int_o^t \varepsilon_R dt'$$

$$= c_o \int_o^t (\varepsilon_I - \varepsilon_R)\, dt' \qquad (3.3)$$

Similarly, the displacement u_2 of the face of bar 2 is obtained from the transmitted strain pulse ε_T as

$$u_2 = c_o \int_o^t \varepsilon_T dt' \qquad (3.4)$$

The engineering strain in the specimen ε_s is then

$$\varepsilon_s = \frac{u_1 - u_2}{\ell_o} = \frac{c_o}{\ell_o} \int_o^t (\varepsilon_I - \varepsilon_R - \varepsilon_T) dt' \qquad (3.5)$$

where ℓ_o is the initial length of the specimen

Assuming the stress across the short compressive specimen is constant, an assumption which becomes more exact as ℓ_o approaches zero, then

$$\varepsilon_R = \varepsilon_T - \varepsilon_I \qquad (3.6)$$

Substituting equation (3.6) into equation (3.5) gives

$$\varepsilon_s = \frac{-2c_o}{\ell_o} \int_o^t \varepsilon_R\, dt' \qquad (3.7)$$

and the engineering strain rate, $\dot{\varepsilon}_s = \frac{-2c_o}{l_o} . \varepsilon_R$ (3.8)

The applied loads F_1 and F_2 on each face of the specimen are:

$$F_1 = EA (\varepsilon_I + \varepsilon_R) \quad (3.9)$$

and $$F_2 = EA \varepsilon_T \quad (3.10)$$

where E is the modulus of elasticity of the pressure bars (i.e. Young's modulus) and A is the cross-sectional area of the pressure bars.

Hence the average stress in the specimen, σ_s, is given by

$$\sigma_s = \frac{F_1 + F_2}{2A_s} = \frac{1}{2} E . \frac{A}{A_s} . (\varepsilon_I + \varepsilon_R + \varepsilon_T) \quad (3.11)$$

Where A_s is in the cross-sectional area of the specimen.

Again using equation (3.6)

$$\sigma_s = \frac{E A}{A_s} . \varepsilon_T \quad (3.12)$$

Hence the engineering stress is directly proportional to the transmitted pulse and the engineering strain rate is directly proportional to the reflected pulse.

By digitising the values of ε_R and ε_T at set time intervals then the complete stress vs. strain vs. strain rate relation can be derived for the compressive test

specimen.

3.4 Validity of Theory

The SHPB theory can be used to derive the mechanical properties of materials at high rates of strain providing that the following assumptions are maintained by the conditions of the experiment:

(a) the specimen is in a state of one dimensional stress
(b) the stress and the strain are uniform throughout the specimen.

These assumptions are invalidated by radial and axial inertia effects and by friction between the specimen and the pressure bars.

Kolsky (1949, 1963) introduced a correction for radial inertia. Assuming small strains, he obtained

$$\sigma_s = \sigma_b - \frac{1}{8} \nu_s^2 d^2 \rho_s \frac{d^2\varepsilon}{dt^2} \qquad (3.13)$$

where σ_b is the axial stress determined by the average of the stresses measured in the two bars, σ_s is the axial stress required to deform the specimen in a one-dimensional stress state, and ν_s, ρ_s, d and ε are Poisson's ratio, density, diameter and axial strain of the specimen, respectively.

In order to minimise friction effects, DAVIES and HUNTER (1963) used specimens whose length-to-diameter ratios were

approximately 0.5, whereas Kolsky, attempting to attain early stress equilibrium in the axial direction, used a ratio of 0.05. Davies and Hunter chose their dimensions as a result of an analysis by SIEBEL (1923) which had:

$$\mu d/3\ell \ << 1$$

as a criterion for neglecting friction effects, where μ is the Coulomb friction coefficient and ℓ is the specimen length.

They added an axial correction to Kolsky's equation (3.13)

$$\text{i.e.} \quad \sigma_s = \sigma_b + \rho_s \left(\frac{\ell^2}{6} - \frac{\nu_s \, d^2}{8} \right) \frac{d^2\varepsilon}{dt^2} \qquad (3.14)$$

Other correction factors arising from friction and radial and axial inertia, have been introduced by RAND (1967) and SAMANTA (1971).

Other analyses of the Hopkinson bar include the one-dimensional calculations by HAUSER et al (1960), CONN (1965), CHIU and NEUBERT (1967) and JAHSMAN (1971). The two-dimensional computer analysis by Bertholf and Karnes (1974) showed that by lubricating the specimen and using a length to diameter ratio of $\nu_s \sqrt{3/4} \approx 1/2$ as proposed by Davies and Hunter then the corrections for friction and inertia can safely be ignored. Assuming that the material is incompressible, which is generally true for plastically deforming materials, then Poisson's ratio is 0.5. Hence a length to diameter ratio of 0.433 satisfies

this criterion. Hence equations (3.7), (3.8) and (3.12) are valid in these circumstances except in the very early period of loading the specimen before stress equilibrium has been attained.

Now in equations (3.7) and (3.8) the elastic wave velocity, c_o, and the projectile length are constants, therefore as the strain rate, $\dot{\varepsilon}_s$, increases so also does the amplitude of the reflected pulse, ε_R, and hence the plastic strain, ε_s, experienced by the specimen, after a given time t, increases as $\dot{\varepsilon}_s$ increases. Hence if a time t_E elapses before stress equilibrium is reached, then a greater specimen strain ε_s occurs before the SHPB equations are valid at a higher strain rate than at a lower strain rate. Therefore when comparing curves of stress vs. strain for a given low plastic strain it is essential to realise that the data become less accurate as the strain rate increases.

3.5 Constant Strain Rate Tests

One of the parameters by which a mechanical test is characterised is strain rate. As evident from the previous section, this is proportional to the amplitude of the reflected pulse. The latter usually varies considerably as the loading pulse is applied. A typical reflected pulse-time profile is indicated in Figure 3.10 (the second pulse on the upper trace) where the amplitude rises to a maximum and then slowly decreases as strain-hardening of the specimen occurs together with an increase in its cross-sectional area. Clearly an average value of strain

rate must be chosen to characterise the test. This average can be derived from a specimen strain vs. time graph (Figure 3.13).

The average plastic strain rate is

$$\dot{\varepsilon}_p = \frac{\varepsilon_B - \varepsilon_A}{t_B - t_A} \quad s^{-1} \qquad (3.15)$$

where ε_B = strain at maximum stress

ε_A = strain at elastic limit

t_B, t_A = time associated with ε_B and ε_A, respectively

The practice of declaring the average strain rate for a test is unsatisfactory. No account is taken of the amplitude variation between the maximum and minimum strain rates during a test. The mechanical behaviour of a material may differ according to the strain rate vs. time profile which is applied to it, even though the average plastic strain rate is identical in each test. Figure 3.14 illustrates three different profiles which represent the same average strain rate.

The conventional SHPB apparatus was modified by ELLWOOD, GRIFFITHS and PARRY (1982a) to produce a constant strain rate during each test. This was accomplished with the introduction of an extra pressure bar (a pre-loading bar) and a 'dummy' specimen which enabled the loading pulse to be 'shaped'. The apparatus is shown in Figure 3.11.

The correct choice of dummy specimen or 'pulse-shaper'

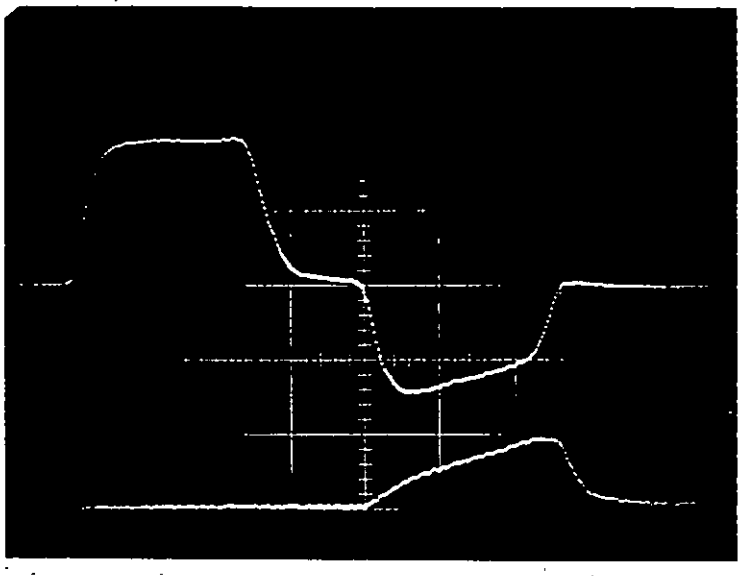

Vertical Scale;
0.125%/div

Horizontal Scale:
40us/div

Filename:
COC60031026SA

Average
Strain Rate:
4697s^{-1}

Figure 3.10 Example of varying high strain rate test recorded with conventional SHPB apparatus

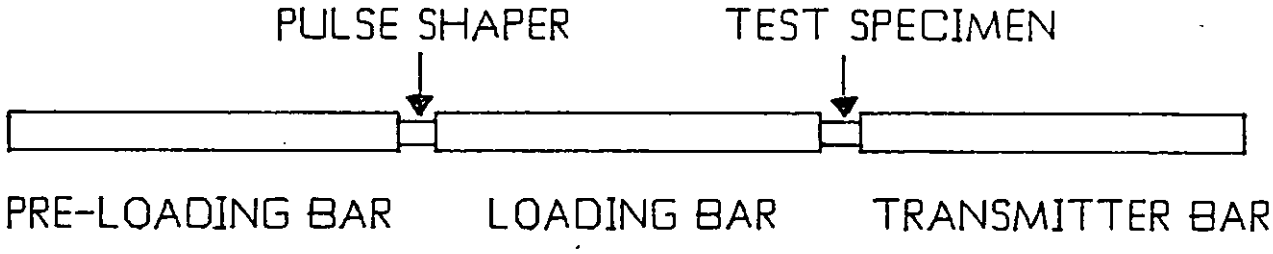

Figure 3.11 SHPB apparatus modified to produce a constant strain rate

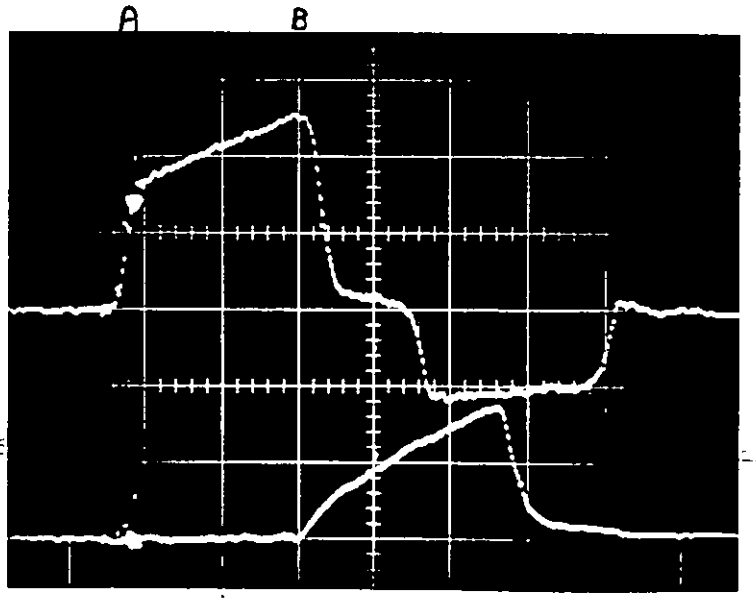

Vertical Scale:
0.06%/div

Horizontal Scale:
40us/div

Filename:
COC02060025SBI

Strain Rate:
1657s^{-1}

Figure 3.12 Example of constant high strain rate test recorded with modified SHPB apparatus

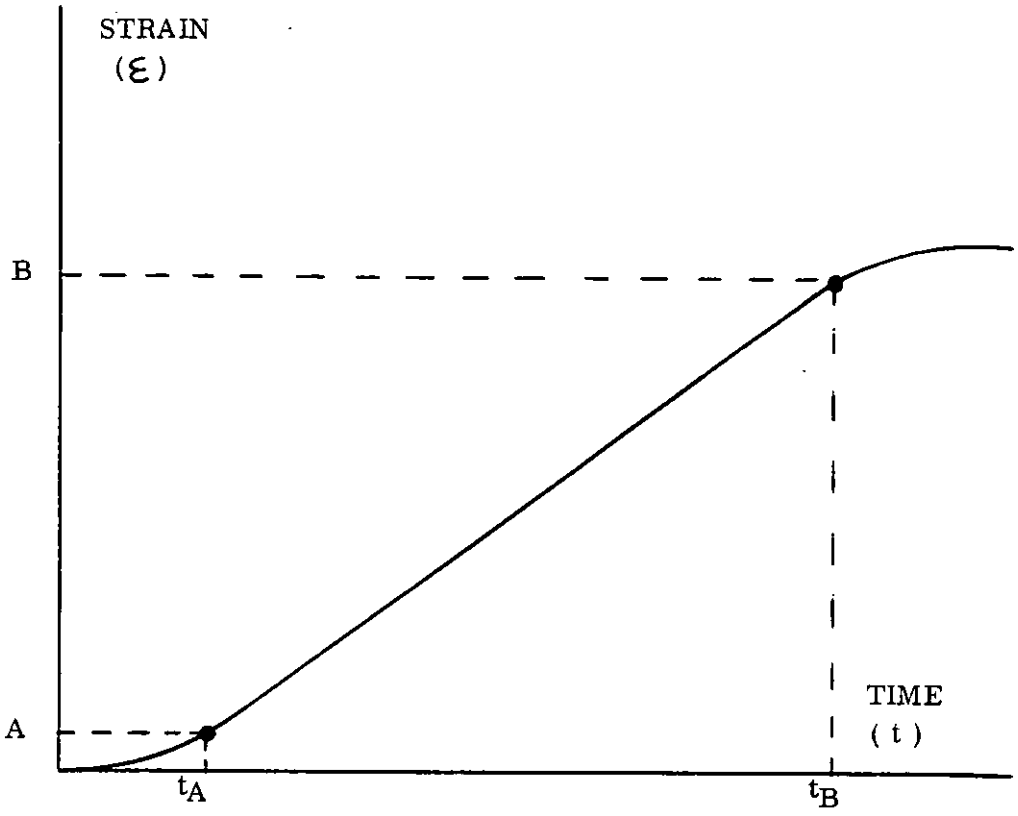

Figure 3.13 Derivation of average value of strain rate

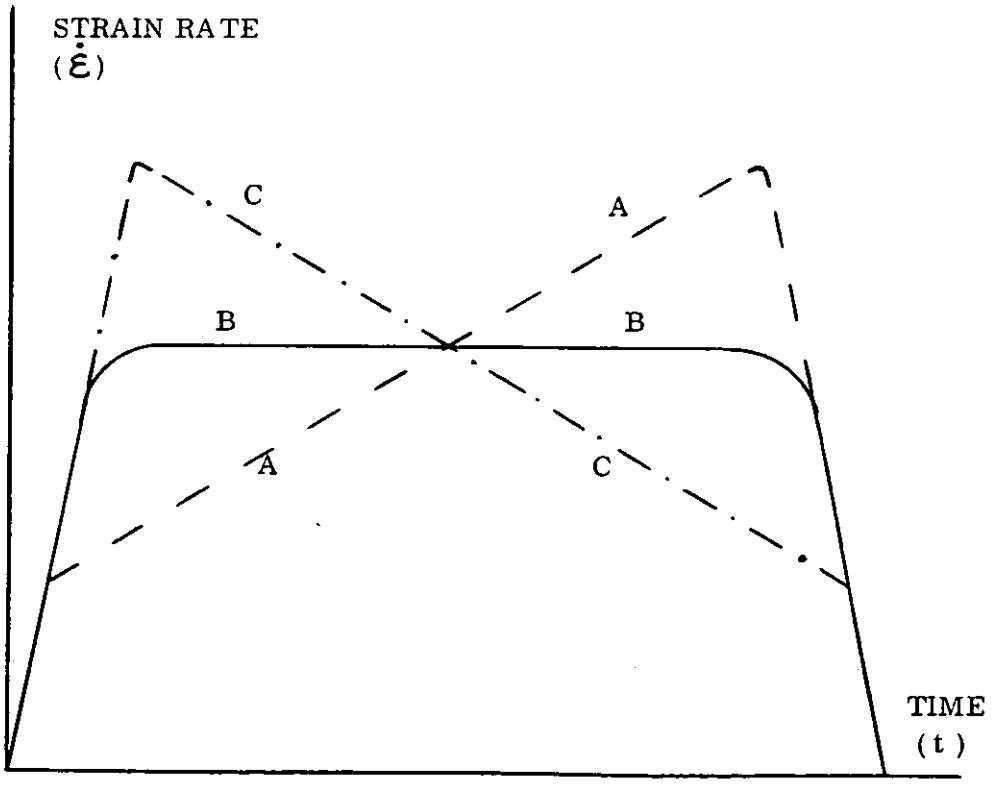

Figure 3.14 Three strain rate profiles (AA, BB and CC).
The average strain rate is the same in each case.

results in a constant amplitude reflected pulse (Figure 3.12), or, in other words, a constant strain rate. The 'flat-topped' incident pulse of the conventional test (Figure 3.10) has been replaced by a 'shaped' incident pulse. The positive gradient of the top of the latter pulse counteracts the effects of work-hardening.

Ellwood et al found from theoretical considerations and experiment that the best material to use as the pulse-shaper is the same as that of the actual test specimen since it automatically has virtually identical yield and flow stress properties under the conditions of the test. Varying the dimensions or the grain size of the pulse-shaper, alters the gradient and amplitude of the 'shaped' incident pulse, which is, of course, the transmitted pulse from the pulse-shaper. Changing the projectile velocity also effects the 'shaped' incident pulse. The latter, which is the stress vs. time response of the pulse-shaper, consists of an elastic region, characterised by a rapid rise in stress, followed by a plastic region of lower gradient. At the yield point of the pulse-shaper, the transmitted pulse

$$\varepsilon_T = \frac{\sigma_y}{E_b} \cdot \frac{A_s}{A} \qquad (3.16)$$

where σ_y = yield stress of the pulse-shaper

E_b = elastic modulus of the pressure bars

A_s = cross-sectional area of the pulse-shaper

A = cross-sectional area of the pressure bars

If the yield stress is very low (i.e. for a very soft material or a small diameter pulse-shaper) then the

transmitted pulse consists of only a plastic region and is then ramp shaped instead of trapezoidal.

Further observations from the trials to determine the best pulse-shaper for each of the various conditions under which the compressive tests were carried out are given in section 7.4.

3.6 Elevated Temperature Tests

3.6.1 Heat Source

The dynamic compressive tests at elevated temperature were also performed using the SHPB system. The heat was supplied by a small electrical furnace which surrounded the test specimen and a short length of the adjacent pressure bars. The furnace consisted of a hollow ceramic cylinder around which was fitted a coil (about 30 turns of 24 swg Ni-chrome wire). The coil was insulated with asbestos tape. The power was supplied using a 2 amp variac and an 8 amp transformer (see Figure 3.15).

3.6.2 Temperature Measurement

The temperature of the specimen was determined by a chromel/alumel thermocouple which was connected in series with a digital voltmeter (DVM). The resolution of the latter was 0.01mV.

Initially each thermocouple was spot welded to the copper specimen but, because of the high thermal conductivity of copper, the weld frequently failed during the test

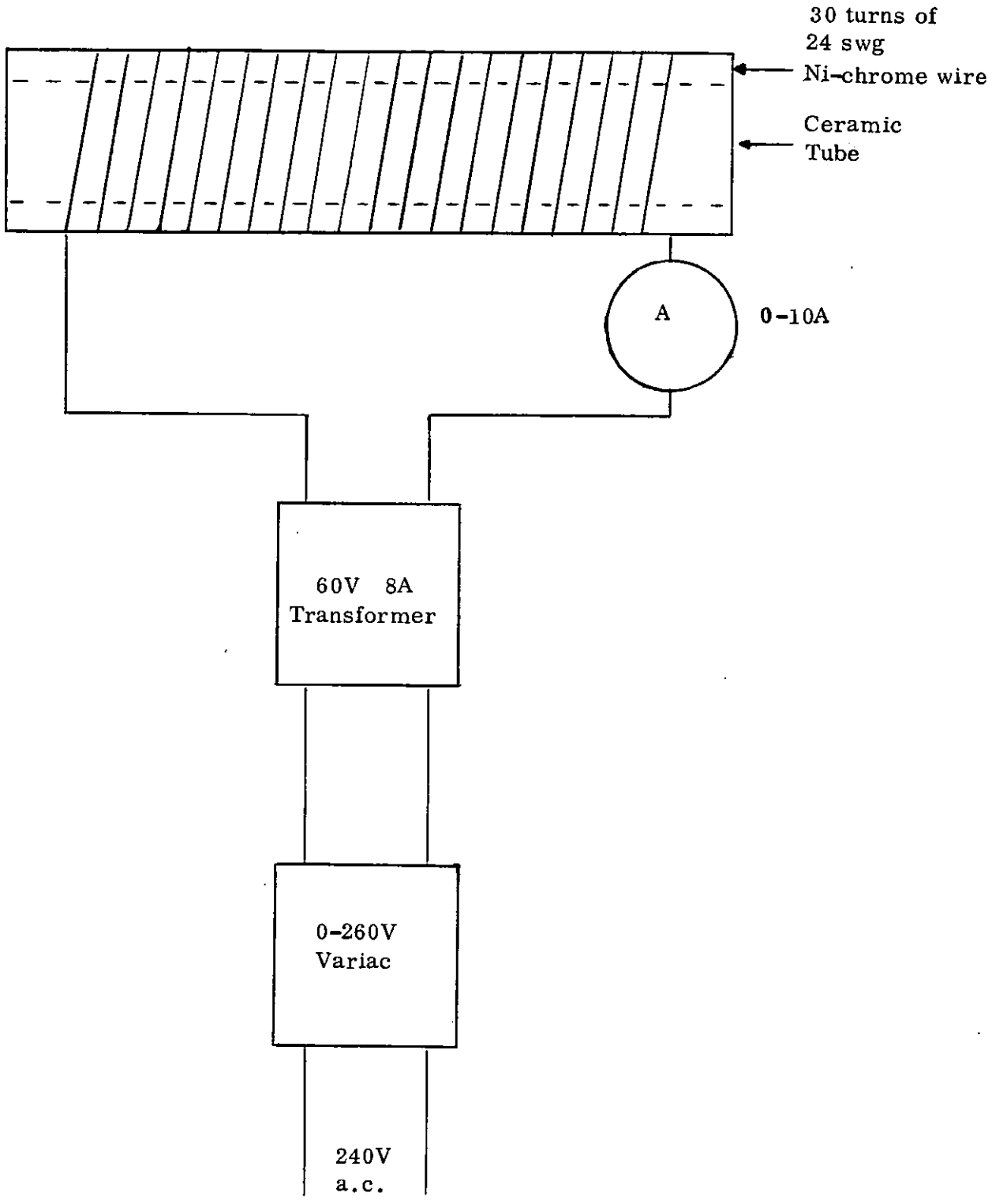

Figure 3.15 Heating system for elevated temperature tests

preparations. Two other methods were then tried, and the DVM readings compared to that with the thermocouple spot welded to the specimen, the measurements being made simultaneously by using 2 DVM's.

(a) the thermocouple was spot welded to the radial surface of one of the pressure bars, as close as possible to the specimen. The maximum error occurred when, according to the thermocouple welded to the specimen, the temperature of the specimen was 600°C. The error was -100°C.

(b) the thermocouple was loosely wrapped around the top of the surface of the specimen after it had been positioned between the two pressure bars. In this case the maximum error was only ± 10°C.

Consequently method (b) was chosen to measure the temperature of the specimen in an elevated temperature compressive test.

3.6.3 Effect of Specimen Heating Prior to Projectile Impact

The furnace was pre-heated before it surrounded the specimen in order to minimise the specimen heating time. In this way any structural changes prior to impact were minimised. The time taken to heat a specimen from room temperature to the maximum elevated test temperature of 600°C was approximately 4 minutes.

Several specimens of the minimum grain size were heated to 600°C, allowed to return to room temperature and then dynamically tested. The results were the same as previous tests on this grain size at room temperature, i.e. heating a specimen prior to performing an elevated temperature test did not invalidate the test by modifying the microstructure of the specimen.

3.6.4 Effect of Heat on Strain Pulses and Pressure Bars

Even at the maximum test temperature it was found (with the use of a thermocouple) that there was no rise in temperature of the pressure bar at a distance of 40cm on either side of the specimen. Consequently the gauges were mounted at this distance on both bars during the elevated temperature tests.

Preliminary trials, performed in the absence of a test specimen, indicated that, even at 600°C, the strain gauge records were unaffected by the increased temperature of the ends of the pressure bars, when the latter were 431 stainless steel. However, when using maraging steel pressure bars, again with no specimen inserted, a large pulse was reflected from the interface of the bars at a temperature of 500°C, even when the applied stress was only a quarter of the room temperature 0.2% proof stress. In fact the bars, especially bar 1, had been plastically deformed by the relatively small applied stress.

Subsequently it was discovered that the maraging steel had been softened by the heating prior to impact. Maraging

steel is austenitized at 815°C to dissolve precipitated phases, and then the relatively soft, low carbon martensite is formed on cooling. To strengthen the material, the alloy is heated to 482°C for 3 hours which causes ageing. Any further heat treatment reduces the high strength life time of the maraging steel. For instance, after a few minutes of heating at 500°C, its strength diminishes rapidly as it decomposes from martensitic to austenitic steel.

Due to the thermal damage produced in maraging steel, all the elevated temperature tests were performed using 431 stainless steel pressure bars.

3.6.5 Specimen Lubrication

The end faces of the compressive specimens were lubricated either with a high melting point grease containing the low friction additive molybdenum disulphide or, better still, graphite.

3.7 True Stress-Strain Relations

Corrections to the engineering equations (3.7), (3.8) and (3.12) must be made to determine the true or natural mechanical properties of a material. The engineering strain, as given by (3.7), takes no account of the change in specimen length during the application of the loading pulse. True strain, ε_t, at any time during the specimen deformation can be expressed as $\delta l / l$, where l is the actual specimen length at time t and δl is the change in length which has occurred in a time δt.

Summing all the infinitessimally small changes in strain from time t = o to t , then the true strain is given by

$$\varepsilon_t = \int_{l_s}^{l} \frac{dl}{l} = \ln (l/l_s) \qquad (3.17)$$

where l_s is the original length of the specimen and l its final length.

$$\text{Hence } l = l_s \pm \Delta l \qquad (3.18)$$

Combining equations (3.17) and (3.18)

$$\varepsilon_t = \ln\left(\frac{l_s \pm \Delta l}{l_s}\right) = \ln\left(1 \pm \frac{\Delta l}{l_s}\right) \qquad (3.19)$$

But, by definition, engineering strain ε_s is $\Delta l / l_s$

$$\text{Therefore } \varepsilon_t = \ln(1 \pm \varepsilon_s) \qquad (3.20)$$

Similarly, engineering stress assumes a constant specimen area. Allowing for the variation of cross-sectional area during deformation, true stress

$$\sigma_t = \sigma_s (1 \pm \varepsilon_s) \qquad (3.21)$$

where σ_s = engineering stress, and + and - are applied for tensile and compressive tests, respectively.

Expressing the results in terms of true stresses and strains allows a comparison to be made between compressive and tensile tests. For isotropic materials, such as

copper, the true stress/true strain curves in compression and in tension should be identical. This is not so for engineering stress vs. engineering strain.

3.8 Summary

The current high strain rate compressive testing technique is a development of the techniques devised by Hopkinson, Davies and Kolsky.

The test specimen, which is sandwiched between two cylindrical steel pressure bars, is loaded by a single stress pulse which travels through the entire bar-specimen-bar system. The loading pulse is generated by the impact of a steel projectile with one of the pressure bars, the former being accelerated in a gas gun.

The strain rate and strain in the specimen are derived from the pulse reflected by the specimen. The specimen stress is proportional to the amplitude of the pulse transmitted by specimen. These engineering values of stress, strain and strain rate are converted to natural or true values in order to facilitate comparison with data from tensile tests.

Tests at constant strain rates have been attempted throughout, using the pulse-shaping technique where necessary, because no account of 'mechanical history' effects is taken in the conventional varying strain rate test.

The combination of selecting the Hunter-Davies length-to-diameter ratio for the specimen and using a lubricant on its faces obviates the need to make friction and inertial corrections.

In the elevated temperature tests, heat was provided by a small electrical furnace, the temperature being indicated by a thermocouple attached to the specimen.

CHAPTER 4

HIGH STRAIN RATE TENSILE TESTING TECHNIQUE

4.1 Introduction

High strain rate tensile testing is far less common than its compressive counterpart. However, over the past two decades several tensile techniques have been devised. Some of these were included in the literature review of copper.

HARDING et al (1960) appear to be the forerunners in developing a tensile version of the Hopkinson-bar technique which involved generating a compressive pulse in a tube surrounding a solid inner rod. The tube and rod are connected by a mechanical joint. When the compressive pulse in the outer tube reaches the joint which is a free end, it reflects back through the solid inner rod as a tensile pulse. A threaded tensile specimen is attached to the inner rod to provide the mechanical connection necessary to transfer the tensile pulse through the specimen and into a second rod. The system achieved strain rates of over $1000s^{-1}$. A similar set up was introduced by HAUSER (1966) and CHRISTMAN et al (1971). This method suffers from the inability to generate tensile waves having very short rise times because of the wave dispersion at the mechanical joint.

LINDHOLM and YEAKLEY (1968) used a conventional loading bar but a specimen in the form of a top hat, the 'rim' of which is pushed away from the 'top' by a hollow transmitter bar.

HARDING (1971) operated a modified SHPB in which the tensile loading pulse was produced by means of a rapidly induced magnetic force.

The kinetic energy of a rotating flywheel has also been used to impart a tensile load. Strain rates up to $2600s^{-1}$ were reported by KAWATA (1979) and up to $1000s^{-1}$ by STURGES et al (1984).

Explosive loading devices have been utilized by several workers including ALBERTINI and MONTAGNANI (1979) and ISOZAKI and OBA (1979). In the same paper, Albertini and Montagnani also reported on the use of the rapid fracture of a clamp in a prestressed bar to generate the tensile pulses in an SHPB system. Strain rates of at least 10^4s^{-1} were achieved by FYFE (1976), FYFE and RAJENDRAN (1979) and BAUER and BLESS (1979) when using an exploding wire or exploding cylinder technique.

DORMEVAL and STELLY (1976, 1979) and REGAZZONI and MONTHEILLET (1984) performed tensile tests using a specially built machine known as Arbalete (Cross-Bow). This machine, which was described in Chapter 2, has enabled strain rates of up to $3 \times 10^3s^{-1}$ to be achieved.

Another technique, in which only a minimal amount of modification is required to convert the normal compressive SHPB system into one for tensile testing, has been developed independently by Bauer and Bless (1979), NICHOLAS (1981) and ELLWOOD, GRIFFITHS and PARRY (1982b). A modified version of this last technique is used in the current

investigation.

4.2 Description of Apparatus and Technique

The technique is based on two simple modifications to the split Hopkinson pressure bar compressive testing technique.

The modifications are:

(a) the short cylindrical compressive specimen is replaced by a tapered or 'dog-bone' shaped tensile specimen which screws into the ends of the adjacent pressure bars;

(b) a steel collar is added to the apparatus. The collar, which is made of the same material as the pressure bars, surrounds the specimen without touching it.

A schematic version of the apparatus is shown in Figure 4.1 and an enlarged view of the coaxial and concentric specimen and collar in Figure 4.2.

The tensile technique is almost identical to the compressive SHPB technique. The main difference is during the initial part of the test in which the compressive pulse initiated in bar 1 by the projectile impact is converted into a tensile pulse of equal amplitude. The latter pulse then loads the specimen and the same theory as used in Chapter 3 is then applied.

Having been generated by impact at the free end of bar 1,

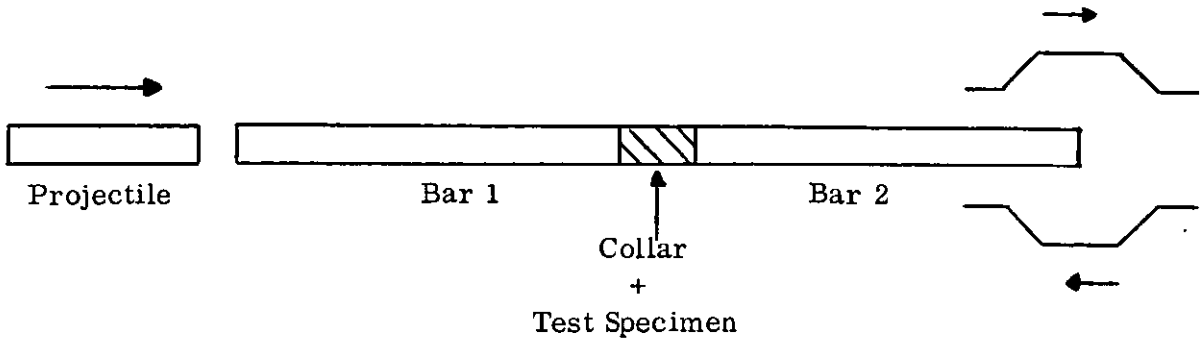

Figure 4.1 Tensile version of the SHPB apparatus

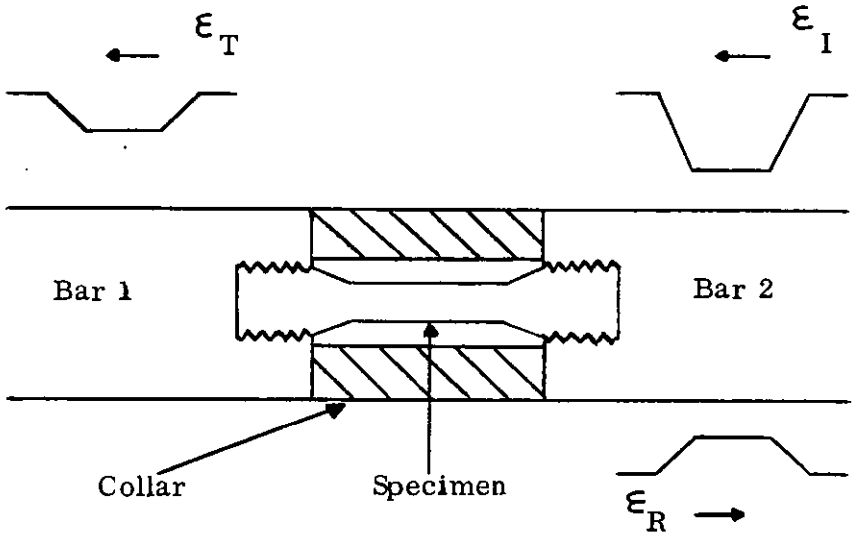

Figure 4.2 Enlarged view of tensile specimen and collar

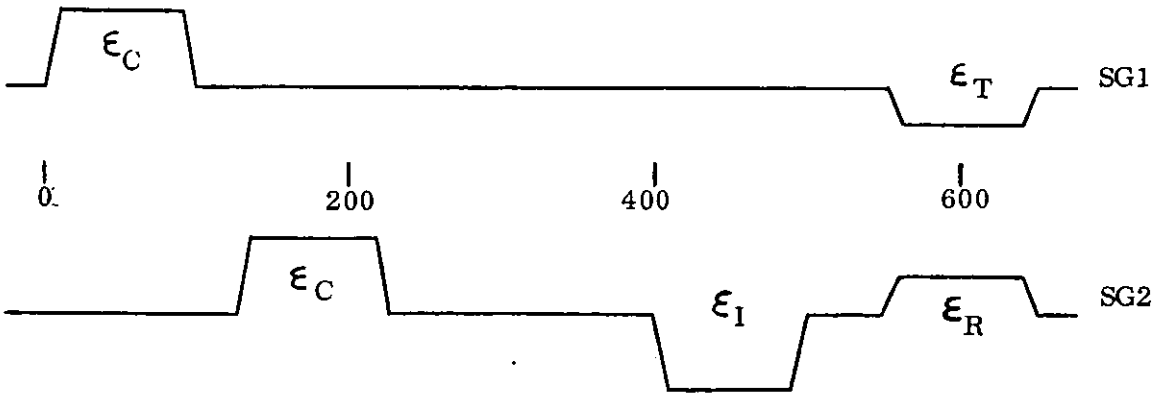

Figure 4.3 Idealised strain pulses recorded by strain gauges SG1 and SG2

the compressive pulse is propagated along the length of bar 1 and then through the steel collar and specimen in parallel. Now, the collar has an inner diameter of 6mm and an outer diameter of 12.7mm (equal to that of the pressure bars), giving it a cross-sectional area of 78% of that of the pressure bars; hence the collar undergoes only marginally more strain than the bars. The specimen and collar are in parallel and so are subject to the same strain, so that, provided the incident compressive pulse is not too large then the latter can pass from bar 1 to bar 2 without work-hardening the tensile specimen.

A tensile pulse is then produced by reflection at the free end of bar 2. On arrival at the specimen/collar interface the collar, which cannot support a tensile pulse, becomes free and the entire stress pulse acts upon the specimen. As the specimen deforms, a compressive pulse is reflected back into bar 2 and a tensile pulse is transmitted into bar 1. The stress/strain/strain rate characteristics of the specimens can then be determined as in Chapter 3 by applying equations (3.7), (3.8) and (3.12) to the reflected and transmitted pulses.

Idealised strain pulses recorded by the strain gauge pairs SG1 and SG2 (mounted on bars 1 and 2, respectively) are shown in Figure 4.3. ε_C is the compressive pulse generated by the projectile impact with bar 1, ε_I is the tensile pulse produced by reflecting ε_C from the free end of the transmitter bar, ε_R and ε_T are, respectively, the pulses reflected and transmitted by the specimen when loaded by ε_I.

The result of a typical dynamic tensile test is shown in Figure 4.4, the upper trace indicating the tensile transmitted pulse, ε_T, and the lower trace the tensile incident pulse, ε_I, and the compressive reflected pulse, ε_R. Note that an almost constant strain rate occurs naturally. This is because, due to the small diameter of the central parallel region of the specimen, nearly all of the flat topped incident pulse is reflected. The rise time of the loading tensile pulse is about 25 μs (c.f. 16 μs for the loading pulse in the equivalent compressive test).

4.3 Effective Specimen Length

In the compressive SHPB test the specimen had a constant cross-sectional area along its length. Consequently the stress and strain are uniform throughout the specimen. Hence the engineering strain is simply the change in specimen length ($\Delta \ell$) divided by the original length, ℓ .

However, for the tensile SHPB test with a tapered specimen (see Figure 7.1) the reference length for strain will not simply be the length of specimen between bar 1 and bar 2. This is because the specimen is composed of a narrow central region, 5mm long and 3mm in diameter, and tapered shoulders, varying in diameter from 3mm to 5mm, the total specimen length being 35mm. Hence the stress applied to the central region which has a smaller cross-section area will be larger than that applied to the broader shoulders and consequently the former region will undergo a larger strain than the latter.

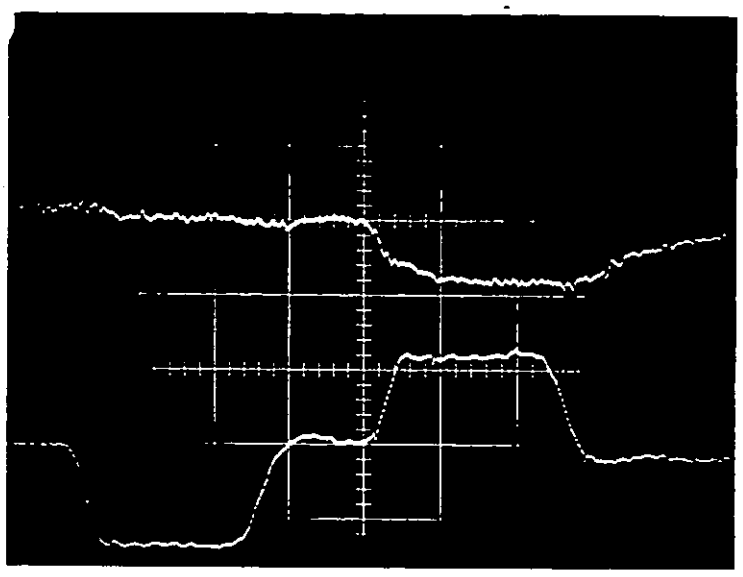

Vertical Scale
(upper trace):
0.005%/div

(lower trace):
0.028%/div

Horizontal Scale:
40us/div

Filename:
COT0203008DG

Average
Strain Rate:
359s^{-1}

Figure 4.4 Typical dynamic tensile test result

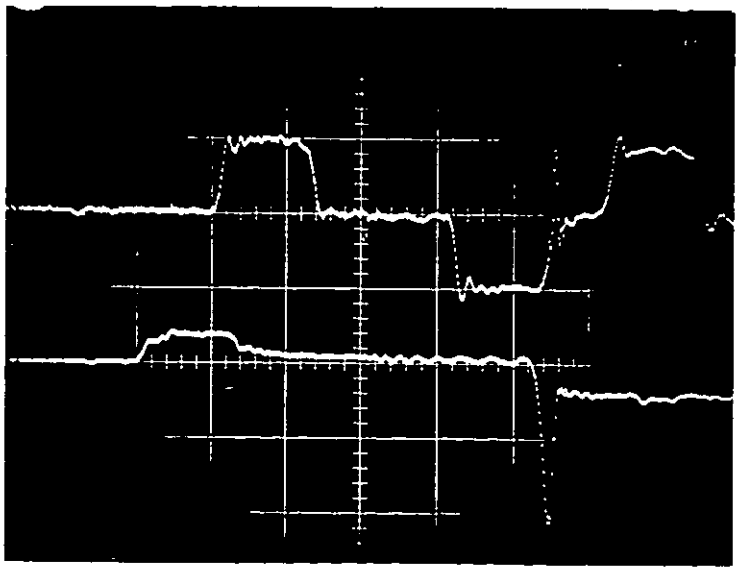

Vertical Scale
(upper trace):
0.08%/div

(lower trace):
0.8%/div

Horizontal Scale:
80us/div

Filename:
COT02050014DA

Figure 4.5 Strain records from gauges on Bar 2 and tensile specimen (upper and lower traces, respectively). Used to determine effective gauge length of tensile specimen. Only the initial part of the tensile loading pulse is seen in the lower trace because the gauge fails.

The length ℓ must be replaced by an equivalent effective length ℓ_E which will give the correct value for the strain in the uniform central region. Then the stress and strain can be compared at the same times for this uniform region using the cross-section of this region as the reference area for stress (A_s in equation (3.12)).

ℓ_E was determined by two different methods:

(a) <u>For small strains in the central region of the specimen (<5%)</u>

A small (1mm length) strain gauge was affixed to the central uniform region of the specimen, parallel to its longitudinal axis. A tensile SHPB test was then performed and the engineering tensile strain (ε_m) in this central region measured by the attached gauge.

The extension of the ends of the specimen is given by a modified form of equation (3.7).

i.e. Specimen extension, $$\Delta \ell = -2c_o \int_o^t \varepsilon_R \, dt \qquad (4.1)$$

where ε_R is measured by the strain gauges SG2.

Now Engineering Strain (ε_m)

$$= \frac{\text{Extension of Specimen } (\Delta \ell)}{\text{Gauge Length or Effective Length } (\ell_E)}$$

Hence $$\ell_E = \frac{\Delta \ell}{\varepsilon_m} \qquad (4.2)$$

From a series of dynamic tensile tests, carried out at various strain rates, it was found that there was very little variation in ℓ_E, its average value being 8.3mm. This length is greater than that of the central region but less than the total length of the specimen. The value of 8.3mm was confirmed with tests at a quasi-static strain rate using an Instron machine (see Chapter 5 for details of the quasi-static tests). As before the strain in the central region was measured with a small strain gauge. The extension of the ends of the specimen was determined using a travelling microscope.

(b) <u>For large strains (> 5%)</u>

At strains greater than about 5% the tensile strain at the centre of the specimen cannot be measured by the affixed gauge because the latter becomes detached. However, the early part of the tensile extension can still be recorded, from which the tensile strain rate ($\dot{\varepsilon}_m$) can be derived. Figure 4.5 indicates the result of a high strain rate ($1250s^{-1}$) tensile test. The upper trace records the strain variations in bar 2. The three pulses are the same as those shown schematically in Figure 4.3, the last pulse being the reflected pulse (ε_R). The lower trace is composed of the transit of the compressive loading pulse through the specimen, the latter being protected by the steel collar, followed by the initial stage of the tensile loading pulse, during which the strain gauge fails. The rise time of this pulse is equivalent to $\dot{\varepsilon}_m$.

From equation (3.8), $\dot{\varepsilon}_m = \frac{2c_o \cdot \varepsilon_R}{\ell_E}$

i.e. the effective gauge length, $\ell_E = \frac{2c_o \cdot \varepsilon_R}{\dot{\varepsilon}_m}$

Again ℓ_E was found to be 8.3mm.

This measurement was corroborated for high strain rate and quasi-static tests by lightly scribing at each end of the 5mm long central region and measuring the extension of the central region with a travelling microscope. From this extension the central region strain (ε_m) can be calculated. By comparing this with the overall extension of the specimen, measured either by the gauge on bar 2 in the high strain rate test or derived from the chart recorder of the Instron machine in the quasi-static test, the effective gauge length (ℓ_E) can again be derived. Once again ℓ_E was estimated at 8.3mm.

4.4 Validity of Tensile Technique

4.4.1 Stress Equilibrium

Since the tensile specimen is longer than the compressive specimen then stress equilibrium will only be achieved at a later stage of the test. However, most of the specimen shoulders remained elastic during a test. Consequently, the time taken for several internal reflections in the plastically deforming region of the specimen principally determines when stress equilibrium is reached.

4.4.2 Inertia

The smaller mass of the tensile specimen ensures that radial inertial errors are minimised.

4.4.3 Friction

Unlike the compressive technique, there are no frictional constraints and the tensile specimen is completely free to laterally contract as it extends longitudinally.

4.5 Advantages of Tensile Technique over Compressive Technique

The tensile SHPB technique is capable of testing materials of higher strengths than its compressive counterpart. This is a consequence of the tapered specimen in which the cross-sectional area of the shoulders of the specimen (at their interface with the pressure bars) is almost three times that of the central parallel region. Hence the stress applied to the interface between the bars and the specimen is magnified by a factor of nearly three in the central region.

Note that in both the compressive and tensile SHPB techniques the upper limit to the specimen stress is determined by the stress set up at the interface of the bars and specimen because this must not exceed the elastic limit of the bars. Hence, the tensile technique has the potential for testing materials which have a yield stress of almost three times that of the pressure bars.

As previously mentioned, with the tensile technique the strain rate is naturally constant and there are no frictional constraints.

4.6 Sources of Error

4.6.1 Work Hardening by the Compressive Loading Pulse

The assumption made by Ellwood et al (1982b) and Nicholas (1981), as stated in section 4.2, that the specimen and collar in parallel, are subject to the same overall strain when loaded by the impact generated compressive pulse, is correct. However, in the case of the compressive pulse, the fact that the strain in the uniform narrow central region can be significantly larger than that in the wider tapered part has been ignored. Hence, even if the overall strain experienced by the specimen is below its elastic limit, it is possible for the central region to be plastically deformed and, thus work hardened by the compressive impact pulse before it is extended by the tensile incident pulse.

In the light of the above hypothesis, experimental and theoretical attempts were made to determine the relation between the compressive strain, ε_b, in the pressure bars and the compressive strain in the central region of the specimen, ε_m, for various values of the former parameter.

(a) Experimental Determination of $\varepsilon_m/\varepsilon_b$

This was carried out in an analogous manner to the effective specimen length determination, i.e. a 1mm strain

gauge was affixed to the central region of the specimen, but this time the extent of the compressive deformation was monitored. Two of the results are shown in Figures 4.5 and 4.6.

In Figure 4.5, the strain in the bars (1st and 2nd pulses of the upper trace) is 0.078% and the compressive strain in the specimen (1st pulse of the lower trace) is 0.326%, i.e. $\varepsilon_m/\varepsilon_b = 4.2$.

In Figure 4.6, $\varepsilon_b = 0.115\%$ and $\varepsilon_m = 0.814\%$ (traces reversed). Hence $\varepsilon_m/\varepsilon_b = 7.1$.

Notice that in Figure 4.5 the strain in the specimen returns to zero after the passage of the transient compressive pulse whereas in Figure 4.6 there is a permanent set at a strain of 0.45%.

In fact, the 0.078% strain of Figure 4.5 was the maximum value of ε_b which did not work harden the tensile specimens. However, 0.078% is virtually the lowest strain that is possible to generate by impact in the pressure bars with the current gas gun/projectile arrangement. It was achieved with a duralumin projectile bar and aperture area of about $32mm^2$. Hence, without modifying the SHPB apparatus, the latter is limited to testing copper in tension at the moderate strain rate of $700s^{-1}$. The apparatus modification which permits tensile testing at higher strain rates is detailed in section 4.7.

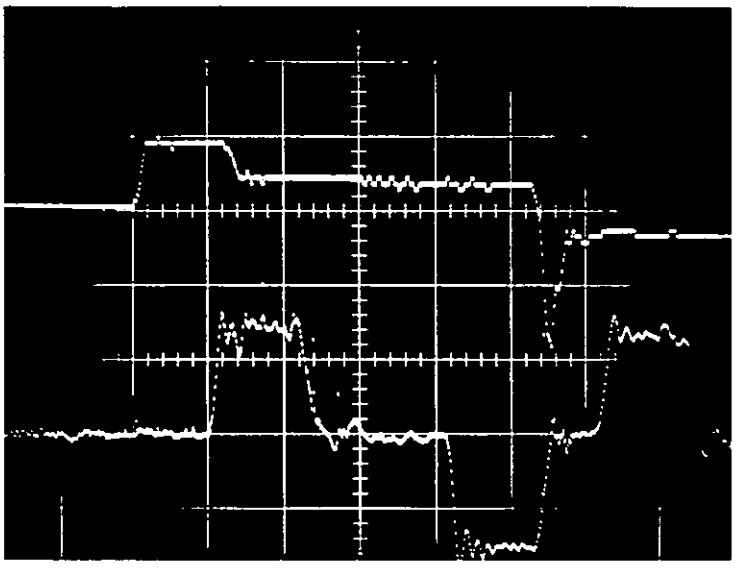

Vertical Scale
(upper trace):
1.1%/div

(lower trace):
0.08%/div

Horizontal Scale:
80us/div

Filename:
COT02031021DA

Figure 4.6 Tensile test result showing work-hardening caused by initial compressive pulse. The upper trace, recorded by strain gauge on tensile specimen, shows the permanent set, i.e. work-hardening, following the compressive pulse. The lower trace is from gauges on bar 2.

(b) Approximate Theoretical Determination of $\varepsilon_m/\varepsilon_b$

Consider a tensile specimen with a step change in cross-section rather than a tapered change. This specimen and the steel collar in parallel are shown schematically in Figure 4.7.

Let force, stress, strain, elastic modulus, cross-sectional area, length and change in length be denoted by F, σ, ε, E, A, L and Δ L, respectively.

Let the suffices corresponding to the pressure bar, collar, large and small cross-sections of the specimen be denoted by b, c, e and m, respectively. The large cross-section is equivalent to the ends of the specimen used in a tensile SHPB test and the small cross-section is representative of the middle section of such a specimen. Consider the equilibrium of forces at one of the interfaces between a pressure bar, and the collar and specimen in parallel.

Hence $F_b = F_c + F_m$

and $\sigma_b A_b = \sigma_c A_c + \sigma_m A_m$

and $\varepsilon_b E_b A_b = \varepsilon_c E_c A_c + \varepsilon_m E_m A_m$ (4.3)

Now $\Delta L_c = \Delta L_m + \Delta L_e$

since the collar and specimen are in parallel and limited to the same reduction in length by the faces of the pressure bars.

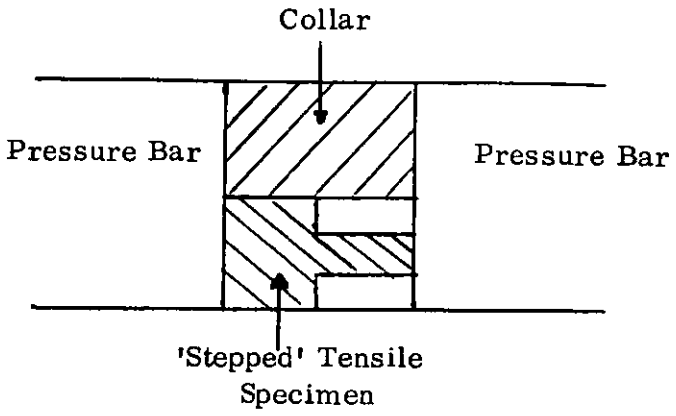

Figure 4.7 Schematic of tensile specimen with 'stepped' change in cross-section in parallel with collar

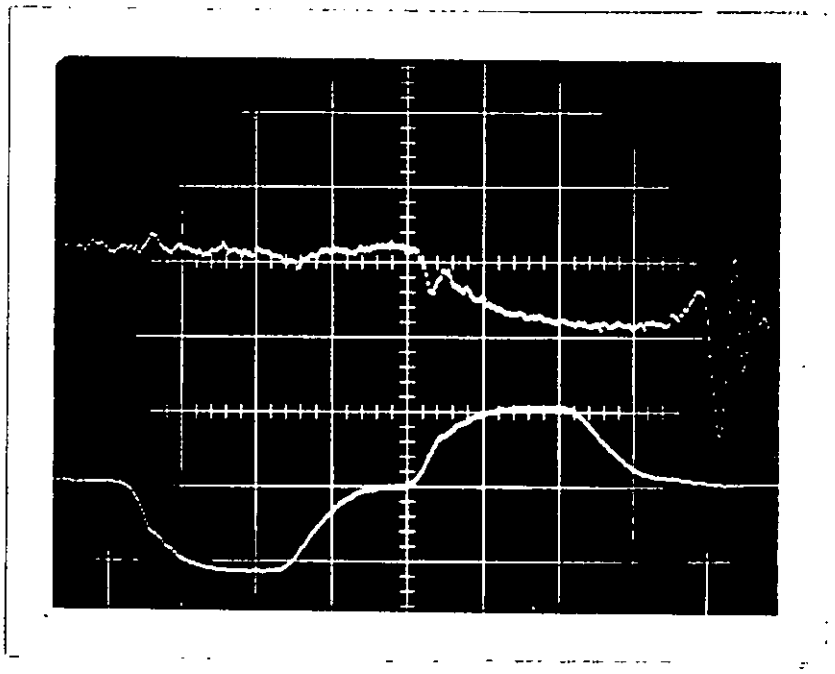

Vertical Scale
(upper trace):
0.006%/div

(lower trace):
0.128%/div

Filename:
COT20060017SA

Figure 4.8 Sudden drop in strain near the start of the tensile transmitted pulse (upper trace) caused by a spurious pulse generated due to the misalignment of bars 1A and 1B. The lower trace shows the incident and reflected pulses.

Therefore $\varepsilon_c L_c = \varepsilon_m L_m + \varepsilon_e L_e$

and $\varepsilon_m = \dfrac{\varepsilon_c L_c - \varepsilon_e L_e}{L_m}$

$$= \frac{\varepsilon_c L_c - \varepsilon_e (L_c - L_m)}{L_m}$$

$$= \varepsilon_c \frac{L_c}{L_m} - \varepsilon_e \left(\frac{L_c}{L_m} - 1 \right) \qquad (4.4)$$

Combining equations (4.3) and (4.4),

$$\varepsilon_m = \varepsilon_c \frac{L_c}{L_m} - \frac{(\varepsilon_b E_b A_b - \varepsilon_c E_c A_c)}{E_e A_e} \left(\frac{L_c}{L_m} - 1 \right) \qquad (4.5)$$

Since the collar and pressure bars are the same material then $E_c = E_b$

Therefore $\varepsilon_m = \varepsilon_c \dfrac{L_c}{L_m} - E_b \dfrac{(\varepsilon_b A_b - \varepsilon_c A_c)}{E_e A_e} \left(\dfrac{L_c}{L_m} - 1 \right)$

(4.6)

Now $E_e \approx 0.5\, E_b$

Therefore $\varepsilon_m = \varepsilon_c \dfrac{L_c}{L_m} - \dfrac{2}{A_e} (\varepsilon_b A_b - \varepsilon_c A_c) \left(\dfrac{L_c}{L_m} - 1 \right)$

(4.7)

But $A_e \approx \dfrac{A_b}{6}$ and $A_c \approx \dfrac{4}{5} A_b = \dfrac{24}{5} A_e$

$$\text{Therefore } \varepsilon_m = \varepsilon_c \frac{L_c}{L_m} - \left(12\varepsilon_b - \frac{48}{5}\varepsilon_c\right)\left(\frac{L_c}{L_m} - 1\right)$$

$$= \varepsilon_c \left[\frac{L_c}{L_m} + \frac{48}{5}\left(\frac{L_c}{L_m} - 1\right)\right] - 12\varepsilon_b\left(\frac{L_c}{L_m} - 1\right)$$

$$= \frac{\varepsilon_c}{5}\left(53\frac{L_c}{L_m} - 48\right) - 12\varepsilon_b\left(\frac{L_c}{L_m} - 1\right) \qquad (4.8)$$

In the current investigation, L_c = 17.5mm & L_m = 5mm

$$\text{Therefore } \varepsilon_m = 27.5\,\varepsilon_c - 30\,\varepsilon_b \qquad (4.9)$$

To make further progress from equation (4.9) the limiting values of ε_c, the strain in the collar, must be found.

Replacing the 2 cross-sectional areas of the specimen by a single 'effective' area permits the following equilibrium of forces to be achieved:

$$F_b = F_c + F' \qquad (4.10)$$

Where F' is the force on the specimen of effective area A'.

$$\text{Hence } \varepsilon_c = \frac{\varepsilon_b E_b A_b}{E_c A_c + E' A'} \qquad (4.11)$$

Where E' is the effective modulus of the specimen

Again taking $A_c = \frac{4A_b}{5}$, and $E_c = E_b$

$$\text{Therefore } \varepsilon_c = \frac{\varepsilon_b E_b A_b}{0.8\ E_b A_b + E' A'} \tag{4.12}$$

The maximum value of $A' = A_e = 0.16\ A_b$
and the maximum value of $E' = E_e \approx 0.5 E_b$

$$\text{Therefore } \varepsilon_c = 1.14\ \varepsilon_b \tag{4.13}$$

Therefore the minimum value of

$$\frac{\varepsilon_m}{\varepsilon_b} = 1.35 \tag{4.14}$$

The maximum value of $\varepsilon_m / \varepsilon_b$ occurs if $E' = 0$

$$\text{i.e. } \left(\frac{\varepsilon_m}{\varepsilon_b}\right)_{max} = 4.38 \tag{4.15}$$

i.e. the strain in the smaller diameter section of the specimen varies between 1.35 and 4.38 times the bar strain, depending on the values of effective area and effective modulus that are chosen.

In conclusion then, two empirical measurements of the effect of the impact-generated compressive pulse on the tensile specimen have indicated that the compressive strain in the central region can be as high as 4.2 or 7.1 times the strain in the pressure bars. An approximate

theoretical model has also confirmed that the central region of the specimen is liable to experience a strain in excess of the compressive strain in the pressure bars; the strain amplication factor predicted by the model varying from 1.38 to 4.38. Hence the collar, as specified by Ellwood et al (1982b) and Nicholas (1981) is inadequate to prevent the tensile specimen suffering considerable plastic deformation in compression prior to its tensile loading.

4.6.2 Generation of Spurious Pulses

As mentioned in section 4.2, because of the narrow central diameter of the tensile specimen, most of incident tensile pulse is reflected. Consequently, the transmitted pulse is extremely small. At the lowest consistently attainable dynamic strain rate of $\approx$ 350 s^{-1}, the value of the transmitted strain pulse was only 0.005% and at the highest attainable strain rate of $\approx$ 1400s^{-1}, it was 0.007%. Contrast these values with the variation in transmitted strains from 0.04% to 0.18% in the compressive tests.

Since the transmitted pulse is so small any spurious pulses produced, for instance, by non-perfect bar alignments can now have serious effects on the results since the latter are of the same order of magnitude as the transmitted pulse.

(a) Flexural Waves

Ideally only a longitudinal compressive pulse should be generated from the impact of the projectile with the first pressure bar. In practice, however, due to the non-perfect

alignment between projectile and bar, a flexural wave or bending wave is frequently generated as well. This flexural wave must be prevented from loading the specimen, and, if possible from reaching the bar 1 gauges, SG1, during the recorded time interval of the test. Fortunately as the flexural wave velocity is less than the longitudinal wave velocity (the velocities ratio being less than 3:5), if the first pressure bar is sufficiently long then the former wave can be delayed until the tensile loading has been completed. If the length of bar 2 is ℓ_2 then the minimum length ℓ_1 of bar 1 so that the tensile loading pulse arrives at the specimen before the flexural pulse is given by:

$$\frac{\ell_1 + 2\ell_2}{c_o} \leq \frac{5}{3}\frac{\ell_1}{c_o} \qquad (4.16)$$

Where c_o is the longitudinal wave velocity

i.e. $\ell_1 \geq 3\ell_2$ (4.17)

In addition, to allow the complete passage of the transmitted pulse through SG1 before the flexural wave arrives at the latter then equation (4.17) becomes

$$\frac{\ell_1 + 2\ell_2 + d + p}{c_o} \leq \frac{5}{3c_o}(\ell_1 - d) \qquad (4.18)$$

Where d is the distance of the strain gauge pair SG1 from the specimen and p is the length of the longitudinal pulse.

The short length of the collar has been ignored in the above equations.

To ensure complete separation of reflected pulses in bar 2, the value of ℓ_2 was chosen to be 1m, d was 0.1m and the pulse length p was 0.5m. Hence the minimum length of bar 1 such that the transmitted tensile pulse is completely separated from any impact generated flexural wave is 4.15m.

In the current series of tests the maximum single bar length available was 2m and consequently bar 1 was replaced by 2 bars, bars 1A and 1B, their respective lengths, ℓ_{1A} and ℓ_{1B}, being 1m and 2m, initially. Thus, the tensile specimen was subject to loading by a flexural pulse before the former had been plastically deformed by the tensile pulse. The accurate alignment of the strain gauge pair SG1, which ensures the cancellation of a flexural wave component from the gauge output, is even more vital in the tensile SHPB test because the transmitted pulse could be of the same order of magnitude as the flexural wave.

(b) Reflections from Misaligned Bars/Collar

The introduction of an extra bar interface between the impact bar face and the specimen proved to be beneficial because a portion of the flexural wave was dissipated across the interface, resulting in a smaller bending wave being propagated towards the specimen.

Conversely, the additional interface also had a deleterious effect. If the bars 1A and 1B are not perfectly aligned

then when the impact-generated compressive pulse arrives at their interface, a small fraction of it will be reflected back towards the gas gun as a tensile pulse. This small tensile pulse will be reflected by the free end of bar 1A as a compressive pulse. Hence a minute additional compressive pulse is propagated towards the specimen and trails the initial large compressive pulse by a time t given by:

$$t = 2\ell_{1A}/c_o \qquad (4.19)$$

If $\ell_2 = n\ell_{1A}$ where n is an integer then an extra compressive pulse will arrive at the specimen at the same time as the loading tensile pulse. The problem is then accentuated by a compressive reflection of the spurious pulse from the bar/large collar interface which will arrive at SG1 simultaneously with the small tensile transmitted pulse. This spurious pulse can be seen at the start of the tensile transmitted in the upper trace of Figure 4.8. It would be easy to misinterpret this pulse, initiated by the misalignment of bars 1A and 1B, as indicating the occurrence of a yield stress drop when copper is dynamically loaded in tension. The various pulses initiated by reflections from misaligned bars/collar are pictorially represented in the Lagrangian diagram of Figure 4.9. The effects of this spurious pulse and the flexural wave were eliminated by increasing the length of bar 1A to 2m.

(c) Bar Supports

Usually any wave reflections from the optical bench supports for the pressure bars, can be ignored as they are

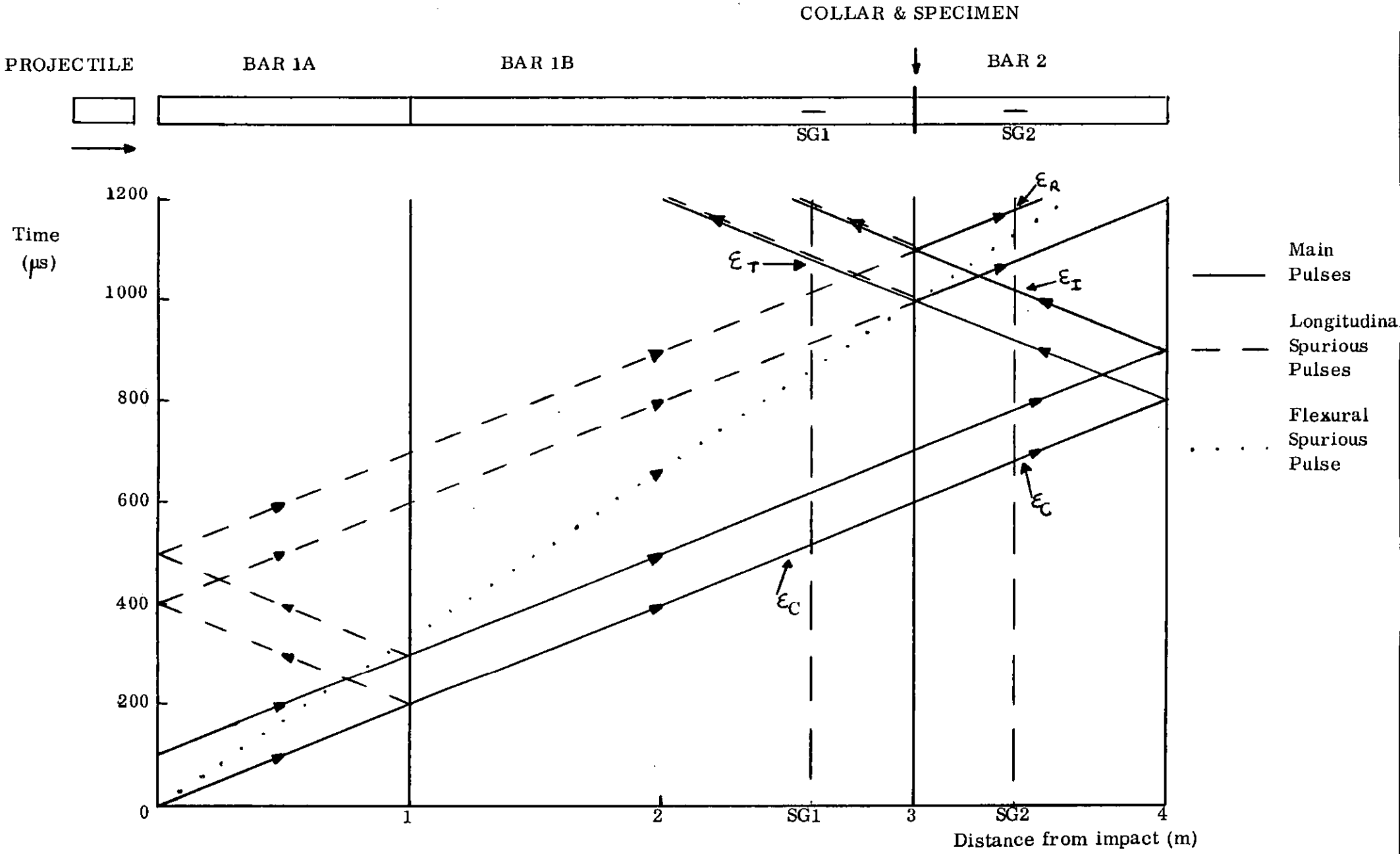

Figure 4.9 Lagrangian showing main and spurious pulses in dynamic tensile test

negligible amplitude compared to the pulses of interest. However, on this occasion if a support is placed too near to the free end of bar 2 then a reflected compressive pulse of significant amplitude will be recorded immediately prior to the start of the tensile transmitted pulse. This makes it extremely difficult to accurately locate the start of the latter pulse. The detrimental effect of this spurious pulse was eliminated by moving the support, that was closest to the free end of bar 2, towards the tensile specimen until the spurious pulse was well removed from the start of the tensile transmitted pulse.

(d) Curved Pressure Bars

If either of the pressure bars adjacent to the tensile specimen is not straight, a definite possibility for the 2m long bar, then it is extremely difficult to prevent an air gap between one collar face and the adjacent bar face, due to the adjacent bar faces not being parallel. When this happens the test is ruined because the specimen is plastically deformed when the gap is closed by the initial compressive pulse. Care must also be exercised when attempting to ensure that there is no air gap that the narrow central region of specimen is not work hardened in shear by the application of excessive torque to bar 2. Additionally there is a danger of bending the specimen.

(e) Specimen Fit

It is essential that there is no longitudinal slackness between the screw threads of the specimen and those of the pressure bars. In the event of this occurring, bar 2 will move freely under the action of the loading tensile pulse,

with no opposition from the specimen until the slack is taken up. During this time interval the loading pulse will be completely reflected from the pressure bar/specimen interface. This is then followed by the sudden application of stress to the specimen's screw threads, resulting in a rapid rise and fall of the tensile pulse transmitted to bar 1B. This again could be incorrectly attributed to a yield stress drop. The start of the transmitted pulse is also delayed until the free play in the threads is removed.

By packing the specimen thread with plasticine or a cement this source of error was successfully eradicated.

4.6.3 Accurate Measurement of Small Transmitted Pulse

The maximum amplitude of the transmitted tensile strain pulse was typically between 0.005% and 0.007%. The error in measuring the former can be consequently large particularly if the zero strain level, or baseline, of the recorded signals is not accurately known. Since nearly all the recorded trace from SG1 is cluttered with a miscellany of pulses the latter is often difficult to ascertain with any degree of certainty.

4.7 Modification to Protective Collar

By doubling the diameter of the 12.7mm protective collar, its cross-sectional area becomes almost five times that of the smaller collar. Consequently the strain in the large collar should be approximately one-fifth of that in the small collar.

In practice, however, because the length of the collar is only 17mm and its diameter is 25.4mm (compared with the bar diameter of 12.7mm), the stress pulse is not uniform over the plane surfaces of the collar. This was established by affixing a strain gauge, in the axial direction, to the surface of the large diameter collar. When the collar was loaded by the compressive pulse the strain gauge actually recorded a tensile pulse. However, when the strain in the specimen was measured directly, this showed a greatly reduced strain. In fact, using the large diameter (25.4mm) protective collars, the strain rate limit was increased to about $1250s^{-1}$ without strain hardening the tensile specimen in compression.

4.8 Very Low Dynamic Strain Rates

Usually the lower limit for strain rates is determined by the combination of impact velocity and the acoustic impedance of the projectile.

Two additional methods were devised to further reduce the strain rate:

(a) The introduction of a 'dummy' specimen between the bars 1A and 1B serves as a pulse attenuator as well as a pulse shaper. It can be used in the former role to reduce the strain rate in tensile testing.

(b) Alternatively the addition of a momentum bar (normally used only in compressive tests) which is made from a material of lower acoustic impedance than that of the

pressure bars will reduce the amplitude of the tensile loading pulse and hence the strain rate. This works on the principle that the compressive pulse generated by the impact is partially transmitted into the momentum bar and partially reflected back into bar 2.

4.9 Elevated Temperature Tests

An alternative method of heating to that used in the compressive tests was devised for the tensile tests because the large diameter protective collar prevented the use of the furnace. Heat was, instead, provided by the flame from a blow lamp. The flame was applied evenly to all of the exposed surface of the collar and to the adjacent pressure bars. Heating times were similar to those of the compressive tests despite the additional requirement of raising the temperature of the steel collar as well as that of the specimen. The temperature was measured with a chromel/alumel thermocouple held lightly in contact with the central region of the specimen.

Further problems were encountered at high temperatures which are similar to those mentioned in 4.6.2(e). There was a rapid rise and fall at the start of the tensile transmitted pulse and also the start of the latter pulse was delayed relative to the start of the reflected pulse. Again a yield stress drop could be falsely attributed to this dynamic tensile test. The magnitudes of the "apparent" yield stress drop and the delay of the transmitted pulse both increased with increase in test temperature. In contrast to the room temperature tests,

these effects are unlikely to be caused by slackness in the screw threads. The thermal coefficient of expansion for copper is greater than that of steel, hence at elevated temperature any slackness should be removed. However, the unrestricted thermal extension of the central region of the specimen could cause a gap to develop between the pressure bars and the protective collar. This gap would increase with increase in temperature. The consequence of this gap, of course, would be to allow the impact-generated compressive pulse to deform the specimen prior to its tensile loading. It is possible, therefore, that the "apparent" yield stress drop and the delay in the transmitted pulse could be attributed to the combination of the compressive deformation and the thermal extension of the tensile specimen.

A photograph of the large diameter protective collar is shown in position between the pressure bars and surrounding the tensile specimen in Figure 4.10. The collar is flanked by bar supports, the usual nylon blocks being replaced by heat resistant tufnol blocks for the elevated temperature tests.

4.10 Summary

The tensile technique is a modified version of that developed independently by Bauer and Bless; Nicholas; and Ellwood, Griffiths and Parry. The apparatus and technique are very similar to the compressive split Hopkinson pressure bar system described in the previous chapter.

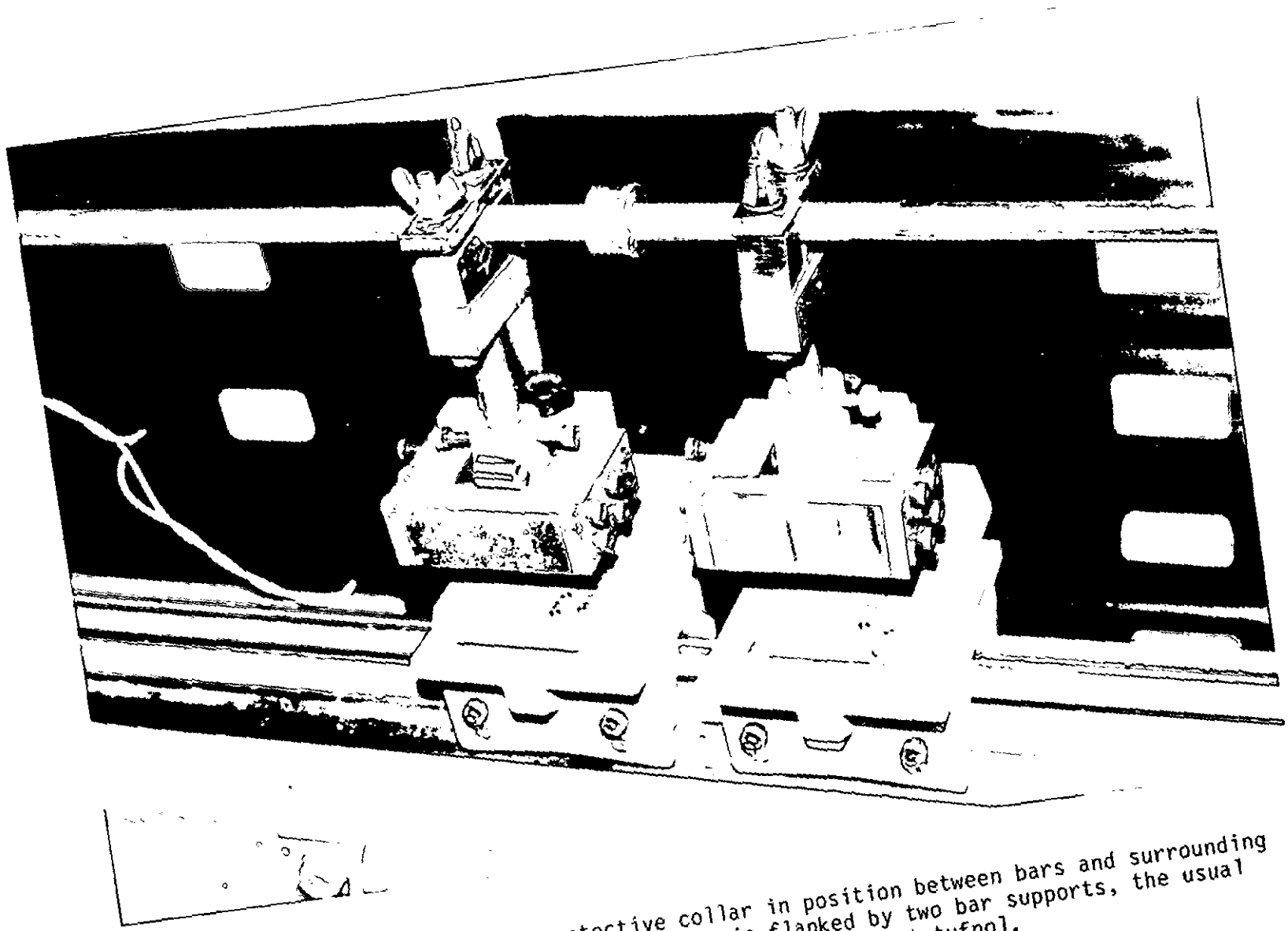

Figure 4.10. Large diameter protective collar in position between bars and surrounding tensile specimen. The collar is flanked by two bar supports, the usual nylon blocks being replaced by heat resistant tufnol.

A tapered tensile specimen screws into the ends of the pressure bars and is protected from the loading compressive pulse by a surrounding steel collar. The compressive pulse is reflected as a tensile pulse of equal amplitude at the free end of the second pressure bar. This tensile pulse returns to the specimen where the collar becomes detached and the specimen is subjected to a high strain rate deformation.

The tensile SHPB system has several advantages over its compressive counterpart. It can test materials of higher strengths, the strain rate is naturally constant and there are no frictional constraints.

Modifications and precautions were taken to ensure that the high strain rate tensile properties of copper were accurately determined. Both experiment and theory proved that at all but the lowest available dynamic strain rate, the steel collar as used by the above authors, did not protect the specimen from compressive permanent deformation prior to the application of the tensile stress pulse. This error was corrected by doubling the external diameter of the collar. This modification increased the acceptable upper strain rate limit to about $1300s^{-1}$.

Due to the extremely small amplitude of the transmitted tensile pulse in this investigation, special precautions were required to prevent the generation of spurious pulses which would invalidate the results. Five sources of spurious pulses were detected, all of which were eradicated or minimised.

The large diameter protective collar prevented the use of the electrical furnace in the elevated temperature tests. Instead a blow lamp provided the heat.

CHAPTER 5

QUASI-STATIC STRAIN RATE TESTING TECHNIQUE

The dynamic tests were complemented by quasi-static strain rate tests. An Instron machine capable of a maximum load of 5000 kg was used for both compressive and tensile tests. This machine displays results on a chart recorder in the form - load vs. displacement.

5.1 Compressive Tests

Figure 5.1 illustrates the arrangement for compressive testing. The moving crosshead and the fixed lower platen are both steel plates, belonging to the Instron machine, between which the test specimen is normally compressed. However, to allow a direct comparison between the dynamic and quasi-static tests, a simple adaptor made from 431 stainless steel was used so that the specimen is compressed by bars of the same diameter and material as in the dynamic tests. The specimen faces were again lubricated.

The Instron machine is designed to operate at various pre-set crosshead speeds. All the quasi-static compressive tests, however, were performed with a crosshead speed of 0.5mm/min, resulting in a constant strain rate of approximately $2 \times 10^{-3} s^{-1}$.

Due to the compliance of the machine components and the adaptor, the crosshead movement as recorded on the chart, is greater than the real displacement of the specimen. Consequently a preliminary test must be performed without

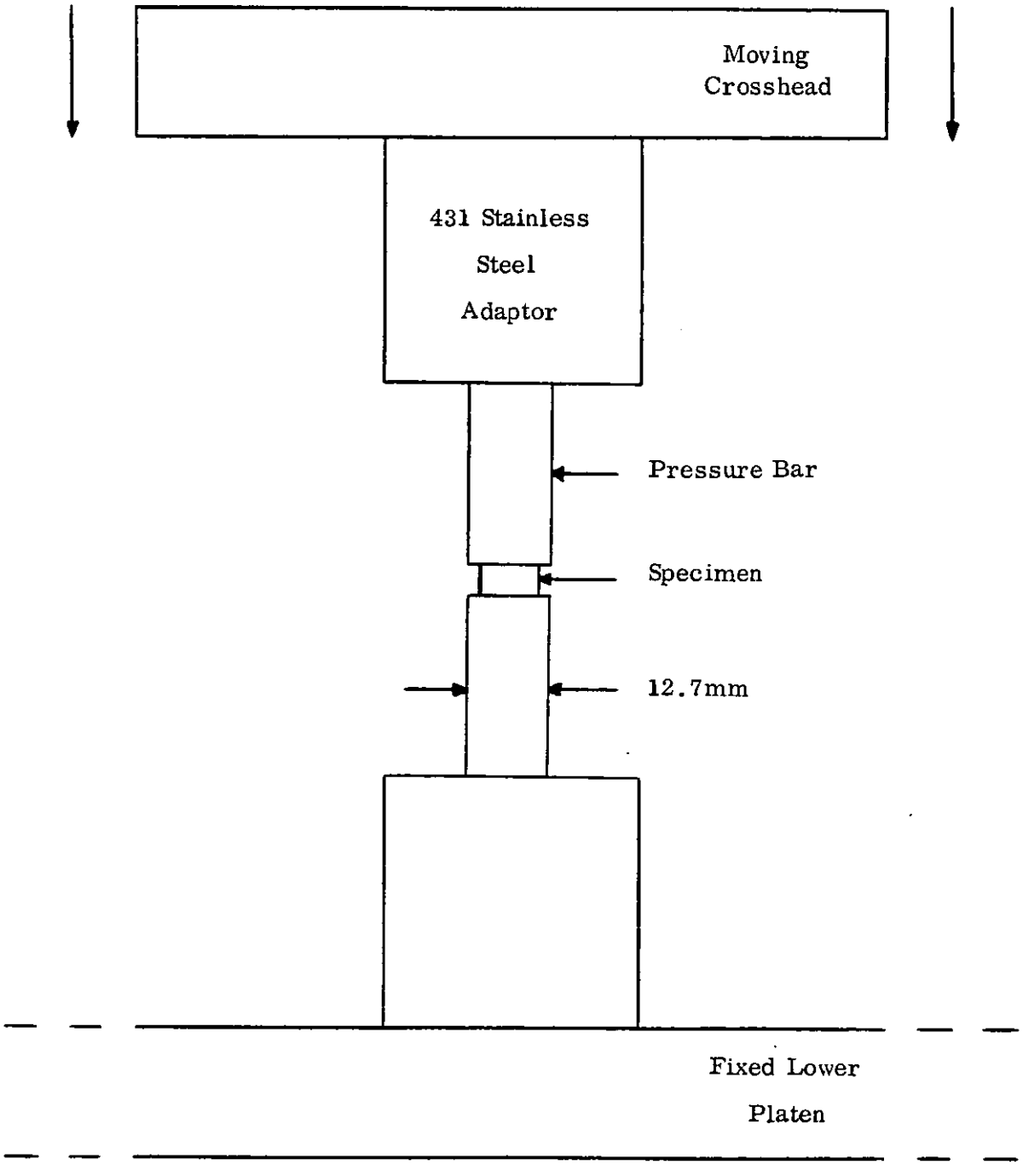

Figure 5.1 Quasi-static apparatus in compressive test arrangement

the test specimen to determine this compliance. Figure 5.2 indicates a chart record of load vs. displacement. The true displacement of the end faces of the specimen results from subtracting the machine compliance from the total crosshead displacement.

The compliance corrected chart recordings were converted to true stress and true strain.

5.2 Tensile Tests

A similar adaptor was used for the quasi-static tensile tests, the ends of the bars being threaded to accommodate the tensile specimen.

The tensile compliance of the system was measured by testing a 'dummy' specimen to full load which remained elastic throughout. The 'dummy' specimen consisted of a constant diameter threaded bar of 431 stainless steel which screwed into the ends of the adaptor bars.

The crosshead speed was identical to that of the compressive tests, consequently a constant strain rate of about $10^{-3}s^{-1}$ resulted, assuming an effective specimen length of 8.3mm as described in Chapter 4.

5.3 Elevated Temperature Tests

A further benefit of the adaptor bars was that the same electrical furnace as used in the dynamic compressive tests could be employed for both the compressive and tensile quasi-static tests.

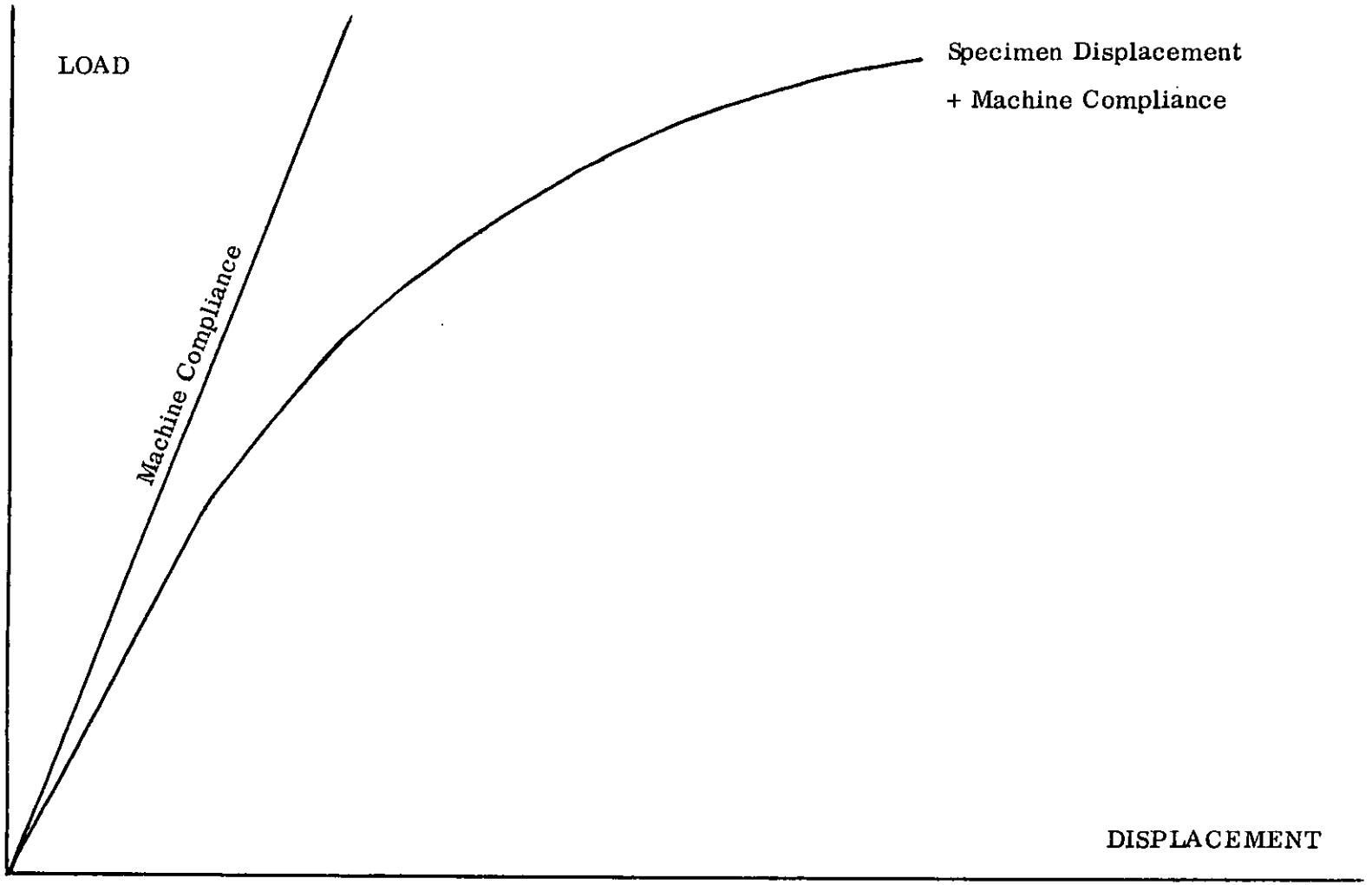

Figure 5.2 Instron chart record of load vs. displacement

CHAPTER 6

DATA ACQUISITION AND ANALYSIS

6.1 Data Acquisition

6.1.1 Introduction

The data acquisition system is outlined in schematic form in Figure 6.1. The transmitted pulse ε_T and the reflected pulse ε_R, which are required to define the specimen stress, strain and strain rate, are transferred in analogue form, i.e. millivolts, from the strain gauge pairs SG1 and SG2 to the input channels of a transient recorder, subsequent to amplification.

The transient recorder performs analogue-to-digital conversions on both signals, their digital equivalents then being passed to the microcomputer for analysis. A plotter, printer and disk drive are available for graphs, results and data tables, and permanent data storage, respectively.

6.1.2 Strain Gauges and Strain Gauge Ciruit

Each strain gauge pair, which is connected in series to cancel flexural or bending waves and double the effect of the plane longitudinal waves, comprises part of a strain gauge circuit. The latter is a simple potential divider circuit (Figure 6.2) comprising a ballast resistor, R_b (2.2K Ω), 2 strain gauges, R_s (total resistance 240 Ω) and a 90V power supply (Farnell stabilised voltage supply - type E350).

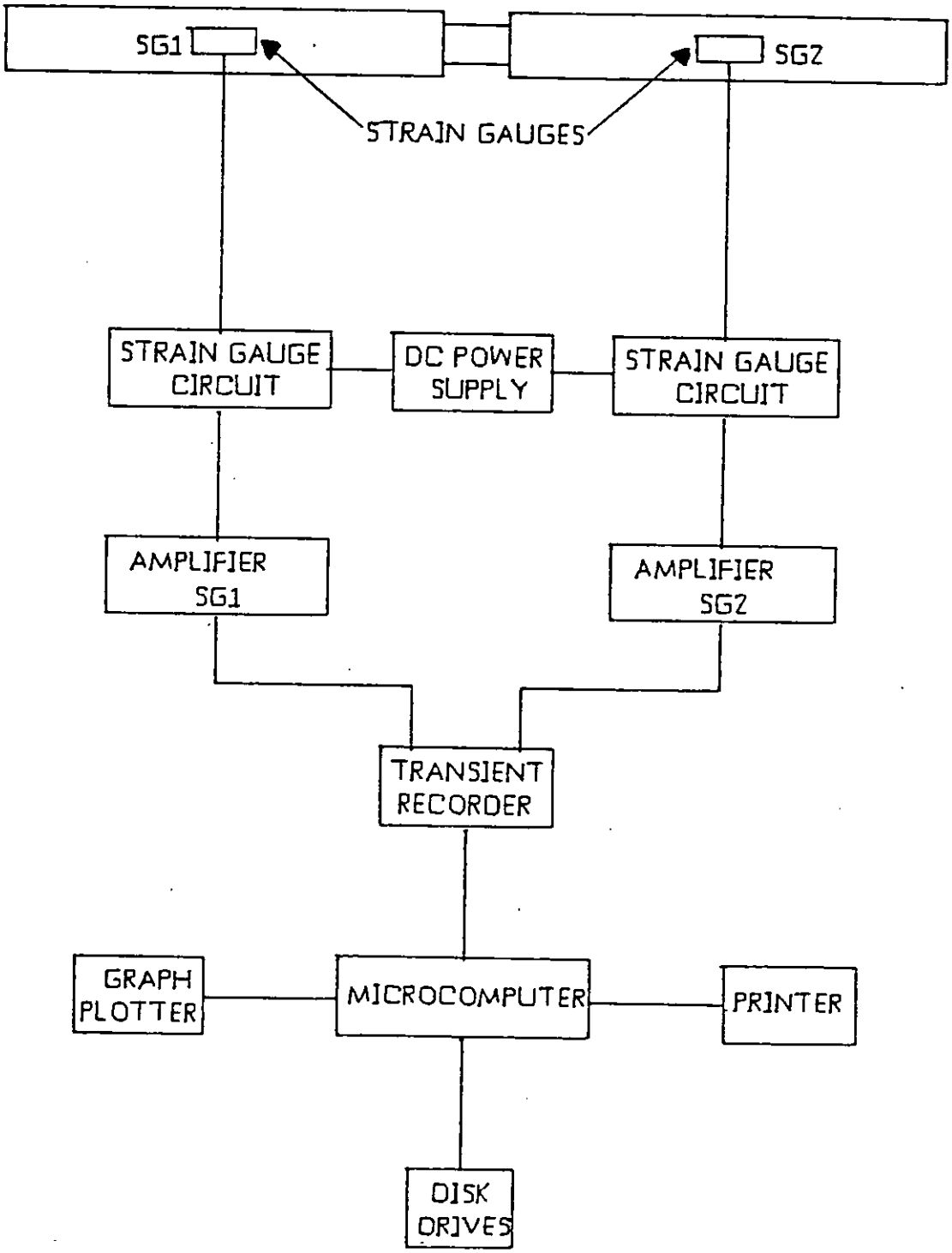

Figure 6.1 Block diagram of Data Acquisition System

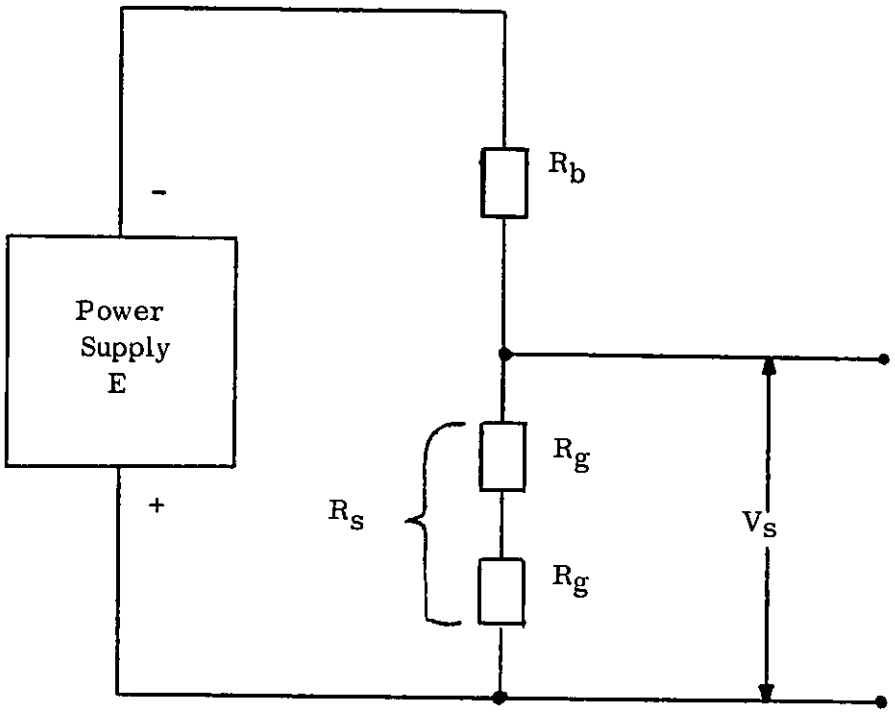

Figure 6.2 Strain gauge potential divider circuit

Power supply E = 90V
Ballast resistor R_b = 2.2KΩ
Strain gauge resistance R_g = 120Ω
Resistance of strain gauge pair R_s = 240Ω

The strain, ε, recorded by a strain gauge is related to the change in its electrical resistance, dRs, by the equation:

$$\varepsilon = \frac{1}{F} \cdot \frac{dR_s}{R_s} \qquad (6.1)$$

where F is the strain gauge factor (typically 2.11) and R_s is the gauge resistance.

In the strain gauge circuit the voltage, V_s, across the strain gauge pair is given by

$$V_s = \frac{R_s}{R_b + R_s} E = \frac{1}{n + 1} E \qquad (6.2)$$

where $n = R_b/R_s$

Differentiating

$$\frac{dV_s}{dn} = - \frac{E}{(n + 1)^2} \qquad (6.3)$$

$$\text{and} \quad \frac{dn}{dR_s} = - \frac{Rb}{R_s^{\,2}} \qquad (6.4)$$

$$\text{Therefore} \quad \frac{dV_s}{dR_s} = \frac{-R_b}{R_s^{\,2}} \left[\frac{-E}{(n + 1)^2} \right] \qquad (6.5)$$

$$\text{and} \quad dR_s = R_s^{\,2} \cdot \frac{(n + 1)^2}{R_b E} \cdot dV_s \qquad (6.6)$$

Substituting for dR_s in (6.1) from (6.6),

$$\varepsilon = \frac{(n + 1)^2}{nFE} \, dV_s \qquad (6.7)$$

Hence ε is also related to the change in voltage across the strain gauges. $(n + 1)^2 / nFE$ is not a constant, of course, because n is inversely proportional to strain gauge resistance. However, the maximum variation of $(n + 1)^2/nFE$ is no more than about $\pm$ 0.5% when applied to the strain levels in the Hopkinson bar. Therefore only a very small error is incurred if it is assumed that ε is directly proportional to dV_s.

N.B. dV_s is positive for compression with the power supply as shown in Figure 6.2.

6.1.3 Strain Gauge Amplifier

The output from each strain gauge circuit is fed to a linear strain gauge amplifier, linearity being implied both in terms of the requisite range of amplitudes and frequencies. Tests were performed with a variety of amplifiers before eventually selecting those contained in the plug-in units of a Tektronix cathode ray oscilloscope (Tektronix type 556 dual beam oscilloscope - type 1A1 dual-trace plug-in units).

Gains of up to 100 were required for the full series of tests. The maximum gain was used exclusively to measure the transmitted tensile pulse in the dynamic tensile tests.

A low pass filter in the form of an 1800pF capacitor was connected in parallel with the outputs of the amplifiers to remove high frequency electrical pick-up, the latter being composed of a fairly regular signal of about 10MHz frequency.

6.1.4 Transient Recorder

The amplified signals are connected to the channel 1 and channel 2 inputs of a transient recorder (Datalab DL912). The transient recorder can be seen in the photograph of Figure 6.3. It is situated on the far left of the bench in the foreground. Its two inputs are connected to the oscilloscope's amplifiers, on the left hand side of the photograph, by two black co-axial cables.

The principal functions of the transient recorder are indicated in the block diagram of Figure 6.4.

The overall gain of the system is determined by the combination of the gain of the strain gauge amplifier and that of the transient recorder amplifier. The latter has 8 different gain settings corresponding to full scale voltage inputs ranging from 100mV to 20V, i.e. a gain ratio of 200:1.

Each strain gauge signal is digitised and stored in separate 4 kilobyte digital memories. Each 8-bit analogue-to-digital converter is capable of a maximum sampling rate of 20MHz, i.e. the analogue signal is digitised at intervals of 0.05μs.

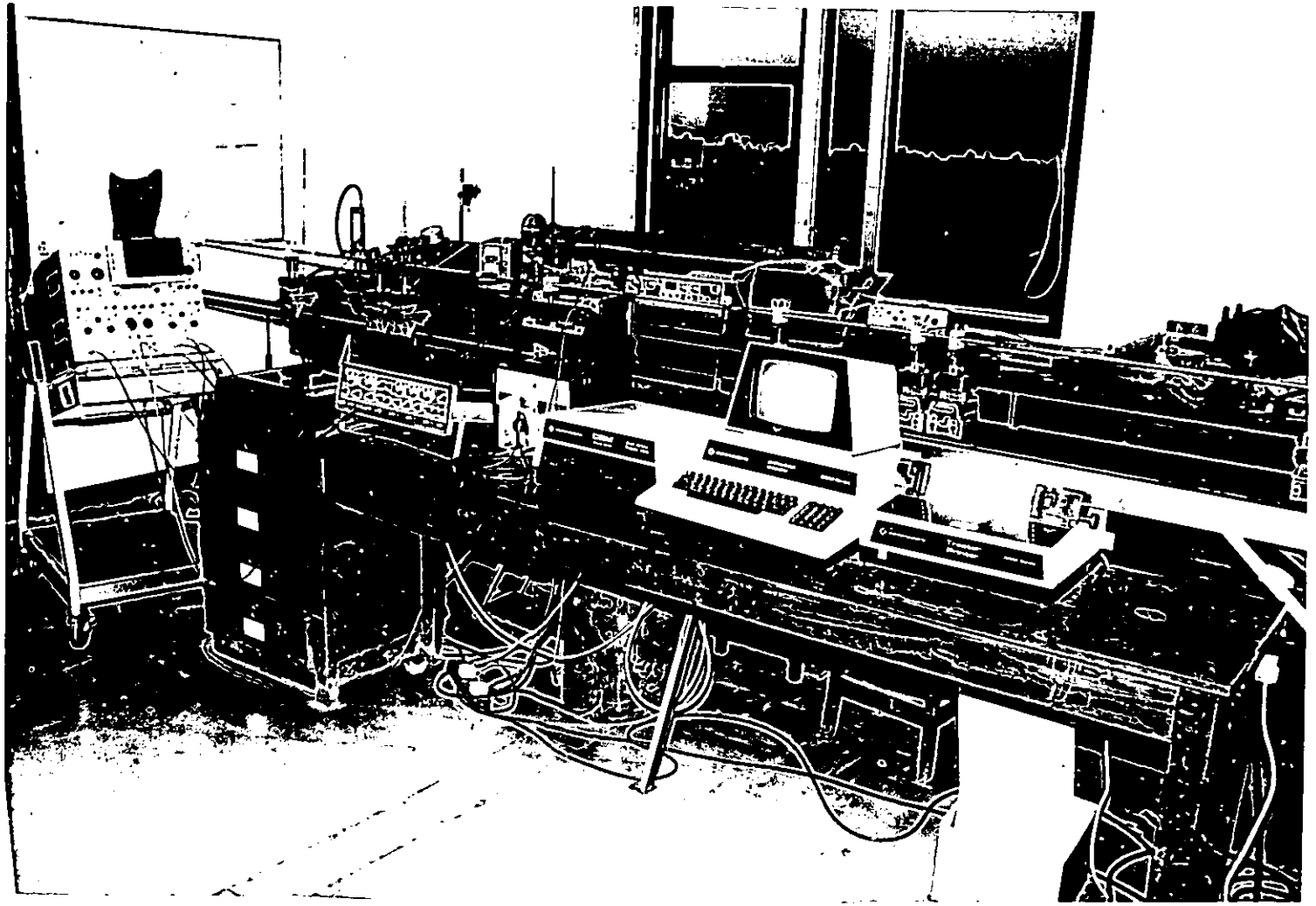

Figure 6.3. Data acquisition and analysis system showing, from left to right, cathode ray oscilloscope, digital plotter, transient recorder, power supply and digital voltmeter, floppy disk drives, microcomputer and tractor printer.

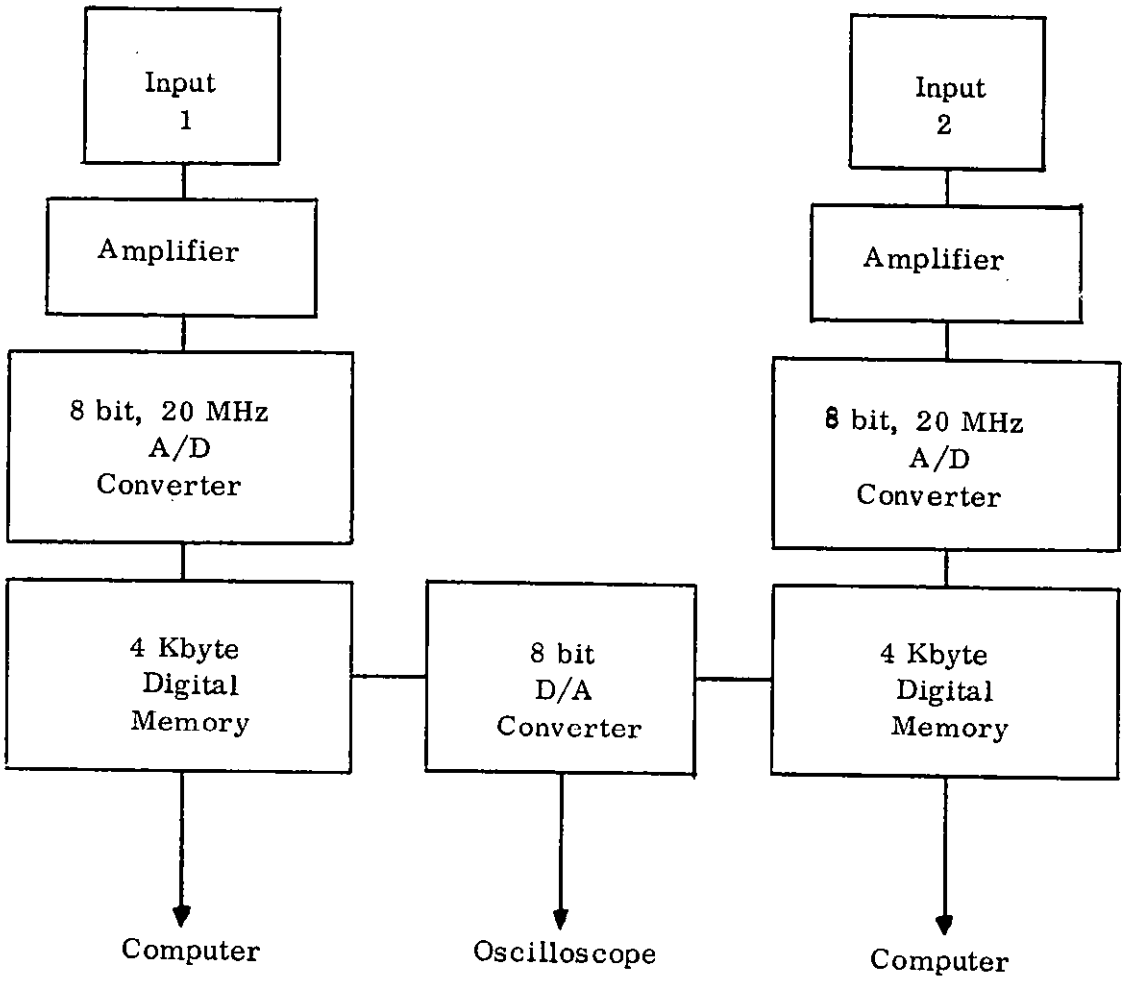

Figure 6.4

Principal functions of the Transient Recorder

As explained in Chapter 3, the temporal resolution (Δt) of the SHPB system is determined by the strain gauge length (ℓ_g) and the longitudinal wave velocity (c_o) in the pressure bars.

$$\Delta t = \frac{\ell_g}{c_o} \tag{6.8}$$

Since ℓ_g = 6mm and $c_o \doteqdot$ 5mm/μs, hence the temporal resolution is approximately 1 μs. Consequently 1MHz is the optimum sampling rate. At this sampling rate, 4ms of data are captured from each strain gauge pair in the 4 kilobyte digital memories.

The resolution of amplitude is ultimately a function of the capability of the transient recorder. By fully utilizing the memory available for each digital sample (8 bits), the best resolution of amplitude is 1 part in 255. Hence, by optimising the system gain so that the digital signal varies from the minimum of the digital memory (zero) to its maximum (255), the signal amplitude can be measured with an accuracy of $\pm$ 2 Δ E where Δ E is the digital error of both extremes of the waveform. In the case of 8 bit digital resolution, Δ E is approximately 0.4%.

When two waveforms of opposite polarities are recorded by the same digital memory, e.g. the incident and reflected pulses, then the amplitude resolution of each waveform is, at best, half of the optimum, i.e. Δ E is 0.8%.

Having captured the waveforms, the transient recorder's

8-bit digital-to-analogue converter transfers the signals to the two inputs of the Tektronix type 556 dual-beam cathode ray oscilloscope (see Figure 6.3). Hence the waveforms from both strain gauge pairs are automatically displayed on the oscilloscope as soon as the Hopkinson bar test has finished. The waveforms remain on the oscilloscope screen until, either the transient recorder is switched off, or the former is switched to the recording mode, in preparation for the next test.

The camera used to photograph the waveforms was manufactured by Shackman Instruments Ltd.

6.1.5 Projectile Velocity Measuring System

The velocity of the projectile is determined from the time taken for the former to travel two consecutive distances of 100mm immediately prior to impact.

The ends of three pairs of optical fibre probes were inserted through holes in the side wall of the gas gun tube at positions A, B and C, as indicated in Figure 3.5. One fibre in each of the pairs acts as a transmitter of white light and the other fibre as a receiver. When the front flange of the 'cotton-reel' shaped PTFE guide passes in turn beneath positions A, B and C the light is reflected to each of the receivers. By converting the light pulse which travels to the other end of each receiver into an equivalent electrical pulse, the time difference between the three pulses and, hence, the time taken for the projectile to travel the distances AB and BC can be

measured by two counter timers.

The conversion of each light pulse to a corresponding electrical pulse is performed by an opto-electronic device. The latter which consists of three identical amplifiers and a 15V power supply, was designed, built and tested by the author during the current investigation.

Figure 6.5 is the circuit diagram of the amplifier. When light is incident upon the high impedance photodiode its resistance is lowered for the duration of this optical pulse. As a consequence the potential of the junction of the photodiode and the 10MΩ resistor is increased during this period of time, i.e. an electrical pulse is generated.

This electrical pulse is fed to the gate of a field effect transistor (f.e.t.) which is operating in the source follower configuration. This has a voltage gain which is only approximately unity but has the virtue of being able to feed a low-impedance load because of its low value of output impedance. The source follower is thus an 'impedance transformer' between the high impedance input (necessary because of the high impedance photodiode) and the following low impedance circuitry.

The following f.e.t. stages provide a total voltage gain of about 130, converting an input of approximately 0.1V to the first stage to an output of 13V.

The fibre optics amplifier is terminated by a bipolar emitter follower stage.

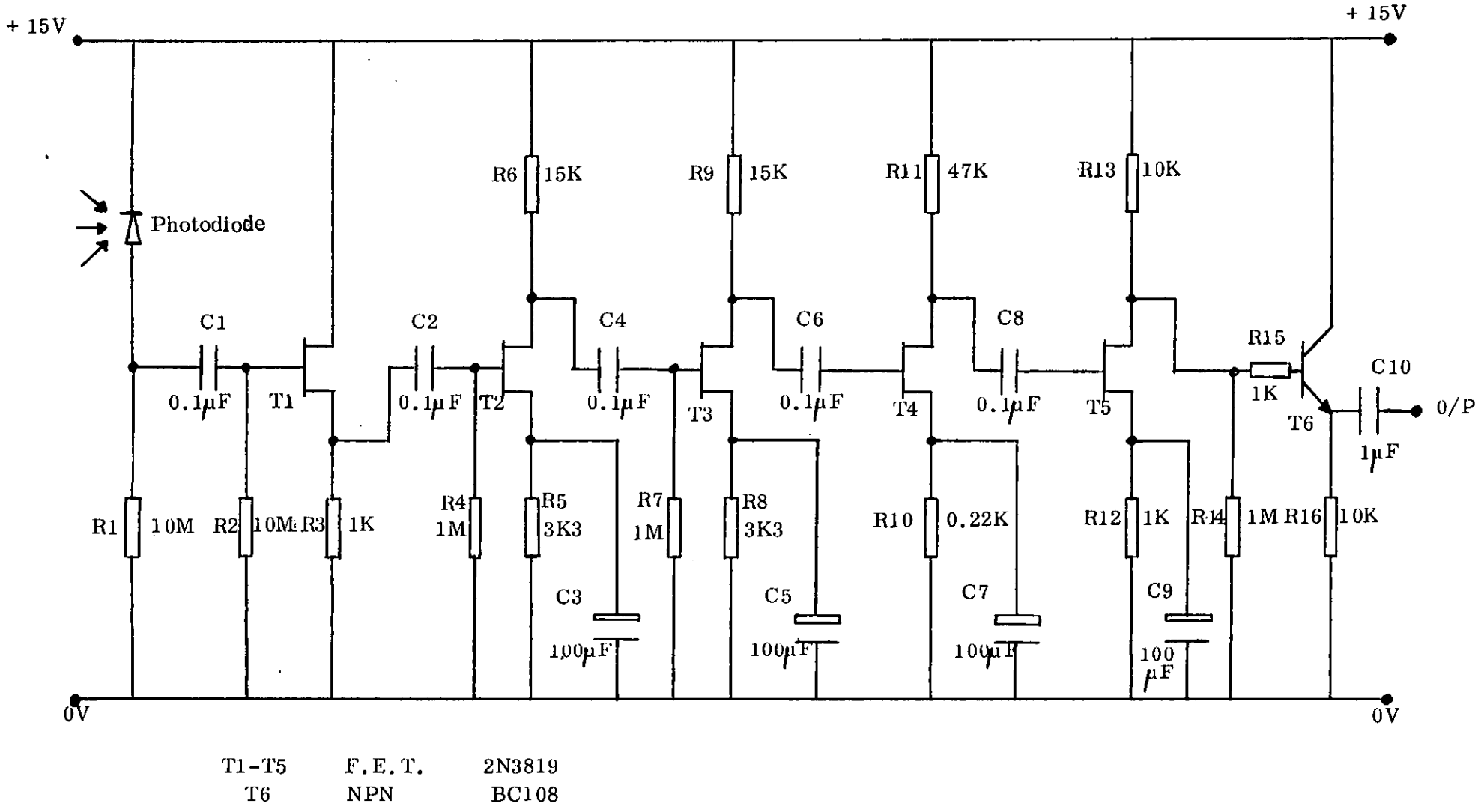

T1-T5	F.E.T.	2N3819
T6	NPN	BC108

Figure 6.5 Circuit diagram of one amplifier in opto-electronic device

The opto-electronic device and the counter timers (RACAL-DANA 9901) can be seen in the left half of Figure 3.4. Note the three pairs of optical fibres connecting the impact end of the gas gun to the opto-electronic device.

6.2 Data Transfer and Analysis

6.2.1 Introduction

A suite of computer programs has been developed for data analysis, data logging and peripheral control. The software was written and executed on a Commodore Professional Computer - 3032 series (commonly known as a PET microcomputer) which was connected to its peripherals via an IEEE 488 interface. The high level language, BASIC was used throughout. The microcomputer and its peripherals are contained in the photograph of Figure 6.3. The micro-computer, slightly to the right of centre, is easily identifiable by its TV monitor. To the left of the PET are the CBM 5 1/4-inch dual floppy disk drives (model 4040) and to the right is the Commodore tractor printer (3022 series). To the left of the main bench of instruments, and adjacent to the transient recorder, is the PD4 digital graph plotter (J.J. Lloyd Instruments Ltd.)

6.2.2 Data Transfer

Immediately following a test, data are transferred, under software control, from the transient recorder to the computer's memory and subsequently for permanent storage to a floppy diskette in one of the disk drives.

The transference to the computer memory is accomplished in less than one second. To reduce the amount of data permanently stored on diskette and to shorten the transfer time, the amount of data passed to a diskette is usually limited to 400 bytes (or samples) from each transient recorder digital memory, i.e. only 10% of the data captured by the transient recorder is permanently stored. The 400 bytes of data, of course, include the incident, reflected and transmitted pulses in their entirety.

6.2.3 Data Analysis and Presentation of Results

Having made 'hard' copies of the strain data from the strain gauges, analysis, according to the Hopkinson Bar theory of Chapter 3, can be completed at any future time without the risk of data loss through power failure etc.

The software routines permit the results of the analysis to be listed either in engineering terms, or in their true or natural, form. Table 6.1 exemplifies both engineering and true stress/strain/strain rate results. The results were produced on the tractor printer. There is also an option for listing the digital data, in the form that they are stored in the transient recorder. Table 6.2 is a typical listing of these digital strain gauge data.

Software written for the digital graph plotter facilitates the display of data and results in a variety of formats. Examples of these are included in Figures 6.6 to 6.10, all of which refer to the same test. These show raw test data and results. No smoothing or averaging has been performed.

Table 6.1 Typical results listing

FILENAME = COC40080026DAP3

TRUE STRESS/STRAIN RESULTS

TIME (10^-6 SEC)	STRESS (MPA)	STRAIN (%)	STRAIN RATE (/SEC)
.00	1.676-	.000	.000
1.00	.000	.003	34.957
2.00	.000	.011	81.571
3.00	6.703	.023	116.542
4.00	15.081	.036	128.211
5.00	21.780	.053	174.860
6.00	35.174	.078	244.857
7.00	46.882	.113	349.899
8.00	55.229	.158	455.052
9.00	61.890	.213	548.672
10.00	68.534	.281	677.499
11.00	71.819	.361	806.590
12.00	66.752	.447	854.057
13.00	63.356	.538	913.361
14.00	61.635	.626	879.019
15.00	68.236	.716	903.265
16.00	73.157	.815	986.311
17.00	78.063	.920	1046.082
18.00	81.300	1.024	1047.178
19.00	84.532	1.127	1024.707
20.00	81.134	1.229	1025.758
21.00	74.433	1.333	1038.620
22.00	77.659	1.438	1051.520
23.00	82.532	1.541	1028.960
24.00	89.042	1.644	1030.020
25.00	90.599	1.746	1019.225
26.00	87.212	1.852	1055.874
27.00	90.404	1.961	1092.639
28.00	88.663	2.072	1105.730
29.00	93.486	2.181	1095.045
30.00	98.302	2.287	1060.479
31.00	96.564	2.390	1025.802
32.00	94.827	2.496	1062.695
33.00	93.090	2.606	1099.704
34.00	97.881	2.716	1100.915
35.00	104.290	2.827	1114.115
36.00	107.431	2.938	1103.357
37.00	107.312	3.048	1104.577
38.00	105.572	3.156	1081.746
39.00	105.459	3.264	1070.878
40.00	108.588	3.371	1072.026
41.00	111.708	3.479	1085.242
42.00	111.585	3.589	1098.499
43.00	111.462	3.699	1099.707
44.00	111.338	3.810	1113.022
45.00	116.050	3.922	1114.262
46.00	115.922	4.032	1103.374
47.00	117.402	4.143	1104.592
48.00	117.272	4.253	1105.814
49.00	117.141	4.365	1119.210
50.00	118.609	4.481	1157.022
51.00	124.874	4.598	1170.563
52.00	124.730	4.713	1147.505
53.00	127.785	4.825	1124.366
54.00	127.641	4.938	1125.638
55.00	127.494	5.053	1151.413
56.00	130.533	5.167	1140.469
57.00	127.200	5.283	1166.341
58.00	128.642	5.399	1155.404
59.00	133.252	5.515	1156.741
60.00	133.096	5.632	1170.401
61.00	137.690	5.748	1159.437
62.00	137.534	5.861	1136.073
63.00	137.374	5.977	1162.103
64.00	140.370	6.093	1151.070
65.00	143.363	6.205	1127.601
66.00	143.198	6.321	1153.698
67.00	144.604	6.436	1155.031
68.00	142.867	6.552	1156.367
69.00	144.270	6.668	1157.705
70.00	148.802	6.784	1159.047
71.00	150.194	6.900	1160.392
72.00	151.582	7.016	1161.740
73.00	151.406	7.132	1163.091
74.00	151.230	7.248	1164.446
75.00	151.053	7.365	1165.803
76.00	150.879	7.481	1154.607
77.00	153.806	7.600	1193.657
78.00	156.732	7.716	1157.323
79.00	156.551	7.831	1158.664
80.00	161.018	7.945	1134.775
81.00	159.288	8.059	1136.065
82.00	160.650	8.174	1150.002
83.00	158.922	8.289	1151.325
84.00	163.363	8.404	1152.653
85.00	163.174	8.519	1153.985
86.00	161.450	8.634	1142.613
87.00	165.878	8.745	1118.485
88.00	168.760	8.857	1119.738
89.00	168.575	8.967	1095.502
90.00	162.255	9.084	1173.263
91.00	169.716	9.198	1136.315
92.00	169.527	9.309	1112.022
93.00	170.862	9.422	1126.071
94.00	175.245	9.532	1101.705
95.00	175.057	9.640	1077.257
96.00	174.875	9.744	1039.884
97.00	174.702	9.843	989.534
98.00	174.542	9.934	913.297
99.00	177.436	10.014	798.209
100.00	178.830	10.082	682.846
101.00	175.702	10.137	554.350
102.00	178.662	10.176	386.937
103.00	172.568	10.198	219.331
104.00	164.993	10.202	38.710
105.00	149.871	10.192	103.224
106.00	131.730	10.172	193.517
107.00	110.559	10.148	245.068
108.00	90.891	10.126	219.220
109.00	71.211	10.107	193.390
110.00	54.553	10.091	154.685
111.00	40.919	10.081	103.110
112.00	28.797	10.072	90.212
113.00	22.736	10.065	64.432
114.00	18.190	10.059	64.428
115.00	13.643	10.054	51.539
116.00	10.612	10.050	38.650
117.00	10.612	10.050	.000

ENGINEERING STRESS/STRAIN RESULTS

TIME (10^-6 SEC)	STRESS (MPA)	STRAIN (%)
.00	1.676-	.000
10.00	68.727	.280
20.00	82.138	1.222
30.00	100.577	2.261
40.00	112.311	3.315
50.00	124.045	4.382
60.00	140.808	5.476
70.00	159.247	6.559
80.00	174.333	7.638
90.00	177.686	8.684
100.00	197.801	9.590
110.00	60.346	9.599
120.00	20.115	9.559
130.00	11.734	9.539

Table 6.2 Typical digital strain gauge data listing

INCIDENT BAR DATA PTS 1 TO 500 COC+0080026DAP3

DATA PT NO	DATA VALUES									
1	132	132	133	134	134	134	135	130	132	134
11	133	133	133	132	132	132	132	134	134	135
21	133	133	133	134	134	134	134	134	134	133
31	134	132	132	133	132	133	132	132	132	132
41	132	133	133	134	133	133	133	133	139	139
51	141	141	145	150	159	171	195	213	230	244
61	252	255	255	251	248	248	251	255	255	255
71	255	255	255	255	255	255	255	255	255	255
81	255	255	255	255	255	255	255	255	255	255
91	255	255	255	255	255	255	255	255	255	255
101	255	255	255	255	255	255	255	255	255	255
111	255	255	255	255	255	255	255	255	255	255
121	255	255	255	255	255	255	255	255	255	255
131	255	255	255	255	255	255	255	255	255	255
141	255	255	255	255	255	255	255	255	255	255
151	255	255	255	255	255	255	255	255	255	255
161	130	166	157	150	144	142	139	239	217	197
171	143	142	140	134	135	137	138	141	142	144
181	133	137	137	133	137	135	134	139	139	139
191	133	136	133	133	137	133	139	137	137	139
201	132	135	132	130	126	123	122	134	131	131
211	94	86	75	64	60	49	42	118	112	103
221	49	55	53	56	49	44	44	37	37	43
231	44	46	46	47	44	41	40	46	46	45
241	44	41	41	40	41	41	43	41	44	47
251	42	42	41	41	42	42	42	44	44	43
261	39	41	41	39	40	38	39	41	38	37
271	41	39	40	42	41	41	41	39	38	39
281	41	41	41	41	42	39	42	41	41	41
291	43	43	43	43	44	46	46	42	44	44
301	47	46	48	50	53	57	63	48	42	45
311	104	117	131	142	149	153	151	72	81	91
321	141	139	139	138	137	134	134	149	146	142
331	139	138	135	134	135	136	135	134	136	137
341	139	136	135	132	132	132	134	134	134	141
351	133	132	133	133	134	135	135	135	134	134
361	133	133	133	132	132	133	134	135	134	134
371	133	134	135	133	132	132	132	133	133	132
381	135	136	132	132	133	134	133	131	133	134
391	134	134	134	133	133	133	135	133	133	135
401	133	133	133	133	133	132	132	135	134	133
411	133	133	135	133	133	133	135	132	132	132
421	133	134	134	130	130	133	136	134	135	134
431	137	139	140	140	144	147	151	135	135	135
441	172	180	186	191	200	207	214	156	160	166
451	237	236	234	231	227	225	226	221	228	233
461	233	234	223	224	223	221	224	223	234	238
471	227	222	222	221	223	223	224	227	227	229
481	223	223	223	226	225	224	223	227	226	224
491	225	223	224	226	226	225	224	223	224	224

TRANSMITTER BAR DATA PTS 1 TO 500 COC+0080026DAP3

DATA PT NO	DATA VALUES									
1	129	128	129	130	131	130	131	125	128	130
11	130	131	129	128	128	128	129	131	131	132
21	130	130	130	129	130	130	131	131	130	129
31	130	129	129	129	129	129	128	129	129	128
41	128	130	131	132	129	129	131	129	135	135
51	134	131	130	129	129	129	127	128	131	130
61	129	129	128	128	128	129	129	128	129	130
71	129	129	129	131	130	129	128	129	128	128
81	127	129	128	128	128	127	127	127	128	134
91	132	131	130	128	129	129	129	129	128	130
101	129	127	127	129	129	129	128	128	129	128
111	128	130	130	130	129	130	130	127	128	130
121	129	129	129	129	129	128	129	129	128	127
131	128	130	128	127	129	131	129	129	129	130
141	128	129	129	129	129	129	128	128	128	128
151	130	129	129	129	127	128	129	130	130	130
161	129	129	128	128	128	129	129	129	130	130
171	128	129	127	122	126	129	130	130	128	128
181	129	129	129	131	130	129	128	130	129	129
191	129	128	129	128	127	128	128	128	128	128
201	130	129	127	129	129	128	128	127	127	128
211	128	132	137	141	152	153	163	167	169	171
221	168	166	165	169	172	175	177	179	177	173
231	175	178	182	183	181	183	182	185	188	187
241	186	185	188	192	194	194	193	193	195	197
251	197	197	197	200	200	201	201	201	202	206
261	206	208	203	208	210	208	209	212	212	215
271	215	215	217	219	219	220	219	220	223	224
281	225	225	225	225	225	227	229	229	232	231
291	232	231	234	234	233	236	238	238	234	239
301	239	240	243	243	243	243	243	245	246	244
311	246	242	237	229	218	204	188	175	162	153
321	147	140	140	137	135	135	137	138	140	141
331	141	138	134	134	137	136	136	136	135	144
341	142	138	135	133	132	132	135	136	135	134
351	134	134	134	134	136	135	134	133	132	132
361	133	132	131	131	133	134	132	132	131	131
371	133	133	132	132	132	132	131	131	133	133
381	133	135	131	131	131	132	132	131	133	135
391	132	132	132	131	132	132	133	133	131	139
401	130	130	132	132	130	130	130	133	131	129
411	131	131	131	130	129	131	132	131	131	130
421	130	130	130	125	128	130	133	132	132	129
431	130	131	131	131	132	128	128	127	125	125
441	123	121	117	111	106	100	95	92	88	87
451	89	90	90	92	91	90	89	86	84	81
461	79	79	79	81	86	82	80	74	70	69
471	72	72	70	68	67	64	63	63	64	63
481	62	61	59	58	56	54	54	54	54	55
491	51	49	50	48	48	47	45	43	44	234

Figure 6.6 STRESS V STRAIN

TEST MATERIAL – COPPER
TEST TYPE – COMPRESSION
TEST TEMP – 020 C
ANNEALING TEMP – 600 C
TEST CODE – COC02060025SBP0

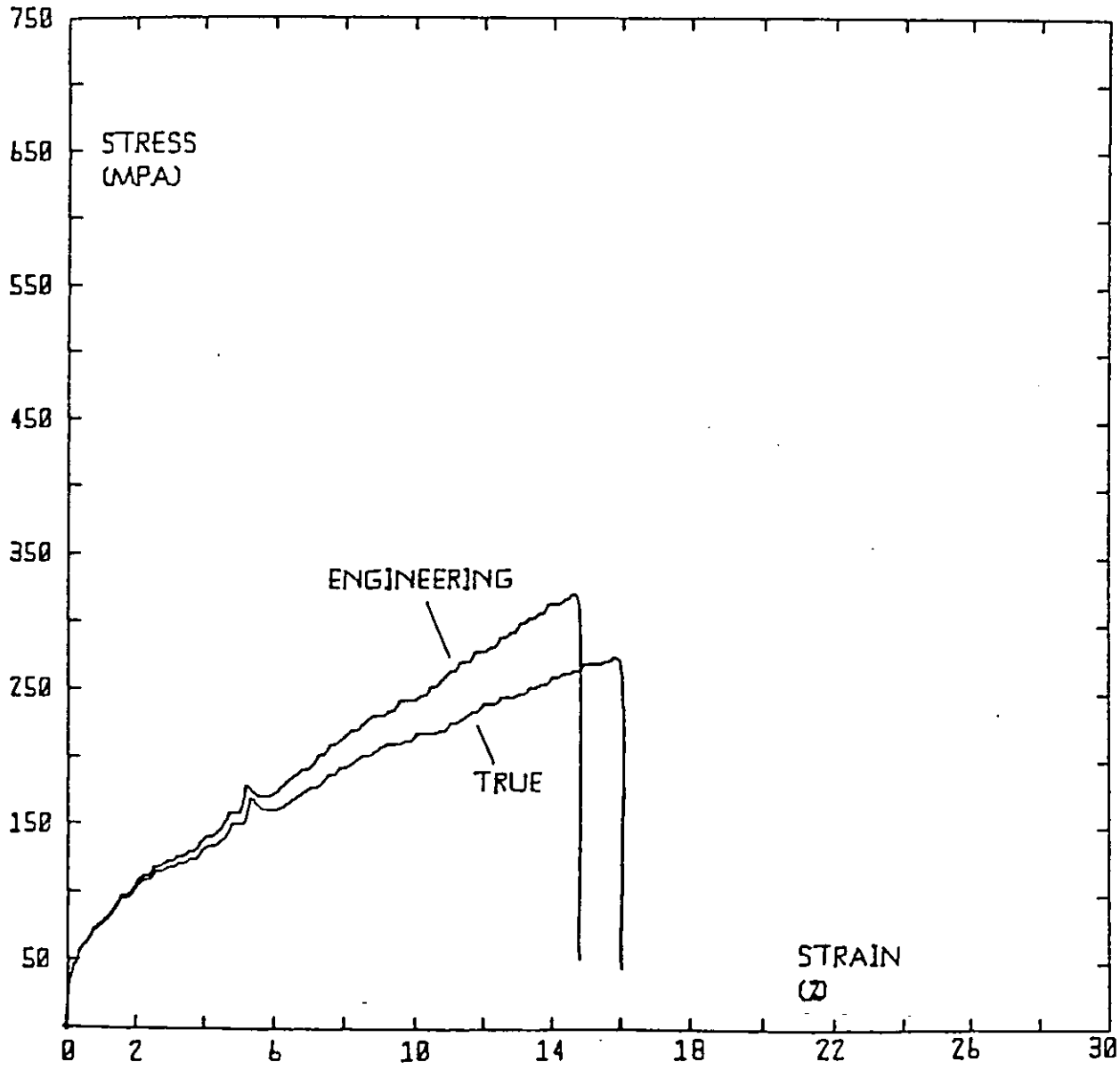

Figure 6.7 STRESS V TIME

TEST MATERIAL - COPPER
TEST TYPE - COMPRESSION
TEST TEMP - 020 C
ANNEALING TEMP - 600 C
TEST CODE - COC020600255BP0

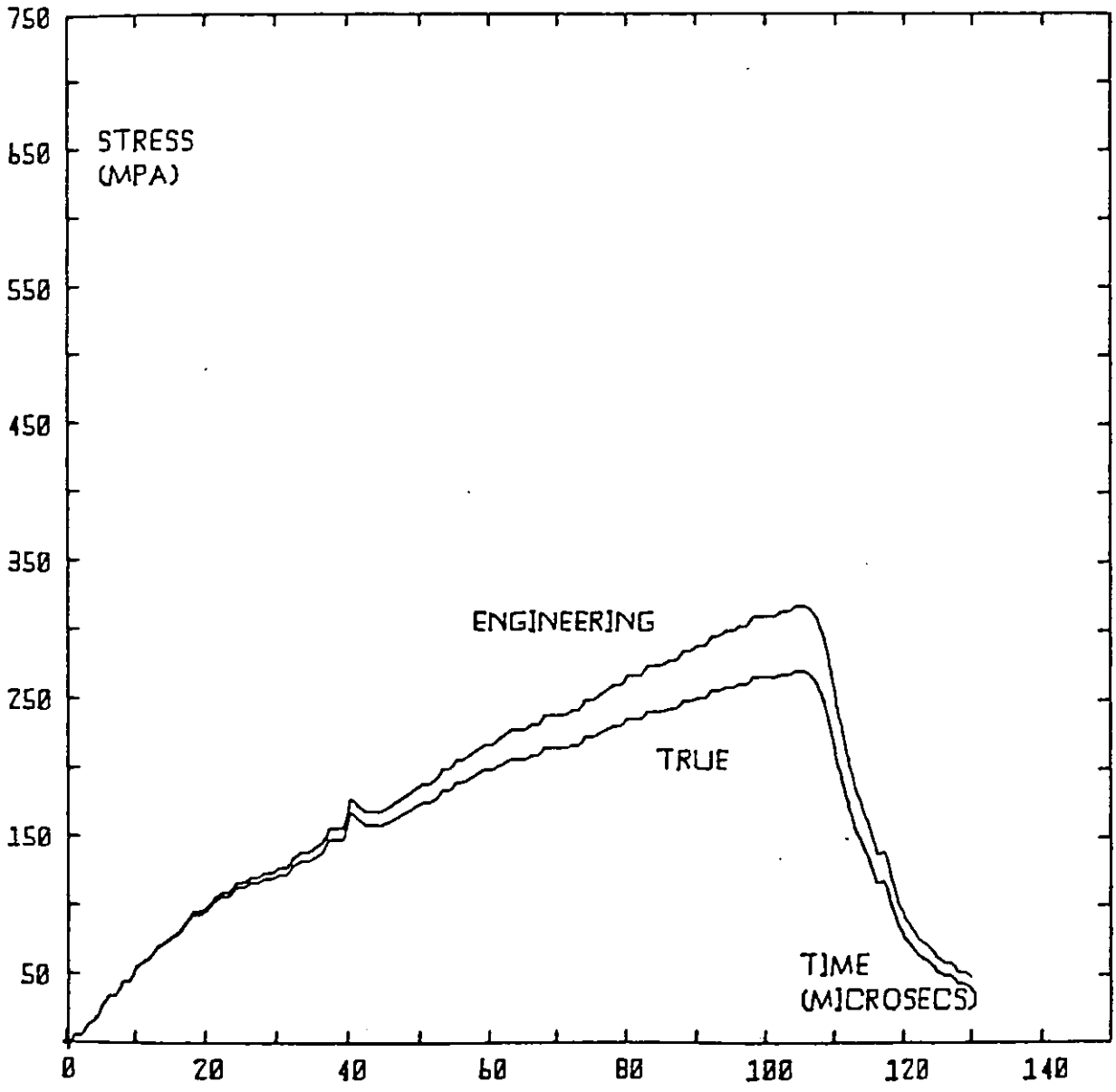

Figure 6.8 STRAIN V TIME

TEST MATERIAL - COPPER
TEST TYPE - COMPRESSION
TEST TEMP - 020 C
ANNEALING TEMP - 600 C
TEST CODE - COC0Z0600Z5SBP0

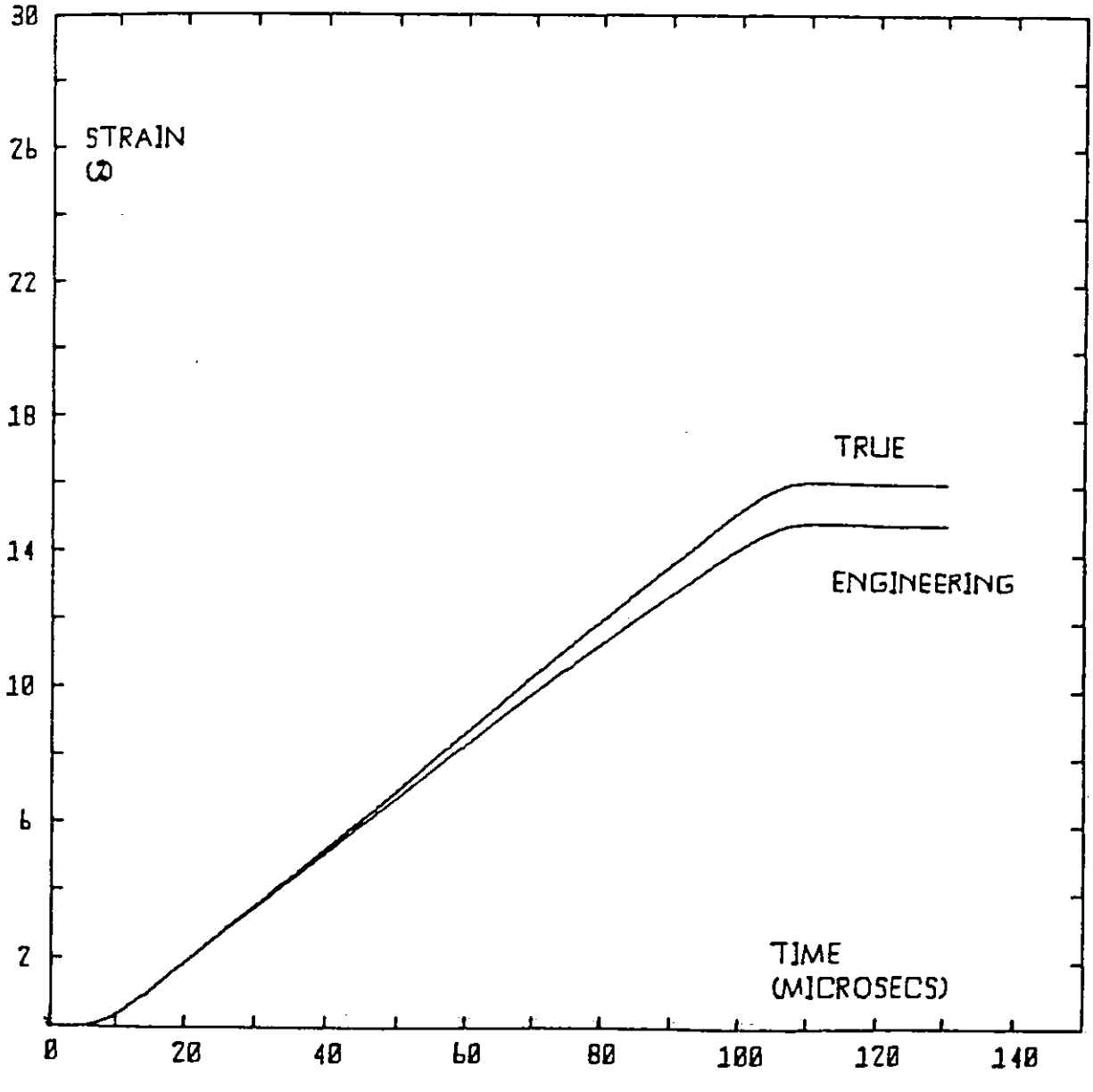

Figure 6.9 TRUE STRAIN RATE V TIME

TEST MATERIAL - COPPER
TEST TYPE - COMPRESSION
TEST TEMP - 020 C
ANNEALING TEMP - 600 C
TEST CODE - COC0206002SSBP0

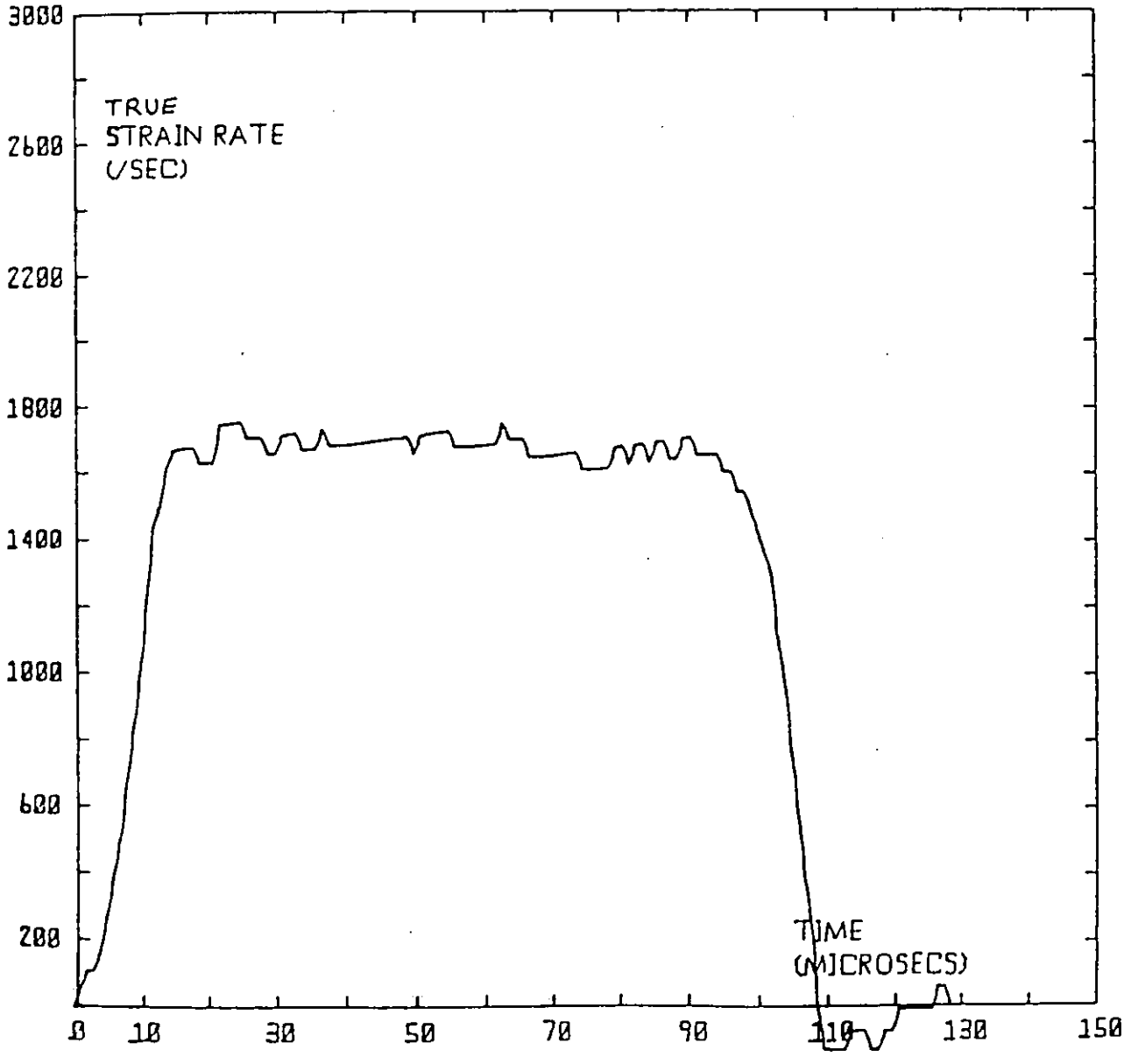

Figure 6.10 STRAIN IN INCIDENT & TRANSMITTER BARS V TIME

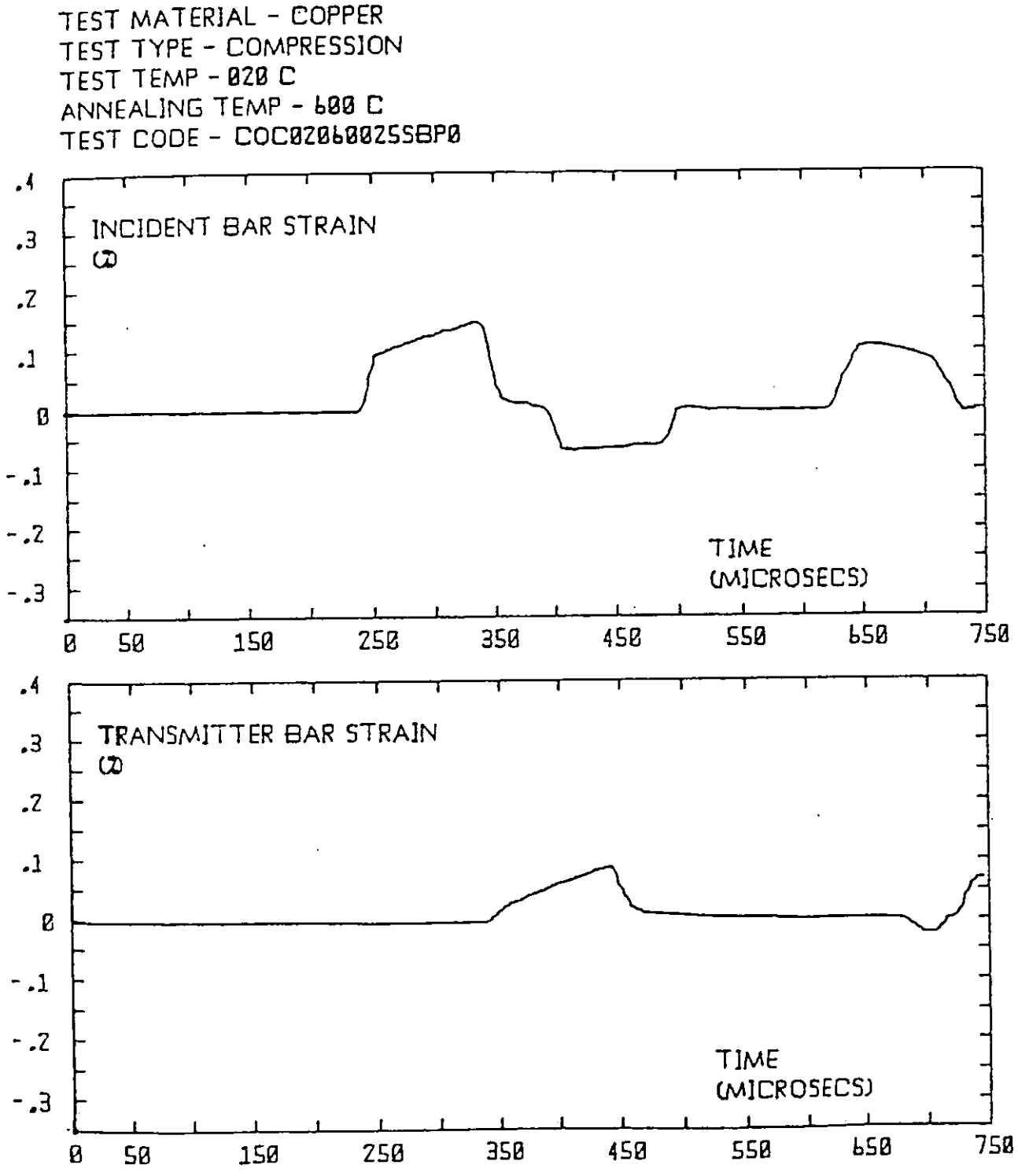

Notice in particular:

(i) the constant true strain rate (Figure 6.9),

(ii) how stress and strain vary in opposite senses when the 'engineering-true' correction is applied (Figures 6.7 and 6.8),

(iii) the smooth strain vs. time curves resulting from the integration of the reflected pulse (Figure 6.8).

6.3 Description of the Software Packages

The suite of computer programs which:

(a) control the transfer of data from the transient recorder to the computer,

(b) control the transfer of data from the computer to a floppy diskette,

(c) analyse the data according to instructions from the computer keyboard, and

(d) control the remaining peripherals, viz the graph plotter and the tractor printer, consist of three software packages. These are:

(i) HOPK-BAR

(ii) GRAPHS

(iii) TR-AUTO-CTRL.

Full program listings are included in Appendices A, B and C.

HOPK-BAR is the main routine and controls the operation of the other two routines. Only one of the routines is present in the computer memory at any one time. This is decreed by the 32 kbytes of random access memory (RAM) of the PET microcomputer which is insufficient for the total memory requirements of the three routines, i.e. 67 kbytes.

6.3.1 HOPK-BAR (listing in Appendix A)

The functions performed by the HOPK-BAR program are listed in Table 6.3. This table - the Hopkinson Bar Directory - is displayed on the computer's visual display unit (VDU) immediately after program initialisation has been completed. The function of each entry in the directory is described from section 6.3.1(c) to 6.3.1(m).

(a) Initialisation (Appendix A: Lines 10-106)

In this portion of the program all variables are assigned their initial or constant values and the initial headings are displayed on the VDU. The values of Young's modulus, longitudinal acoustic velocity and mechanical impedance are selected by the program according to the pressure bars' material (see lines 102-106).

(b) Display of Hopkinson Bar Directory (Appendix A: Lines 108-260)

See Table 6.3.

Table 6.3

Hopkinson Bar Directory

1. Transfer data from transient recorder to PET
2. Hopkinson Bar data analysis
3. Instron data input & analysis
4. List data
5. List results
6. Draw graphs
7. Parameters entered from keyboard
8. Bar strain & impact velocity
9. Execute transient recorder operational software
10. Average of results files
11. Finish

Table 6.4

Directory of Graphs

1. Stress v. Strain
2. Stress v. Time
3. Strain v. Time
4. Strain Rate v. Time
5. Strain Gauge Data v. Time
6. Bar Strain v. Time
7. Incident Pulse v. Time
8. Reflected Pulse v. Time
9. Transmitted Pulse v. Time
10. Hopkinson Bar Menu

(c) Transfer Data from T.R. (Transient Recorder) to Pet (Microcomputer) (Appendix A: Lines 1000-1500)

In preparation for the transfer of the data from channels 1 and 2 of the transient recorder to files on a floppy diskette, 2 filenames are created which correspond to the parameters of the dynamic tests which has just been completed (lines 1003-1025).

For example, if the test parameters are:

Material tested: COpper
Compressive or Tensile: Compressive
Test Temp: 400^{o}C
Annealing Temp: 310^{o}C
Projectile Time (1 to 2) : 5ms
Projectile Time (2 to 3): 5ms
Steel or Duralumin Projectile: S
Identity Letter: A

then the filename for the channel 1 data is:

COC40031020SA1

and the filename for the channel 2 data is:

COC40031020SA2

where 20 is the projectile velocity in ms^{-1} corresponding to the projectile times of 5ms between the optical probe positions 1 and 2, and 2 and 3. If a pulse shaper is also

used and its annealing temperature is 600^{o}C (say) then the filenames will be COC40031020SAP61 and COC40031020SAP62, respectively. The disk drive for data storage is chosen in lines 1030 and 1031. In lines 1032 to 1048 the number of bytes of data to be stored from channel 1 of the transient recorder, is selected.

The routine TR-AUTO-CTRL is loaded into RAM (replacing HOPK-BAR) at line 1100. This routine then controls the transfer of data from the transient recorder, channel 1, to the floppy diskette. The whole process is repeated for channel 2 data in lines 1200 to 1320.

A third filename, e.g. COC40031020SAP63, is created into which further parameters, entered via the computer keyboard, are stored. These parameters are listed in lines 1342 to 1399, and transferred to the floppy diskette in lines 1400 to 1500.

(d) Hopkinson Bar Data Analysis
(Appendix A: Lines 3000 - 4999)

This function of HOPK-BAR can be used at any time after a test has been completed and the recorded data stored on the three diskette files.

In lines 3010-3092, the third file, i.e. the file containing parameters previously entered via the computer keyboard, is read back into RAM.

If the strain gauge amplifiers invert the Hopkinson Bar

signals then lines 3150-3170 set flags A1 and A2 accordingly.

Lines 3210-3260 relate to equation (6.7), which converts the change in voltage (dVs) across each strain gauge to strain (ε). Gain factors are also included, i.e. G1 and G2 - the gains of the strain gauge amplifiers, V1 and V2 - the full scale voltages of the input channels of the transient recorder.

Lines 3799 - 3800 determine whether the transmitted pulse is stored in the file with a suffix of 1 or a suffix of 2. The multiplying factor PP is set to + 1 or - 1, accordingly.

The number of data points comprising the transmitted pulse, and consequently, also the combined incident and reflected pulses, are determined and displayed on the VDU in lines 3805-3812. The transmitted pulse is read into RAM using the subroutine call in line 3820 and its starting point is automatically found from the subroutine call of line 4025.

If any large, high frequency 'spikes' appear in the transmitted pulse data, these are removed in lines 4100-4290.

The baseline or zero voltage level of the transmitted pulse is determined by averaging the 15 data points occurring immediately prior to the start of the pulse (lines 4297-4345). If an inspection of the transmitted pulse data casts doubt on the computer determined baseline value, the operator can override this value in lines 4346-4349.

Engineering stress versus time is calculated in lines 4370-4394, using equation 3.12.

The file containing the incident and reflected pulses is read into memory in lines 4410-4426 and the starting times of each pulse are found in lines 4427-4441.

The most reliable means of automatically determining the baseline for the incident and reflected pulses was to average the data occurring immediately after the reflected pulse (lines 4445-4456). As before, this baseline value can be altered by the operator (lines 4457-4460).

The next stage of the data analysis determines whether the pressure bars were aligned correctly with the test specimen. In the case of imperfect alignment there will be a delay in the arrival of the transmitted pulse at the bar 2 strain gauges, relative to the arrival of the reflected pulse at the bar 1 gauges (see lines 4470-4485). Figures 6.11(a) and 6.11(b) indicate the shape of the reflected pulse for perfect and imperfect alignments, respectively. When such an imperfect impact occurs, either, the test data can be discarded or the reflected pulse modified. The latter is achieved by removing the initial part of the pulse, which relative to the transmitted pulse arrived too soon so that the modified pulse rises as shown by the dotted line in Figure 6.11(b). The portion of the program which automatically performs this pulse modification runs from line 4487 to line 4530. Lines 4535-4568 permit the operator to override the start and end points of the modified portion of the reflected pulse.

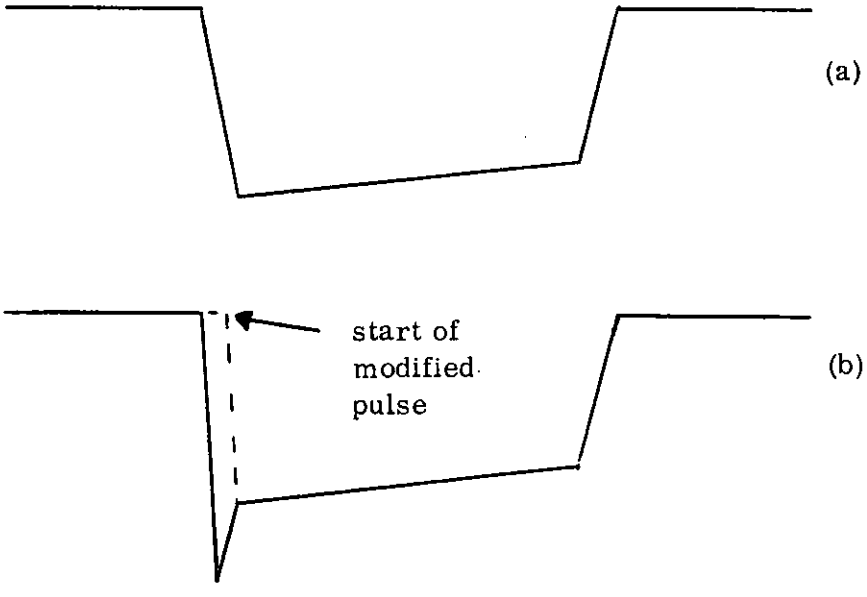

Figure 6.11

(a) Reflected pulse from perfectly aligned specimen
(b) Reflected pulse from imperfectly aligned specimen

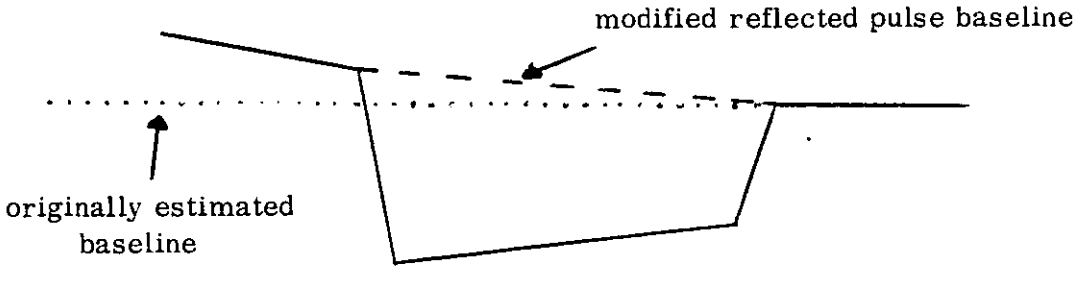

Figure 6.12

Reflected pulse sloping baseline correction

Lines 4561-4579 perform a further, and final, correction to the reflected pulse data, if necessary. This correction is required if the reflected pulse commences or terminates at a strain level above or below the zero strain level of the baseline. In effect, the correction introduces a sloping baseline so that the values of strain at either end of the reflected pulse are set to zero. An example of this sloping baseline correction is incorporated in Figure 6.12, where the dotted line indicates the previously estimated horizontal baseline, and the dashed line is the sloping baseline correction. The sloping baseline correction is defined by the expression contained in line 4577.

The variation of engineering strain in the specimen with time is calculated in lines 4589-4703 (see equation 3.7).

The computer code in lines 4910-4962 is used to convert the engineering values of the mechanical parameters into their true counterparts, i.e. true stress, strain and strain rate. Line 4930 is equivalent to equation 3.20 and line 4940 to equation 3.21. Notice that the value of PP is + 1 or -1 for tensile tests or compressive tests, respectively.

The option to store the values of true stress, strain and strain rate on a floppy diskette is given in line 4970; lines 4975-4995 being used to transfer these values from RAM to diskette.

(e) Instron Data Input and Analysis
(Appendix A: Lines 18000-18410)

This directory option permits the input of data obtained from the Instron quasi-static tests, via the computer keyboard, and then performs analyses on these data, eventually ending up with results in the true stress, strain, strain rate format, as in the previous Hopkinson Bar Data Analysis option.

Data are entered in the form of load, chart displacement equivalent to specimen displacement and chart displacement equivalent to machine compliance (lines 18035-18060). Note that all three variables are expressed in millimetres, as read directly from the chart. Having input all the data from the keyboard, this can now be stored on diskette, the filename being constructed, as in 6.3.1(c) (lines 18085-18185). Data Analysis can now proceed immediately or at a later time by recalling these data from diskette to memory (lines 18021-18030). During the analysis further information is entered via the keyboard, i.e. cross head speed (mm/min), chart speed (mm/min), full scale load (kg), specimen gauge length (mm) and specimen diameter (mm). Specimen extension (mm) v. load (kg) is calculated in lines 18327-18345, and engineering stress (MPa) and strain in lines 18375-18395. Finally true stress, strain and strain rate are calculated using the same statements as in 6.3.1(d), i.e. lines 4910-4962.

(f) List Data (Appendix A: Lines 2000-2390)

Having entered the name of the file holding the data (line 2000), via the computer keyboard, the disk file is read into the PET's memory. The number of data points in this file is printed on the VDU from line 2187 and the operator then selects how much of this data is to be displayed (lines 2190-2200). In lines 2201-2260 one of two display media is chosen, i.e. either the VDU screen or the printer. The program determines in lines 2352 and 2353 whether the data are from bar 1, i.e. incident pulse data from a compressive test, or from bar 2, i.e. transmitted pulse data from a compressive test. For data from a tensile test, of course, incident and transmitted pulse data are derived from bar 2 and bar 1, respectively. The remainder of the List Data option prints the heading, below which the data is listed (see Table 6.2).

(g) List Results (Appendix A: Lines 5000-5620)

This section of the HOPK-BAR program commences (lines 5010-5040) by listing, on the VDU, a short directory or menu of options of the form:

RESULTS

1. TRUE STRESS/STRAIN
2. ENGINEERING STRESS/STRAIN
3. RETURN TO HOPK BAR MENU

SELECT CODE:

From the appropriate choice of code 1 or code 2, the results are printed as in Table 6.1.

The options of displaying the results on the VDU or the printer are given in lines 5050-5090.

Line 5100 allows the operator to choose the time interval (in microseconds) between each line of results, i.e. although stress/strain/strain rate results are calculated from every microsecond of data, the results can be summarised by, for example, printing the results at intervals of 5 microseconds.

Lines 5301-5345 print the results headings on the chosen medium and these are followed by the table of results (lines 5350-5368). If the results to be printed are not currently in RAM and have been previously stored on diskette file, then lines 5500-5620 permit the operator to select the results' filename, the contents of which are then transferred to RAM.

(h) Draw Graphs (Appendix A: Lines 6000-6100)

Line 6050 indicates that the graph plotting program is being loaded into memory from a diskette filename. Line 6100 performs this transfer.

Full details of the graph plotting program (GRAPHS) are given in section 6.3.2.

(i) Parameters Entered From Keyboard
(Appendix A: Lines 7000-7300)

A list of all parameters entered from the computer keyboard prior to an impact test can be obtained by selecting this option. The format of this list is given in lines 7110-7276.

The list can either be displayed on the screen or the printer according to the operator's reply to line 7023.

(j) Bar Strain and Impact Velocity
(Appendix A: Lines 8000-8160)

This option calculates and prints the strains recorded by the pairs of strain gauges mounted on bars 1 and 2. In addition, it can be used to translate the strain produced by impact into the projectile velocity; the latter can then be compared with that calculated from the projectile velocity measuring system. Results agreed to better than 10%.

(k) Execute T.R. (Transient Recorder) Operational Software
(Appendix A: Lines 14000-14010)

Option number 9 loads the third software package into the computer memory. This package, TR-AUTO-CTRL, is a modified version of the DL912 transient recorder control software written by the manufacturers, Datalab.

TR-AUTO-CTRL includes the control software which transfers the strain gauge data from the transient recorder to the

microcomputer.

(l) Average of Results Files
(Appendix A: Lines 15000-15680)

This is an unfinished option to permit the user to automatically find the mean of several stress-strain curves taken from tests with nominally the same strain rate.

(m) Finish (Appendix A: Lines 20000)

By selecting this option the operator exits from the suite of computer programs.

The memory requirements of HOPK-BAR are 22 kbytes for the BASIC program and 10 kbytes for the data, i.e. a total of 32 kbytes are required.

6.3.2 GRAPHS (listing in Appendix B)

This software package also commences by displaying a directory or menu of options on the VDU. This directory of graphs is listed in Table 6.4.

The function of each entry in the directory is described from section 6.3.2(c) to 6.3.2(l).

(a) Initialisation (Appendix B: Lines 85-336)

As in 6.3.1(a), a number of variables are assigned their initial or constant values in this section of the program.

In addition, line 200 activates the graph plotter, line 310 determines the size of the print used in labelling the axes, line 320 selects the orientation of the print and in lines 330-336 the position of the origin of each graph is chosen.

(b) Display of Graphs Directory
(Appendix B: Lines 400-950)

See Table 6.4.

(c) Stress v. Strain
(Appendix B: Lines 2200-2251 & Lines 2600-2652)

The two groups of lines listed above perform very similar tasks. The former group (lines 2200-2251) deal with engineering stress and engineering strain data, whereas the latter deal with true stress and true strain data.

In lines 2216-2240 and 2610-2625 the data are converted to stress in MPa and strain in %, respectively. If the results are extracted from a disk file then the latter is converted in lines 2637-2640.

Lines 2344-2350 and 2644-2650 arrange that the axes are correctly labelled, i.e. STRESS (MPa) and STRAIN (%), respectively.

(d) Stress v. Time

(Appendix B: Lines 2300-2352 & Lines 2700-2752)

This is performed in identical fashion to (c). The data conversion is performed in lines 2310-2340 and 2714-2725 (or 2735-2742). The axes' labels are chosen in lines 2344-2350 and 2744-2750, respectively.

(e) Strain v. Time

(Appendix B: Lines 2400-2452 & Lines 2800-2852)

Here the relevant lines are 2415-2440 and 2812-2825 (or 2835-2842) for the data conversion, and 2444-2450 and 2844-2850 for the selection of the labels for the axes.

(f) Strain Rate v. Time

(Appendix B: Lines 2900-2952)

This routine permits only the plotting of true strain rate v. time. Otherwise it is similar to (c) - (e), with the data conversion and axes labelling code being contained in lines 2910-2940 and 2944-2950, respectively.

(g)-(k) Strain Gauge Data, Bar Strain, Incident Pulse, Reflected Pulse, Transmitted Pulse

In these five options the above variables can be plotted versus time.

The strain gauge data plot is the raw digital data from both pairs of strain gauges. The bar strain graph is the

same data but converted to strain values.

In the three other graphs the individual pulses are plotted separately in the format of bar strain vs. time.

The relevant code for options (g) - (k) in Appendix B are:

Lines 2252, 2253, 3000-3060, 3100-3160, 3200-3260.

In addition, both options (g) and (h) call the subroutine in lines 10000-10200. This subroutine reads the relevant data files from diskette and, in the case of option (h), converts the data into the strain in bars 1 and 2.

Options (i), (j) and (k) call the subroutine in lines 16000-16330. This subroutine performs a similar task to the one commencing at line 10000 except that it finds the individual pulses contained in the data and converts the selected pulse into strain values.

(l) Hopk Bar Menu (Appendix B: Lines 25000-25200)

Selecting this final option results in the main program being re-loaded into RAM.

Following the selection of one of the ten options the following six subroutines are executed consecutively irrespective of the initial choice.

(m) Find Maximum Values (Appendix B: Lines 4000-4120)

If the graph to be plotted consists of a single curve only then this subroutine determines the maximum values of the data described by the titles of both axes. This is the initial stage in determining the scale to which the curve is to be plotted. The maxima are found in lines 4010-4060.

Alternatively, if more than one graph uses the same set of axes then the operator enters the maxima in lines 4080-4120.

(n) Calculate Axes Limits (Appendix B: Lines 5000-5440)

The length of the X axis (used for both strain and time) is fixed at 150mm but the Y axis (stress, strain or strain rate) can be 150mm or 200mm, as selected in lines 5003-5004.

In labelling each axis, the maximum value of the corresponding parameter (i.e. stress, strain, strain rate and time) is determined by the following:

The ratio of the length of the axis in mm to the upper value labelled on the axis is (1, 2 or 5) x 10^n, where n is an integer. The ratio is chosen so that the maximum value of the data described by the axis is as close as possible to the upper value labelled on the axis. For example, if the maximum value of stress is 200MPa and the length of Y axis was chosen to be 150mm then the upper limit of stress on the Y axis would be 300 MPa, i.e. the ratio of the axis

length to the maximum value labelled on the axis = 150 : 300 = 5×10^{-1}.

Similarly, if the maximum value of strain on the X axis is 10% then the upper limit of strain on the X axis would be 15%, i.e. a ratio of 150 : 15 = 1×10^{1}.

The maximum value of each parameter as labelled on the X or Y axis is determined in the following lines:

(i)	maximum value of stress on the Y axis	5100-5130
(ii)	maximum value of strain on the Y axis	5150-5180
(iii)	maximum value of strain rate on the Y axis	5200-5240
(iv)	maximum value of strain on the X axis	5300-5330
(v)	maximum value of time on the X axis	5400-5440

The scales of the strain gauge data and bar strain, plotted on the Y axis, are fixed, the maximum value being determined by the length of the Y axis (i.e. 150mm or 200mm).

In all cases, except when strain gauge data are plotted on the Y axis, the maximum value of time on the X axis is 150 microseconds.

(o) Draw and Label Axes (Appendix B: Lines 6000-6900)

The graph plotting routines can be used either to draw curves on previously drawn and labelled axes or to perform the complete operation of drawing and labelling axes followed by plotting one or more curves.

In the former case, instructions are given in lines 6005-6022 to align the pen of the digital plotter with the origin of the axes.

The rectangular "box" axes are drawn by the code contained between lines 6025 and 6520. Short linear intercepts are also drawn perpendicular to the axes, separated by distances of 10mm.

The numerical labels on the axes are plotted by lines 6700-6900.

The values of the test parameters are printed above the axes in lines 6538-6563 and the titles of the variables being plotted are printed adjacent to the corresponding axes using the code in lines 6566-6680.

(p) Convert X Data (Appendix B: Lines 7000-7550)

This short subroutine converts the values of the X axis data into lengths in mm corresponding to the scale of the X axis.

(q) Convert Y Data (Appendix B: Lines 8000-8700)

This subroutine performs an identical function for the Y axis date.

(r) Draw Graphs (Appendix B: Lines 9000-9910)

The graph(s) are plotted as individual points or continuous

curves according to the response to the question in line 9001.

The memory requirements of GRAPHS are 14 kbytes for the BASIC program plus 6 kbytes for the data, i.e. a total of 20 kbytes.

6.3.3 TR-AUTO-CTRL (Listing in Appendix C)

The third and final package is the transient recorder automatic control software. This is a modified version of the software provided by Datalab, the manufacturers of the DL912 transient recorder. It can be selected by the operator, from within the HOPK-BAR routine, to perform the six data control functions designed by Datalab, or, alternatively, it is called by the HOPK-BAR routine to perform the task of transferring data from both digital stores of the transient recorder to the memory of the PET microcomputer.

The six data control functions are listed in lines 210-260. RE. + T´FER DATA, which is an abbreviation of read and transfer data, combines the actions of the first and second data control functions.

The memory requirements of TR-AUTO-CTRL are 7 kbyte for the BASIC program plus 8 kbytes for the data, i.e. a total of 15 kbytes.

6.4 Summary

The experimental data were acquired by the conversion of the transmitted and reflected pressure pulses into equivalent electrical pulses by strain gauge transducers. These transients were digitised and stored in two separate memories of a transient recorder. A suite of computer programs then controls the subsequent data handling and analysis.

The main program, HOPK-BAR, was used to

(a) transfer the data from the transient recorder to files on a floppy diskette;
(b) analyse the data according to the Hopkinson bar equations of Chapter 3.

The analysis includes:

(i) filtering out high frequency components in the transmitted pulse;
(ii) finding the zero strain level of each pulse, i.e. the baseline;
(iii) identifying the start of each pulse;
(iv) a correction for misaligned pressure bars;
(v) an adjustment of the reflected pulse data if the latter commences or terminates below or above the baseline;
(vi) conversion of the engineering stress and strain data into true or natural values;

(c) input data from the quasi-static Instron tests and perform the subsequent analysis;

(d) list the recorded digital strain data from each pressure bar;

(e) list the stress/strain results in engineering or true terms;

(f) select the graph plotting routine, GRAPHS;

(g) miscellaneous minor functions such as listing the parameters entered via the computer keyboard, estimate the projectile impact velocity from the strain gauge data and select the transient recorder operational software.

The GRAPHS routine converts the data into the requisite format to plot the selected graph from the nine possible choices. In addition, the axes are automatically drawn and labelled by this routine.

An opto-electronic device was designed and constructed to measure the impact velocity of the SHPB projectile. The impact velocity is used to calibrate the system.

CHAPTER 7

RESULTS AND DISCUSSION

7.1 Test Specimens - Chemical and Physical Data

7.1.1 Material Composition

The test material was oxygen-free high conductivity (OFHC) copper. A chemical analysis revealed the following impurities:

Silver 0.005%, Carbon 0.01%, Oxygen 0.003% and Sulphur < 0.0003%.

Hence the material ws 99.98% pure copper. The chemical analysis was carried out by RARDE, Fort Halstead.

7.1.2 Annealing Temperatures

Prior to producing the specimens, the raw material was divided into 5 blocks. Each block was annealed at a different temperature for one hour at atmospheric pressure in a circulating air furnace. The annealing temperatures chosen were 310^{o}C, 400^{o}C, 500^{o}C, 600^{o}C and 800^{o}C. Recrystallisation did not occur for temperatures less than 310^{o}C.

Due to insufficient material being annealed at the start of the research programme, additional material was prepared in identical fashion to the above, on two further occasions during the course of the three year investigation.

Annealing was performed by Dr. R.M. Bateman of RARDE.

7.1.3 Specimen Dimensions

All the test specimens were machined from the annealed copper blocks by RARDE.

(a) Compressive Specimens

The length of the cylindrical specimen was (4.3 $\pm$ 0.1)mm and the diameter (10.0 $\pm$ 0.05)mm. This satisfies the criterion for length to diameter ratio given in section 3.4. A surface finish of approximately 1 micron, for the specimen faces was produced, whilst the faces were parallel to within 4 microns.

(b) Tensile Specimens

The dimensions of the tensile specimen are shown in Figure 7.1. Its gauge length is not equal to the length of the specimen between the bar faces because of its tapered shape. A preliminary investigation indicated a specimen gauge length of 8.3mm (see section 4.3). The specimen size and geometry were recommended by JRC, Ispra and AWRE, Foulness. The geometry is not material dependent.

7.1.4 Grain Sizes

The average grain size for each annealing temperature was determined from photomicrographs of the sectioned specimens using a linear intercept method. Grain size measurements of representative specimens from the first of three batches of copper specimens to be prepared by RARDE, were made by

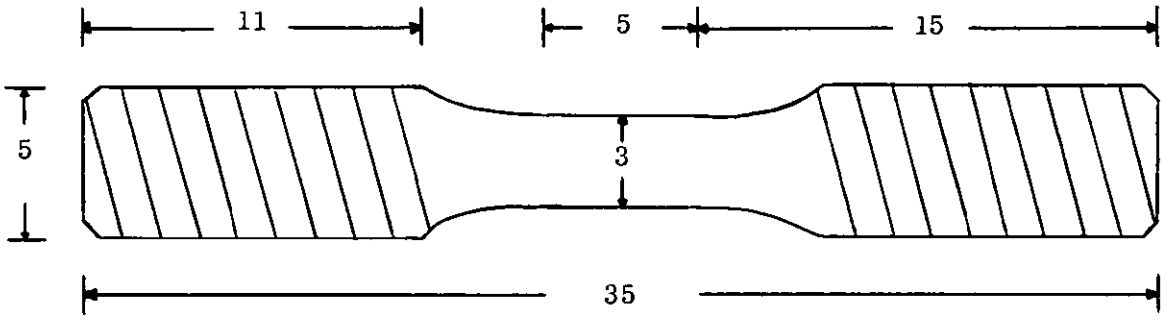

Figure 7.1 Tensile Specimen
(Dimensions in mm. Magnification x 4)

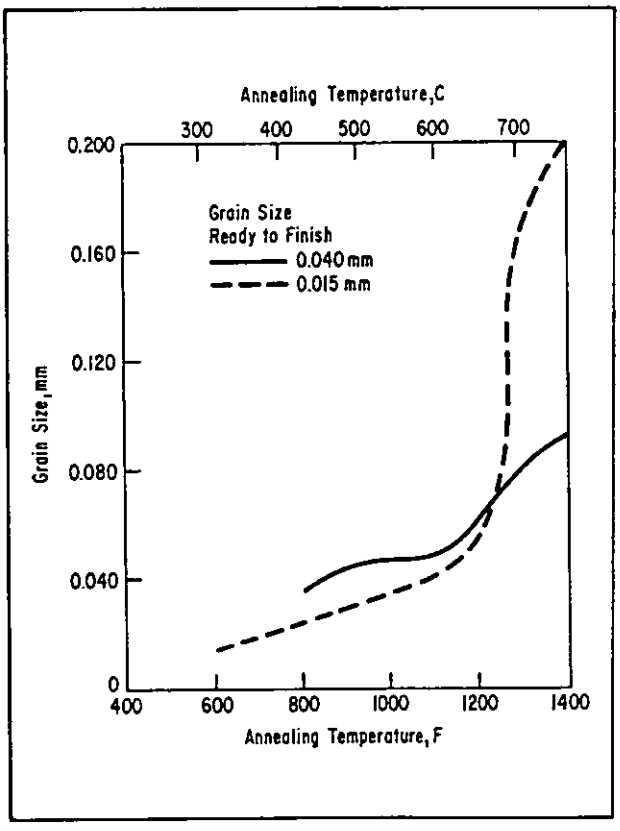

Effect of annealing on grain size of OFHC copper strip cold rolled 50%

Figure 7.2

Dr. Bateman and the author. Measurements on the third batch of specimens were made by Charnwood Consultants Ltd., Kegworth. Grain boundaries only were deliberately included in the grain size measurements, although at times it was not possible to distinguish between grain boundaries and twins. No attempt was made to determine the grain size of the copper prior to its annealing.

There was reasonably good agreement between the two batches which were inspected for all annealing temperatures except 600°C. The initial batch yielded an average grain size of 48μm, whilst the final batch was 200μm. A possible explanation for these widely differing grain sizes being produced from nominally identical heat treatment can be derived from the graph of grain size versus annealing temperature (Figure 7.2) produced by WILKINS and BUNN (1943), in which there is a rapid increase in grain size for annealing temperatures greater than 600°C for the material initially composed of 15μm grains. Hence a relatively small temperature difference between the batches nominally annealed at 600°C would produce a large difference in grain size. Rather than exclude the mechanical test results of material annealed at 600°C, a mean grain size of 124μm is quoted for this annealing temperature. These test results are, of course, treated with extreme caution due to the potentially large error in the grain size estimate.

Table 7.1 lists the grain sizes corresponding to the five annealing temperatures.

Table 7.1

Annealing Temperature (^{o}C)	Grain Size (μm)
310	20
400	29
500	32
600	124
800	240

7.2 Loading Pulse Characteristics

Amplitudes up to 700MPa or approximately 45 tons/sq.in. were attainable in the pressure bars. Prior to pulse shaping the incident strain pulse, or loading pulse, had either a flat top (Figure 7.3(a)) or it had Pochhammer - Chree oscillations at its maximum amplitude (Figure 7.3(b)). The latter pulse is predicted by theory (see, for example, FOLLANSBEE and FRANTZ, 1983). The occurrence of the two types of pulse depends on the bar material and the impact velocity. In the present investigation, the pressure bars were initially 431 martensitic stainless steel. These produced flat-topped loading pulses for all but the lowest impact velocity. At a late stage of the research, pressure bars made from the higher strength maraging steel were used so that very high strain rate tests could be performed. Pochhammer-Chree oscillations were always recorded in the latter. The lack of oscillations at the maximum amplitude of the loading pulse in the 431 bars (except at lower stresses) is probably due to the higher stress wave attenuation of this material. This damping also increases with stress amplitude. Hence when high amplitude pulses are being propagated it is preferable to use maraging steel to avoid errors due to attenuation, particularly if the gauges on bar 1 are further from the specimen that those on bar 2. After pulse-shaping (which was only performed with the 431 bars) the loading pulse is ramp shaped (Figure 3.12).

A 25cm long projectile was used throughout. Consequently the pulse length was 50cm and its duration approximately

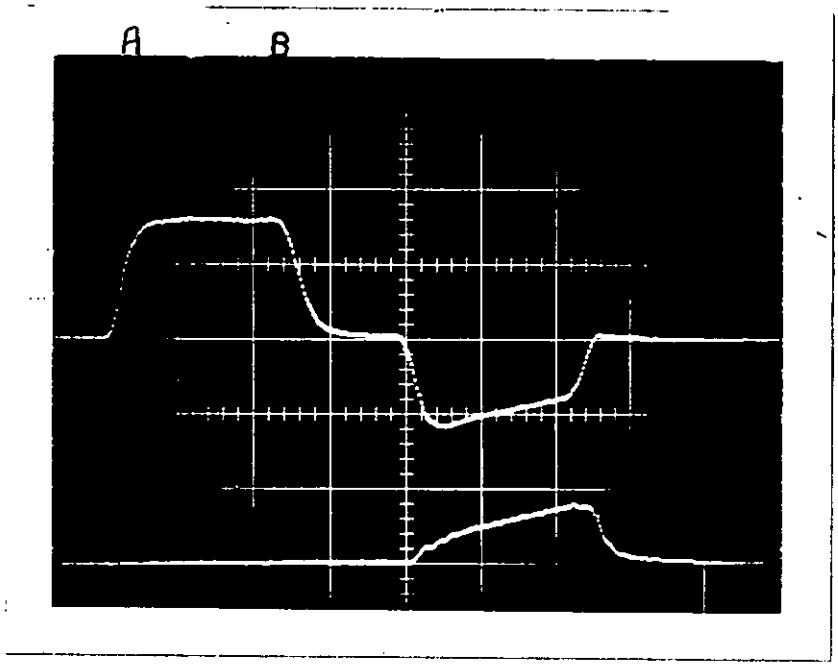

Vertical Scale:
0.13%/div

Horizontal Scale:
40us/div

Average Strain Rate:
$3534s^{-1}$

Filename:
COC600500205A

Figure 7.3(a) Incident strain pulse with a flat top
(1st pulse on upper trace)

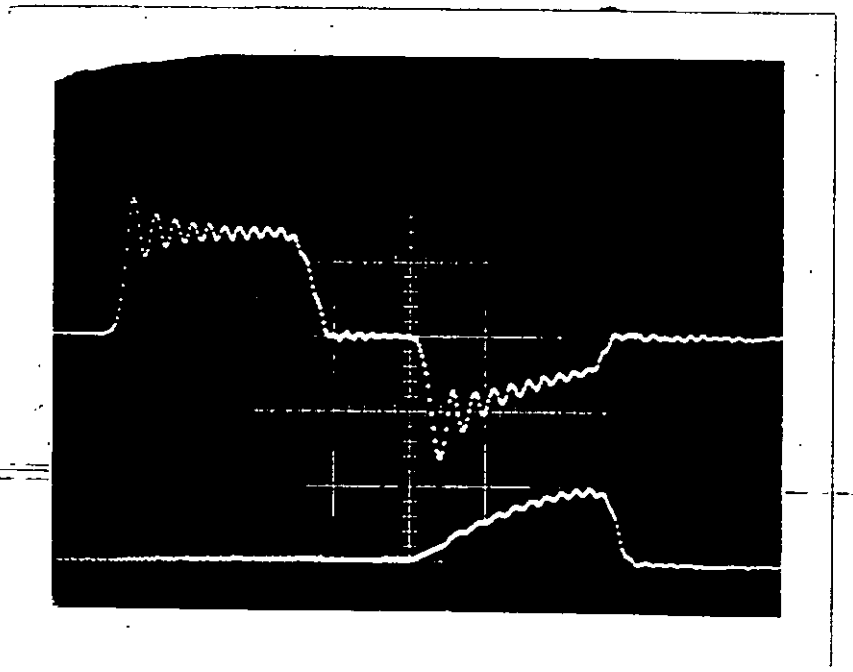

Vertical Scale:
0.26%/div

Horizontal Scale:
40us/div

Average Strain Rate:
$5887s^{-1}$

Filename:
COC020800365B

Figure 7.3(b) Incident strain pulse with Pochhammer-Chree oscillation
(1st pulse on upper trace)

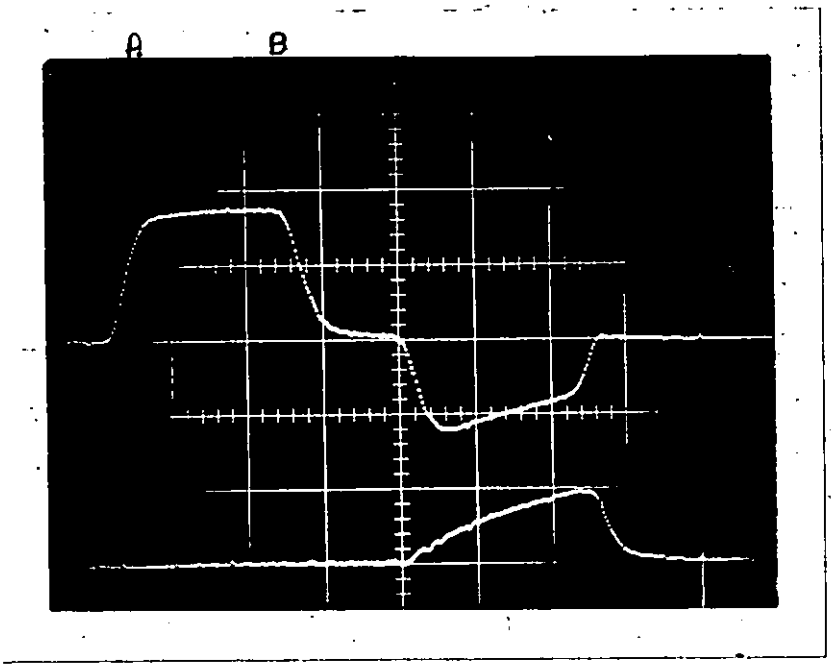

Vertical Scale:

0.13%/div

Horizontal Scale:

40us/div

Average Strain Rate:

$3645s^{-1}$

Filename:

COC40080026SA

Figure 7.3(c) Incident strain pulse with a positive gradient top achieved with an impact velocity of $26ms^{-1}$ without using a pulse shaper (1st pulse on upper trace).

100 microseconds. All these tests were performed with either a steel projectile or a duralumin projectile, the latter being able to impart lower stresses to the loading bar as a consequence of its lower density (see equation 3.1).

7.3 SHPB System Calibration

As previously stated the impact velocity of the projectile is controlled by the hole size in the aperture plate adjacent to the gas gun sliding valve. The seven circular holes vary in diameter from 2mm to 20mm. By repeatedly firing the projectile, in the absence of a test specimen, the impact velocity and the strains in bars 1 and 2 can be recorded for each permissible combination of holes that are uncovered. Hence calibration curves can be plotted of both impact velocity versus aperture area (Figure 7.4) and strain versus aperture area (Figure 7.5) for the steel and duralumin projectiles. These two figures refer to the calibration of the gas gun in conjunction with the 431 steel pressure bars. The calibration curves were used to enable a strain rate estimate to be made prior to testing a specimen.

Both during system calibration and specimen testing the impact velocity was used to monitor the correct functioning of the strain gauges. The relation between stress (which is the product of strain and elastic modulus) and impact velocity is given by equation 3.1. The attenuation of the stress pulse during its transit between the gauges of bars 1 and 2 was found to be negligible in the absence of a test

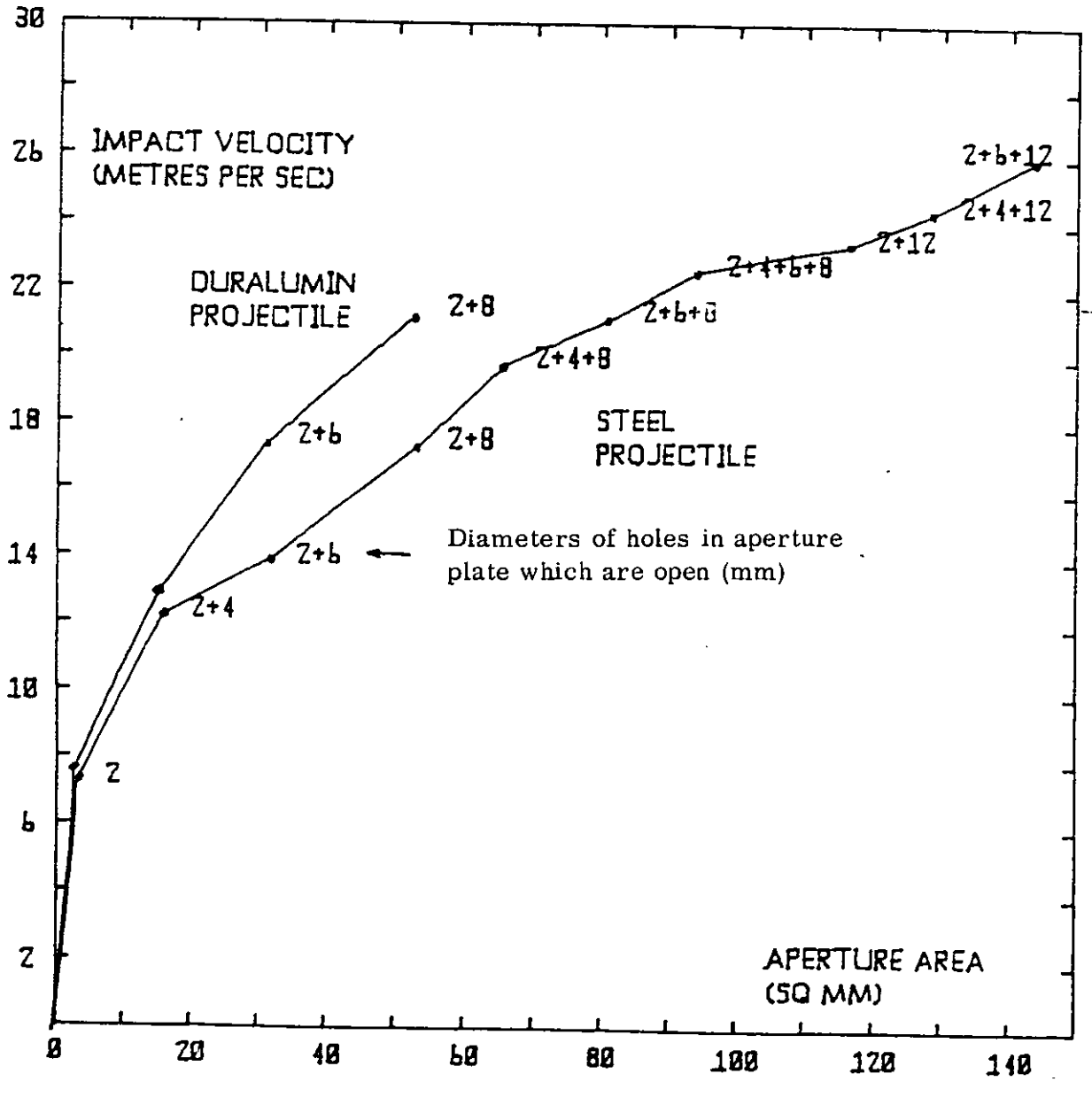

Figure 7.4 Impact velocity versus aperture area

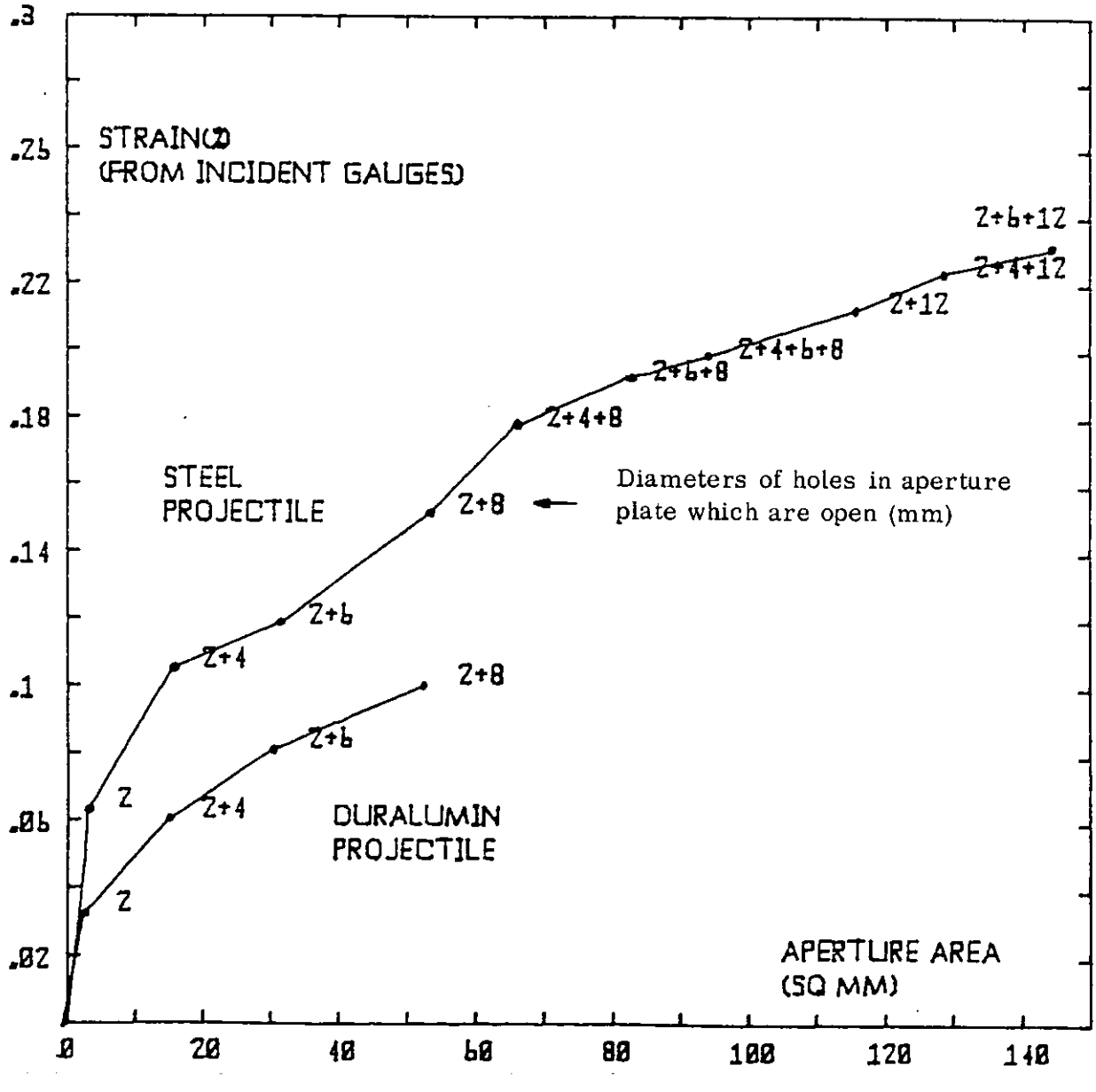

Figure 7.5 Strain versus aperture area

specimen (except in the 431 bars at high impact velocity) and hence the impact velocity could be used to check the calibration of both pairs of strain gauges.

7.4 Pulse Shaping

The exact dimensions and grain size of the copper pulse shaper required to produce a constant strain rate for a given grain size of compressive test specimen, test temperature and impact velocity, were determined empirically. However, in arriving at the correct values for these parameters, the theoretical considerations outlined in section 3.5 were taken into account.

The following observations were recorded during the pulse shaping trials, which relate to shape of the loading pulse in the 431 steel pressure bar after the pulse has been modified by its transmission through the dummy specimen; the dummy specimen being inserted at the interface of bar 1A and bar 1B:

(a) Refer to the flat-topped pulse in Figure 7.3(a), where the flat top is denoted by AB. This is the shape of the loading pulse prior to its passage through the dummy specimen. The pulse transmitted through the dummy specimen (or pulse shaper) is no longer flat-topped but the gradient of AB is now positive (as would be expected for a transmitted pulse) (Figure 3.12). The amplitude of A can be reduced, and hence the gradient of AB increased, by increasing the grain size of the pulse shaper, thereby reducing its yield

stress and reducing the amplitude of the pulse which is initially transmitted into bar 1B.

(b) High constant strain rates (approximately $1500s^{-1}$) are produced with unannealed pulse shapers of identical dimensions to the test specimens and impact velocities with the steel projectile of approximately $25ms^{-1}$. Low constant strain rates of ($< 50s^{-1}$) can be achieved with pulse shapers of 5mm diameter and 6mm length which were annealed at $300^{o}C$ for 1 hour; the requisite impact velocity using the duralumin projectile being approximately $14ms^{-1}$.

N.B. It was found that at impact velocities greater than about $20ms^{-1}$ a trapezoidal pulse, with AB having a positive gradient, could be produced without using a pulse shaper (Figure 7.3(c)). This is probably due to a differential damping or internal friction mechanism between the low and high frequency components of the pulse propagated in the 431 stainless steel pressure bar. At high impact velocities, attenuation is no longer negligible and the low frequency component of the pulse, which according to theory travels faster than the high frequency component, is subjected to higher damping than the higher frequencies. The latter statement is only true for wave propagation in small diameter bars or other bounded media of narrow cross-section. In unbounded polycrystalline material, attenuation is an increasing function of frequency.

7.5 Dynamic Strain Rate Ambit

Constant strain rates, produced by the pulse shaping technique, varied from about $10s^{-1}$ to slightly more than $1500s^{-1}$ in the compressive tests.

Further tests using the conventional system achieved an upper limit of $6250s^{-1}$. The attenuation produced by the pulse-shaping technique precluded its use at the highest strain rates. However, natural mechanical behaviour, as noted in section 7.4, yielded fairly constant rates in the latter case.

Strain rates up to $3 \times 10^3 s^{-1}$ were attained with 431 martensitic stainless steel pressure bars (0.2% proof stress = 700MPa). Above this rate of strain, maraging steel bars (0.2% proof stress = 1381MPa), supplied by RARDE, were used.

In the tensile tests, the upper strain rate of approximately $1300s^{-1}$ was limited by the degree of allowable initial compression suffered by the specimen. Below about $300s^{-1}$ the transmitted tensile pulse was too small to accurately assess.

7.6 Test Parameters

7.6.1 Compressive Tests

At room temperature, each of the 5 grain sizes of specimen was tested at a minimum of 5 strain rates.

The elevated temperature tests, performed at 200°C, 400°C and 600°C, were limited to three grain sizes (20μm, 32μm and 240μm), results being presented for three strain rates.

For any given set of selected test parameters (i.e. impact velocity, type of projectile, test temperature and grain size) several tests were performed to ensure repeatability and the results averaged.

The quasi-static tests were performed at a strain rate of $2 \times 10^{-3} s^{-1}$. Average results were again used.

7.6.2 Tensile Tests

The variety of tensile tests carried out was far more limited than the compressive tests because of the difficulties in attaining the requisite conditions for a valid result. As a consequence, tests were repeated many times with the same test parameters. Eventually consistent results were obtained following many modifications to the apparatus to reduce the sources of error. These sources of error and the modifications to eradicate them were described in the sections 4.6 and 4.7.

At room temperature, specimens annealed at 310°C, 500°C and 800°C (i.e. grain sizes of 20μm, 32μm and 240μm) were tested at 2 dynamic strain rates plus one quasi-static strain rate of approximately $10^{-3} s^{-1}$. For the elevated temperature tests, at 200°C, 400°C and 600°C, only the specimens annealed at 800°C (i.e. 240μm grain size) were deformed dynamically at 2 strain rates. Quasi-static tests

were performed on the same grain sizes as the compressive quasi-static tests quoted in the previous section.

7.7 Results of Mechanical Tests

Figures 7.6 - 7.19 and 7.32 - 7.37 show the graphical representation of the results of the mechanical tests in the form of true stress vs. true strain rate for various constant true strain levels. (Unless otherwise specified 'true' stress, 'true' strain and 'true' strain rate are implied henceforth whenever those macroscopic mechanical variables are used). Each figure represents a particular testing mode, test temperature and grain size. These graphs were generated from stress-strain curves, each of which was an average of several tests. This averaging process is illustrated by Figure 7.20 which contains the 'raw' data from 3 nominally identical tests and also the mean curve. Figure 7.20 exemplifies the high degree of repeatability of compressive tests for strain rates in the region of $10^3 s^{-1}$.

When comparing results of tests conducted at different strain rates, the stress vs. strain rate format is the usual and most convenient presentation of SHPB test results. The alternative format of stress vs. strain for constant strain rates is more difficult to construct due to the limited control over strain rate in these tests. The latter is, of course, a function of the test material's mechanical properties and the dimensions of the specimen, as well as being dependent on the projectile impact velocity.

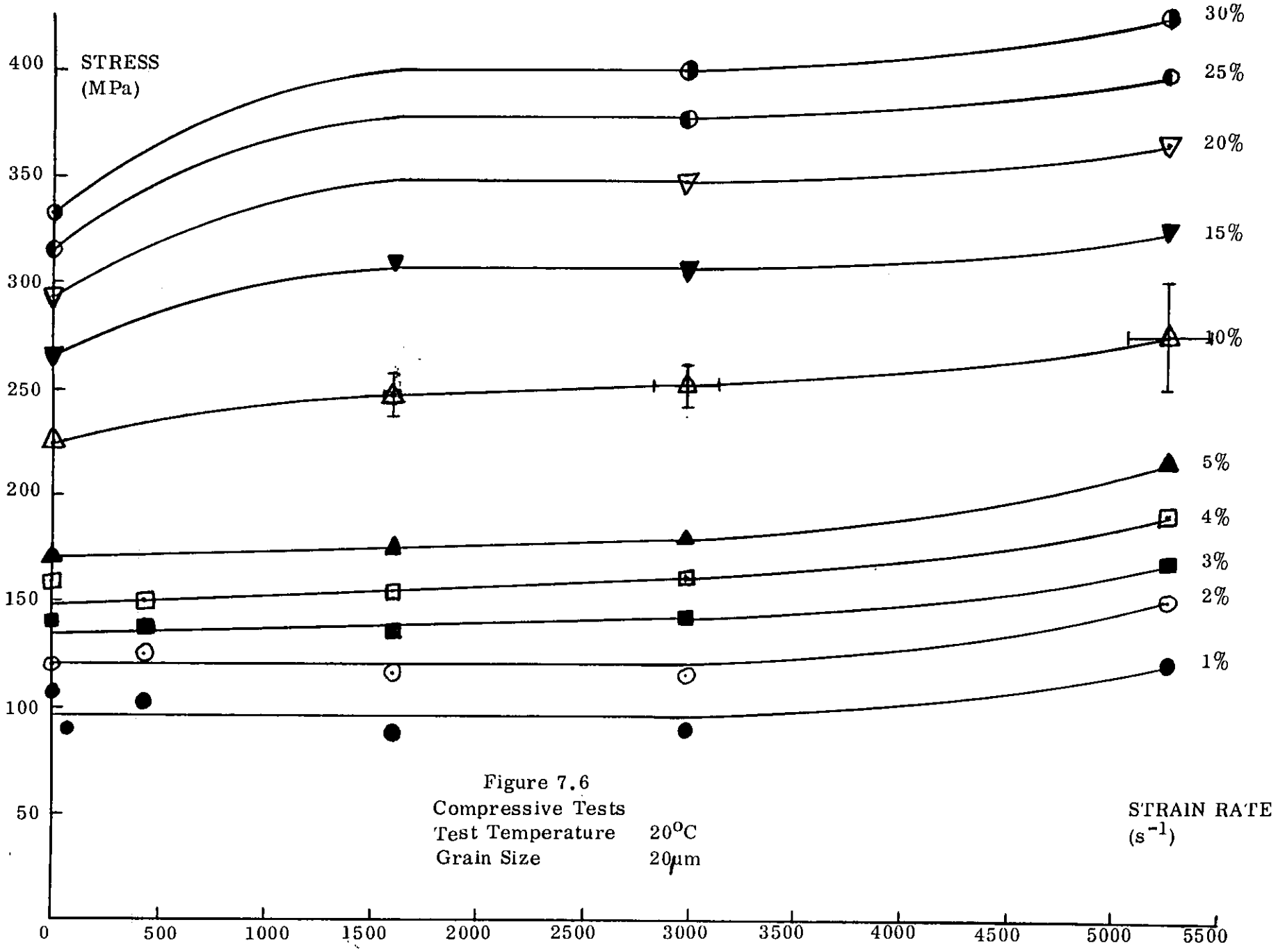

Figure 7.6
Compressive Tests
Test Temperature $20^{o}C$
Grain Size $20\mu m$

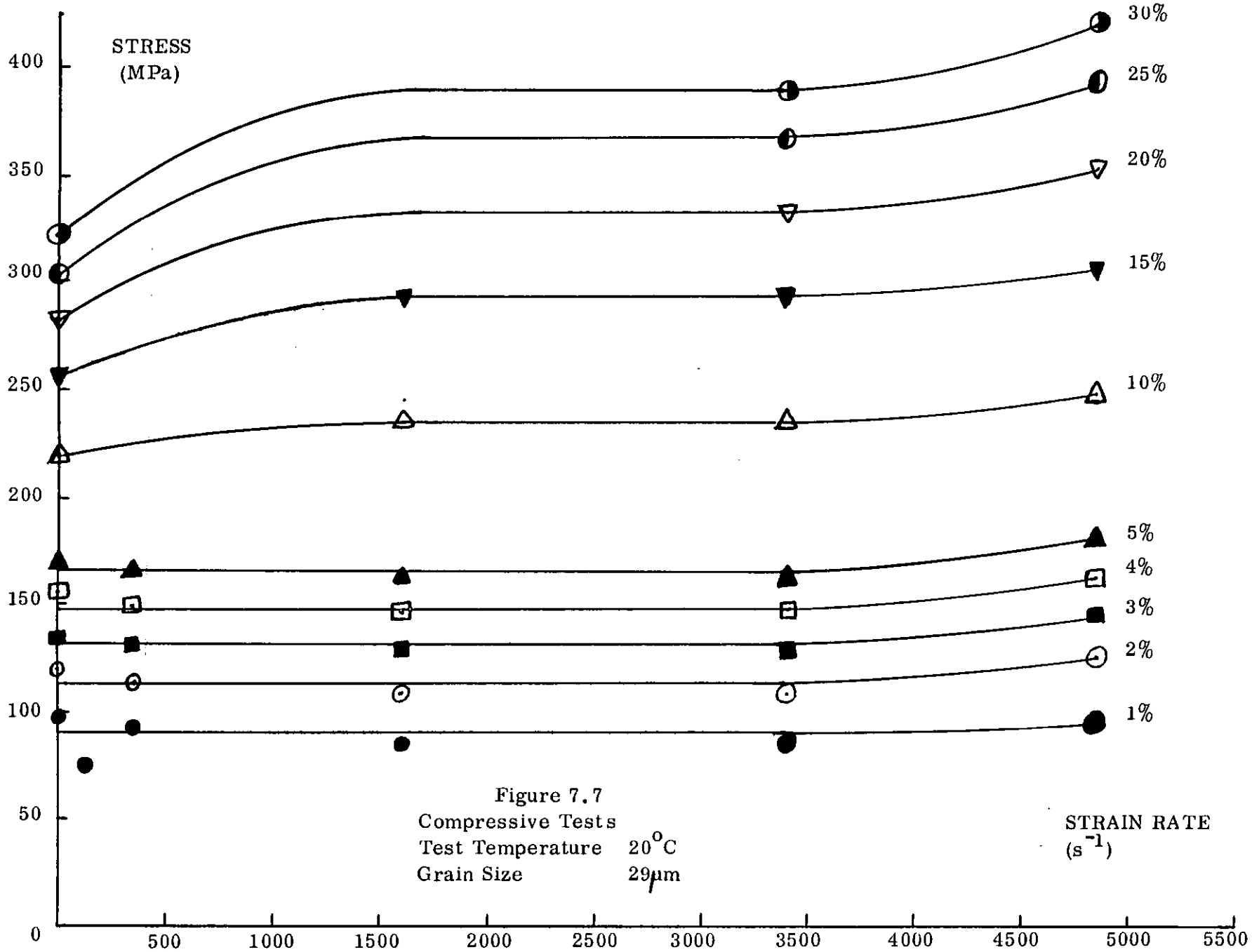

Figure 7.7
Compressive Tests
Test Temperature 20°C
Grain Size 29μm

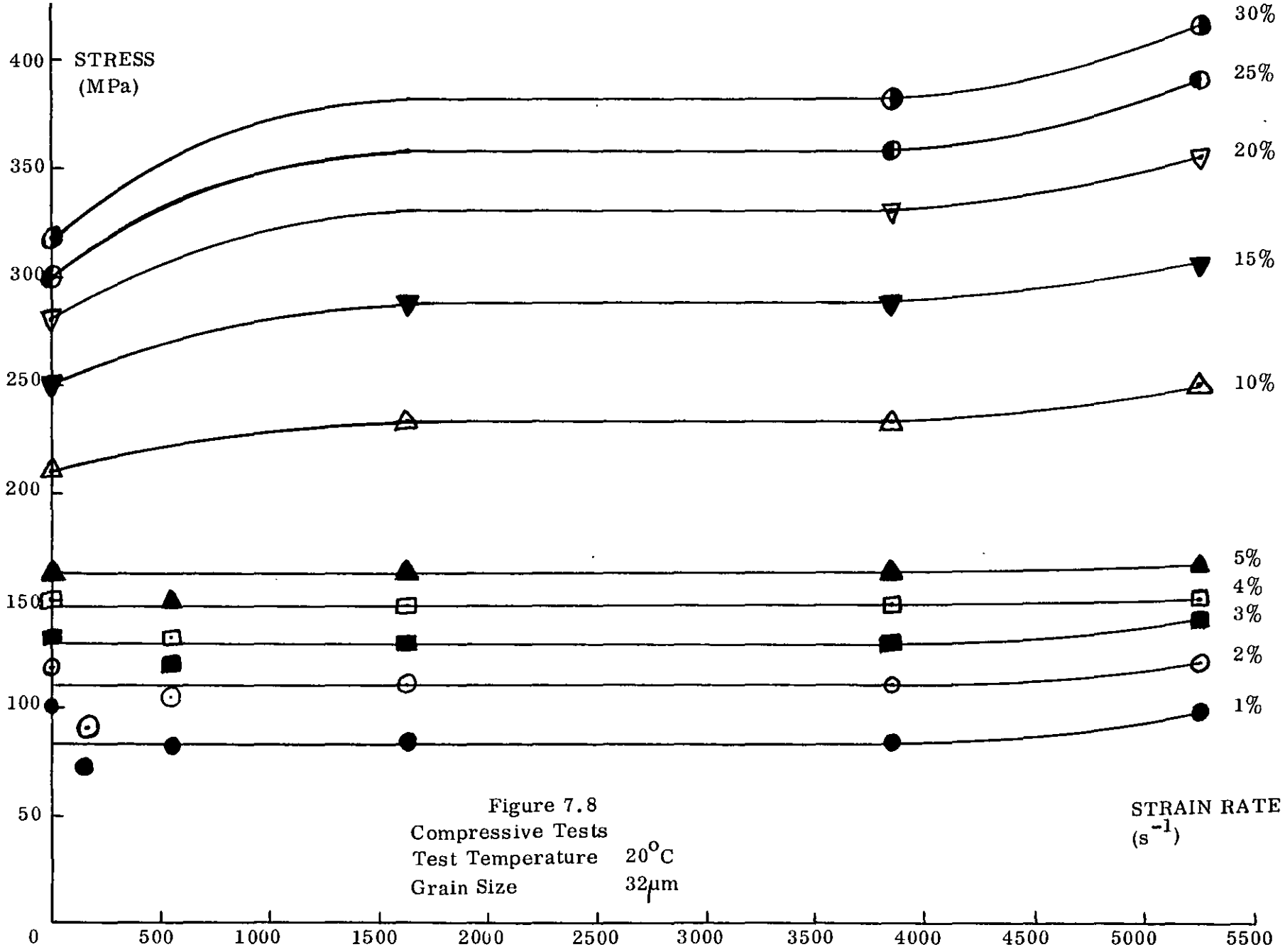

Figure 7.8
Compressive Tests
Test Temperature $20^{o}C$
Grain Size $32\mu m$

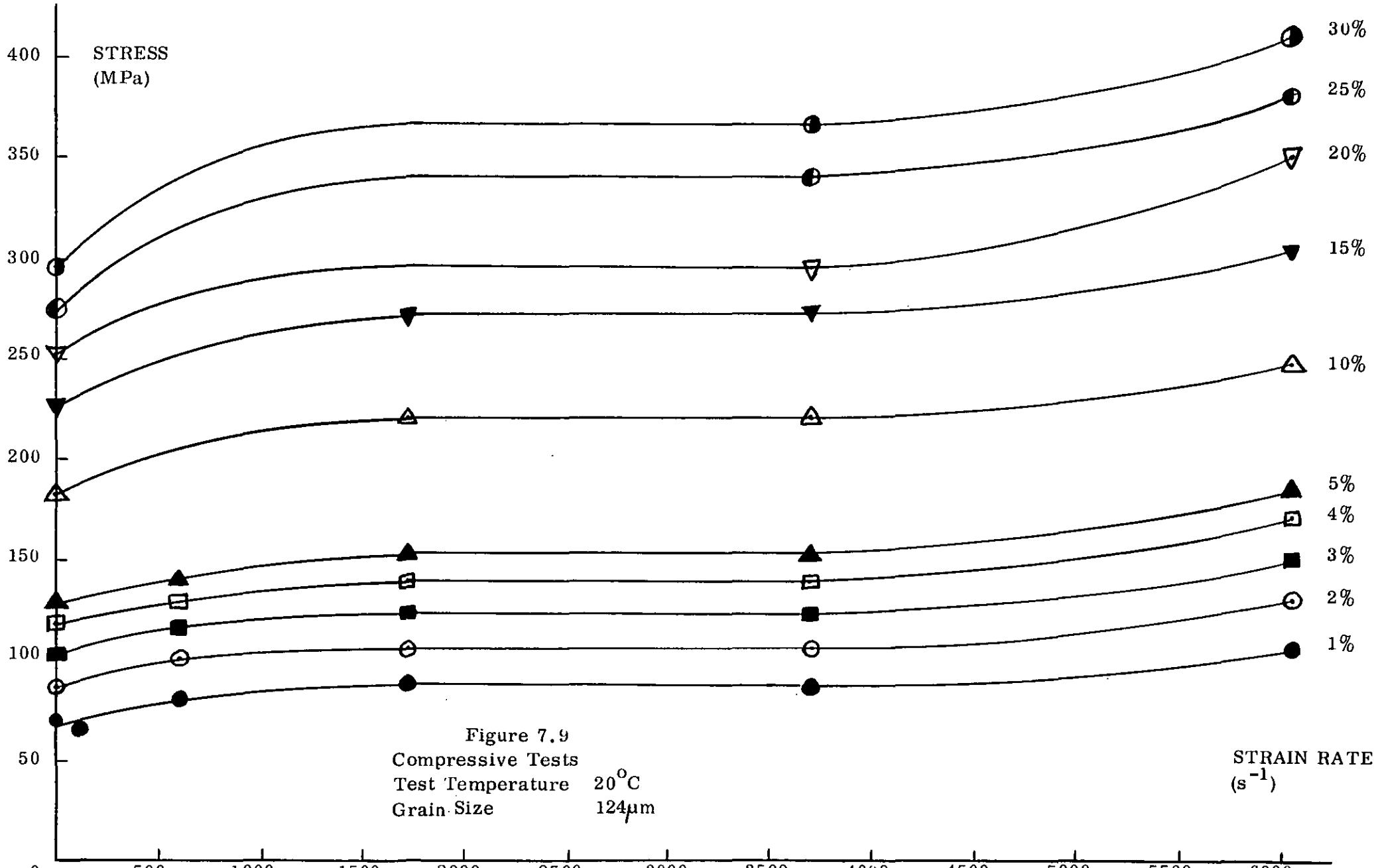

Figure 7.9
Compressive Tests
Test Temperature 20°C
Grain Size 124μm

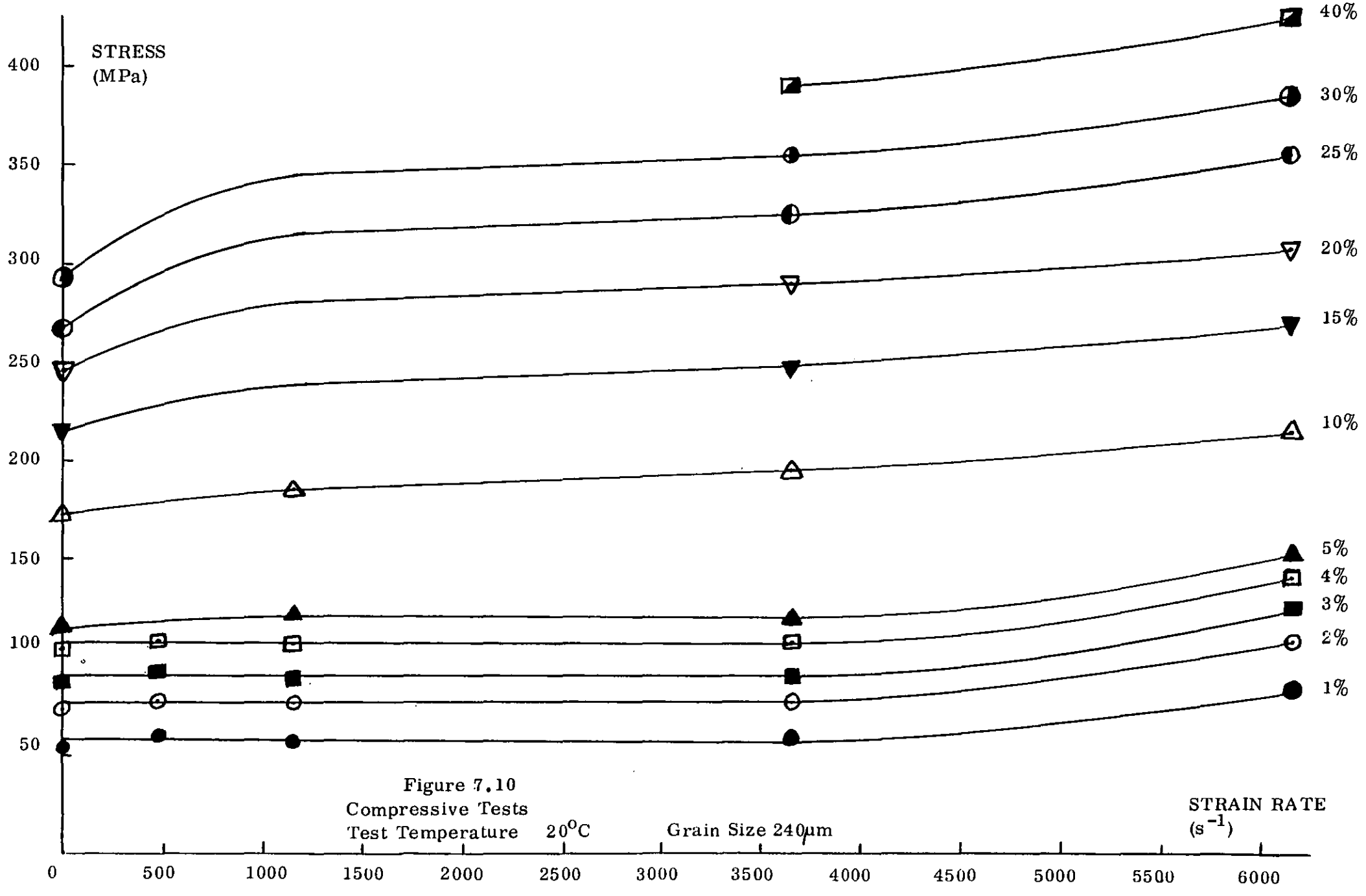

Figure 7.10
Compressive Tests
Test Temperature 20°C Grain Size 240μm

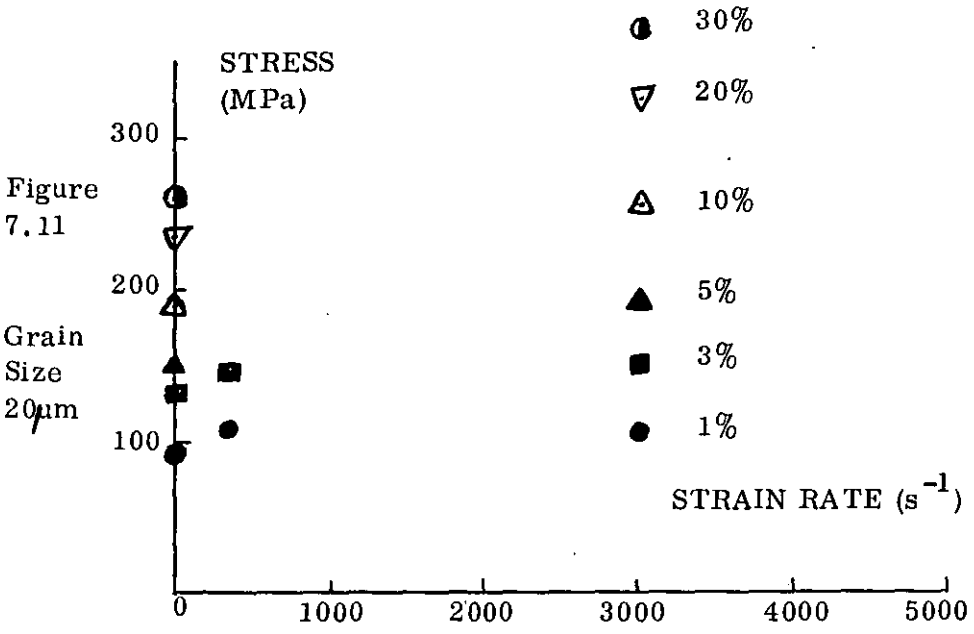

Figure 7.11

Grain Size 20μm

COMPRESSIVE TESTS

AT

200°C

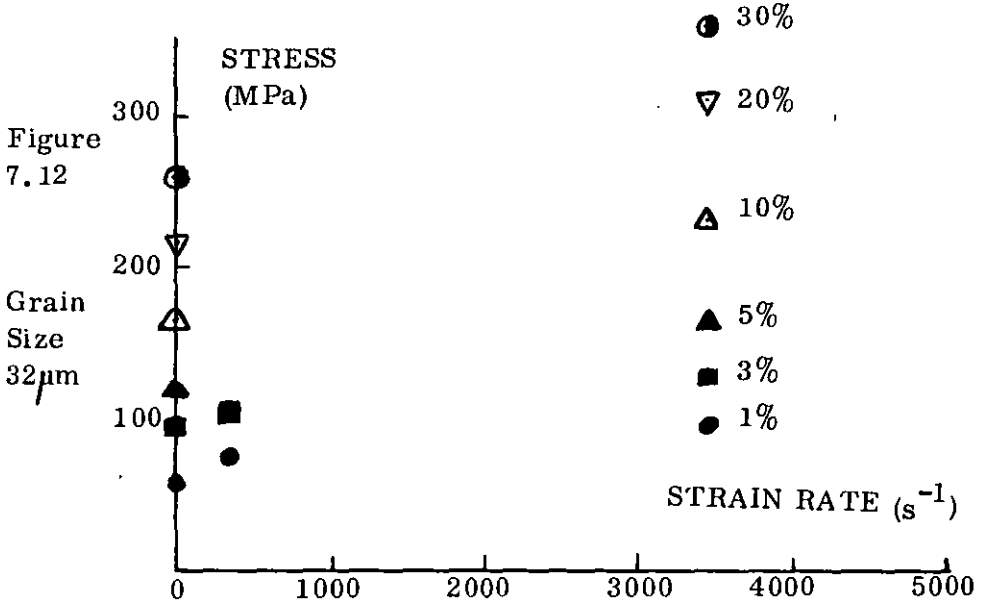

Figure 7.12

Grain Size 32μm

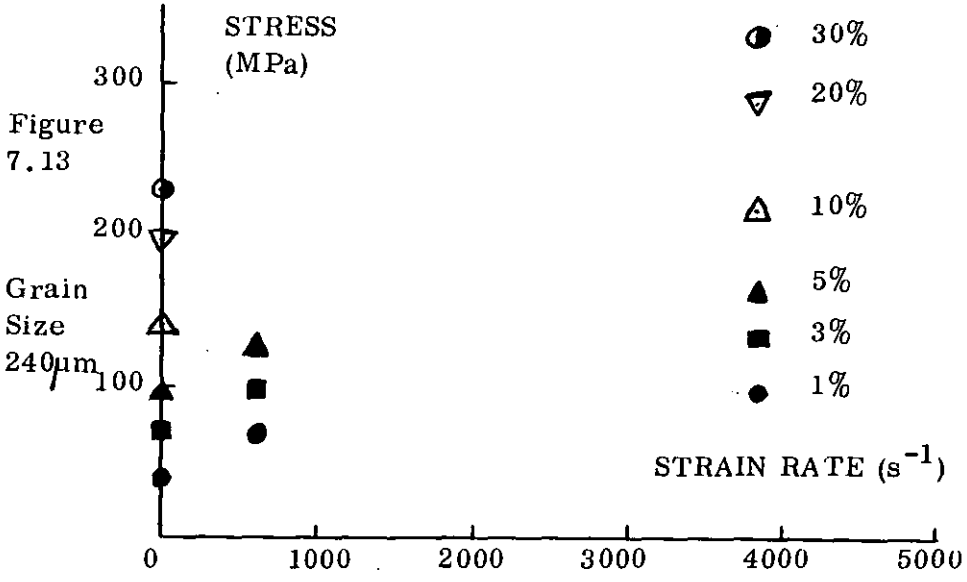

Figure 7.13

Grain Size 240μm

Figure 7.14

Grain Size 20μm

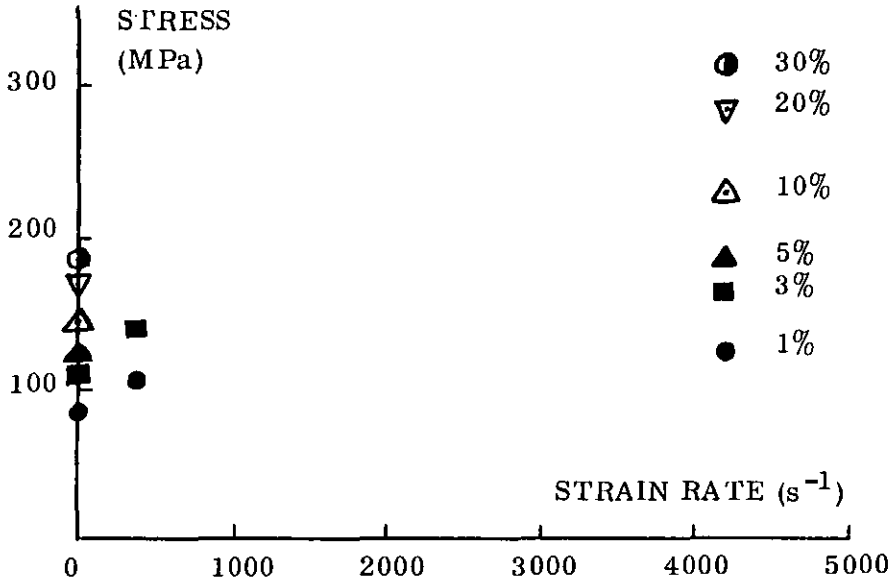

COMPRESSIVE TESTS

AT

400°C

Figure 7.15

Grain Size 32μm

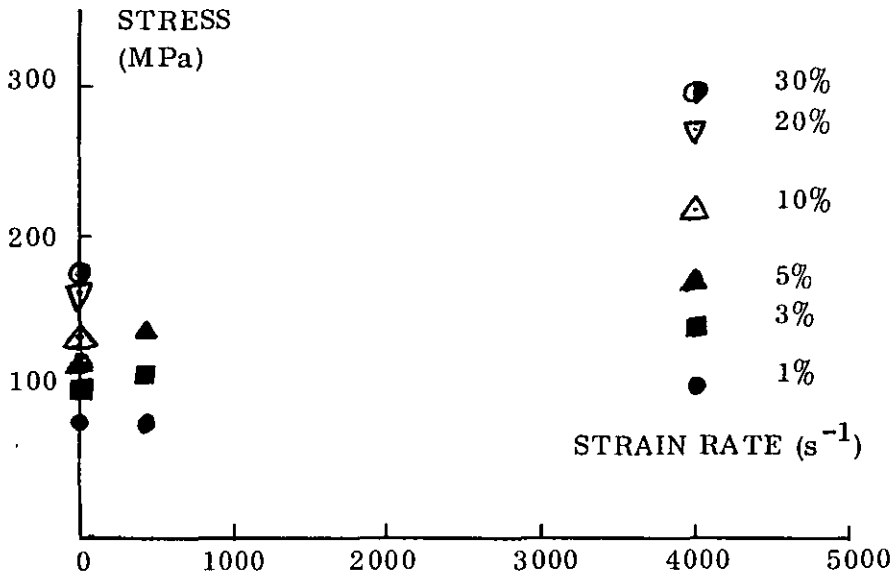

Figure 7.16

Grain Size 240μm

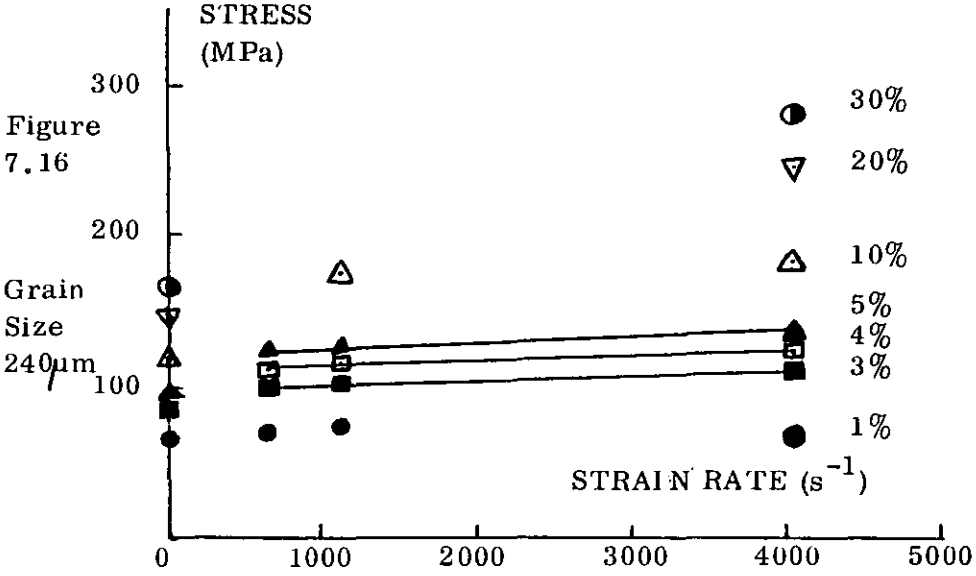

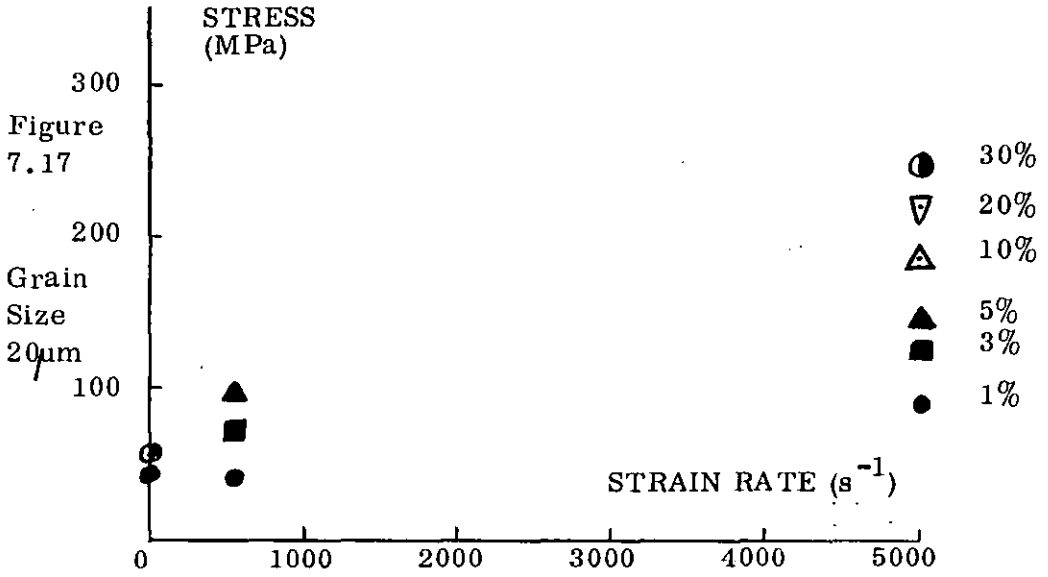

Figure 7.17 Grain Size 20μm

COMPRESSIVE TESTS AT $600^{o}C$

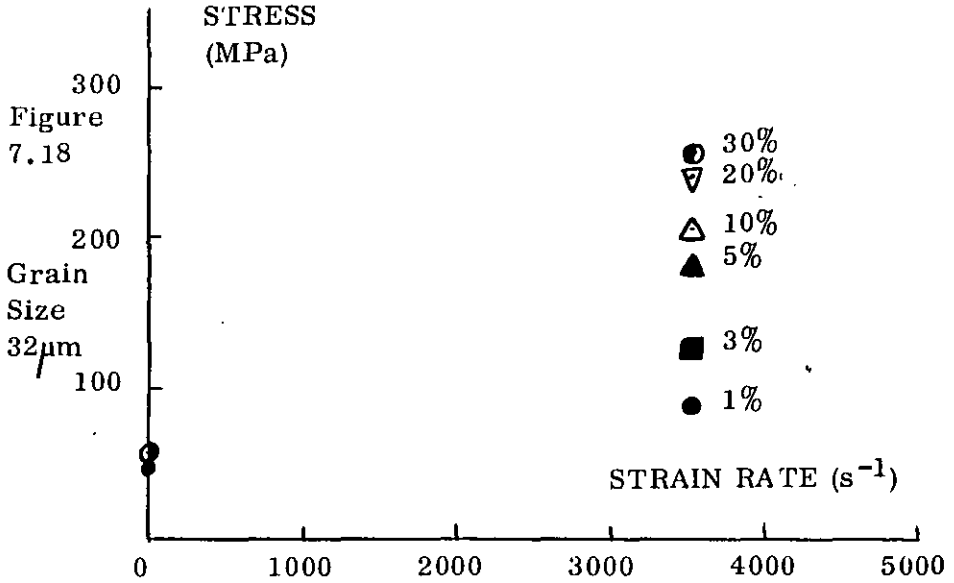

Figure 7.18 Grain Size 32μm

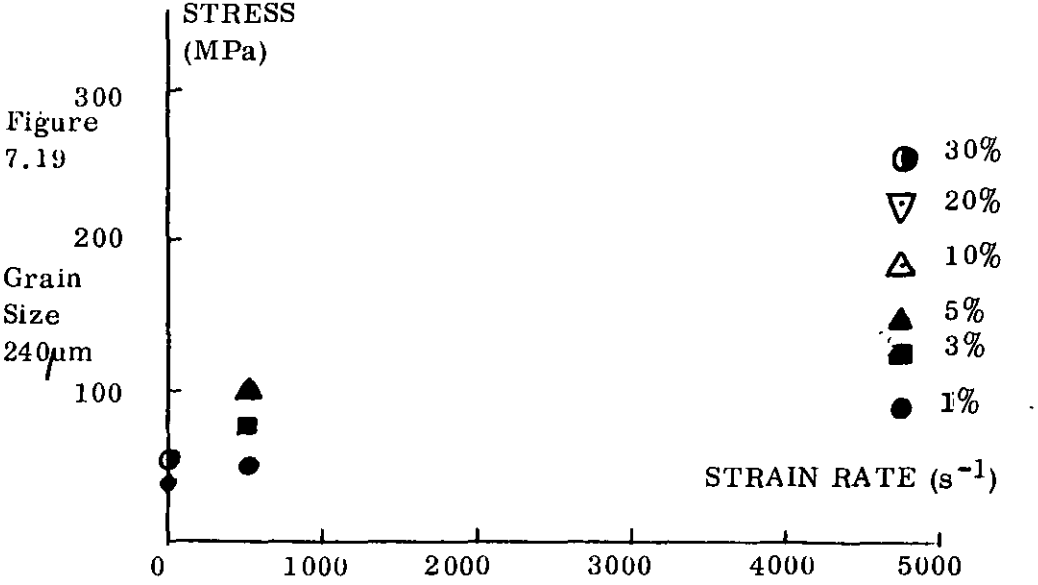

Figure 7.19 Grain Size 240μm

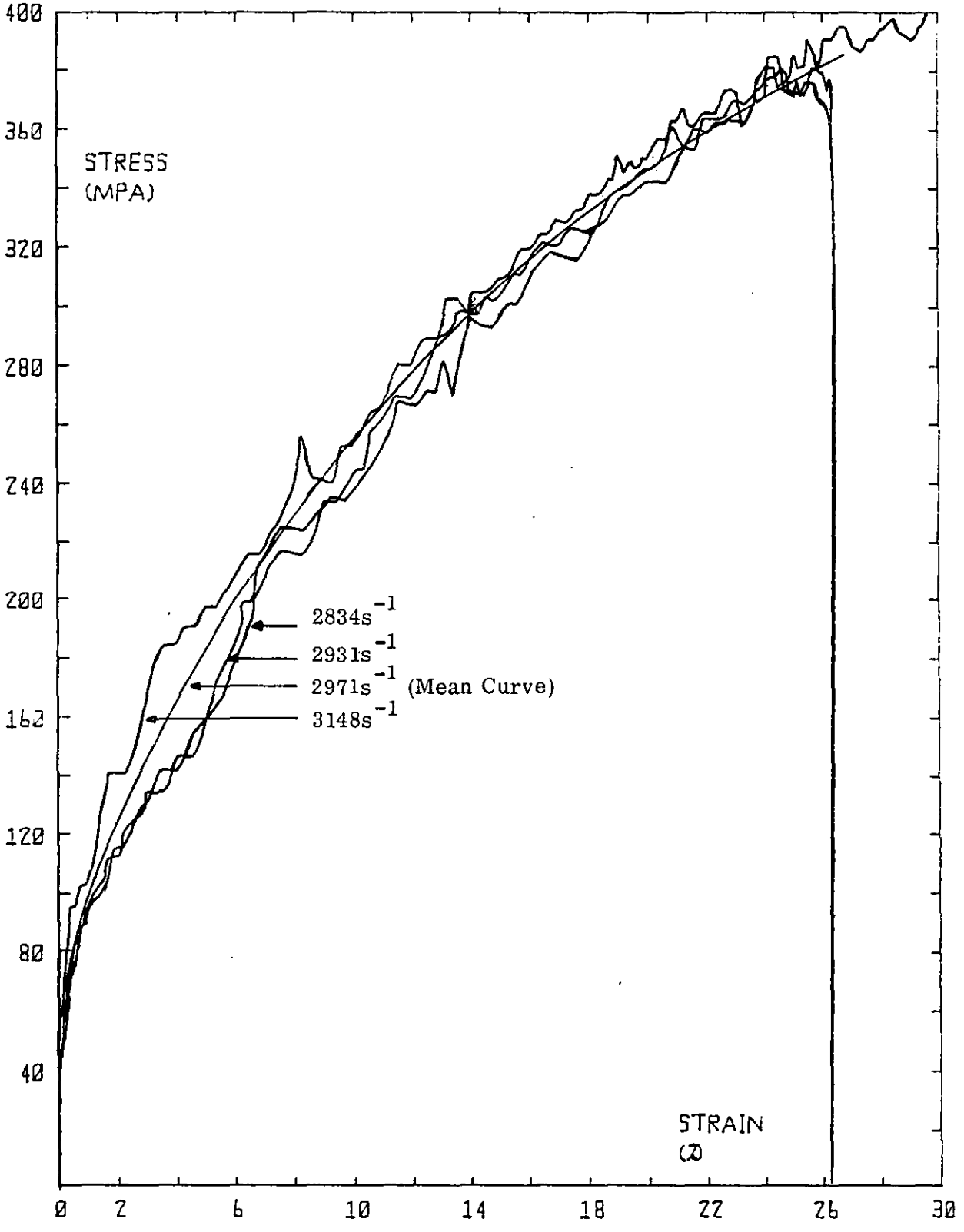

Figure 7.20 Experimental curves and mean curve.
Compressive tests at 20^{o}C on 20μm grain size.
Mean strain rate = 2971s^{-1}

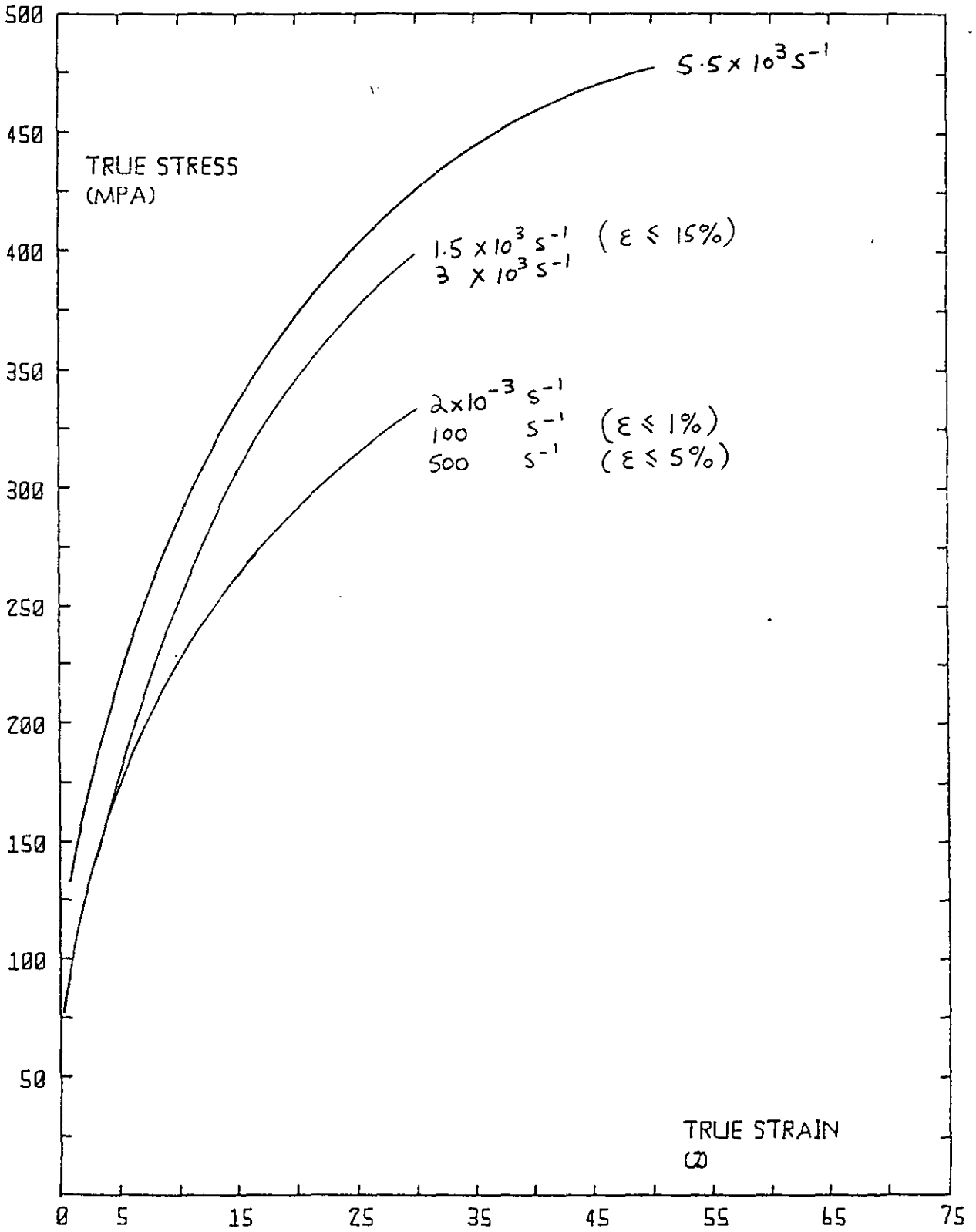

Figure 7.21 Compressive tests at 20°C, Grain size 20μm

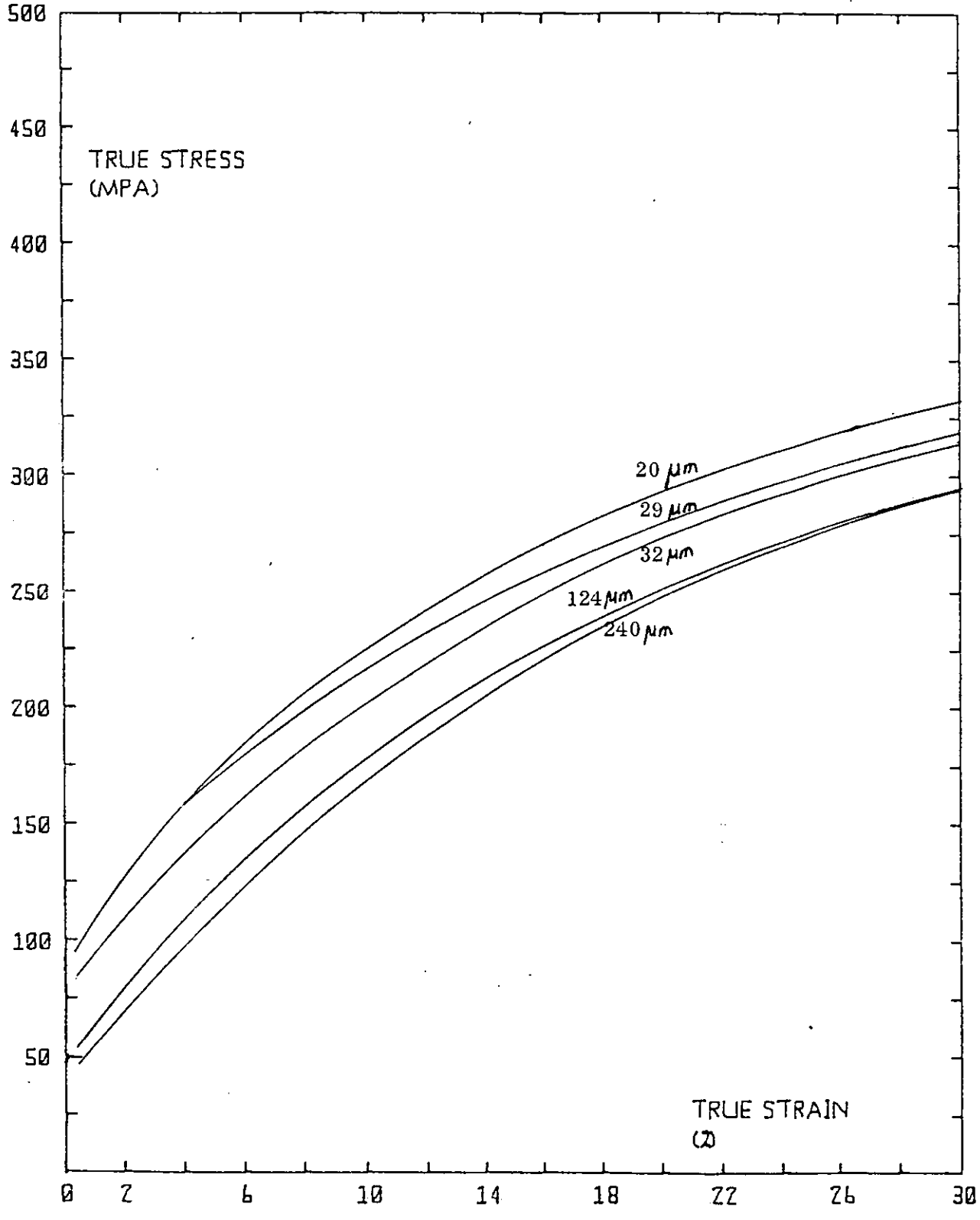

Figure 7.22 Quasi-static compressive tests at 20°C -5 Grain Sizes (20 - 240μm)

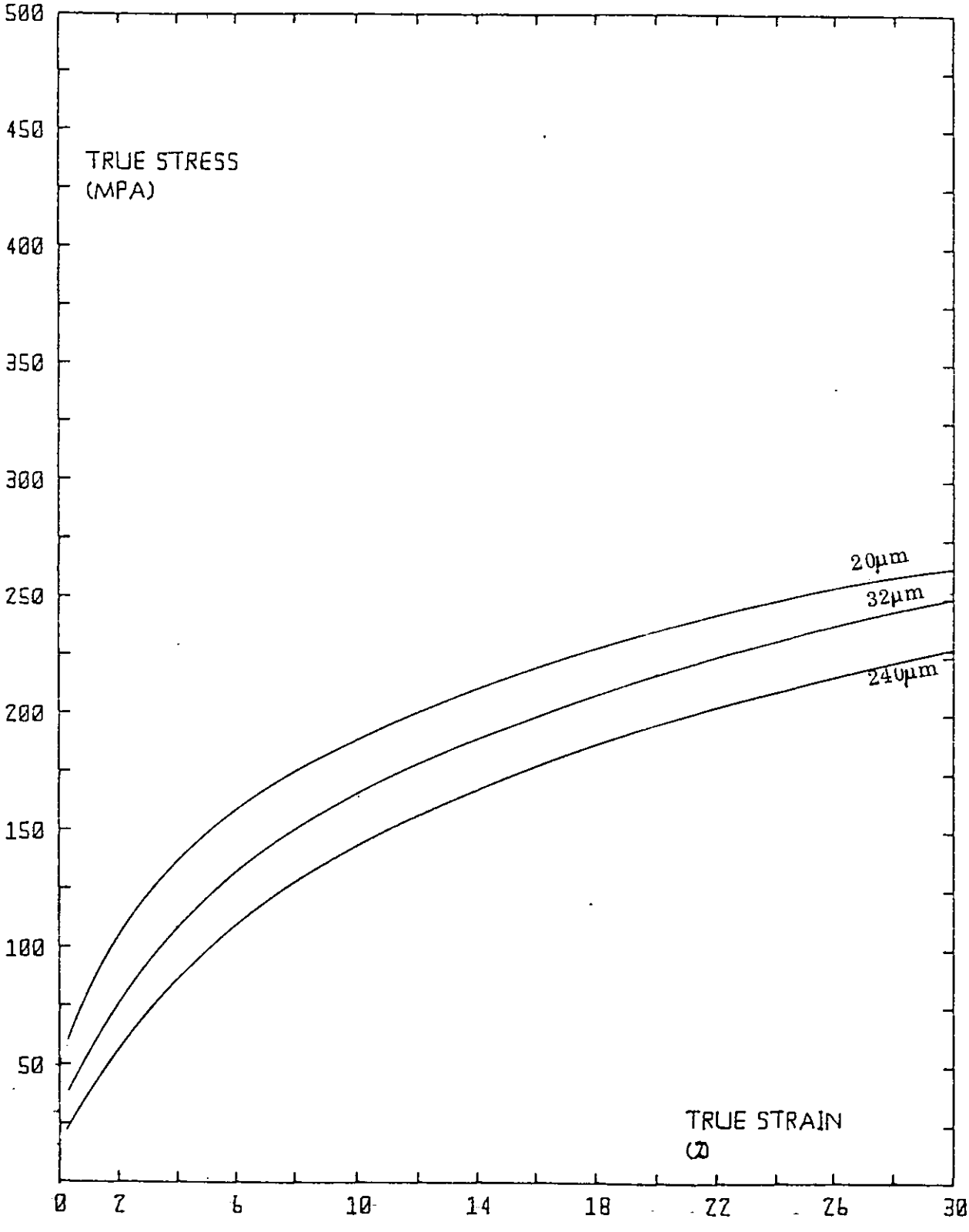

Figure 7.23 Quasi-static compressive tests ($2 \times 10^{-3} s^{-1}$) at 200°C on grain sizes 20, 32 and 240μm

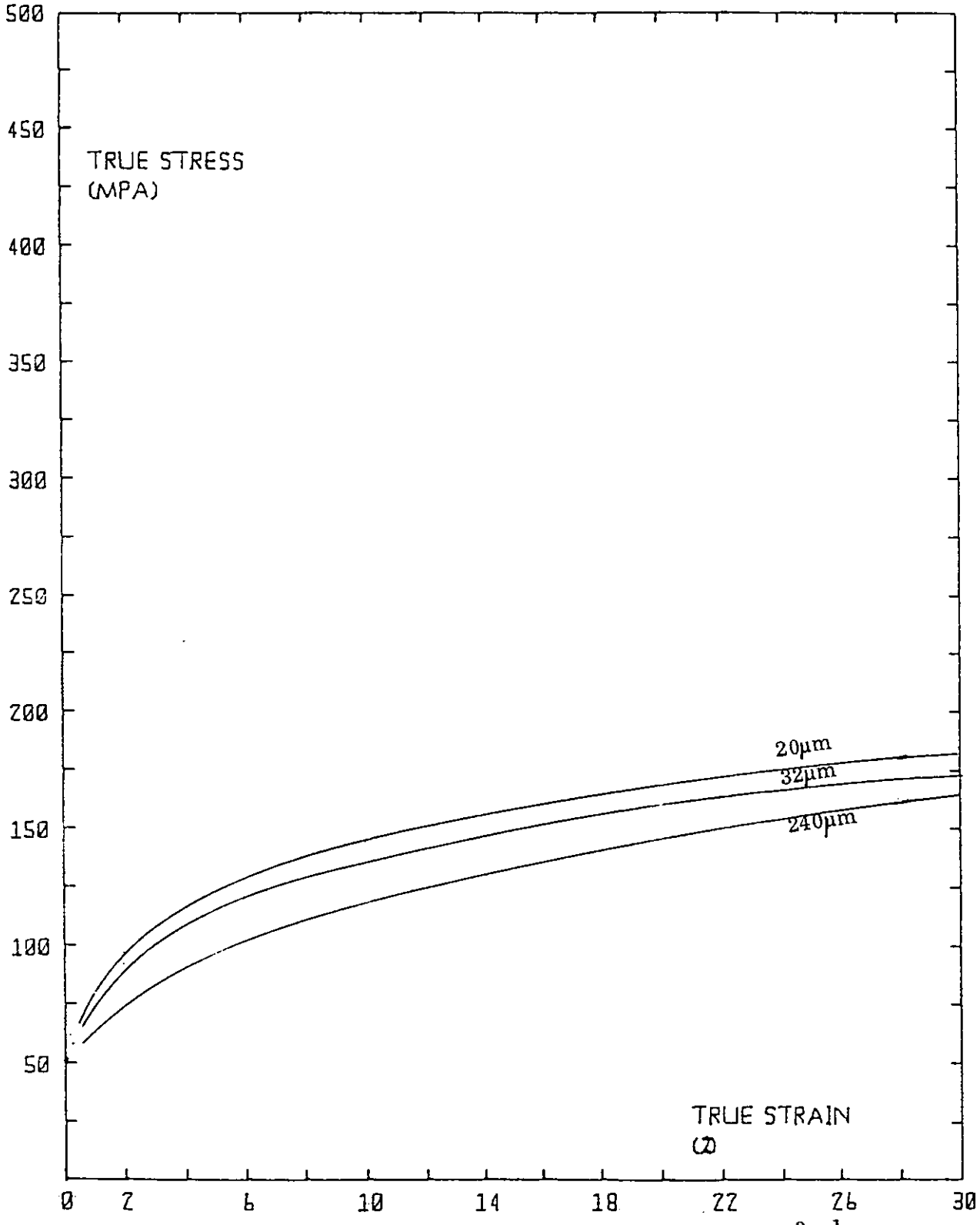

Figure 7.24 Quasi-static compressive tests ($2 \times 10^{-3} s^{-1}$) at $400^{o}C$ on grain sizes 20, 32 and 240μm

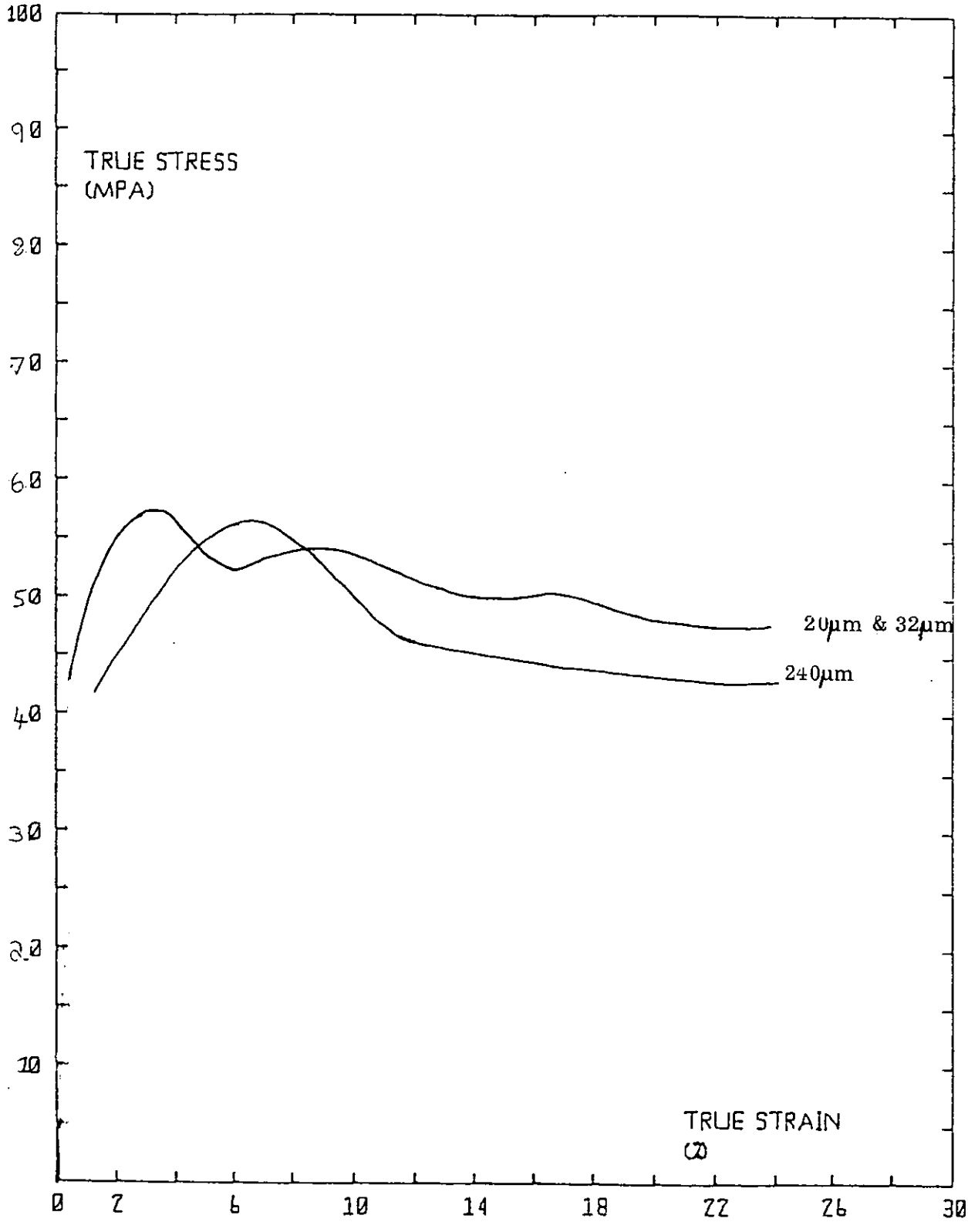

Figure 7.25 Quasi-static compressive tests ($2 \times 10^{-3} s^{-1}$) at $600^{\circ}C$ on grain sizes 20, 32 and 240μm

If desired, stress-strain curves can be generated subsequent to the construction of the stress-strain rate curves. A series of well-defined values of strain rate are chosen which correspond fairly closely with actual strain rate values. For each selected strain rate, the values of flow stress on each constant strain curve are read off. Take, for example, Figure 7.6. If a strain rate of $3000s^{-1}$ is selected, then the flow stresses corresponding to the ten constant strain levels are, starting from the 1% strain level, 95, 120, 142.5, 162.5, 180, 252.5, 307.5, 347.5, 377.5 and 400MPa. Using these stress figures a stress-strain curve at the constant strain rate of $3000s^{-1}$ can be drawn. A typical set of stress vs. strain curves for the room temperature compressive tests on the 20 μm grain size specimens appears in Figure 7.21. If this process were to be repeated for the other stress-strain rate figures, i.e. Figures 7.7 to 7.25, then the variations of stress with strain for the same set of well-defined constant strain rates could be compared in each case. Figure 7.21 indicates three stress-strain curves but 6 different strain rates. This is because at $\dot{\varepsilon} = 2 \times 10^{-3}s^{-1}$, $100s^{-1}$ and $500s^{-1}$ the curves overlap. The same is true for $\dot{\varepsilon} = 1500s^{-1}$ and $3000s^{-1}$. Where the curves overlap there is no difference in strain rate sensitivity within the strain rate ambit covered. At $100s^{-1}$ the curve only extends to 1%. Likewise at $500s^{-1}$ and $1500s^{-1}$, these curves are limited to 5% and 15%, respectively.

7.7.1 Compressive Tests

(a) Variation of Flow Stress with Strain Rate

(i) at room temperature (Figures 7.6 to 7.10)

These figures can be split up into three approximate strain rate regions:

(1) $\dot{\varepsilon} \leqslant 1.5 \times 10^{3} s^{-1}$

For all grain sizes, except 124um, there is virtually zero variation of flow stress with strain rate for constant strain levels up to 5%. Above 5%, flow stress increases with strain rate for all grain sizes; the average gradient of the curves increasing with strain, up to the maximum strain level of 30%.

(2) $1.5 \times 10^{3} s^{-1} < \dot{\varepsilon} \lesssim 3 \times 10^{3} s^{-1}$

This is a plateau region for nearly all grain sizes and strain levels, i.e. the flow stress remains constant irrespective of strain rate.

(3) $\dot{\varepsilon} > 3 \times 10^{3} s^{-1}$

In this region flow stress increases again with strain rate.

A few of the stress-strain rate curves exhibit a fairly linear region with a positive gradient. An example of this is the curve for the largest grain size (Figure 7.10) at a constant strain level of 10%, which is approximately linear

from $1150s^{-1}$ to $6150s^{-1}$.

(ii) <u>at elevated temperatures (Figures 7.11 to 7.19 and 7.23 to 7.25)</u>

At 200°C there is a much greater reduction in quasi-static flow stress levels than in dynamic stresses compared with the room temperature results.

At 400°C there is a more general reduction in flow stresses at all strain rates. There is a linear variation between stress and strain rate (Figure 7.16) between strain rates of $650s^{-1}$ and $4050s^{-1}$, for strain levels of 3%, 4% and 5%, for the 240μm grain size.

At 600°C the flow stress at the highest strain rates are now between 60% and 80% of their equivalent room temperature values. The flow stress reduction increases as the strain level increases. The quasi-static flow stresses exhibit a dramatic decrease, oscillating slightly as the strain increases about a mean flow stress level of about 50MPa (Figure 7.25). Similar observations about oscillatory stress fluctuations at elevated temperatures were also noted by BLAZ et al (1983), in their quasi-static tests of copper. They attributed their findings to dynamic recrystallisation. If the temperature is sufficiently high and the strain rate low enough, then recrystallisation occurs as a specimen is being strained. (N.B. The time taken to complete each compressive quasi-static test was about 10 minutes).

(b) Variation of Flow Stress with Grain Size

(i) at room temperature

Flow stress decreases with increasing grain size for a given strain rate and strain level. This decrease is almost independent of strain. For example, in the aforementioned plateau region there is a stress difference of approximately 60MPa between any strain level for the 20μm grain size (Figure 7.6) and the same strain level for the 240μm grain size (Figure 7.10). This relation between stress difference and strain level has been investigated in greater detail for each of the grain sizes 20μm, 29μm, 32μm and 124μm, relative to the largest grain size of 240μm.

For the strain rate of $2 \times 10^{-3} s^{-1}$, in each of the four curves of stress difference vs. strain (Figure 7.26), there are two approximately linear regions. The strain at which the linear 'regions' intersect varies between 5% and 7%.

At the dynamic strain rate of $2 \times 10^{3} s^{-1}$, the stress difference data follow a similar trend, except that for three of the four curves the stress difference is constant between approximately 5% and 20% (or 25%) (Figure 7.27). The intersecting points vary from 3% to 6%.

(ii) at elevated temperatures

The stress differences $\sigma_{20} - \sigma_{240}$ and $\sigma_{32} - \sigma_{240}$ were computed for the elevated temperature tests at 200°C and 400°C. Two linear regions were again discernible.

However, the strain levels at which the lines intersect show a wider variation (5% - 20%). At 200°C, all the lines

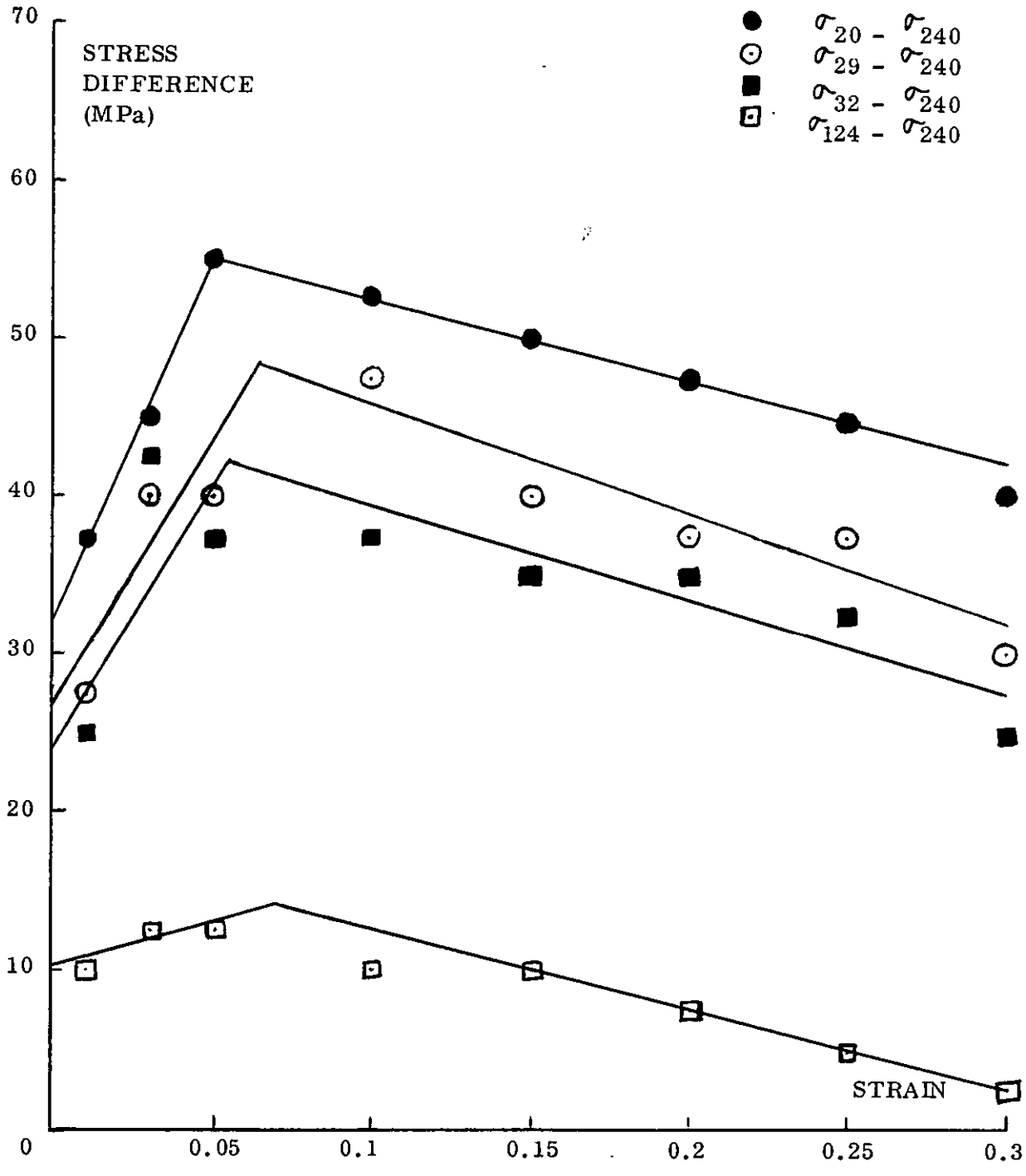

Figure 7.26 Variation of stress difference with strain

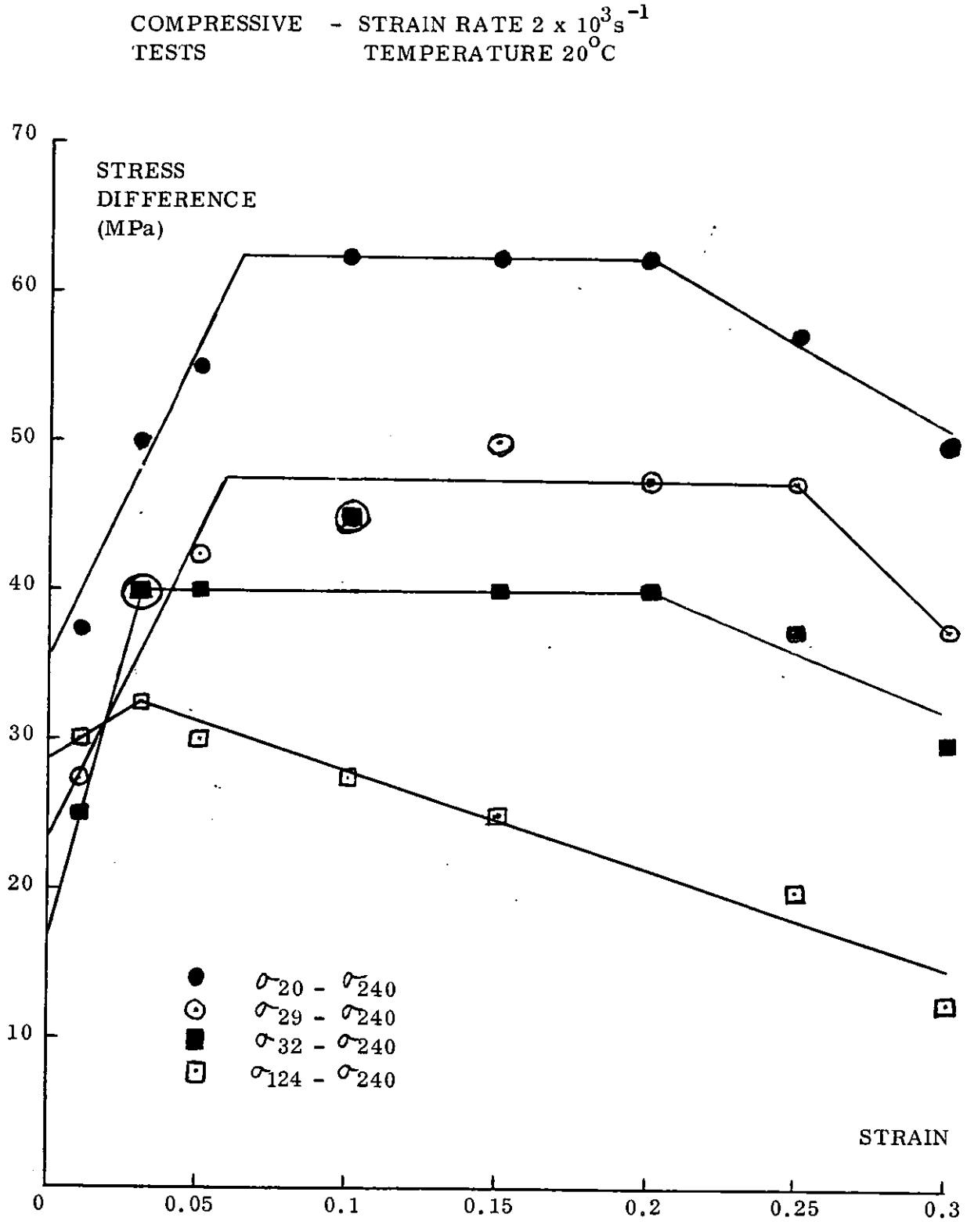

Figure 7.27 Variation of stress difference with strain

have positive gradients, whereas at 400°C, the gradients are all less than or equal to zero.

(c) Strain Rate Sensitivity

(i) at room temperature

Defining strain rate sensitivity (λ) at constant strain as

$$\lambda = \frac{\partial \sigma}{\partial \log \dot{\varepsilon}} \quad ,$$

the room temperature compressive test results can be split into two regions of strain rate sensitivity according to strain rate. This can be seen more easily from Figure 7.28(a), where a representative cross section of the results has been re-plotted as σ vs. log $\dot{\varepsilon}$.

Above approximately $10^3 s^{-1}$ there is a rapid increase in λ for all grain sizes and at all strain levels. Below about $10^3 s^{-1}$, there is a linear relation between λ and log $\dot{\varepsilon}$. λ is zero (or near zero) at strains less than or equal to 5%. This is true for all grain sizes. Above strains of 5%, λ increases with strain for all grain sizes. λ decreases slowly with increasing grain size.

The variation of the mean strain rate sensitivity (λ_m), for the strain rates between $2 \times 10^{-3} s^{-1}$ and $3 \times 10^3 s^{-1}$, with strain for the grain size of 240μm is shown in Figure 7.29. The curves for the other grain sizes are qualitatively very similar.

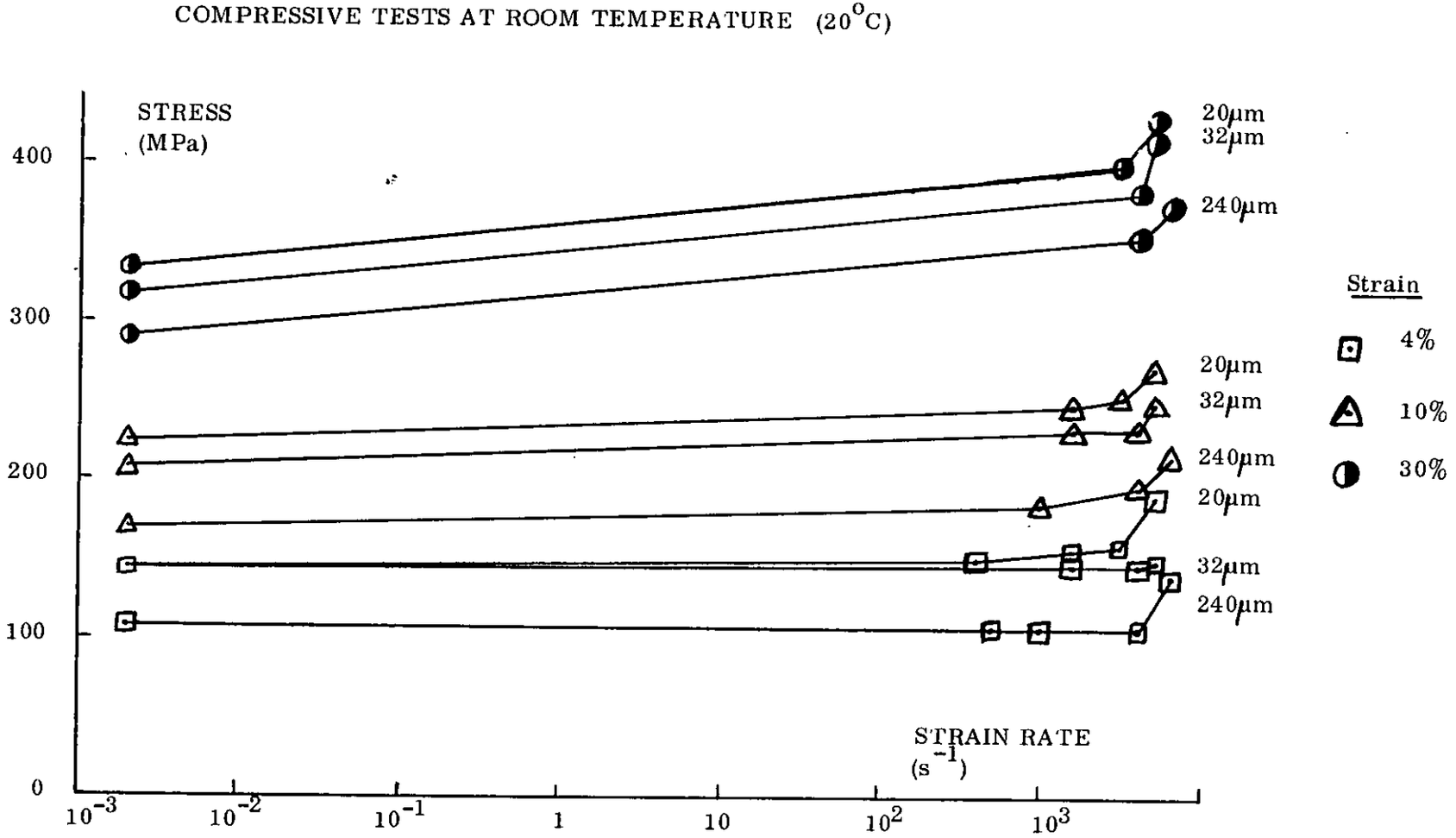

Figure 7.28 (a) Flow Stress versus Log Strain Rate

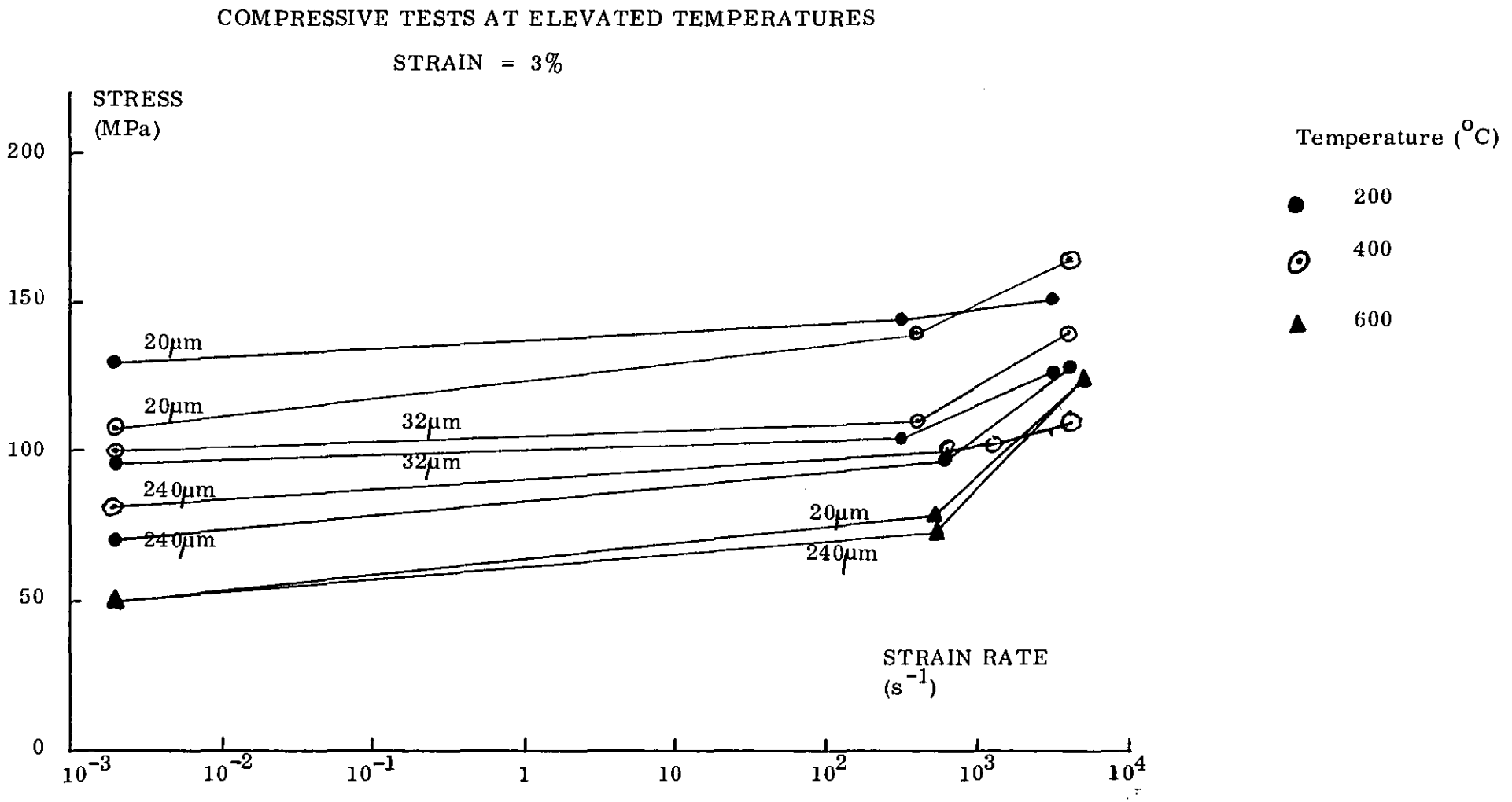

Figure 7.28(b) Flow Stress versus Log Strain Rate

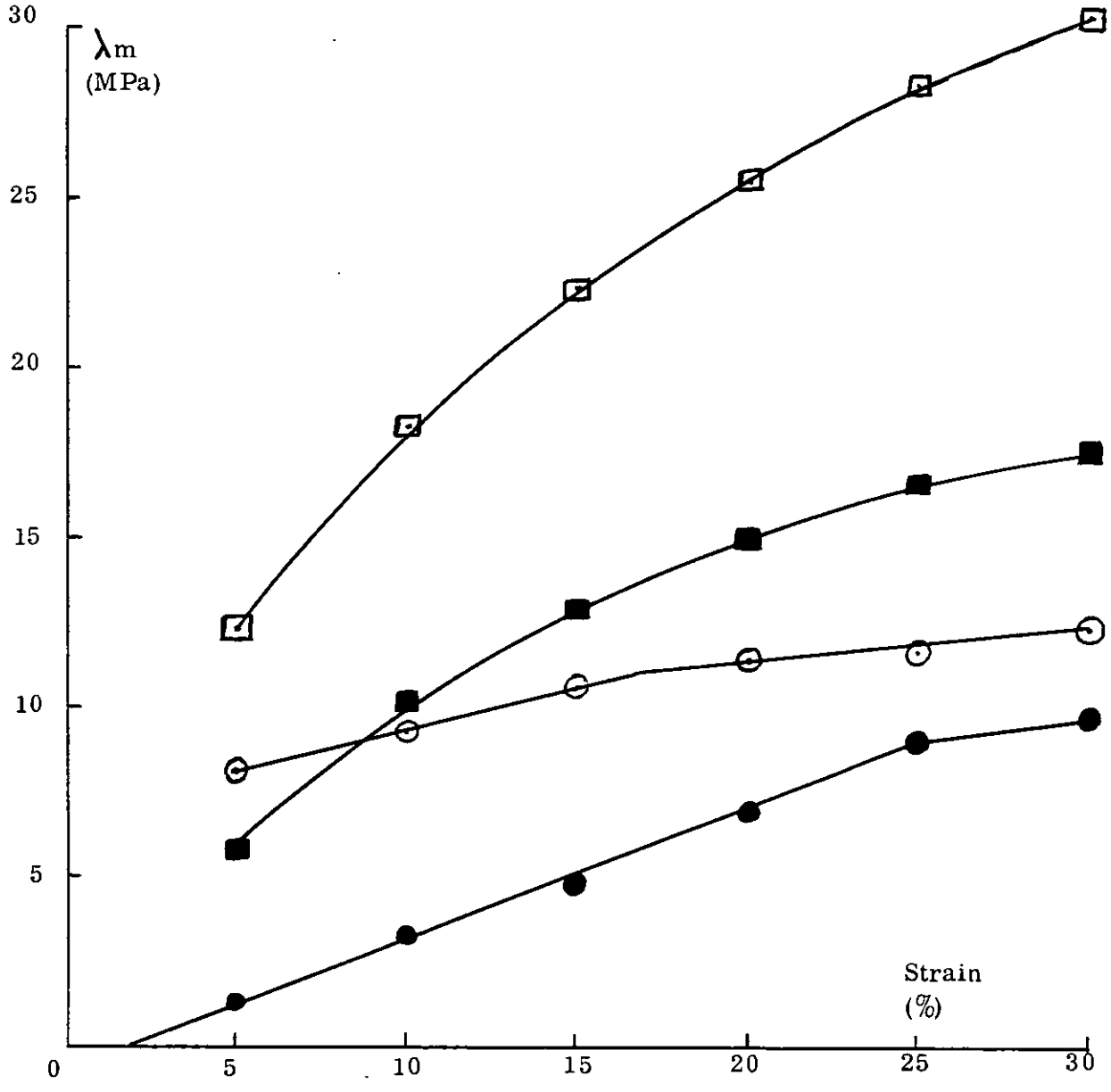

Figure 7.29

Mean Strain Rate Sensitivity (λ m) v. Strain
- Strain Rate Region $2 \times 10^{-3} s^{-1}$ to $3 \times 10^{3} s^{-1}$
- Grain Size 240μm

Test	●	20°C	⊙	200°C
Temperatures	■	400°C	⊡	600°C

Between 3 x $10^3 s^{-1}$ and 5 x $10^3 s^{-1}$, there is a less uniform variation of λ_m with strain. The λ_m maxima for the same three grain sizes, 20μm, 32μm and 240μm, are 53MPa, 44MPa and 24MPa, respectively. The maxima for the first two grain sizes occur at strains of 5% and 25%, respectively. For the 240μm grain size there were 3 maxima, each of 24MPa, which occurred at strains of 15%, 25% and 30%.

(ii) <u>at elevated temperatures</u>

At low strain levels (e.g. 3%) there is again an up turn in the stress vs. log strain rate curve, occurring between $10^2 s^{-1}$ and $10^3 s^{-1}$ (Figure 7.28(b)), especially at 600°C. Due to insufficient data, a similar observation cannot be made for strain levels larger than approximately 3%.

At all strain rates, λ is an increasing function of strain and temperature. In general, λ decreases with increasing grain size, although there are a couple of anomalies.

The variations of λ_m with strain, for the 240μm grain size, are shown in Figure 7.29 for the three elevated testing temperatures. The strain rate region is 2 x $10^{-3} s^{-1}$ to 3 x $10^3 s^{-1}$. Again the curves for the other grain sizes exhibit similar profiles.

The maximum values of λ_m for the three grain sizes and all four testing temperatures are listed in Table 7.2. These maxima all occur at the highest strain level recorded, i.e. 30%.

Table 7.2

Variation of the Maximum Value of Mean Strain Rate Sensitivity

Strain rate region: $2 \times 10^{-3} s^{-1}$ to $3 \times 10^{3} s^{-1}$

Temperature (°C)	Grain Size (μm)	Maximum λ_m (MPa) ($\varepsilon = 30\%$)
20	20	10.8
20	32	10.4
20	240	9.7
200	20	17.5
200	32	14.3
200	240	12.2
400	20	17.8
400	32	17.2
400	240	17.8
600	20	27.9
600	32	28.3 ($\varepsilon = 25\%$)
600	240	30.4

(d) Work Hardening Exponent

The most common empirical description of work or strain hardening is a simple power law, i.e.

$$\sigma = K\varepsilon^n, \tag{7.1}$$

where n, the work hardening or strain hardening exponent or coefficient, is a measure of the increase of flow stress with strain during plastic deformation; strain rate, grain size and temperature being constant.

From equation (7.1),

$$n = \frac{\partial \log \sigma}{\partial \log \varepsilon} \tag{7.2}$$

Figure 7.30 shows the relation between log σ and log ε for the grain size of 20μm. In general, for each constant strain rate, the data form two linear regions which intersect at strain levels between 15% and 20%. The gradient of each linear region, of course, corresponds to the work hardening exponent for that region. The other grain sizes exhibit qualitatively similar results.

Table 7.3 lists the work hardening exponents for 3 grain sizes, 4 test temperatures and 2 or 3 strain rates.

Excluding the quasi-static tests at 600°C, n only varies from 0.18 to 0.6 over the large range of strain rates, temperatures and grain sizes. The work hardening exponent in the lower strain region is always larger than or equal to that in the higher region. There is a tendency for greater strain hardening for the largest grain size and for

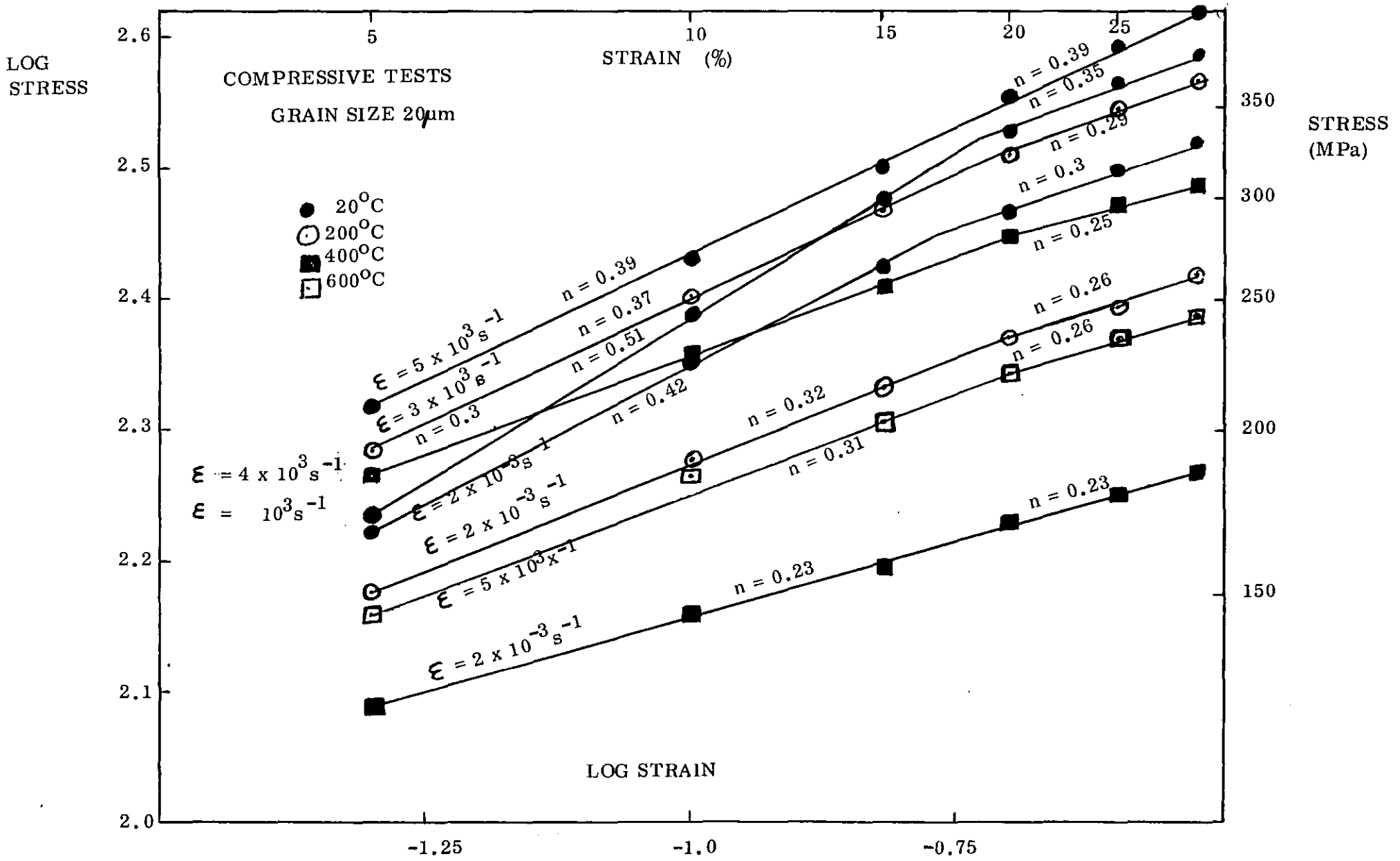

Figure 7.30 Dependence of work hardening exponent n on strain and strain rate

Table 7.3

Variation of Work Hardening Exponent

Temperature (°C)	Grain Size (μm)	Strain Rate (s^{-1})	Work Hardening Exponent n	
			Lower Strain Region	Higher Strain Region
20	20	2×10^{-3}	0.42	0.3
20	20	1×10^{3}	0.51	0.35
20	20	5×10^{3}	0.39	0.39
20	32	2×10^{-3}	0.4	0.33
20	32	1×10^{3}	0.48	0.36
20	32	5×10^{3}	0.53	0.36
20	240	2×10^{-3}	0.57	0.42
20	240	1×10^{3}	0.6	0.52
20	240	5×10^{3}	0.57	0.5
200	20	2×10^{-3}	0.32	0.26
200	20	3×10^{3}	0.37	0.29
200	32	2×10^{-3}	0.42	0.42
200	32	3.5×10^{3}	0.49	0.36
200	240	2×10^{-3}	0.5	0.36
200	240	3×10^{3}	0.42	0.37
400	20	2×10^{-3}	0.23	0.23
400	20	4×10^{3}	0.3	0.25
400	32	2×10^{-3}	0.25	0.18
400	32	4×10^{3}	0.32	0.24
400	240	2×10^{-3}	0.32	0.24
400	240	4×10^{3}	0.43	0.33
600	20	2×10^{-3}	0	0
600	20	5×10^{3}	0.31	0.26
600	32	2×10^{-3}	0	0
600	32	3.5×10^{3}	0.24	0.24
600	240	2×10^{-3}	0	0
600	240	5×10^{3}	0.3	0.3

a decrease in strain hardening as the test temperature increases. Comparing the values of n at high strain rates with those at quasi-static rates, in more than 83% of these comparisons n is larger at the higher rate.

(e) Variation of the dynamic to quasi-static flow stress ratio (σ_D/σ_S) with homologous temperature

The ratio of dynamic flow stress to quasi-static flow stress is plotted again the ratio of test temperature (K) to melting point (K) in Figure 7.31. The latter ratio is known as the homologous temperature. In Figure 7.31 the dynamic strain rate is $3 \times 10^{3} s^{-1}$, the quasi-static strain rate is $2 \times 10^{-3} s^{-1}$ and the strain level in both cases is 15%. For homologous temperatures below 0.5 there is a linear increase of σ_D/σ_S with temperature and the gradient is small. Above 0.5 there is a rapid increase in σ_D/σ_S. This is caused by the large reduction in σ_S due to dynamic recrystallisation. The average gradient in the lower temperature region is 1.3. This increases to 17.9 in the upper region.

7.7.2 Tensile tests

(a) Comparison with Compressive Tests

The tensile test results, in the stress-strain rate format, are included in Figures 7.32 to 7.37 and the quasi-static tensile test results, in the stress-strain format, in Figures 7.38 to 7.41. For the reasons previously indicated, these results are far less comprehensive than their compressive counterparts. Where comparisons are possible, however, there is excellent agreement between the

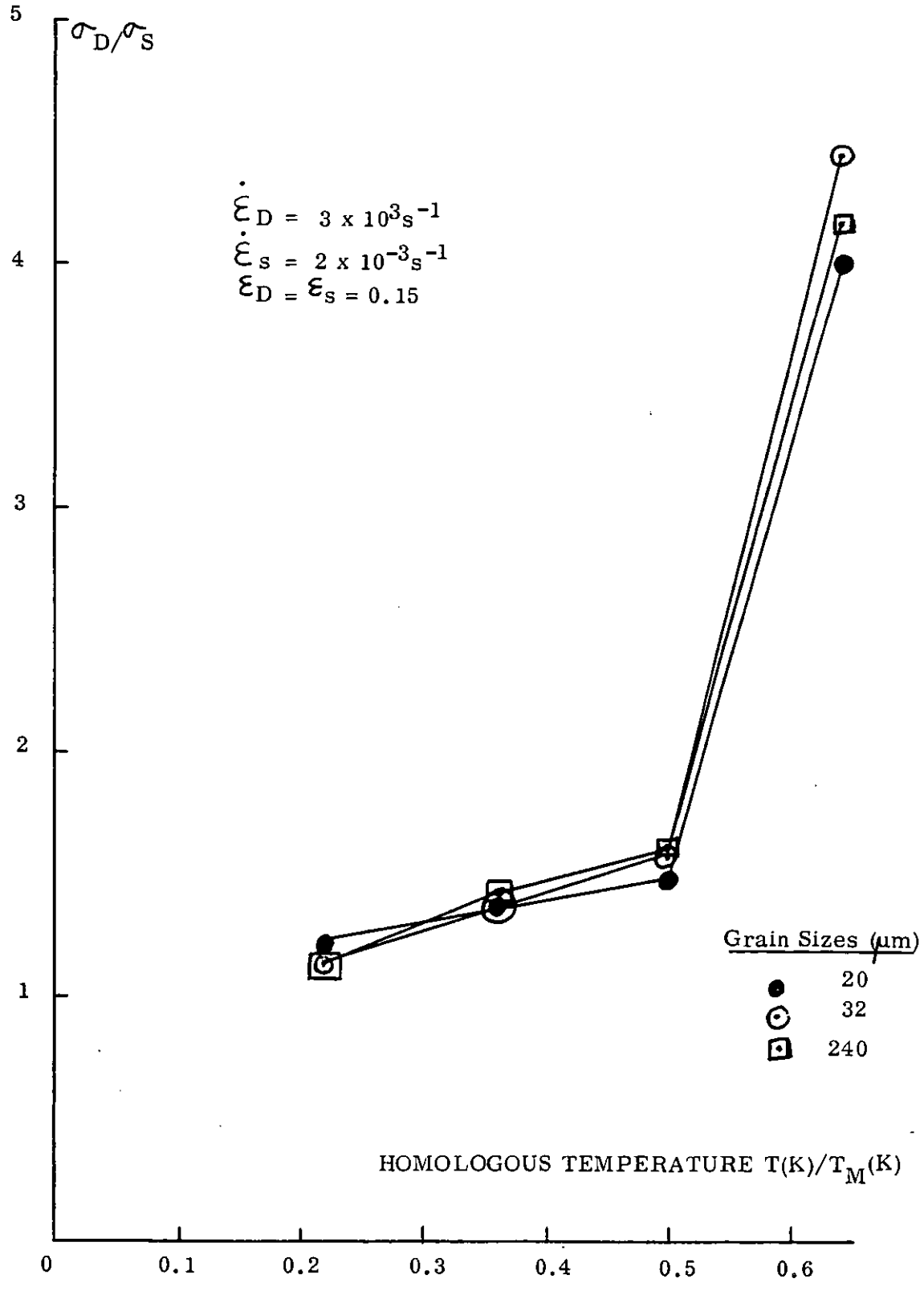

Figure 7.31 Variation of dynamic/static flow stress ratios with homologous temperature for three grain sizes

Figure 7.32 Grain Size 20μm

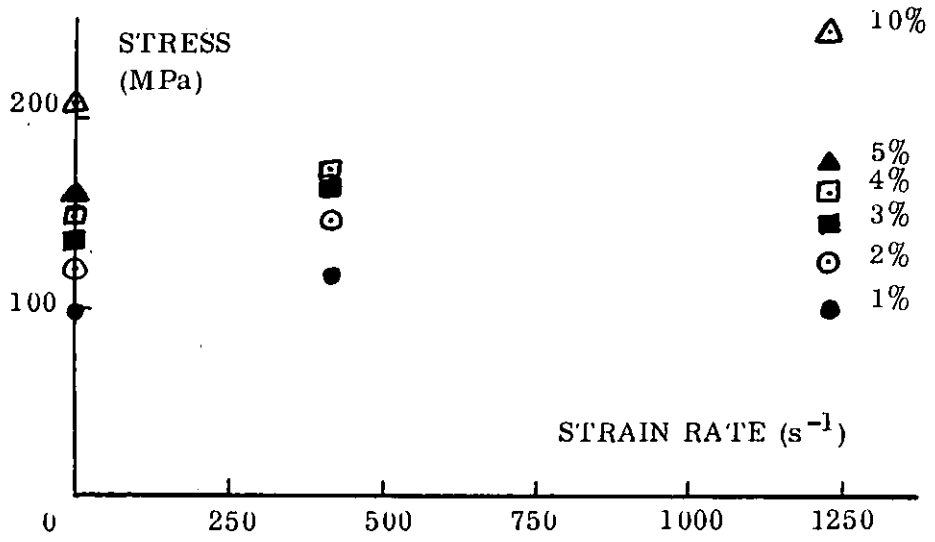

TENSILE TESTS

AT

$20^{o}C$

Figure 7.33 Grain Size 32μm

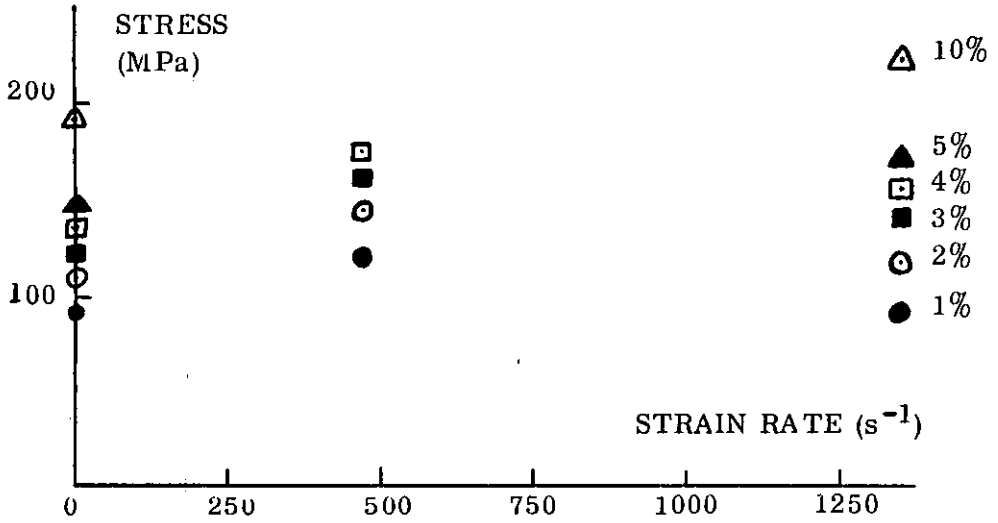

Figure 7.34 Grain Size 240μm

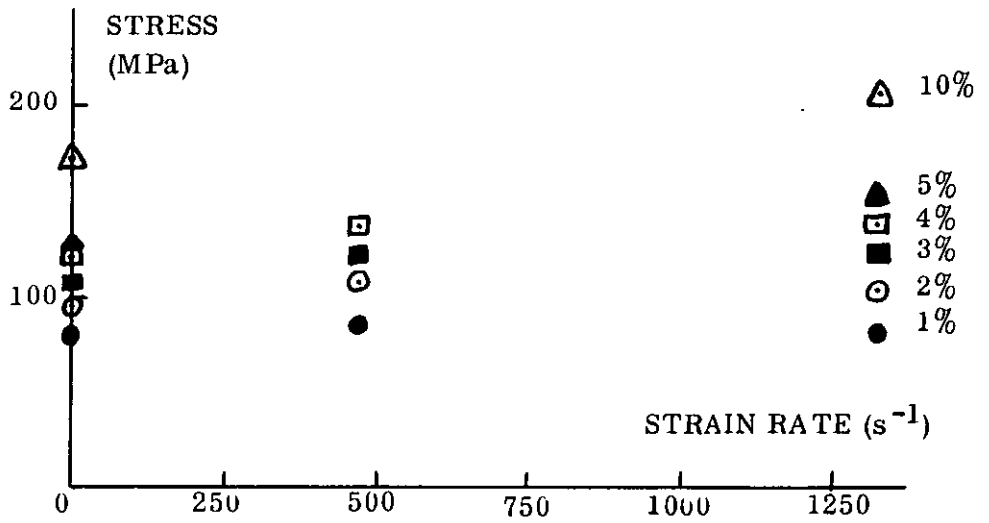

Figure 7.35 Test Temp. 200°C

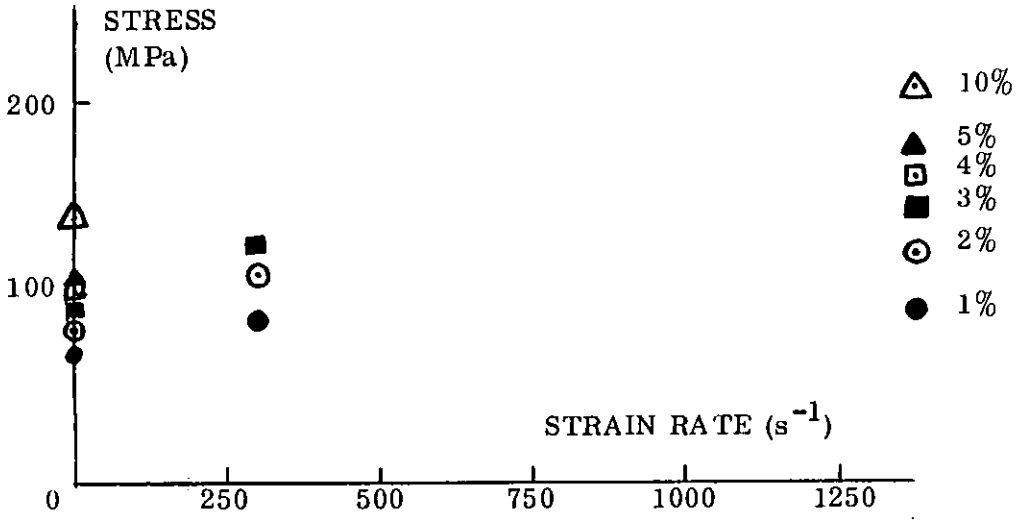

ELEVATED TEMPERATURE

TENSILE TESTS

GRAIN SIZE 240μm

Figure 7.36 Test Temp. 400°C

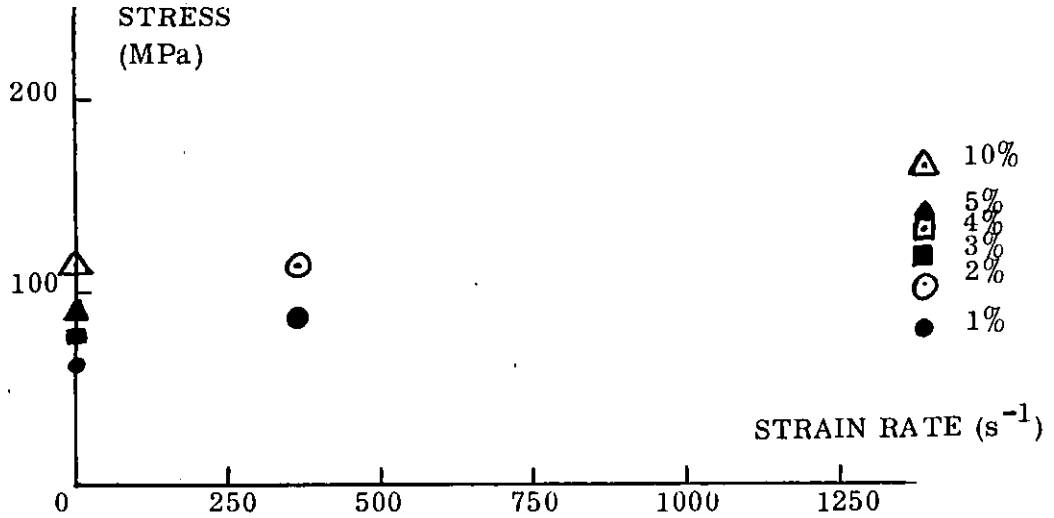

Figure 7.37 Test Temp. 600°C

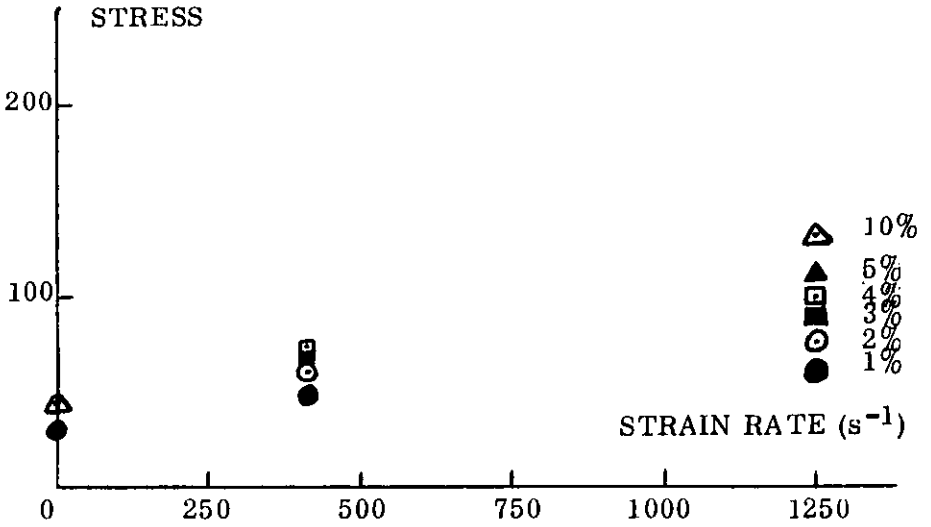

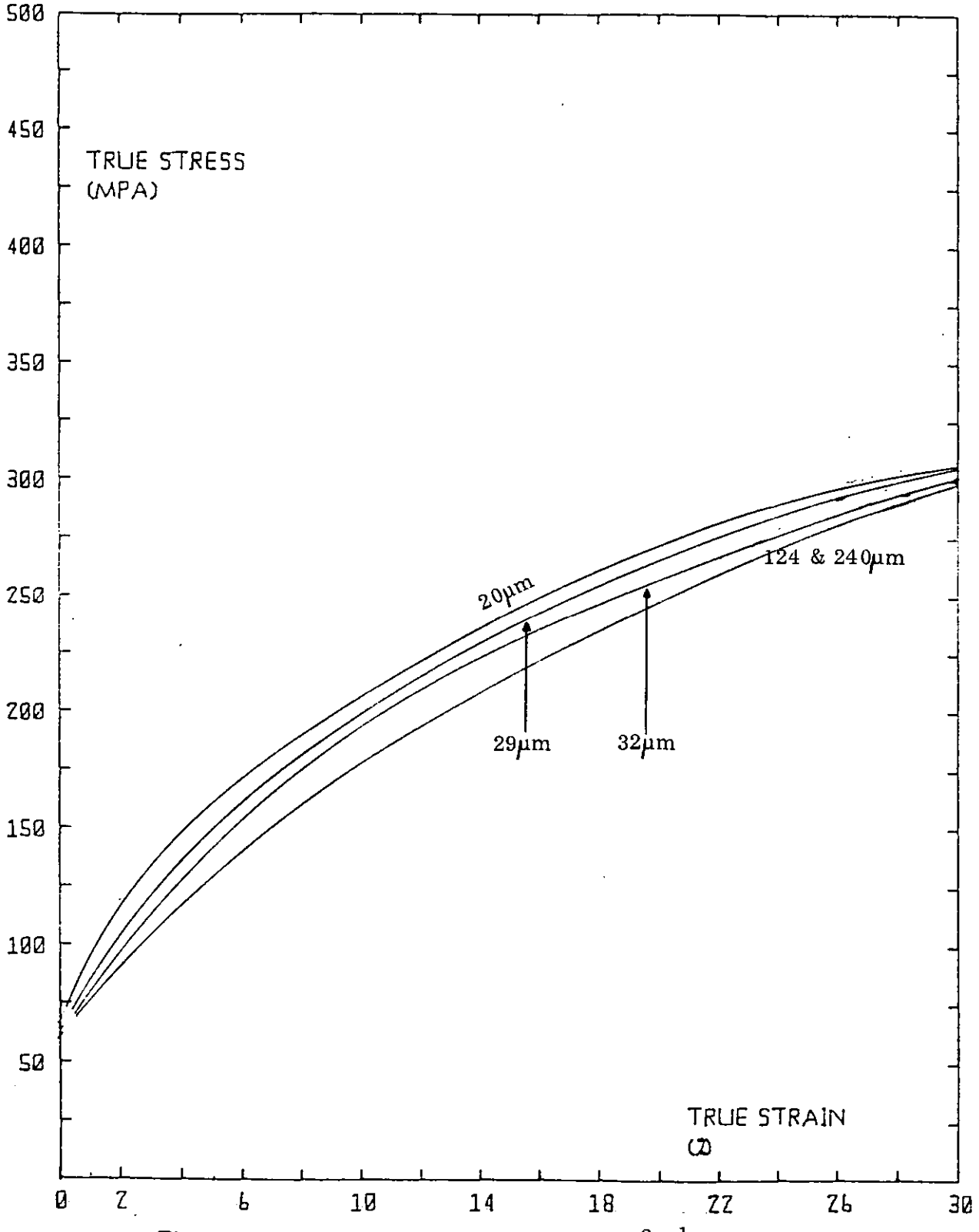

Figure 7.38 Quasi-static tensile tests ($10^{-3}s^{-1}$) at 20°C on grain sizes 20, 29, 32, 124 and 240μm

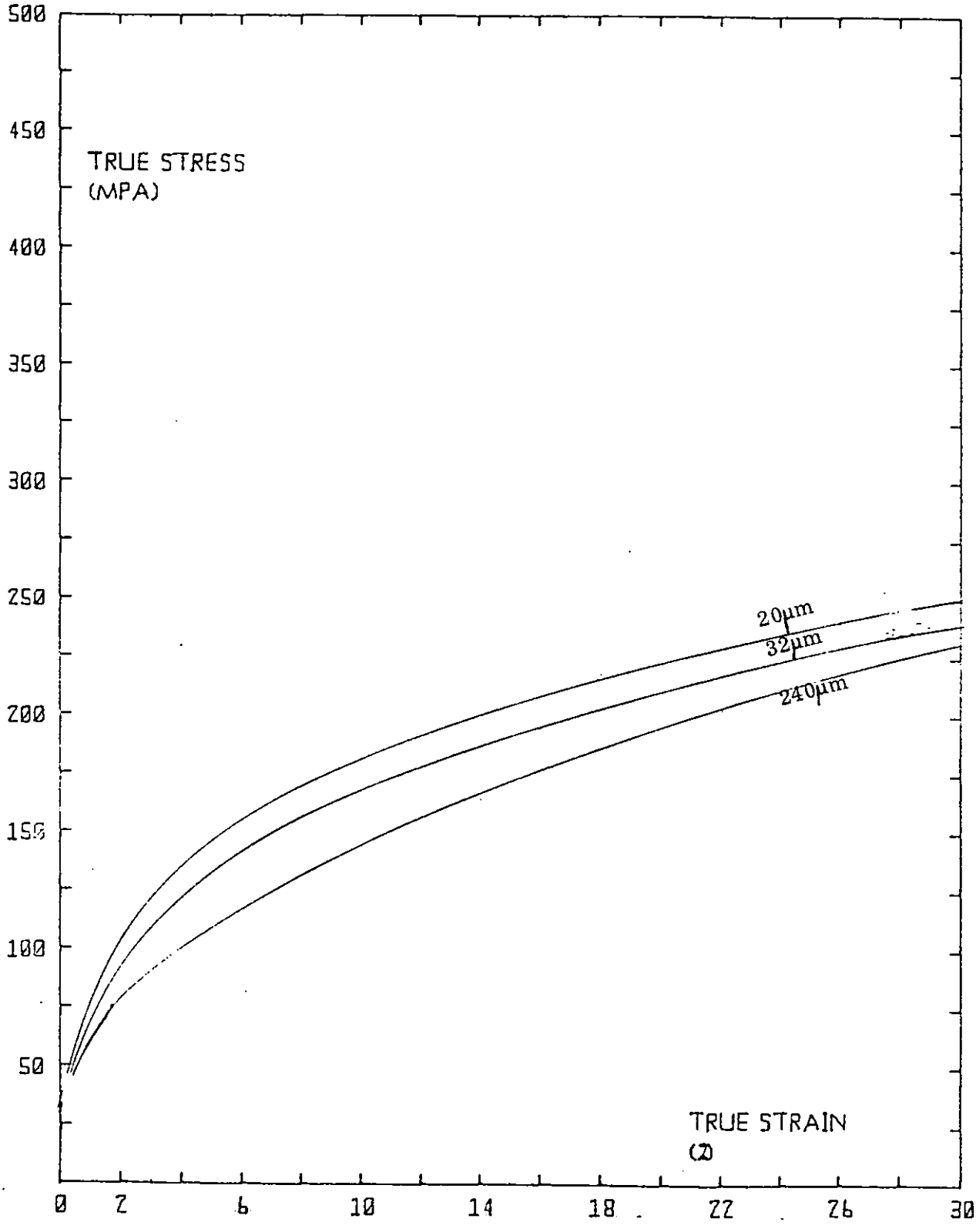

Figure 7.39 Quasi-static tensile tests ($10^{-3}s^{-1}$) at 200°C on grain size 20, 32 and 240μm

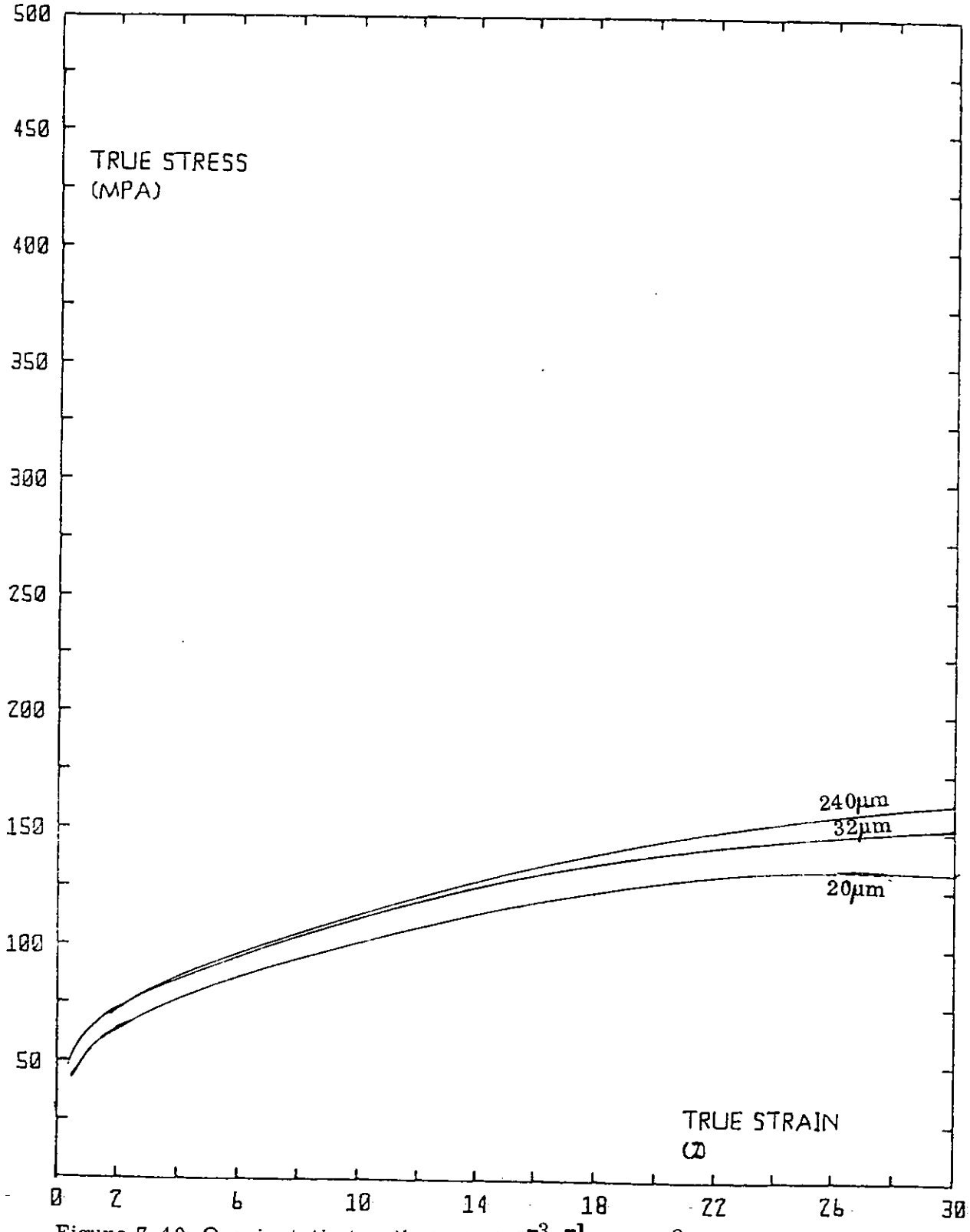

Figure 7.40 Quasi-static tensile tests ($10^{-3}s^{-1}$) at 400°C on grain sizes 20, 32 and 240 μm

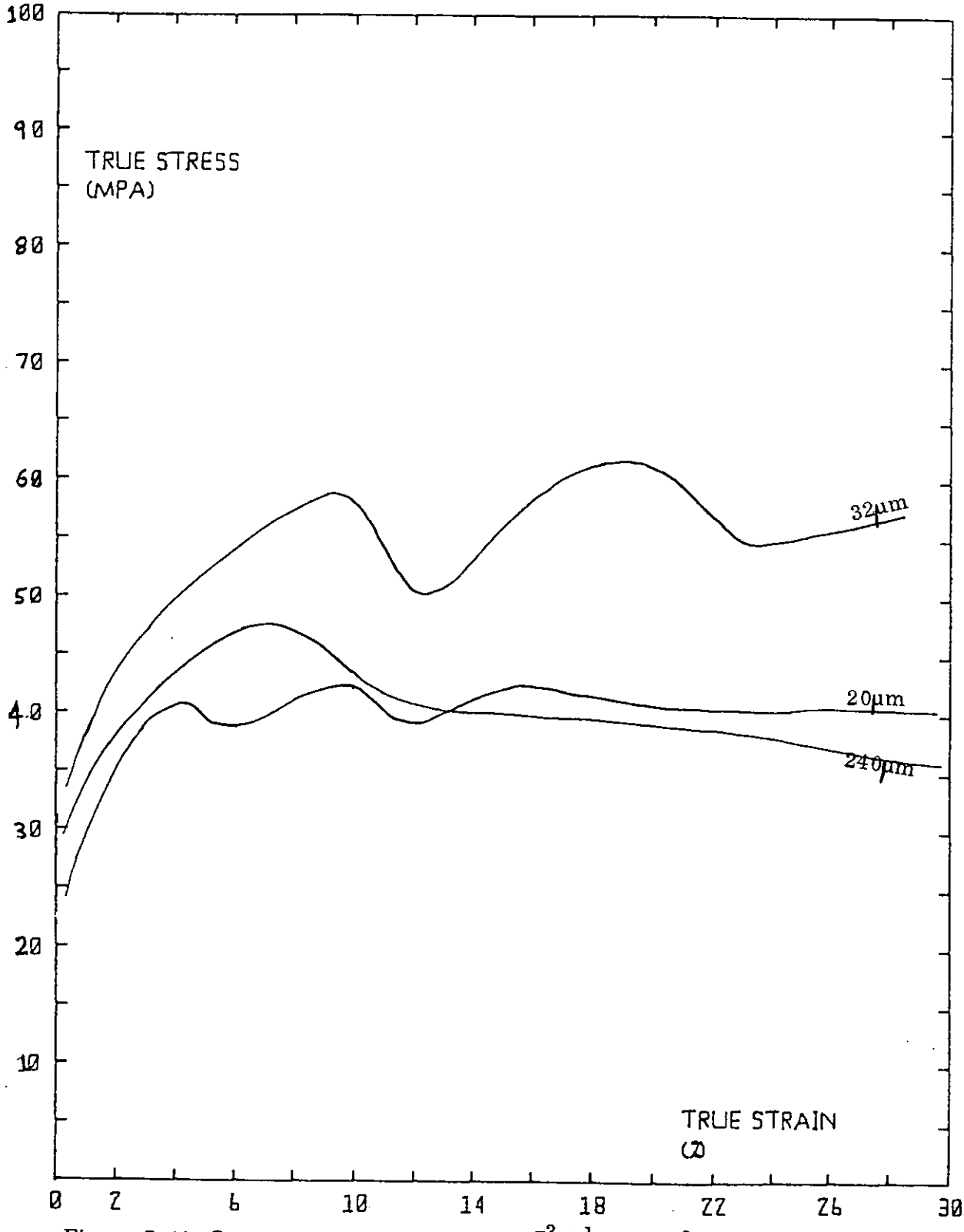

Figure 7.41 Quasi-static tensile tests ($10^{-3}s^{-1}$) at 600°C on grain sizes 20, 32 and 240 um

two modes of testing in the majority of cases.

To quantify this comparison, the differences between the compressive flow stresses and the tensile flow stresses were determined at corresponding strain rates, grain sizes and temperatures for a given number of constant strain levels. For instance, for the room temperature quasi-static strain rate tests, the tensile flow stress at the 5% strain level was subtracted from the compressive flow stress at the same strain. This process was repeated for strains of 10%, 15%, 20%, 25% and 30%. These flow stress differences were then summed and the average flow stress difference found. A mean was also found by dividing the latter by the mean compressive flow stress, calculated from the same strain levels.

The results of these compressive-tensile test comparisons are listed in Tables 7.4(a) to 7.4(e). A negative stress difference indicates that the mean tensile stress is greater than the mean compressive stress.

The variations of flow stress with strain rate, grain size, strain and temperature all follow the same trends as the results of the compressive tests.

The work hardening exponent again has a lower and higher value for each quasi-static stress-strain curve, at constant temperature and grain size. The critical strain is always 20% for this mode of testing. With the exception of tests at 600^{o}C, where dynamic recrystallisation is again effective, the value of n in the lower strain region varies

Table 7.4

Variation of Mean Flow Stress Difference with Grain Size

(a)

Quasi-static strain rate
Test temperature: 20°C
Constant strain levels considered: 5, 10, 15, 20, 25 & 30%

Grain Size (μm)	Mean Flow Stress Difference (MPa)	Mean Relative Stress Difference (%)
20	19.8	7.4
29	16.6	6.4
32	18.9	7.5
124	3.9	1.7
240	-4.0	-1.8

(b)

Strain rate: $1.25 \times 10^{3} s^{-1}$
Test temperature: 20°C
Constant strain levels considered: 1, 3, 5 & 10%

Grain Size (μm)	Mean Flow Stress Difference (MPa)	Mean Relative Stress Difference (%)
20	-2.5	-1.5
32	-4.4	-2.9
240	-26.3	-23.2

(c)

Quasi-static strain rate
Test temperature: 200°C
Constant strain levels considered: 5, 10, 15, 20, 25 & 30%

Grain Size (μm)	Mean Flow Stress Difference (MPa)	Mean Relative Stress Difference (%)
20	10.2	4.7
32	5.3	2.7
240	-0.8	-0.5

(d)

Quasi-static strain rate
Test temperature: 400°C
Constant strain levels considered: 5, 10, 15, 20, 25 & 30%

Grain Size (μm)	Mean Flow Stress Difference (MPa)	Mean Relative Stress Difference (%)
20	52.1	32.5
32	20.8	13.7
240	3.8	2.8

(e)

Strain rate: $1.25 \times 10^{3} s^{-1}$
Grain size: 240μm
Constant strain levels considered: 1, 3, 5 & 10%

Temperature (°C)	Mean Flow Stress Difference (MPa)	Mean Relative Stress Difference (%)
200	-29.4	-23.6
400	-3.8	-3.2
600	2.5	2.5

from 0.29 to 0.46 (c.f. in the compressive mode, 0.25 to 0.57). In the higher strain region, n varies from 0.05 to 0.38 (c.f. in the compressive mode, 0.16 to 0.42).

(b) Multiple Loading Dynamic Tensile Fracture

At strain rates of approximately $1300s^{-1}$ in tensile tests, all the specimens fractured. Analysis of the pulse reflected from the specimen indicated a total strain of only 13% for a pulse length of approximately 100us. However, fracture strains of between 60% and 85% were recorded in the quasi-static tensile tests.

The reason for this large discrepancy is that the specimen is not fractured by a single loading pulse in a dynamic test but by the application of several pulses in rapid succession. A tensile loading pulse is reflected from the specimen as a compressive pulse (refer to Figure 4.4). Because of the small cross-sectional area of the specimen, relative to the pressure bars, a very high percentage of the incident pulse is reflected, which is then re-converted to a tensile pulse without attenuation at the free end of bar 2. Consequently, the specimen is loaded for a second time by a pulse whose amplitude is only slightly less than that of the first tensile pulse.

In order to produce further plastic deformation in the specimen on re-loading, a higher stress must be applied because the specimen is now work hardened. Since the cross-sectional area of the specimen has been reduced by the first loading pulse, the second, slightly smaller tensile pulse can still apply a larger stress to the

specimen if the area reduction is sufficient.

Support for this hypothesis is given by Figure 7.42. This is a strain vs. time oscilloscope record of the variation of strain in bar 2 during a tensile test. The initial pulse, which is compressive, is travelling towards the free end of bar 2 and has just passed through the specimen and collar in parallel, prior to the specimen being loaded in tension. The second pulse is the tensile loading pulse, the magnitude of which is equal to that of the initial compressive pulse. The third pulse has been reflected from the specimen after its initial tensile deformation. The subsequent pulses are alternately tensile loading pulses (generated from the reflection of the previous reflected pulse at the free end of bar 2) and compressive pulses reflected from the specimen as it is being plastically deformed. Whilst the specimen is intact, a small percentage of the loading pulse is transmitted through the specimen into bar 1. Hence, prior to fracture the multiple reflections in bar 2 diminish in amplitude as time proceeds.

In Figure 7.42 the multiple reflections have constant amplitude after the fifth loading tensile pulse. Bar 2 is now free at both ends, i.e. the specimen has fractured.

The average engineering strain rate, as determined from the first reflected compressive pulse, is $1700s^{-1}$ and the corresponding strain is 16%. Ignoring changes such as the increasing gauge length of the specimen as the multiple dynamic loadings proceed, the total strain at fracture can

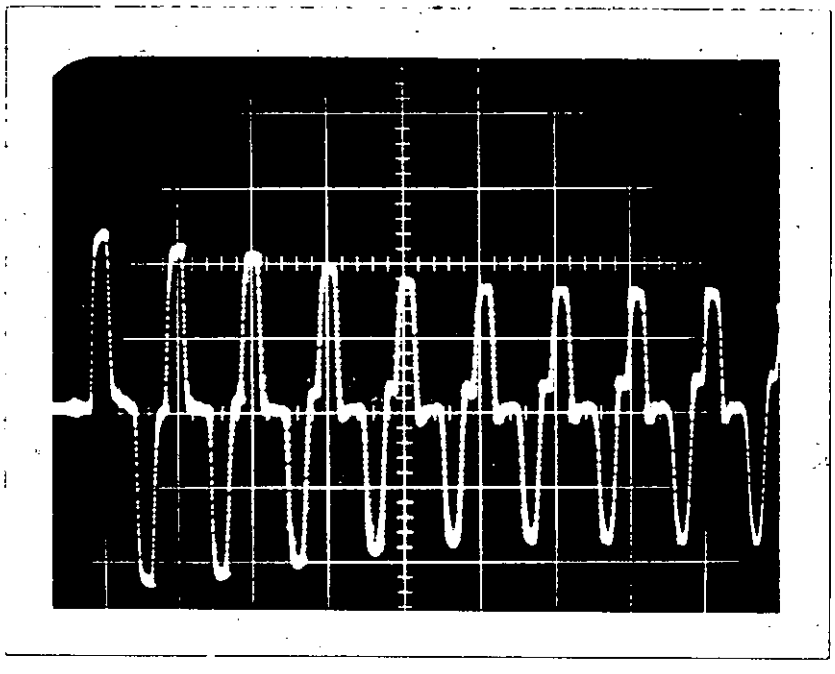

Vertical Scale:
0.06%/div

Horizontal Scale:
400us/div

Average Strain Rate:
1700s^{-1}

Filename:
COT02080016SE

Figure 7.42 Strain pulses in bar 2 during multiple loading dynamic tensile fracture. Fracture occurred after the fifth tensile loading pulse. After fracture, pulses are of equal amplitude.

be very approximately estimated by summing the amplitudes of the reflected pulses up to the time at which fracture occurs. This yields a fracture strain of 71%. The fracture strain was also measured subsequent to the dynamic test by determining the elongation of the central region of the specimen at fracture, from marks placed on the specimen. Dividing this elongation by the original gauge length resulted in a fracture strain of 69%. Hence the multiple reflections which occur during a dynamic tensile test yield a reasonably accurate value of the strain at fracture.

(c) Elongation at Fracture

Figure 7.43(a) indicates the elongation or extension of the tensile specimens at fracture, as a function of grain size. For the quasi-static tests, the 32μm grain size shows the least variation in elongation at fracture as the testing temperature is increased; this grain size yielding the largest extension at room temperature.

In the dynamic room temperature tests, in which fracture occurred by means of multiple loading, the elongation at fracture is approximately 1mm greater than its quasi-static counterpart, for each corresponding grain size.

The variation of elongation at fracture with test temperature is illustrated in Figure 7.43(b) for the 240μm grain size. The dynamic elongations are greater than those occurring in the quasi-static tests, except at 600^{o}C where the large extension of almost 6.5mm is a consequence of dynamic recrystallisation.

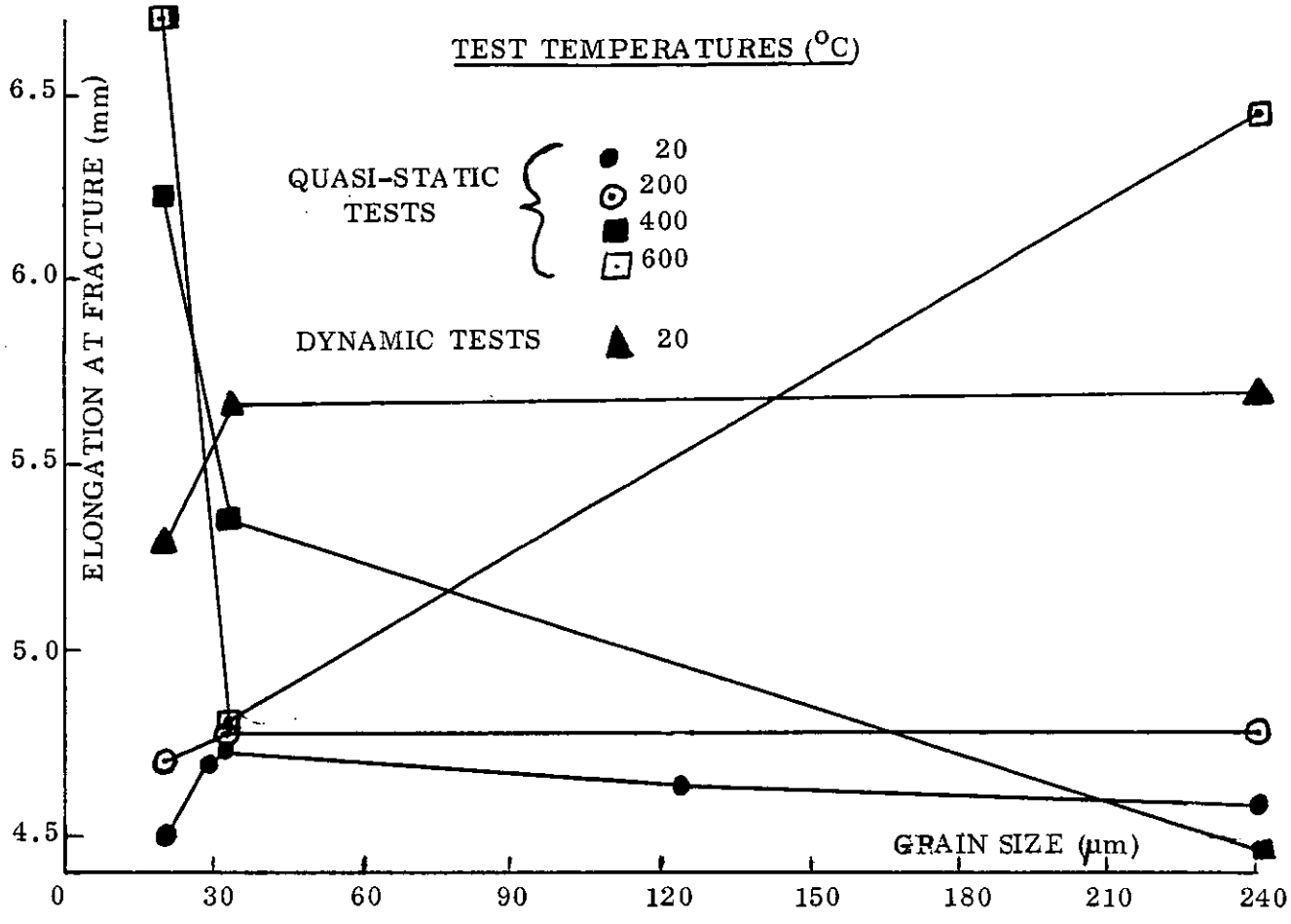

Figure 7.43(a) Elongation at fracture as a function of grain size

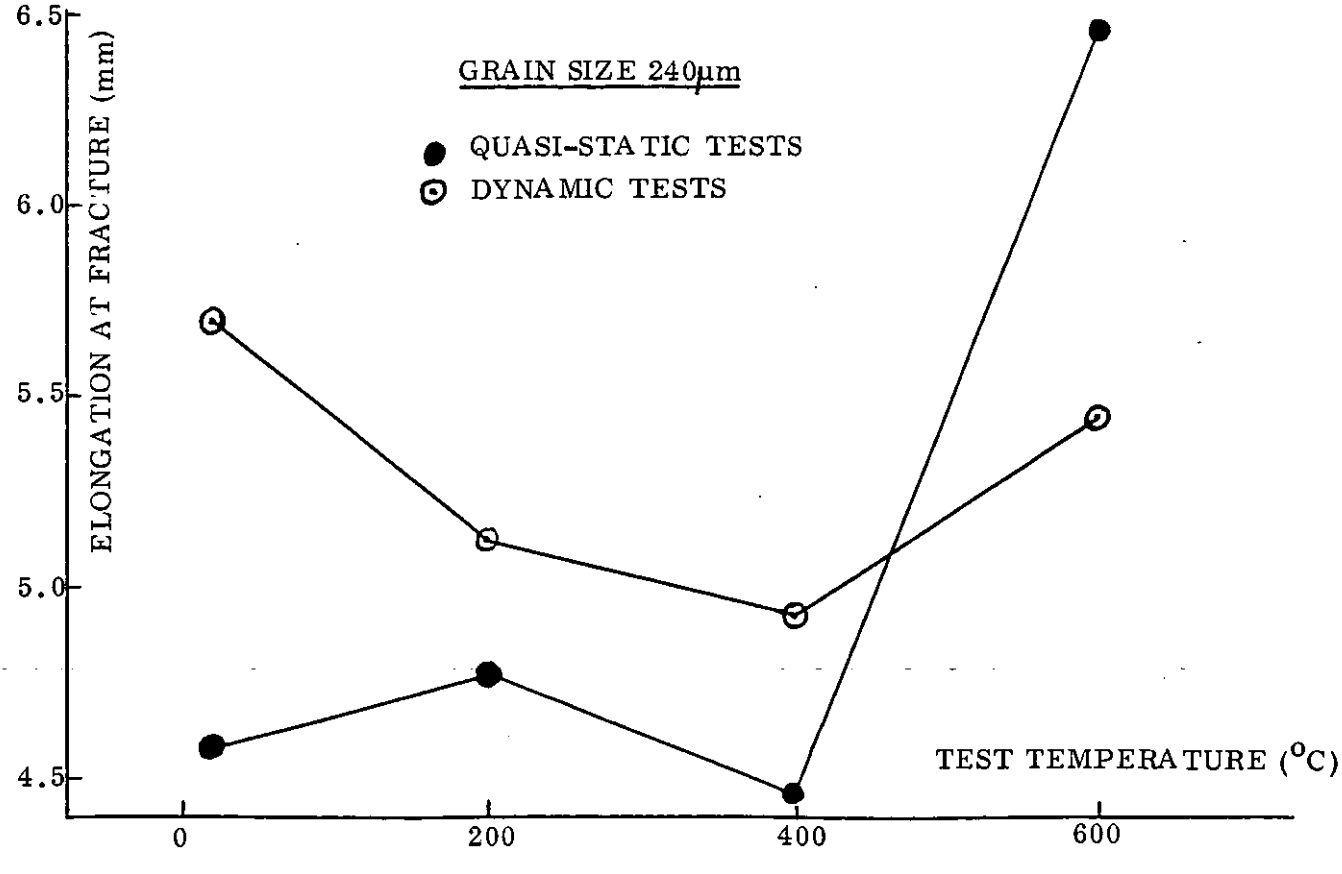

Figure 7.43(b) Elongation at fracture as a function of temperature

(d) Fracture Surfaces

The fracture surfaces of the tensile specimens were examined subsequent to failure and failed specimens representative of each test condition photographed. The quasi-static fracture surfaces are shown in Figures 7.44(a) to 7.44(d) (labelled B, C, D & E). Here the 20μm and 32μm grain sizes exhibited the 'cup and cone' type of fracture surface at all test temperatures except 600°C. The 'cup and cone' type of fracture is extremely common in ductile metals. At 600°C, the 32μm grain size failed by shearing-off or cleavage. The cross-sections of the 20μm specimens, when fractured at 600°C, were reduced to such an extent that very sharp points resulted. This type of fracture surface, of course, corresponds to the dynamic recrystallisation process. For the 240μm grain size, failure occurred by the cleavage process at room temperature and at 200°C. At 400°C, 'cup and cone' fracture was exhibited, whereas at 600°C, dynamic recrystallisation again produced pointed surfaces.

In the dynamic tests, 'cup and cone' occurred at room temperature for the 20μm and 32μm grain size and at 600°C for the 240μm grain sizes. The remainder of the dynamic tensile specimens were fractured by the cleavage process. Photographs of representative dynamic fracture surfaces are contained in Figures 7.45(a) and 7.45(b).

(e) Surface Texture

The surface texture of the 240μm grain size compressive and tensile specimens differed from the smaller grain size specimens subsequent to mechanical testing. This

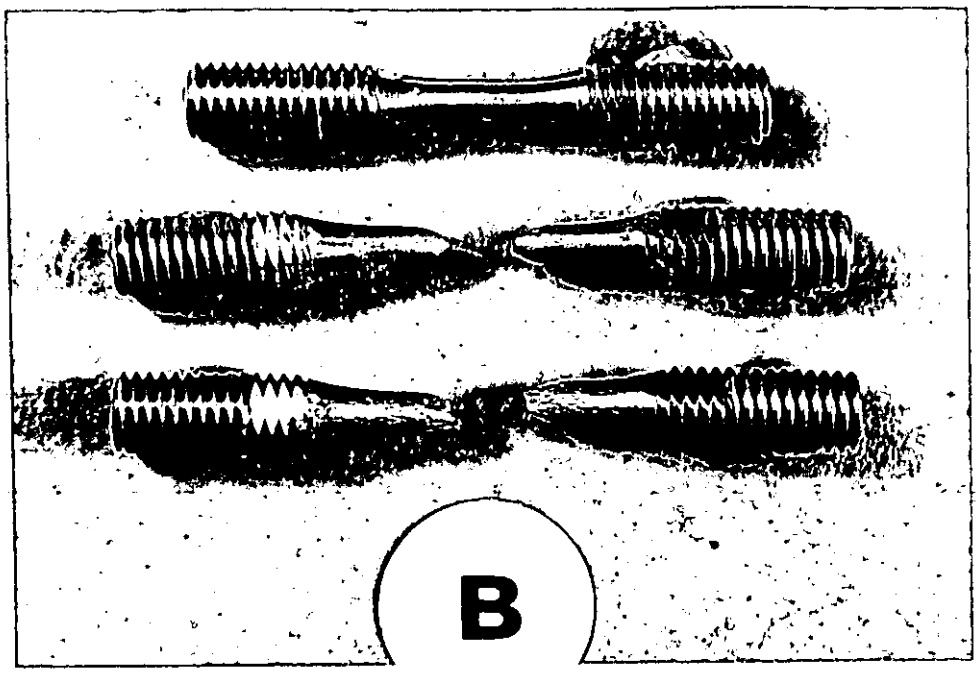

Figure 7.44(a). An undeformed tensile specimen (top) and two specimens fractured in quasi-static strain rate tests at room temperature. The 20 μm (middle) and 240 μm grain size specimens exhibit 'cup and cone' and 'cleavage' fracture surfaces, respectively.

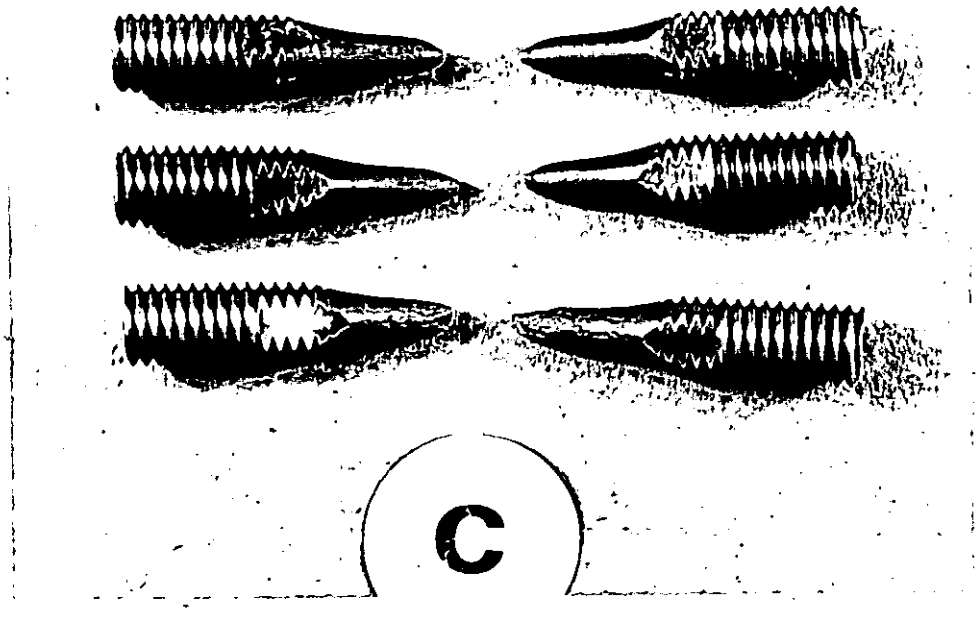

Figure 7.44(b). From top to bottom 20, 32 and 240 μm grain size specimen quasi-statically fractured at 200°C. Failure by the cleavage process is exhibited for the largest grain size and 'cup and cone' for the remainder.

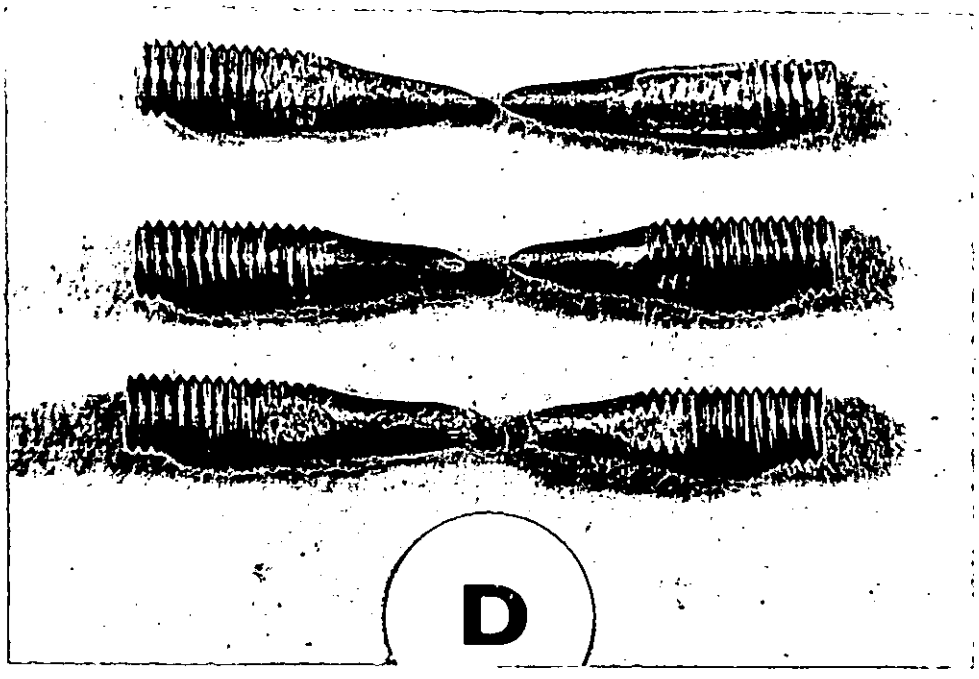

Figure 7.44(c). Specimens quasi-statically fractured at 400 ^{o}C. All three specimens, show 'cup and cone' fracture surfaces.

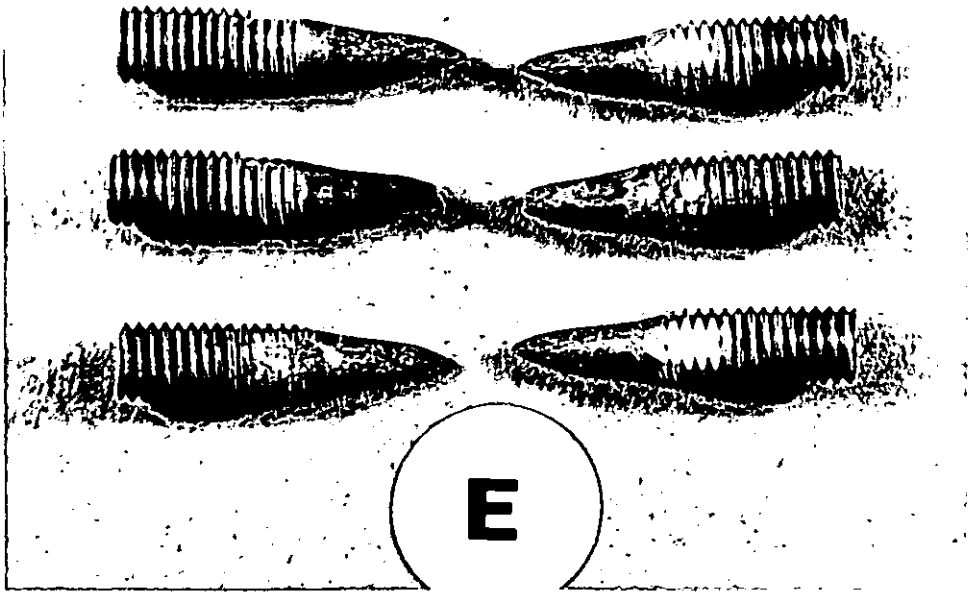

Figure 7.44(d). Specimens quasi-statically fractured at 600 ^{o}C. Both the 20 and 240 μm specimens (top and bottom, respectively) have very sharp points due to dynamic recrystallisation. The 32 μm specimen failed by the 'cleavage' process.

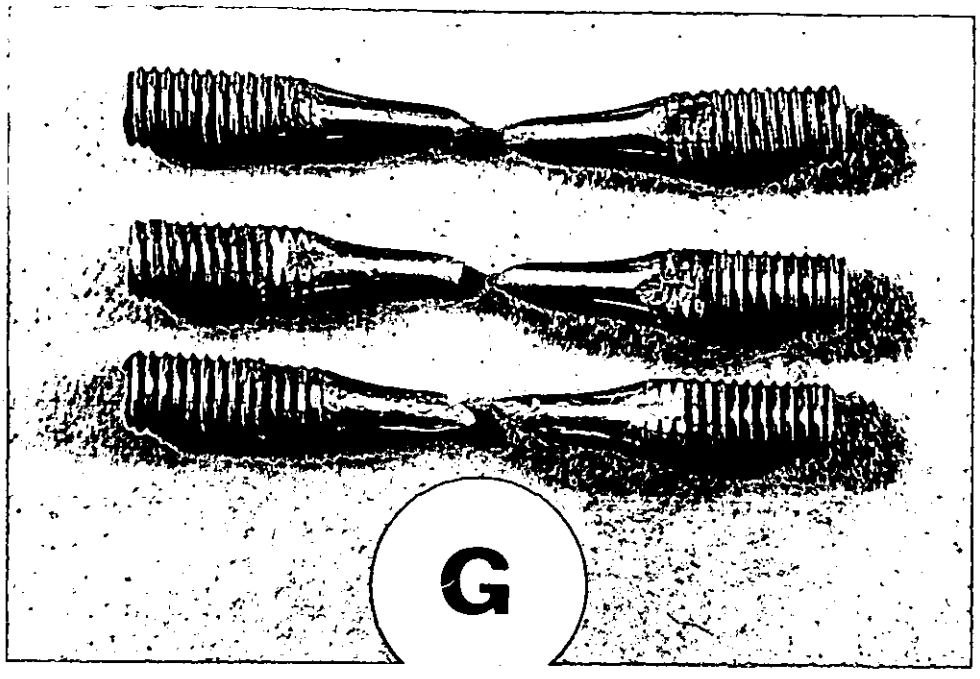

Figure 7.45(a). Specimens dynamically fractured at room temperature. The 20 and 32 μm grain specimens (top and middle, respectively) indicate 'cup and cone' fracture surfaces. The 240 μm specimen failed by the 'cleavage' process.

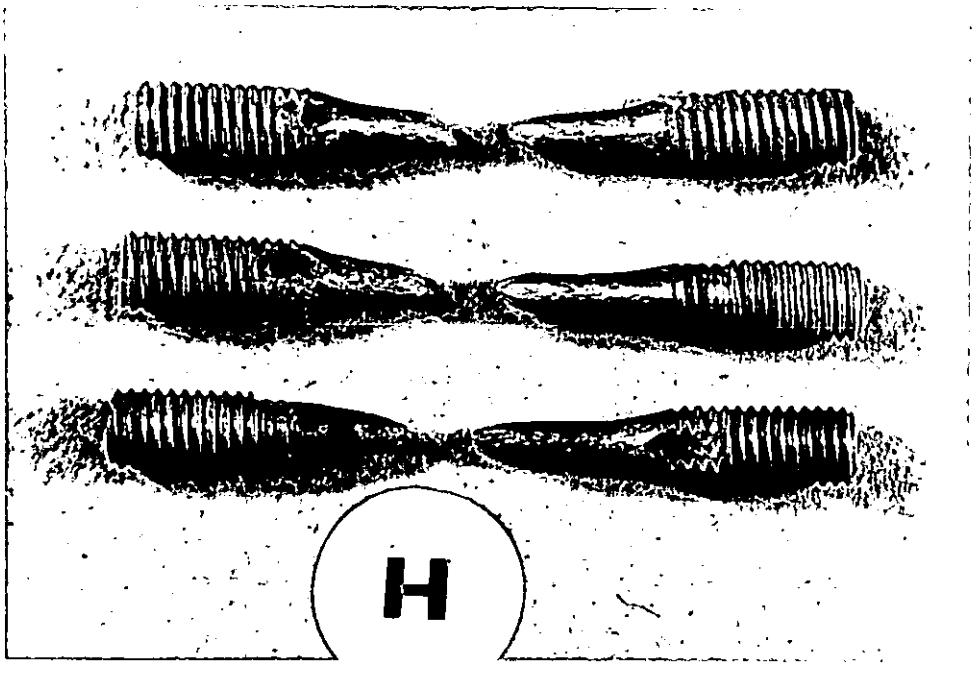

Figure 7.45(b).240 μm grain size specimens dynamically fractured at 200 °C (top), 400 °C (middle) and 600 °C. The lower specimen exhibits 'cup and cone' fracture and the remainder the 'cleavage' process.

difference was noticeable irrespective of strain rate or test temperature. Whereas the lower grain sizes retained their smooth surface finish, the surfaces of the specimens containing the largest grains attained a mottled or 'orange peel like' appearance. This can be seen on the compressive specimens in Figure 7.46 and on the tensile specimen in Figure 7.44(a). The mottled appearance is a grain structure effect. The grains have various orientations within the specimen and are hence deformed to varying degrees by the applied stress, resulting, in the case of the largest grain size, in a visibly undulating surface.

7.7.3 Comparison of Results with Previous Investigations

The results of the current investigation have been compared with those of other authors. These results have been reproduced in the stress-strain rate format for strain levels of 10%.

(a) Room Temperature Tests

The results of the current investigation for the smallest (20μm) grain size and largest (240μm) grain size are shown as dashed lines in Figure 7.47. All the curves indicate that the strain rate sensitivity of copper increases above about $10^3 s^{-1}$. As would be expected, because of their intermediate grain sizes, the curves of REGAZZONI and MONTHEILLET (25μm), and DOWLING et al (37μm) fall between those of the author (except at low strain rates where the curve of Dowling et al is slightly below the 240μm grain size results of the current investigation. The stress-strain rate curve from the more recent of

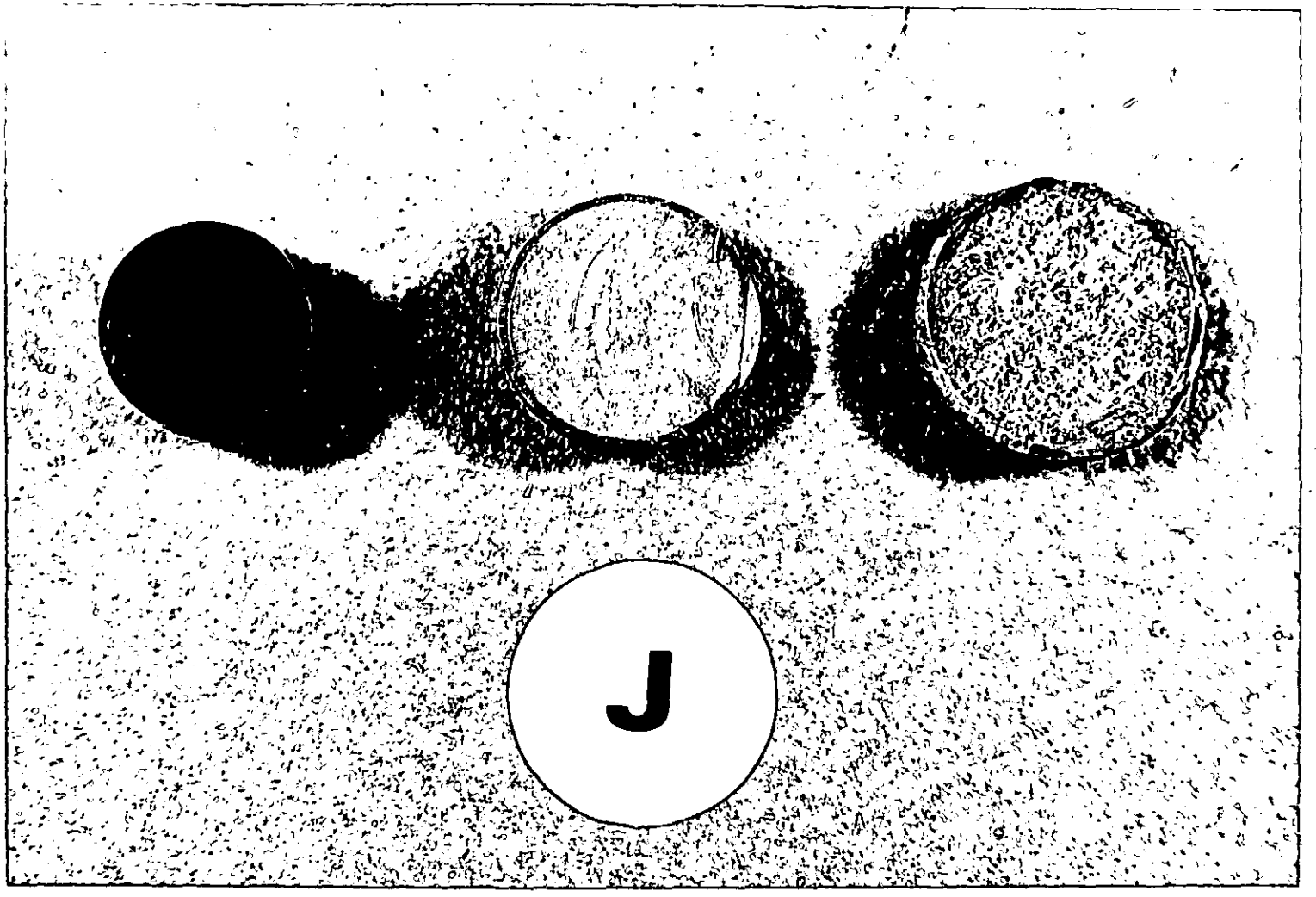

Figure 7.46. Surface texture of compressive specimens. On the left, a polished undeformed specimen. In the middle, the dull, but smooth surface of a 20 μm specimen deformed at a high strain rate. On the right, the mottled appearance of a dynamically compressed 240 μm specimen.

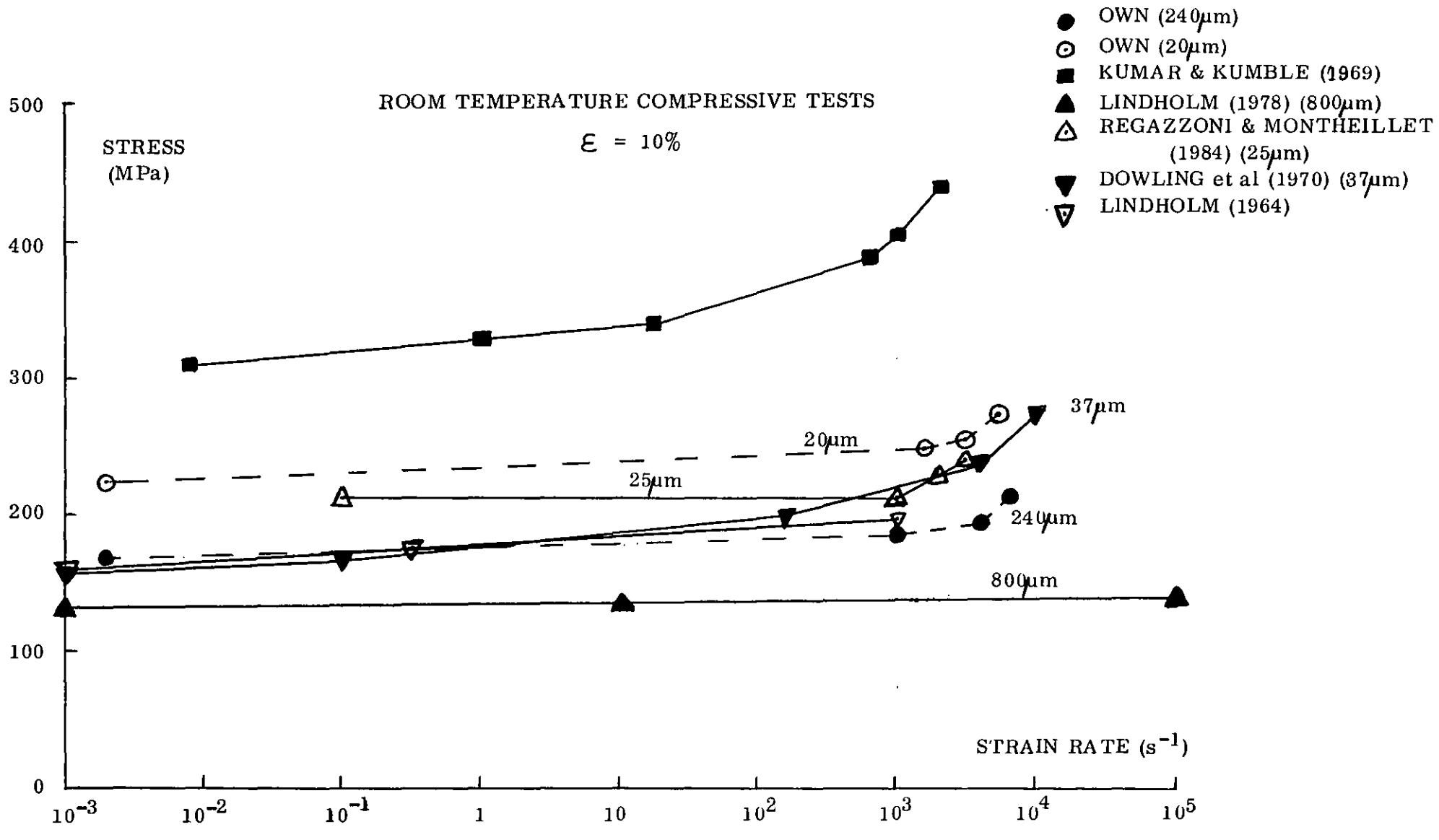

Figure 7.47 Comparison of results with previous investigations

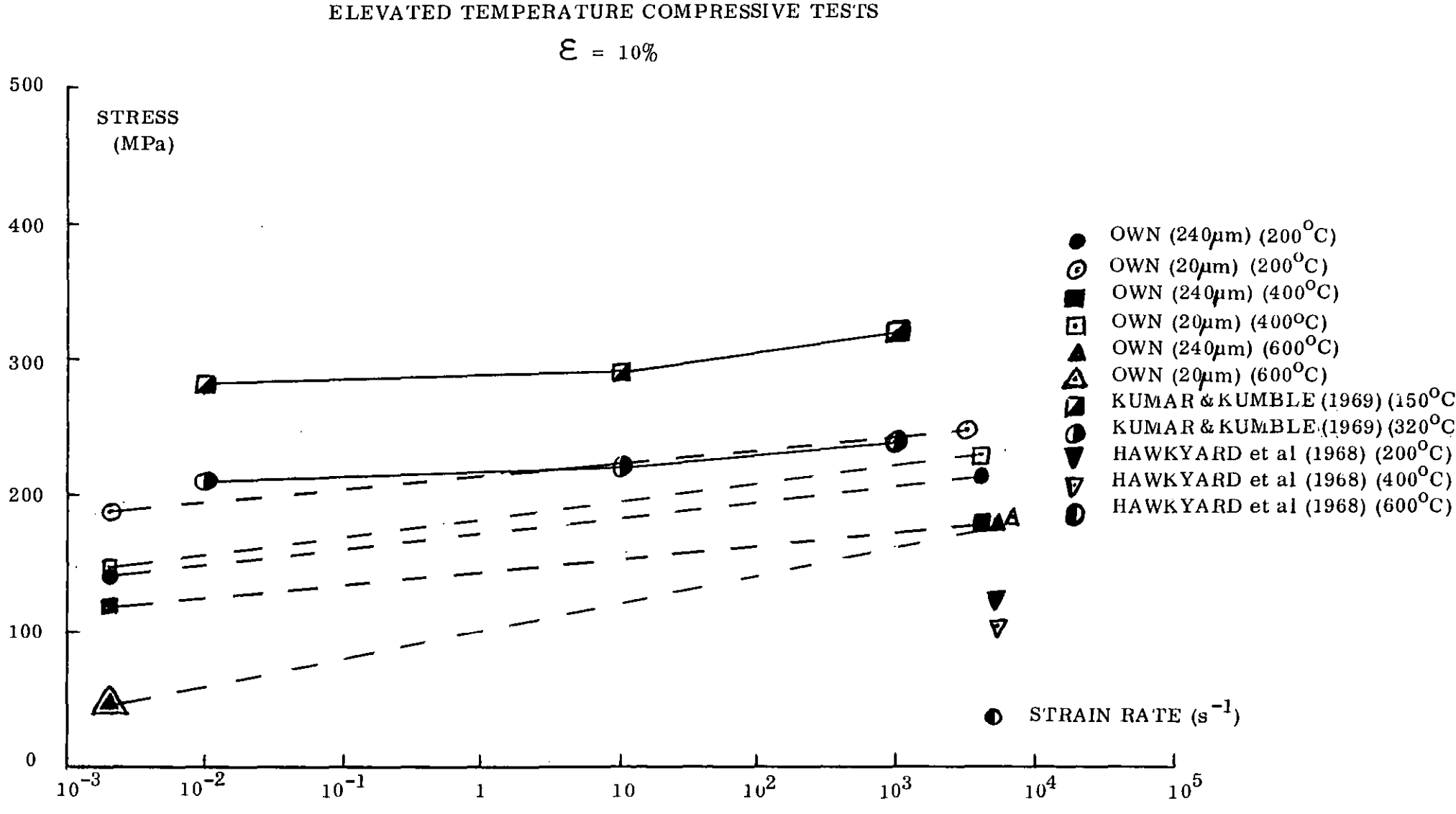

Figure 7.48 Comparison of results with previous investigations

LINDHOLM's two investigations falls below both of the author's curves, the very large grain size of 800μm producing lower stresses. Hence there is excellent quantitative agreement between the room temperature tests of the current investigation and those of the above authors. Comparisons cannnot be made with the results of KUMAR and KUMBLE (1969), and Lindholm (1964) due to the lack of grain size information.

(b) Elevated Temperature Tests

The paucity of high strain rate data for copper at elevated temperatures is evident from Figure 7.48, in which the results from the current investigation for the minimum and maximum grain sizes are again indicated by dashed lines. Kumar and Kumble (1969) have tested copper at two elevated temperatures (150°C and 320°C) and at three strain rates, whereas HAWKYARD et al (1968) have produced results for three elevated temperatures (200°C, 400°C and 600°C) but only one strain rate. The results of Kumar and Kumble are qualitatively very similar to those of the author. Quantitative comparisons are impossible because no grain size is stated by Kumar and Kumble or by Hawkyard et al.

7.8 Summary

99.98% pure, oxygen-free high conductivity copper has been tested in compression and tension.

7.8.1 Compressive Test Results

The tests were performed over a strain rate ambit of 2 x $10^{-3}s^{-1}$ to $6250s^{-1}$ and at temperatures of 20, 200, 400 and 600°C. At room temperature (20°C), five grain sizes were investigated, i.e. 20, 29, 32, 124 and 240μm. The elevated temperature tests were performed with grain sizes of 20, 32 and 240μm.

(a) Stress vs. Strain Rate

At room temperature, the vast majority of the results can be split into 3 strain rate regimes. In the lower regime ($\dot{\varepsilon} \lesssim 1500s^{-1}$), flow stress increases with strain rate except at strains of less than 5%. In the intermediate regime ($1500s^{-1}$ - $3000s^{-1}$), flow stress remains virtually constant irrespective of strain rate. In the upper regime ($\dot{\varepsilon} > 3000s^{-1}$), flow stress increases with strain rate for all strains. In a few isolated cases, the stress-strain rate curves exhibit linear regions with positive gradients.

The main features of the stress-strain rate curves at elevated temperatures are the proportionally greater reduction in the flow stress values of the quasi-static tests relative to the values in the equivalent dynamic tests, and the occurrence of dynamic recrystallisation at 600°C.

(b) Stress vs. Grain Size

Flow stress decreases with increasing grain size for a given strain rate and strain level in a manner which is almost independent of strain. Plotting stress difference

(between grain sizes at constant strain rate and strain) versus strain, results in many cases, in a dual linear relation. At room temperature these lines intersect at strains between 5% and 7%.

(c) Strain Rate Sensitivity (λ)

At room temperature below about $10^3 s^{-1}$, λ is linearly related to log $\dot{\varepsilon}$. λ increases with strain, being zero for strains of less than or equal to 5%. λ decreases as the grain size increases.

From the much smaller data set at elevated temperatures, it appears that results follow a similar trend. In addition, λ increases with temperature.

(d) Work Hardening Exponent (n)

For each temperature, grain size and strain rate, n has two constant values depending on the strain level. There are upper and lower strain regions which intersect at between 15% and 20%. There is little variation of n over the wide range of test parameters, its minimum and maximum values being 0.18 and 0.6, respectively, it is always larger in the lower strain region and, finally, in a high percentage of cases it is larger at high strain rates than at the corresponding quasi-static rate.

(e) Temperature Dependence of the Dynamic to Quasi-Static Flow Stress Ratio

Below a homologous temperature of 0.5 there is a linear relation, the gradient being small. The ratio increases rapidly above 0.5.

7.8.2 Tensile Test Results

In the tensile tests, the strain rate was varied from $10^{-3}s^{-1}$ to $1300s^{-1}$. At room temperature, three grain sizes were investigated, i.e. 20, 32 and 240μm. The same elevated temperatures were selected as in the compressive tests, but were applied only to the largest grain size, i.e. 240μm.

(a) Tensile - Compressive Comparison

In most cases there is excellent agreement between the smaller number of tensile test results and the corresponding compressive results. The work hardening exponent is again bi-valued, the critical strain always being 20%.

(b) Multiple Loading Dynamic Tensile Fracture

All the specimens fractured at a strain rate of about $1300s^{-1}$, even though the results indicated a tensile strain of only 13%. Fracture was caused by multiple loading. Records of multiple reflections in the second pressure bar indicate that fracture occurs after the fifth tensile loading.

(c) Elongation at Fracture

At room temperature the 32μm grain size extends the most and the multiple loading dynamic fracture extends the specimens approximately 1mm more than the corresponding quasi-static fracture.

(d) Fracture Surfaces

Three different fracture surfaces were identified according to the test conditions and grain size. These were 'cup and cone', cleavage and pointed surfaces. The last of these was the result of dynamic recrystallisation.

CHAPTER 8

CONSTITUTIVE EQUATIONS & MICROMECHANICS OF PLASTIC FLOW

8.1 Introduction

It is now well established that the predominant mechanism of plastic deformation or flow in metals and alloys is slip caused by the motion of dislocations. The latter are imperfections in the crystal lattice, their presence being the principal cause of a crystalline material being permanently deformed below its theoretical or ideal yield stress. The dislocations are prevented from moving freely through the lattice by a variety of barriers. The interaction between dislocations and barriers is dependent on factors such as the rate at which the stress is applied and the ambient temperature. There is no universally applicable empirical law or constitutive equation that permits the resultant experimentally determined strain rates to be related to applied stresses, strains, temperatures and grain sizes over wide ranges of these variables.

The effect of strain rate on the plastic flow behaviour of metals has been rationalized in terms of the dynamics of dislocations. In general, there are four main types of deformation mechanism which control plasticity. Although all four types of mechanism contribute simultaneously to the observed net strain rate effects, a dominant mechanism, which depends on the strain rate and temperature, usually prevails.

Most metals deform by diffusion-controlled creep at low stresses and at temperatures above about half of their melting temperature. Over low temperatures and for rates of strain up to approximately $10^3 s^{-1}$, plastic flow in crystals is usually dominated by one or more of a series of thermally-activated mechanisms. At higher temperatures, the yield stress becomes independent of the strain rate and the athermal deformation mechanisms predominate. Finally, at very high strain rates ($\dot{\varepsilon} > 10^3 s^{-1}$), viscous drag mechanisms are operative. This typical behaviour of metals is illustrated in Figure 8.1 (KUMAR & KUMBLE, 1969).

In the strain rate and temperature ambits chosen in the current investigation the thermally activated and viscous drag mechanisms are expected to be predominant.

8.2 Stress-Strain Rate Relations

8.2.1 Thermally Activated Mechanisms

In this type of mechanism the dislocation motion is aided by thermal fluctuations. The dislocations are obstructed at barriers and a combination of thermal agitation and applied stress field is required to activate the dislocations over the obstacles. As the strain rate increases the time spent by a dislocation waiting for a large enough thermal fluctuation to overcome a barrier decreases. Hence a higher external stress is needed for the continued motion of the dislocation. With increasing temperature, more energy is supplied by thermal agitation and a smaller effective stress is needed to move the dislocation, resulting in a lower yield stress.

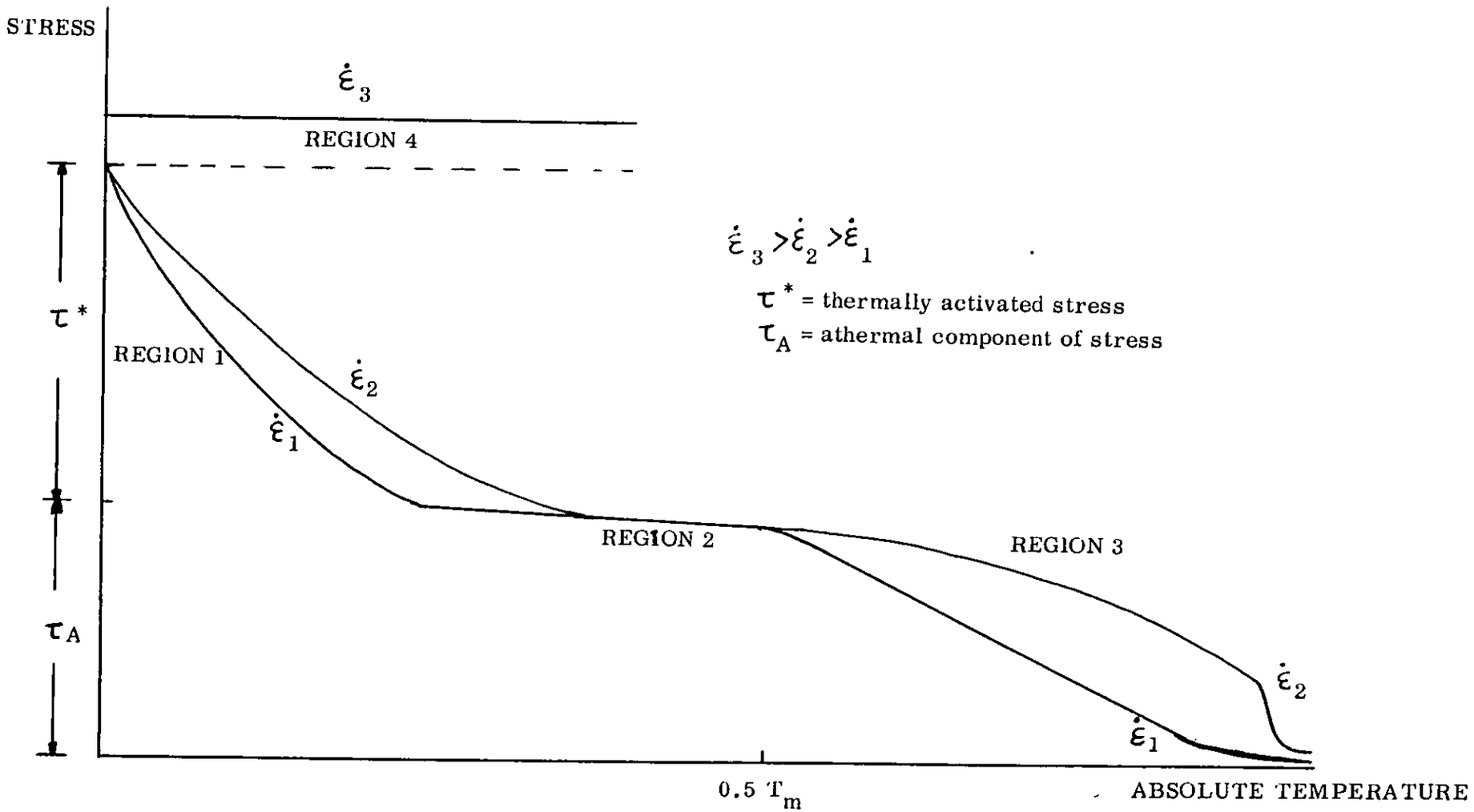

Figure 8.1

Typical behaviour of metals subjected to increasing temperature and strain rate.
(Region 1 - thermally activated, Region 2 - athermal, Region 3 - diffusion controlled & Region 4 - viscous damping)

The theory of a single thermally activated process was developed by SEEGER in a series of papers (1954a, 1954c, 1955d and 1956a). It was applied to comparatively low strain rates but has been shown to be valid at high rates of strain by DORN and HAUSER (1963) and LINDHOLM (1964), in their investigations on aluminium and copper, respectively. From Seeger's theory, the shear strain rate ($\dot{\gamma}$) is related to the stress-dependent activation energy (U_a) and the absolute temperature (T) by

$$\dot{\gamma} = (\rho_m/L)\ Ab\ \nu \exp\left(\frac{-U_a}{kT}\right) \qquad (8.1)$$

where ρ_m is the mobile dislocation density,

L is the average length of the dislocation segments,

A is the average area swept out by a dislocation after it overcomes a barrier,

b is the Burgers' vector,

ν is the vibration frequency of the dislocation segment,

k is the Boltzmann constant.

Combining the first five variables on the right hand side of equation (8.1) into a single strain-rate or frequency parameter and applying the numerical factor $\sqrt{3}$ to convert from shear to normal values:

$$\dot{\varepsilon} = \dot{\varepsilon}_o \exp\left(\frac{-U_a}{kT}\right) \qquad (8.2)$$

From ELLWOOD et al (1984), the activation energy (at high strain rates) is related to the applied stress (σ) by

$$U_a = U_b - V^* (\sigma - \sigma^*) \qquad (8.3)$$

where U_b is associated with the local barrier energy

σ^* is an internal stress field

V^* (= bdL) is the activation volume

d is the distance moved by the dislocation in overcoming the barrier

Assuming that b and L are independent of σ and σ^* then from (8.2) and (8.3)

$$\sigma = \sigma^* + \frac{U_b - kT \ln(\dot{\varepsilon}_o/\dot{\varepsilon})}{V^*}$$

$$= \left(\sigma^* + \frac{U_b}{V^*} - 2.303 \frac{kT}{V^*} \log \dot{\varepsilon}_o\right)$$

$$+ 2.303 \frac{kT}{V^*} \log \dot{\varepsilon} \qquad (8.4)$$

Hence if σ^*, U_b, $\dot{\varepsilon}_o$ and V^* are constants at a given temperature, grain size and strain, then plots of σ against log $\dot{\varepsilon}$ for various constant strain levels and grain sizes will produce a set of straight lines, each line having a gradient of $2.303\ kT/V^*$.

The theory is apparently borne out by Figure 7.28(a) at strain rates below about $10^3 s^{-1}$. Even though there are no intermediate strain rate data between 2×10^{-3} and approximately $10^3 s^{-1}$, the increase in stress over six orders of magnitude of strain rate is so small that the variation of

stress with strain rate in this region of Figure 7.28(a) is almost certainly linear. The gradients of these linear portions increase with strain but at each strain level there is virtually no variation of gradient with grain size. From these gradients the variation of activation volume (V*) with strain can be calculated, since V* is equal to 2.303 kT divided by the gradient. At ε = 30%, V* = 8.7 x $10^{-28} m^3$. V* then increases as ε decreases, until at ε = 4%, V* is infinite for the zero gradient curve at 240μm. (KLEPACZKO (1974) found V* to be 2.06 x $10^{-28} m^3$ for copper at a strain of 15%).

8.2.2 Viscous Drag Mechanisms

The sharp increase in strain rate sensitivity illustrated in Figures 7.28(a) and (b) by the rapid increases of gradients above about $10^3 s^{-1}$, has been interpreted by all except LINDHOLM (1978) as a transition in the dominant plastic deformation mechanism from thermal activation to a viscous drag mechanism, i.e. when the applied stress is raised above some critical level, thermal activation is no longer necessary to assist a dislocation past a barrier and dislocation motion becomes limited by dissipative forces during continuous glide.

FOLLANSBEE et al (1984) stated that the continuous motion of a dislocation moving through a lattice is resisted by the lattice potential itself, as well as by interactions with phonons, electrons, radiation and point defects. These dissipative processes are viscous in nature and lead to a linear dependence of the dislocation velocity V on the

net driving force $\sigma_e b$ according to

$$V = \sigma_e b/B = (\sigma - \hat{\sigma})b/B \qquad (8.5)$$

where B is the drag coefficient

σ_e is the effective stress on the dislocation or the overstress

$\hat{\sigma}$ is the internal back stress or threshold stress

KLAHN et al (1970) have listed 5 viscous drag mechanisms, namely thermoelastic, phonon scattering, electron scattering, phonon viscosity and electron viscosity. In copper, at room temperature, phonon viscous drag is thought to provide the dominant resistance to dislocation motion. Phonon viscosity is caused by the difference in the shear strain rate as the dislocation moves, causing a separation of the vibration frequencies of the different phonon modes. Energy loss is due to dissipation of heat from the phonons which have a higher temperature than the cooler ones. The drag coefficient vanishes at a temperature of T = 0K and increases up to the Debye temperature (343K for copper) and thereafter increases only slightly with increasing temperature. (The Debye temperature (θ_o) is given by

$$\theta_o = h \nu_{max}/k$$

where h = Planck's constant

ν_{max} = maximum frequency of crystal vibration

k = Boltzmann's constant)

A density ρ_m of mobile dislocations, moving through a field of obstacles with an average velocity V determined

almost entirely by their waiting time at obstacles, produces a strain rate (OROWAN, 1940) of

$$\dot{\varepsilon} = \rho_m b V / \sqrt{3} \qquad (8.6)$$

Combining (8.5) and (8.6)

$$\sigma = \hat{\sigma} + \frac{B\sqrt{3}}{\rho_m b^2} \cdot \dot{\varepsilon} \qquad (8.7)$$

$$\text{i.e. } \sigma = \hat{\sigma} + \beta\dot{\varepsilon} \qquad (8.8)$$

In other words, in the viscous drag region the applied stress is linearly related to the strain rate.

According to Follansbee et al (1984) the average value of B for copper from the literature is 4.3×10^{-5} Pa.s and from FROST and ASHBY (1982) the value of Burgers' vector b for copper is 2.56×10^{-10}m. Hence by measuring the slope β of the graph of σ versus $\dot{\varepsilon}$, the mobile dislocation density ρ_m can be calculated.

Figures 7.6 to 7.19 indicate the variations of σ with $\dot{\varepsilon}$ for all the strain rates, temperatures and grain sizes at which the copper specimens were tested in compression. Some of these curves are linear in certain strain rate ambits. In these linear regions the mobile dislocation density ρ_m has been calculated. The results are listed in Table 8.1.

Hence the mobile dislocation density (ρ_m) only varies

Table 8.1

Linear Stress-Strain Rate Results.

T(K)	D(μm)	ε	$\dot{\varepsilon}$ (s^{-1})	β(10^{-3}MPa.s)	ρ_m($10^{11}m^{-2}$)
293	20	0.03	$2x10^{-3}$-$3x10^{3}$	2.08	5.46
293	20	0.04	$2x10^{-3}$-$3x10^{3}$	4.17	2.72
293	20	0.05	$2x10^{-3}$-$3x10^{3}$	3.33	3.41
293	240	0.1	$1.15x10^{3}$-$6.15x10^{3}$	6.0	1.89
673	240	0.03	$6.5x10^{2}$-$4.05x10^{3}$	3.68	3.09
673	240	0.04	$6.5x10^{2}$-$4.05x10^{3}$	3.68	3.09
673	240	0.05	$6.5x10^{2}$-$4.05x10^{3}$	3.68	3.09

between 1.9×10^{11} and $5.5 \times 10^{11} m^{-2}$ over a wide range of temperatures, grain sizes, strains and strain rates. The values of ρ_m in Table 8.1 compare well with previously published values, e.g. WULF (1974): $\rho_m = 10^{11} m^{-2}$, STELLY and DORMEVAL (1978): $\rho_m = 4 \times 10^{10} m^{-2}$ to $3 \times 10^{11} m^{-2}$, and Follansbee et al (1984): $\rho_m = 3.7 \times 10^{11} m^{-2}$ to $5.1 \times 10^{11} m^{-2}$.

The remaining room temperature stress-strain rate curves from the current investigation contains a plateau region or inflexion which has not previously been reported in the literature. These curves are examined in the next section.

8.2.3 Combined Thermally Activated and Viscous Drag Mechanisms

REGAZZONI and MONTHEILLET (1984) reported that their high strain rate results from tests on copper were consistent with a transition regime where the deformation is controlled simultaneously by thermal activation and viscous drag. They found that the dissipative process, which is synonymous with the viscous drag mechanism, is detectable at stresses below the threshold stress $\hat{\sigma}$ (the stress at which dislocations overcome the obstacles without thermal activation); the dislocation velocity is then controlled by both thermal activation and viscous drag.

Follansbee et al (1984) analysed the high strain rate behaviour of copper in terms of this transition in the rate controlling mechanism from thermal activation to viscous drag. They raised objections to the equation relating

overstress (σ_e), applied stress (σ) and threshold stress, i.e.

$$\sigma_e = \sigma - \hat{\sigma} \tag{8.9}$$

which was used to derive the linear relation between stress and strain rate in the viscous drag region.

They suggest that $\hat{\sigma}$ should be replaced by $\sigma(y)$, an internal back stress, which is a function of a dislocation's position, y, along the glide plane. At an obstacle $\sigma(y) = \hat{\sigma}$, but between obstacles $\sigma(y)$ is negligible, i.e. the glide resistance is very small. Since the distance between obstacles is large compared with the width of the obstacle then the majority of time during continuous glide the driving force is simply the applied stress (σ) multiplied by the Burgers' vector (b).

Therefore equation (8.8) becomes

$$\sigma = \beta \dot{\varepsilon} \tag{8.10}$$

Thus if viscous drag is the sole rate controlling mechanism, then a linear plot of stress versus strain rate should result which should extrapolate through the origin. In fact, all experimental results have shown that the linear plot extrapolates to a value on the stress axis which is well removed from the origin.

Now the dislocation velocity, V, can be expressed in terms of the distance between obstacles, λ , and the times t_w and

t_m, which are respectively the time which a dislocation spends awaiting thermal activation to overcome an obstacle and the time moving between successive obstacles, i.e.

$$V = \frac{\lambda}{t_w + t_m} \tag{8.11}$$

From thermal activation theory, (e.g. see Kumar & Kumble (1969)

$$t_w = \nu^{-1} \exp \Delta G/kT \tag{8.12}$$

where $\Delta G = F_o [1 - (\sigma/\hat{\sigma})^{1/2}]^{3/2}$,

F_o is the total free energy or activation energy

and $t_m = MB\lambda/\sigma b$. (8.13)

M is the average Taylor orientation factor and is numerically equal to 3.1.

Combining equations (8.11), (8.12) and (8.13) with (8.6) yields

$$\dot{\varepsilon} = \frac{\hat{\dot{\varepsilon}}\,\sigma/\hat{\sigma}}{1 + \psi(\sigma/\hat{\sigma}) \exp(\Delta G/kT)} \tag{8.14}$$

where $\hat{\dot{\varepsilon}} = \frac{b^2 \rho_m \hat{\sigma}}{M^2 B}$,

and is the strain rate at which the transition from thermal

activation to viscous drag is complete,

and $$\psi = \frac{\nu^{-1} b \hat{\sigma}}{MB\lambda}$$

Before the results produced by the current investigation can be fitted to equation (8.14), the values of the quantities $\hat{\sigma}$, λ and F_o must be determined. The threshold stress $\hat{\sigma}$ is the value of the flow stress, for a particular strain, when the temperature is at absolute zero, i.e. where there are no thermal fluctuations. Now the thermal activation equation for jerky glide is

$$\dot{\varepsilon} = \dot{\varepsilon}_o \exp \left\{ \frac{-F_o}{kT} [1 - (\sigma/\hat{\sigma})^{1/2}]^{3/2} \right\} \qquad (8.15)$$

Re-arranging, $$\sigma^{1/2} = C.T^{2/3} + \hat{\sigma}^{1/2} \qquad (8.16)$$

where $$C = \hat{\sigma}^{1/2} \left[\frac{k}{F_o} \ln \left(\frac{\dot{\varepsilon}}{\varepsilon_o} \right) \right]^{2/3}$$

Hence at constant strain rate, $\sigma^{1/2}$ should be linearly related to $T^{2/3}$. By plotting $\sigma^{1/2}$ versus $T^{2/3}$ a straight line should be obtained which can be extrapolated to the $\sigma^{1/2}$ axis, from which the value of threshold stress $\hat{\sigma}$ can be found. $\hat{\sigma}$ was determined in the current investigation for the grain sizes 20μm and 240μm, and the strain levels 5%, 10% and 20%, from the quasi-static compressive data obtained at temperatures of 293K, 473K and 673K (Figures 7.22, 7.23 and 7.24). The resultant plots are shown in Figure 8.2 for the six combinations of strain and

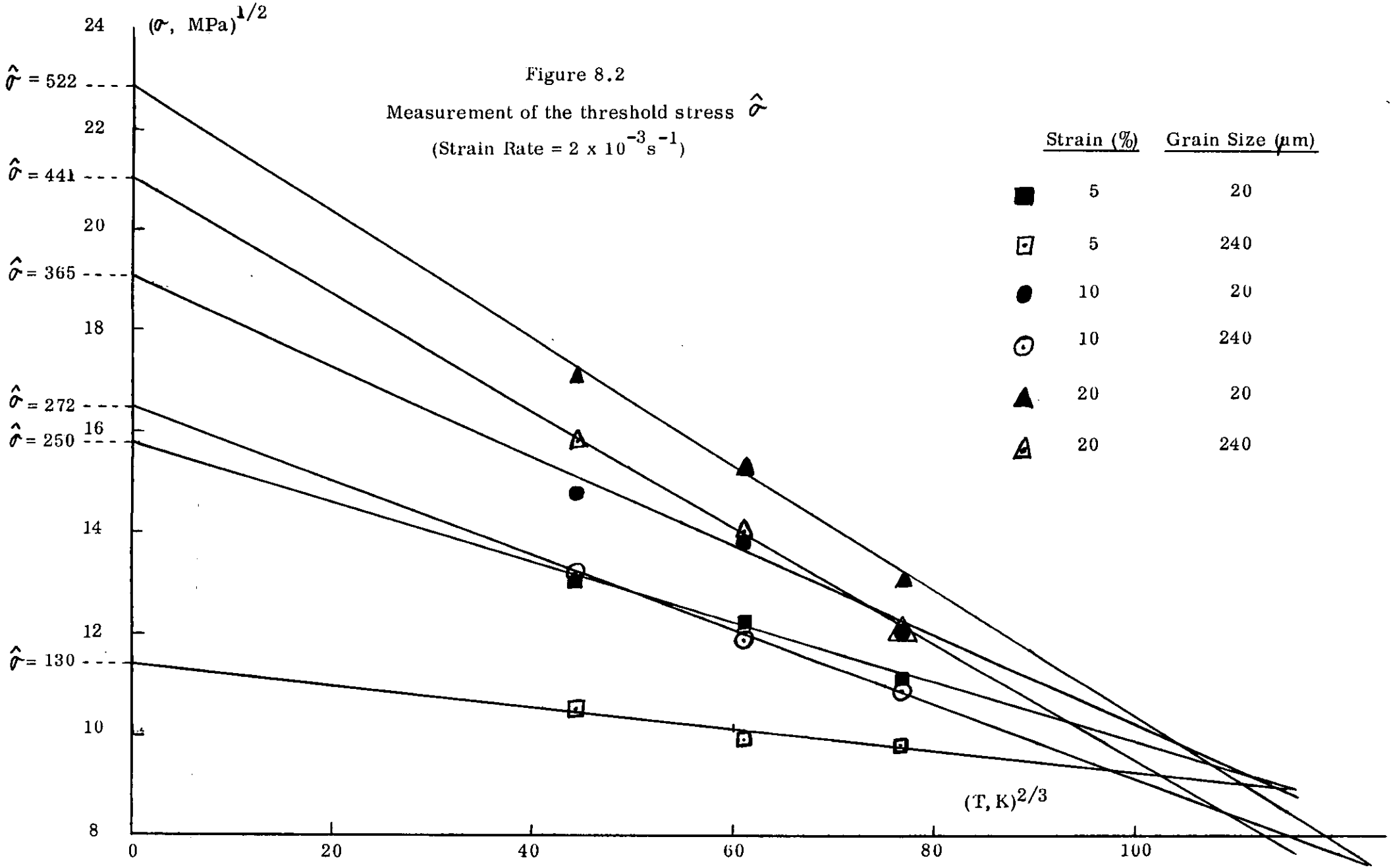

Figure 8.2

Measurement of the threshold stress $\hat{\sigma}$

(Strain Rate = $2 \times 10^{-3} s^{-1}$)

grain size. An approximately linear relation is exhibited in each case. Extrapolating the curves to the $\sigma^{1/2}$ axis, the threshold stresses were calculated and these are listed in Table 8.2.

Follansbee et al (1984) quoted threshold stresses for a 37 μm grain size of 170, 275 and 415 MPa for strains of 5, 10 and 20%, respectively.

The curves in Figure 8.2 have also been extrapolated in the positive temperature direction and it is interesting to note that the six curves very nearly intersect at a common point. In fact, at a temperature of 1154K the stress is 78 ± 8MPa, for all strains and grain sizes.

In Follansbee's paper, it is stated that F_o/kT is related to the gradient of the graph of $\ln \dot{\varepsilon}$ against $\ln \sigma$ at a low strain rate. However, in the current work, insufficient low strain rate data is available to produce an accurate value for this gradient. Consequently, equation (8.14) was modelled, varying F_o/kT until a best fit to the experimental data was achieved. Choosing the value of 40μm for λ as in Follansbee's paper, the representative curves of Figure 8.3 resulted, in which stress has been plotted against strain rate for the 20μm and 240μm grain sizes, both at a strain of 10%. By varying F_o/kT the shape of the curves was not altered, it merely had the effect of raising or lowering the stress level by an amount which is constant for all strain rates, i.e. adjusting the value of F_o/kT offsets the stress by a constant value. For the 20μm curve F_o/kT equals 140, and for the 240μm curve F_o/kT

Table 8.2

Variation of Threshold Stress with Strain and Grain Size

Strain (%)	Grain Size (μm)	Threshold Stress (MPa)
5	20	250
5	240	130
10	20	365
10	240	272
20	20	522
20	240	441

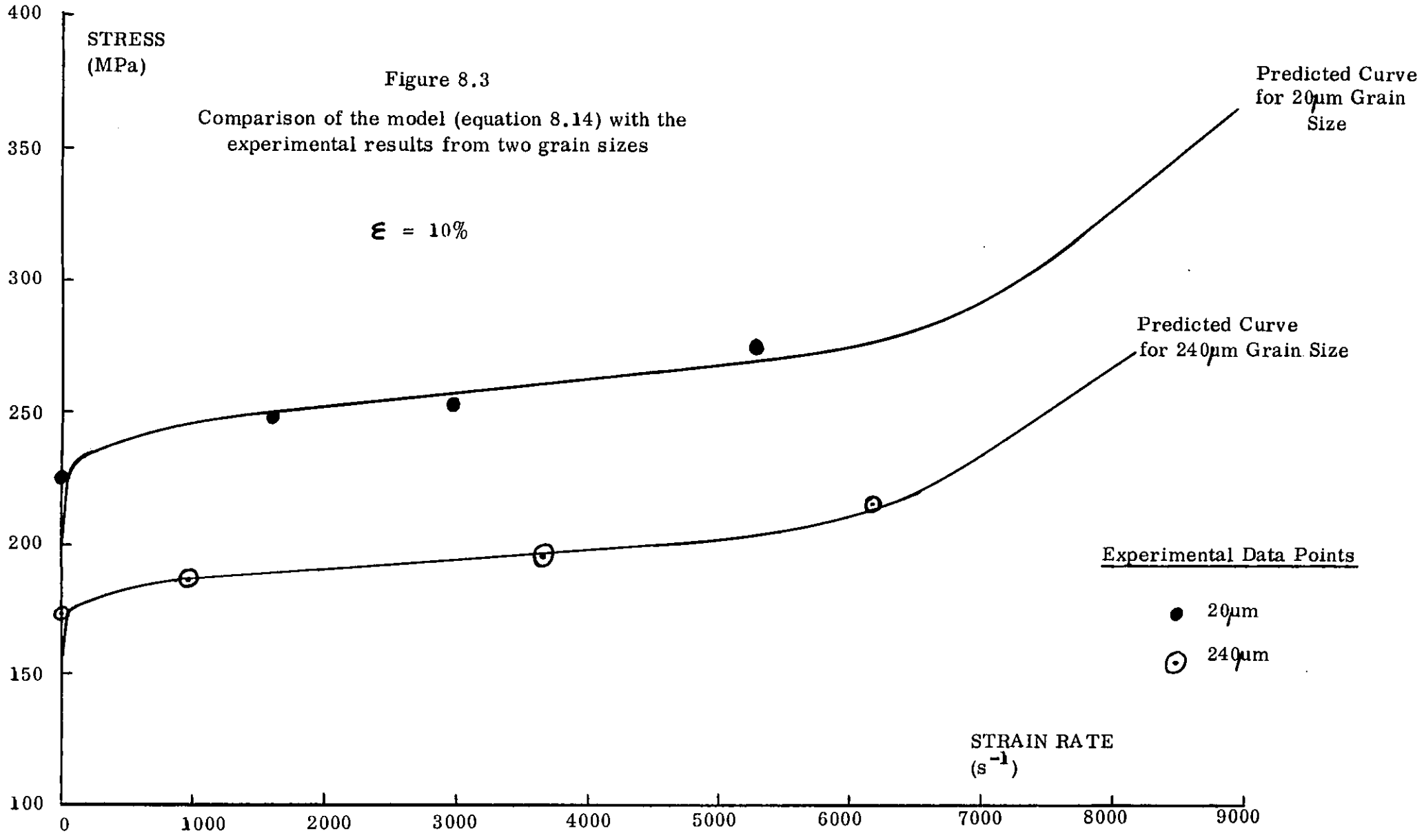

Figure 8.3

Comparison of the model (equation 8.14) with the experimental results from two grain sizes

ε = 10%

equals 150 (the value of F_o/kT used by Follansbee et al was 220, the grain size being 37μm).

The model correlates excellently with the experimental data. Consequently, the current high strain rate test results on copper, which uniquely indicate an inflexion in the stress-strain rate curve, serve to validate the mathematical model proposed by Follansbee et al (1984). Notice that the model predicts a much larger increase in stress with strain rate up to about $100s^{-1}$ than is determined experimentally. At high strain rates, the sharp upturn in stress is not expected, according to the model, until $\dot{\varepsilon} > 5000s^{-1}$. In the current investigation only one data point, per grain size tested, exists above this strain rate serve to validate the mathematical model proposed by Follansbee et al (1984).

8.3 Stress-Grain Size Relation

8.3.1 Introduction

HALL (1951) and PETCH (1953) determined that the tensile yield and brittle fracture stresses (σ) of mild steel were related to the mean grain diameter (D) according to

$$\sigma = \sigma_o + KD^{-1/2} \qquad (8.17)$$

where σ_o and K are constants.

ARMSTRONG et al (1962) showed that equation (8.17) also applied for the complete stress-strain behaviour of various metals and their alloys at low strain rates.

However, at high strain rates, very few reports have been published which investigate the influence of grain size on flow stress.

8.3.2 Variation of Flow Stress with Grain Size

The validity of the Hall-Petch relation in the current series of tests has been investigated by plotting flow stress (σ) versus the inverse square root of grain size ($D^{-1/2}$) for various temperatures, strain rates and strains as shown in Figures 8.4 - 8.17. The inverse square roots of the grain sizes 20, 29, 32, 124 and 240μm are 7.07, 5.87, 5.59, 2.83 and 2.04mm$^{-1/2}$, respectively.

All the data in the σ vs. $D^{-1/2}$ curves were derived from the compressive stress-strain rate results of Figures 7.6 - 7.19 and the tensile stress-strain rate results of Figures 7.32 - 7.37. In the dynamic test results, data points were interpolated from the stress-strain rate curves to permit the variation of flow stress with the inverse square root of grain size to be investigated for a particular strain rate.

The Hall-Petch relation between stress and grain size, indicated by a linear relation between stress and inverse square root of grain size, was evident in the cases quoted in Table 8.3.

Of the remaining compressive data in Figures 8.4 - 8.17, which contain more than 3 data points, the quasi-static room temperature results (Figure 8.4) exhibit dual linear

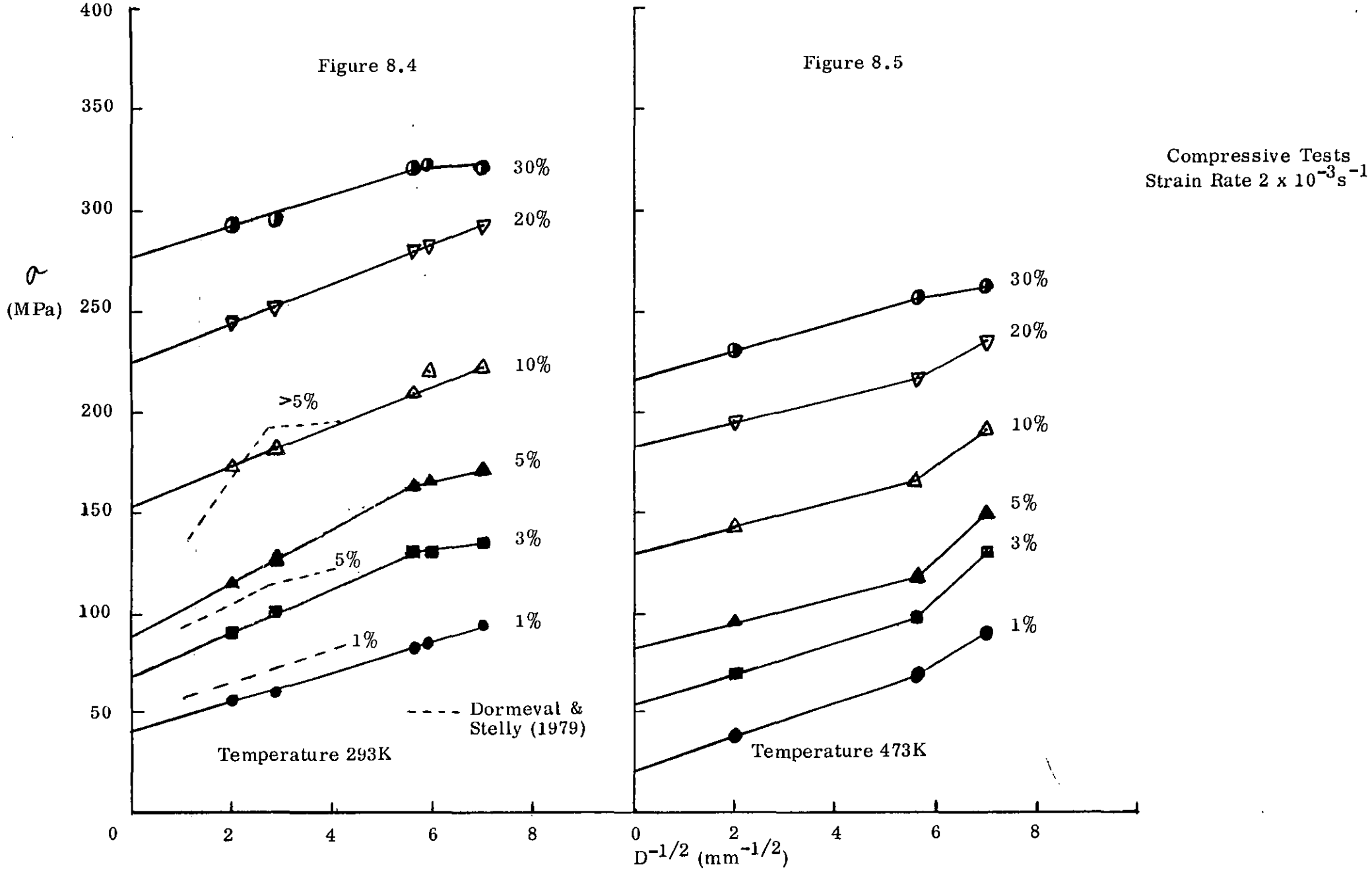

Influence of grain size on flow stress

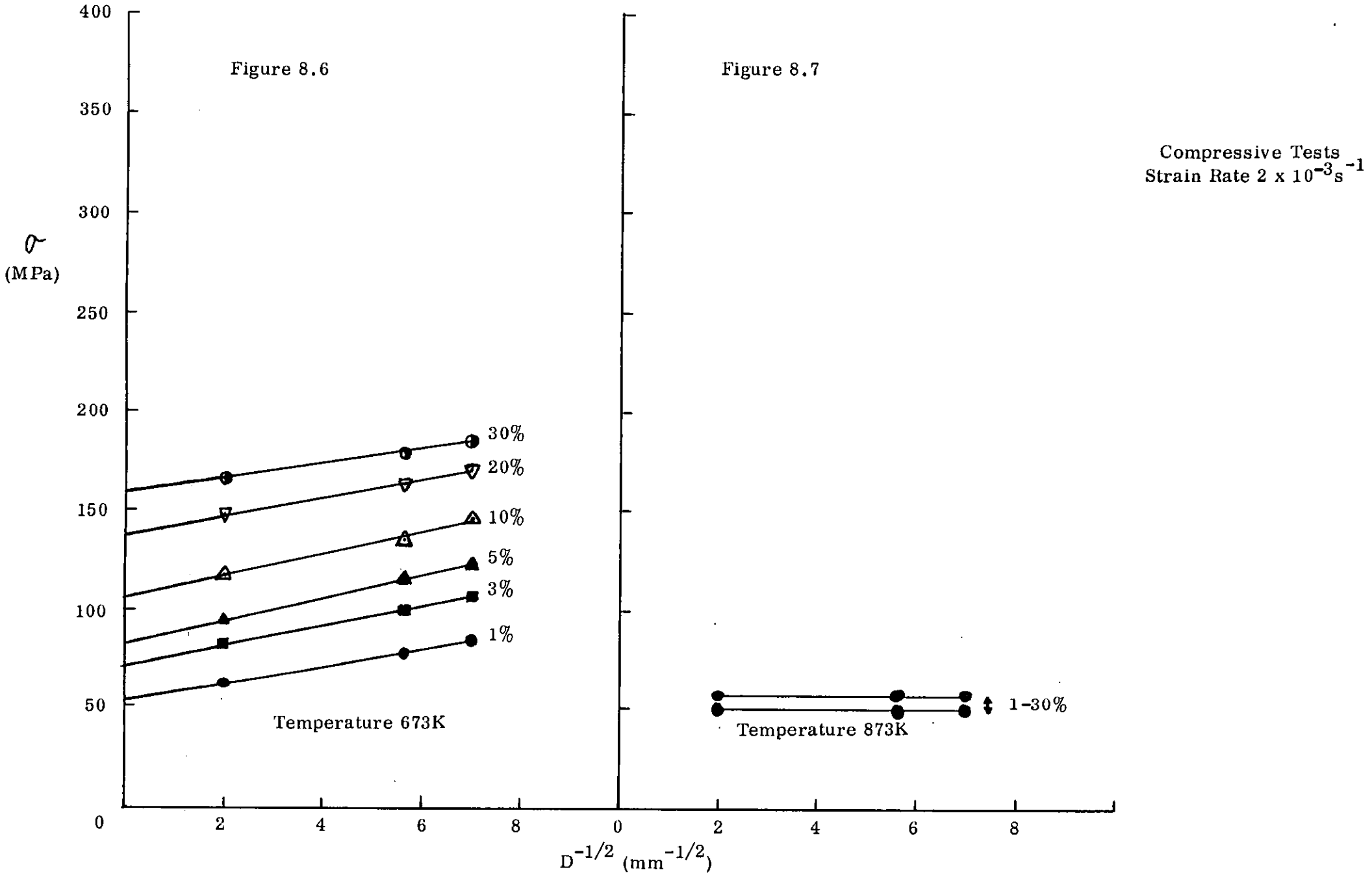

Influence of grain size on flow stress

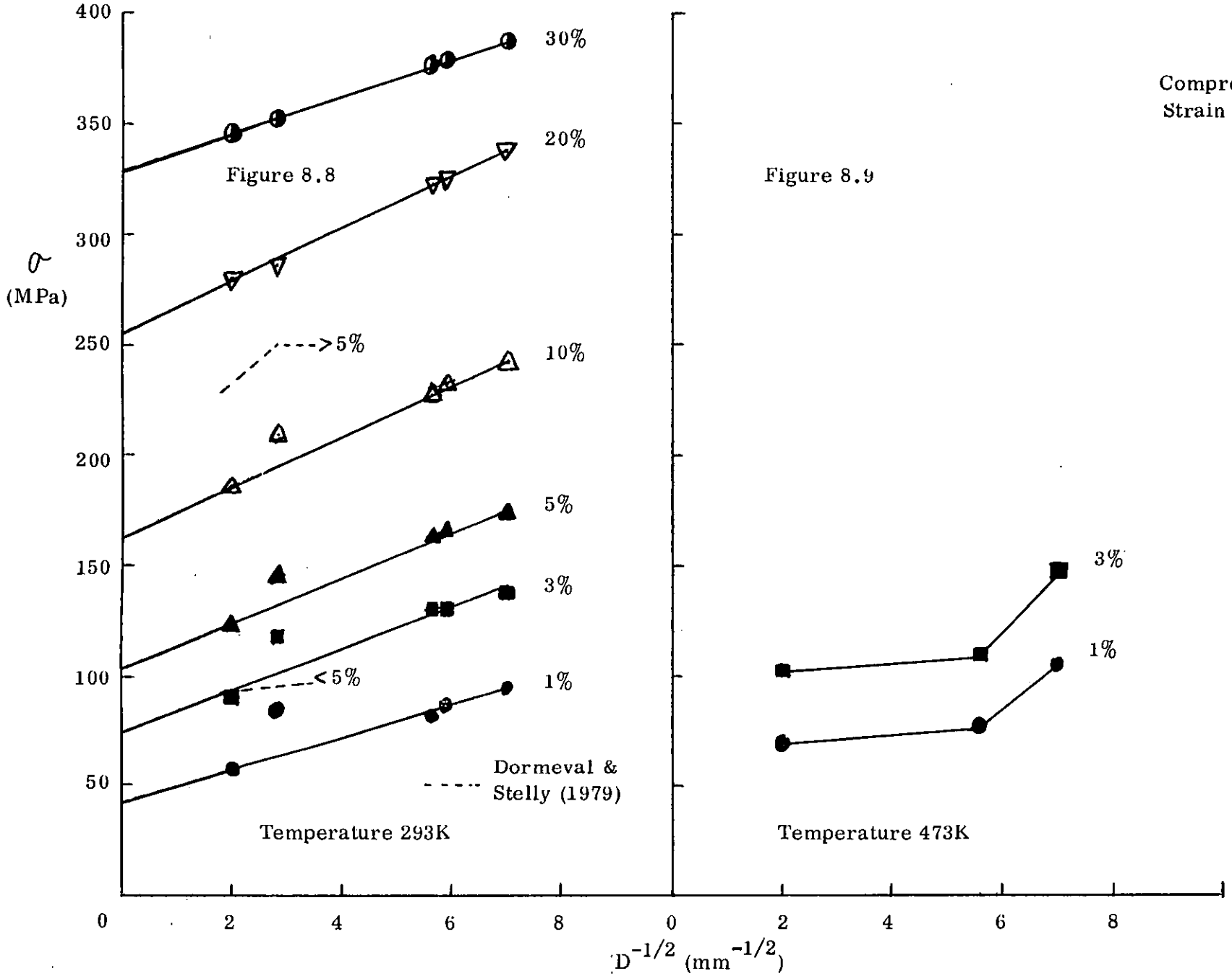

Influence of grain size on flow stress

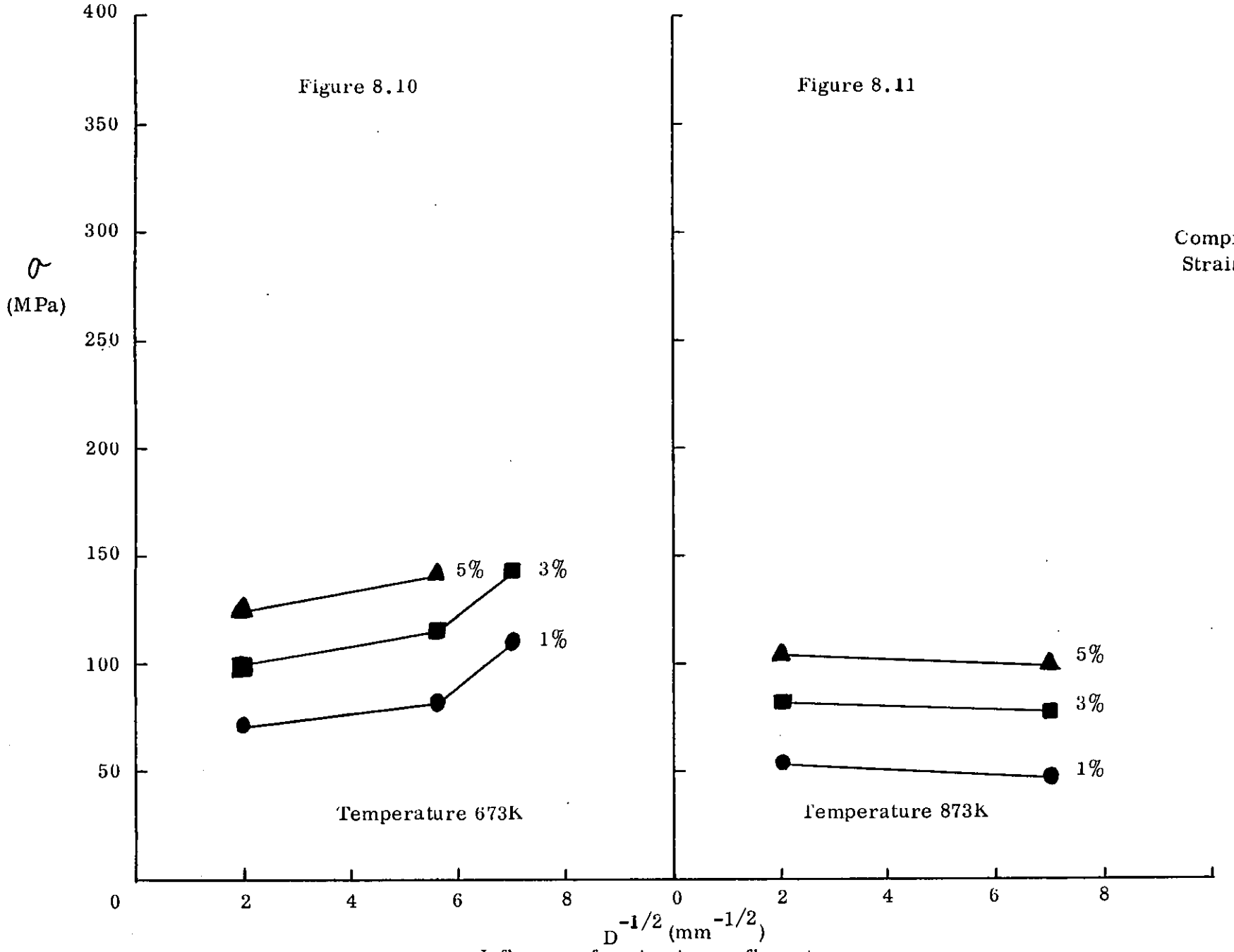

Influence of grain size on flow stress

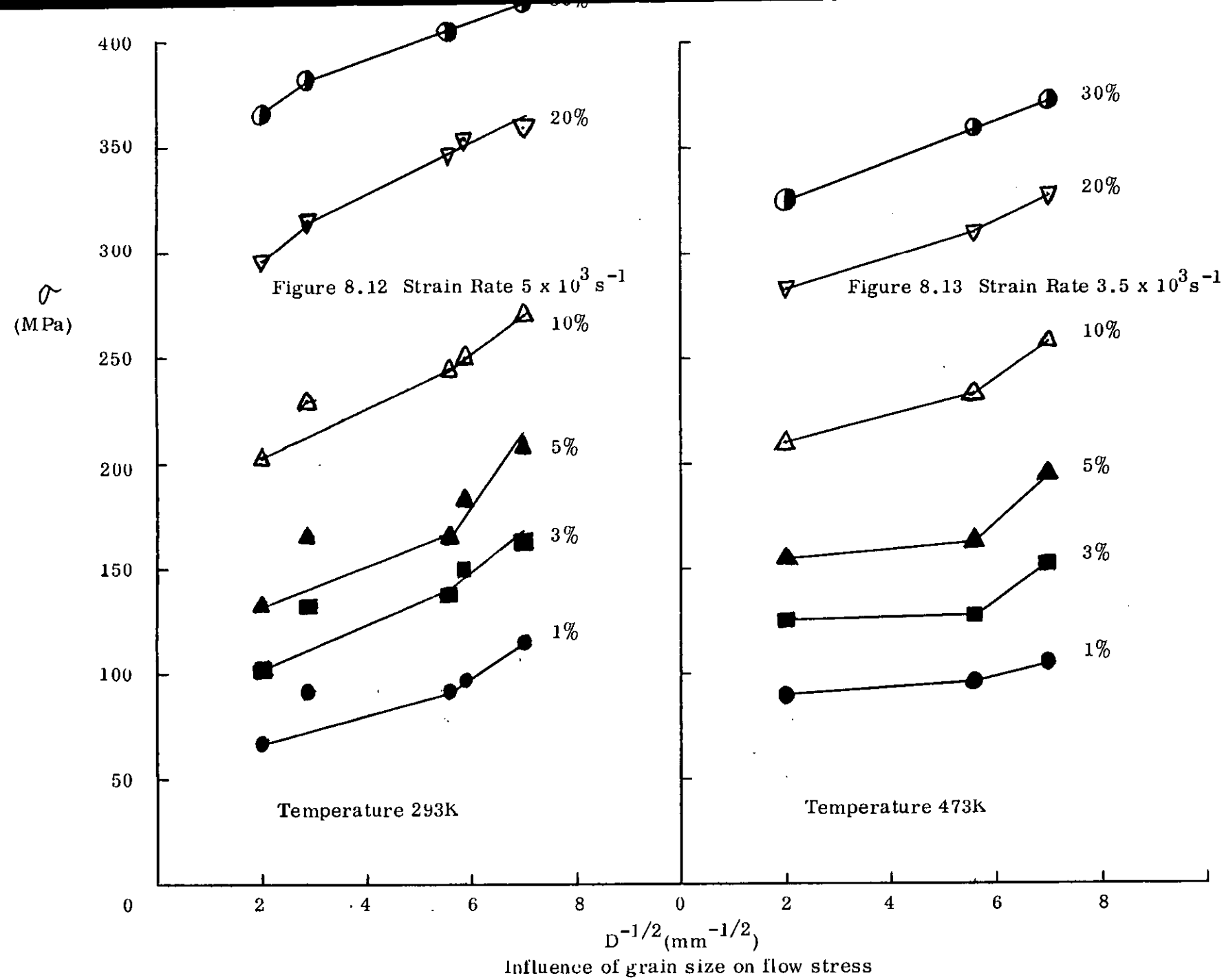

Figure 8.12 Strain Rate $5 \times 10^{3}\ s^{-1}$

Figure 8.13 Strain Rate $3.5 \times 10^{3} s^{-1}$

Compressive Tests

Influence of grain size on flow stress

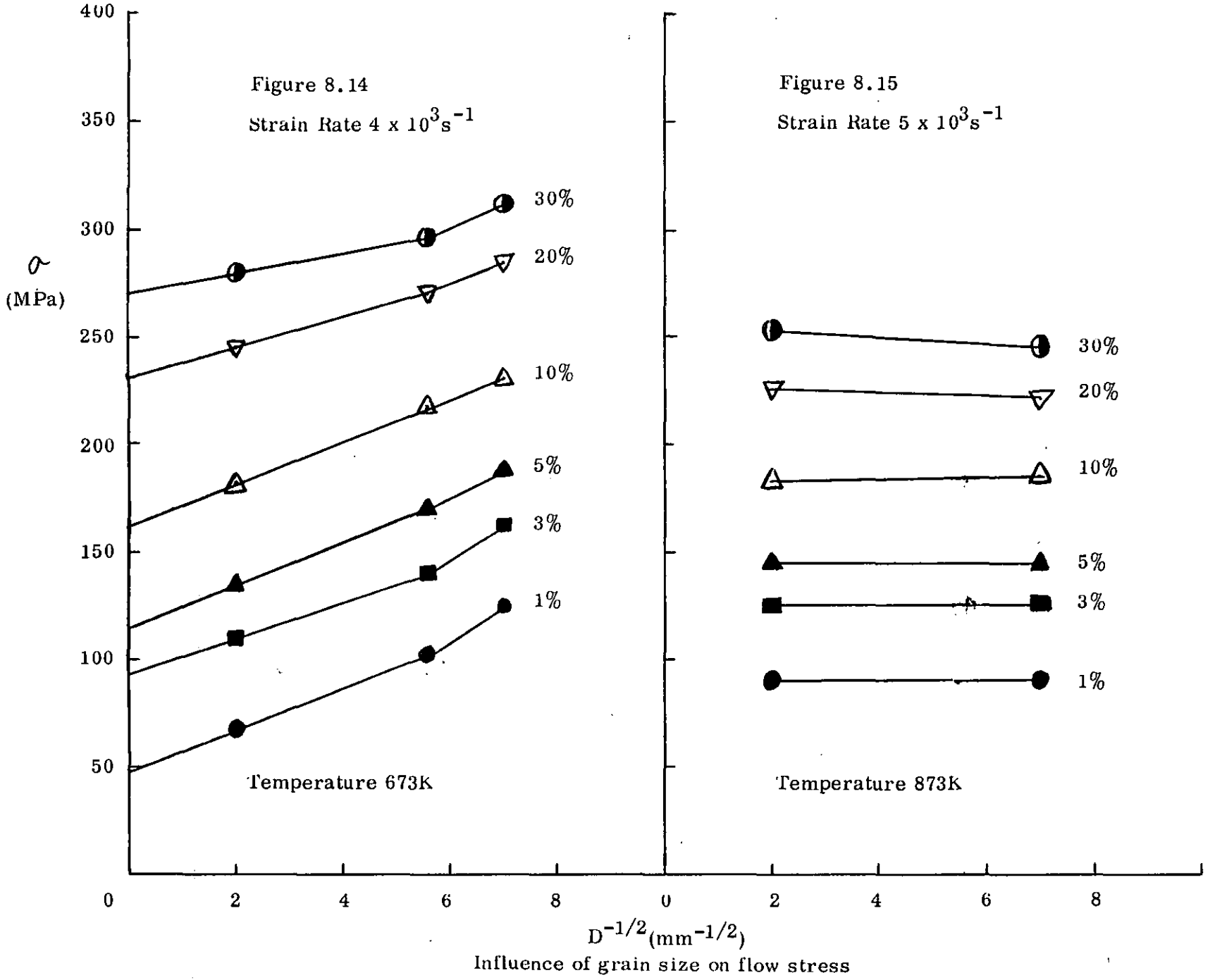

Influence of grain size on flow stress

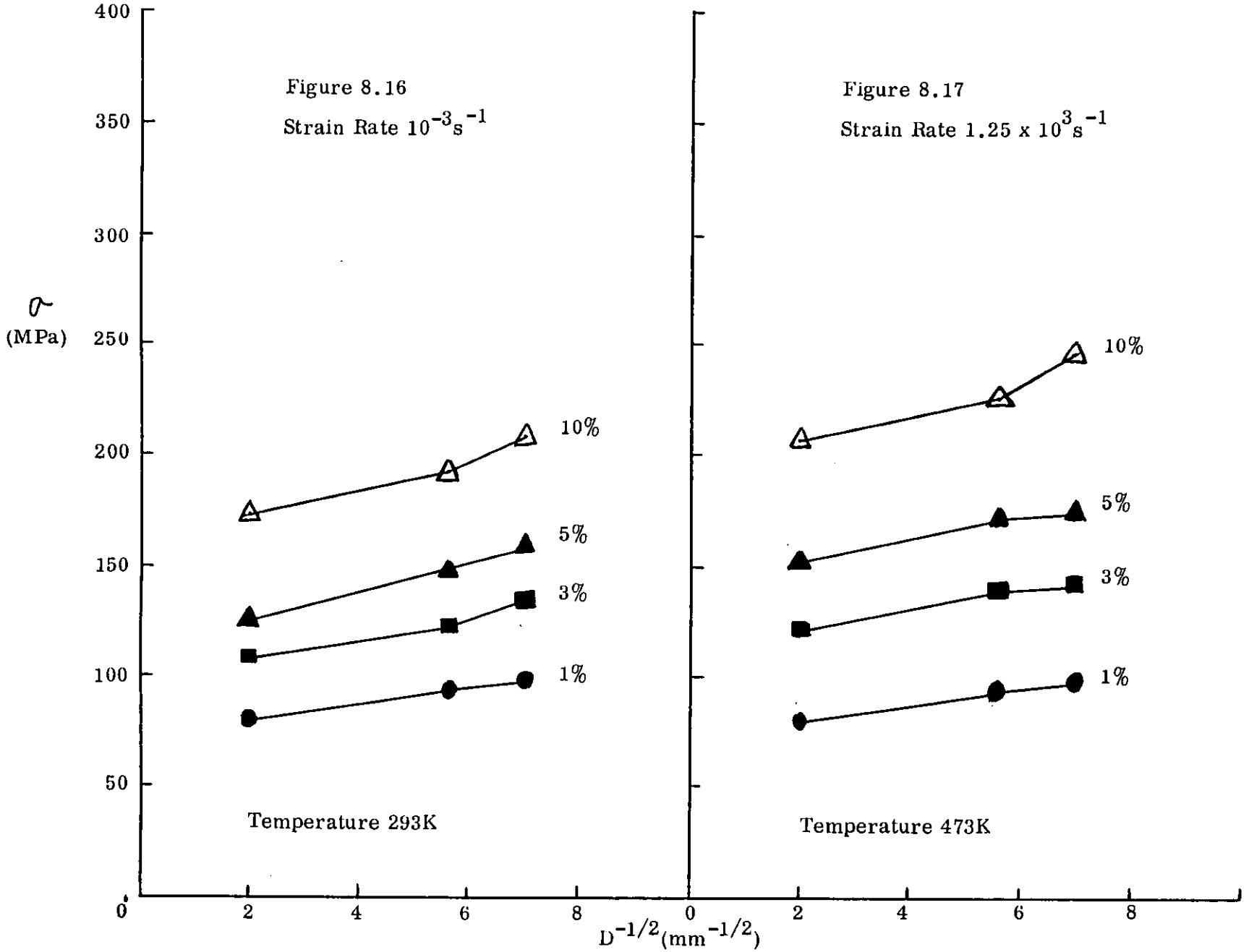

Influence of grain size on flow stress

Table 8.3

Compressive Tests exhibiting the Hall-Petch Relation

Strain Rate (s^{-1})	Temperature (K)	Strain (%)
$2x10^{-3}$	293	1,10 & 20
$2x10^{-3}$	673	1-30
$2x10^{-3}$	873	1-30
$1x10^{3}$	293	1-30*
$3.5x10^{3}$	473	30**
$4x10^{3}$	673	10**

* the 124μm grain size data have been ignored for strains 1-20% (N.B. as explained in 7.1.4, 124μm is the mean of 2 grain sizes)

** only 3 data points

regions at strains of 3, 5 and 30%. The room temperature results at a strain rate of $5 \times 10^{3} s^{-1}$ (Figure 8.12) also indicate the possibility of two linear regions, although the anomalous 124μm grain size data make these results difficult to interpret. Where dual linearity exists the point of intersection is at 32μm (i.e. at a value of $D^{-1/2}$ of $5.59 mm^{-1/2}$).

The tensile results of Figures 8.16 and 8.17 (strain rates of $10^{-3} s^{-1}$ and $1.25 \times 10^{3} s^{-1}$, respectively) show approximately linear relations in both figures at 1% strain. As the strain increases the deviation from linearity increases for both the quasi-static and dynamic curves.

DORMEVAL and STELLY (1979) also investigated the influence of grain size on the mechanical behaviour of high-purity polycrystalline copper at various strain rates. Their tensile tests were performed on specimens of 90, 130 and 300μm grain sizes. They found that in both quasi-static tests and dynamic tests (at 350, 700 and $1000 s^{-1}$) their results were only in agreement with the Hall-Petch relation for strains less than 5%. Due to only three data points it is not possible to deduce whether there are two linear relations between σ and $D^{-1/2}$ at higher strains. The results of Dormeval and Stelly have been included with those of the author in Figures 8.4 and 8.8. The two curves of Dormeval and Stelly where the strains are quoted (Figure 8.4, ε = 1% and 5%), are reasonably close to the equivalent curves of the current investigation.

At the quasi-static strain rate, the gradients of the

compressive curves of Figures 8.4 - 8.7 decrease as the test temperature increases. At room temperature (Figure 8.4) the gradient of the linear region between $D^{-1/2}$ = $2.04mm^{-1/2}$ and $D^{-1/2}$ = $5.59mm^{-1/2}$ increases with increase in strain from 1 to 10% and then decreases at higher strains. The same pattern is followed at 673K except that the maximum gradient is at a strain of 5%. At 473K the gradient of the same portion of each curve decreases from 1% strain to 20% before increasing at 30% strain. At $10^3 s^{-1}$ and room temperature (293K) (Figure 8.8), once again the gradient increases with strain up to 10% and then decreases at higher strains.

Extrapolating the curves of Figures 8.4 - 8.17 back to the stress axis yields the value of σ_o, which corresponds to the flow stress at infinite grain size or the single crystal flow stress. In Figures 8.4, 8.5, 8.6, 8.8 and 8.14, σ_o and the strain ε are related by equations of the form:

$$\sigma_o = c\varepsilon^n \qquad (8.18)$$

where c and n are constants

Equation 8.18 is a work hardening equation for copper of infinite grain size or single crystals. It was previously mentioned in section 7.7.1(d) (equation 7.1) to describe the work or strain hardening of polycrystalline copper. Therefore n is the work hardening exponent. The values of c and n for single crystals are tabulated in Table 8.4.

For comparison the work hardening exponent for the 240μm

Table 8.4

Values of C and n for Single Crystals

Temperature (K)	Strain Rate (s^{-1})	C	n	n_{240}
293	$2x10^{-3}$	575	0.6	0.57
473	$2x10^{-3}$	486	0.6	0.50
673	$2x10^{-3}$	236	0.35	0.32
293	$1x10^{3}$	730	0.65	0.60
673	$4x10^{3}$	440	0.45	0.43

grain size in the lower strain region has been re-plotted from Table 7.3. The values of n (infinite grain size) and n_{240} are remarkably similar, the former always being slightly greater. As in Table 7.3, at infinite grain size n decreases with increasing temperature and n increases with increasing strain rate.

8.4 Summary

8.4.1 Stress-Strain Rate Relations

Previous investigations have established that the predominant mechanisms which control the plastic deformation or flow in metals are thermal activation and viscous drag.

Below about $10^3 s^{-1}$ the majority of authors indicate that dislocation motion, which is arrested by various kinds of barriers, is assisted by a combination of thermal agitation and applied stress.

The sharp increase in strain rate sensitivity, above about $10^3 s^{-1}$ has been interpreted by most as a transition from thermal activation to a viscous drag mechanism. In the latter mechanism when the applied stress is raised above a critical level, thermal activation is no longer necessary to assist a dislocation past a barrier, the motion being limited by dissipative forces during continuous glide.

Recently it has been suggested combined thermally activated and viscous drag mechanisms control the flow of copper at high rates of strain. Follansbee et al have produced a mathematical model to describe the combined mechanisms.

This model correlates excellently with the experimental data from the current investigation, particularly in the case of the tests on the 240μm grain size specimens. Hence the results presented in this dissertation uniquely match the inflexion in the stress-strain rate curve (at high strain rates) predicted by the mathematical model of Follansbee et al.

8.4.2 Variation of Flow Stress with Grain Size

The well-known Hall-Petch relation, in which stress is inversely proportional to the square root of grain diameter has almost exclusively been used to characterise the material behaviour of metals and alloys at low strain rates. However, in the present research, this relation has proved to be valid also for certain dynamic strain rates strains and temperatures. In fact, at room temperature and at $10^3 s^{-1}$ the Hall-Petch relation has been shown to be applicable at all strains for compressive tests. In certain other combinations of strain rate, strain and temperature, dual linear regions were found.

Where there are sufficient data, the graphs of flow stress versus inverse square root of grain size have been extrapolated back to the stress axis, where, in many cases, it was found that the flow stress for an infinite grain size (σ_o), i.e. the single crystal flow stress, is related to strain by the work hardening equation.

$$\sigma_o = C\varepsilon^n$$

where C and n are constants.

The values of the work hardening exponent, n, are almost identical to those previously calculated for the 240μm grain size in the lower strain region.

CHAPTER 9

METALLOGRAPHIC EXAMINATION

9.1 Introduction

The metallographic examination consisted of optical microscopy of representative compressive and tensile specimens before and after deformation in order to investigate the variation in grain structure. The author is indebted to Dr. R. Bateman of R.A.R.D.E., Fort Halstead and Dr. D.H. Houseman of Charnwood Consultants Limited who carried out grain size assessments and photomicrography on some of the specimens. The results of their grain size estimates, together with those of the author, were reported previously in Chapter 7.

Also contained in this chapter are the results of hardness tests performed on compressive specimens with a Vickers Pyramid Hardness Testing Machine.

9.2 Specimen Preparation

9.2.1 Polishing

Before the material to be inspected will reveal its crystalline structure, its surface must be polished and etched. In the latter process, a chemical solution preferentially attacks the grain boundaries, twins, pits etc., so that the surface structure will be revealed under a microscope.

Representative unstrained compressive and tensile specimens from each annealing temperature group were chosen and sectioned with a hacksaw along the axis which is parallel to the split Hopkinson pressure bars when the specimen is positioned for testing, i.e. the specimens were sectioned along their longitudinal axes. Having bisected the specimens, their bulk structure could then be observed. In addition to the unstrained specimens, representative specimens were also prepared for metallographic inspection that had been dynamically or quasi-statically strained at room temperature or 600^{o}C. A few tensile specimens were sectioned in the transverse direction to their longitudinal axis.

Each specimen was mounted in bakelite. The bakelite powder and specimen were compressed to a pressure of approximately 200 bars by means of a hydraulically operated mounting press. After reaching the desired pressure the bakelite was heated for 5 minutes and then cooled for a further 5 minutes by circulating cold water. The cylindrical mount so produced, was 4cm in diameter and 1 1/2 to 2cm deep.

The initial stage of surface polishing was performed successively on 4 grinding wheels, each rotating at 2 to 3 revs per second. Wheel number 1 carried a 120 grade silicon carbide paper - the coarsest grade. This was followed by further grinding with grades 220, 400 and 600. Grade 600, the finest grade, gives a comparable finish to 20/25 micron diamond paste. All wheels were operated with water continuously running onto the silicon carbide paper to prevent removed particles from damaging the surface of

the specimen.

The mounted specimens were then further polished on 'diamond' wheels. Each wheel carried a cloth which was frequently impregnated with diamond paste of the appropriate grade. The specimens were successively polished with 6μm, 3μm and 1μm paste. Prior to each stage of polishing the specimens were washed with teepol and warm water, and then placed for a short time in a sonic cleaner. Finally, they were washed with alcohol and immediately dried with hot air to prevent staining.

Prior to each stage of polishing the specimens were examined at a magnification of X300 with an optical microscope. The appearance of excessive scratching or pitting, usually caused by too much pressure or dirt on the diamond wheel, or too little time spent on the grinding wheels, resulted in further polishing with a coarser grade of paste or a return to the silicon carbide (wet and dry) papers. No scratches should be visible to the 'naked eye' after polishing with 3 μm paste.

The specimens prepared by Charnwood Consultants Limited were polished to 0.1μm.

9.2.2 Etching

A 5% ferric chloride solution was initially chosen to etch the copper specimens. This consisted of 5g of $FeCl_3$ dissolved in 100mls of solvent (50mls alcohol and 50mls distilled water) and 5mls of concentrated hydrochloric

acid. This solution proved to be inadequate as it etched the copper far too quickly. Even when using a weaker solution it tended to produce pits in the surface and not clear grain boundaries.

A boiling ammonium persulphate solution was far more effective, giving fairly clear grain boundaries, the etching time per specimen being of the order of 5 seconds. The strength of the ammonium persulphate (ammonium peroxo-disulphate $(NH_4)_2S_2O_8$) etch was 100g/litre of distilled water.

An ammonia/hydrogen peroxide etch was employed by Charnwood Consultants Limited.

9.3 Microscopy

A UNIMET-UNION 7579 optical microscope was used for viewing the etched specimens. This had a top magnification of X2000 but for the purpose of examining the grain structure of the copper specimens, magnifications of X300 and X600 were perfectly adequate. The scale of each photomicrograph is shown in each figure. Three magnifications were represented in the photomicrographs provided by Charnwood Consultants Limited, viz. X60, X120 and X300. The author's photomicrographs can be identified by the superimposed graticules.

In the case of all the compressive specimens the photomicrographs were taken in an orientation such that the horizontal axes of the prints are perpendicular to the

direction of stress application. The longitudinally sectioned tensile specimens are displayed such that the horizontal print axis is parallel to the direction of stress application. The transverse sections of the tensile specimens were polished to remove all evidence of the fracture surface and, in general, the viewing plane is within 1mm of the actual fracture site. All photomicrographs were taken as close as possible to the centres of the specimens, where the grains were larger and more uniform.

9.4 Discussion of Photomicrographs

The main features in all the photomicrographs are grain boundaries and annealing twins. The latter can be identified by pairs of closely spaced, parallel and linear markings which often bisect a grain. The area enclosed by a twin has usually a different monochromatic intensity than the surrounding grain. The high density of twins in the microstructures of all the specimens is typical of most annealed f.c.c. metals. The large number of twins made the grain size measurements very difficult because it was not always possible to distinguish between grain boundaries and twins.

Figures 9.1 to 9.6 cover the range of the annealing temperatures for the unstrained compressive specimens. In each figure the grain dimensions are fairly similar along both the longitudinal and transverse axes. It is immediately noticeable that the average grain size is increasing from Figure 9.1 to 9.6. The average grain sizes

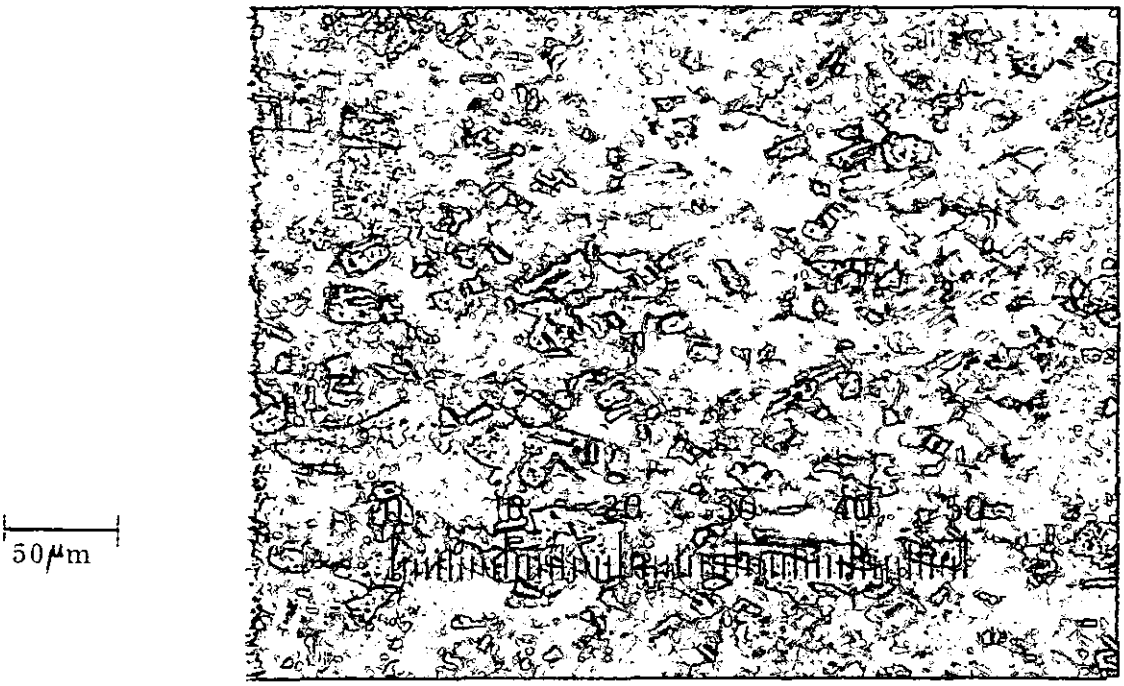

Figure 9.1 Unstrained Compressive Specimen - Annealing Temperature 310°C

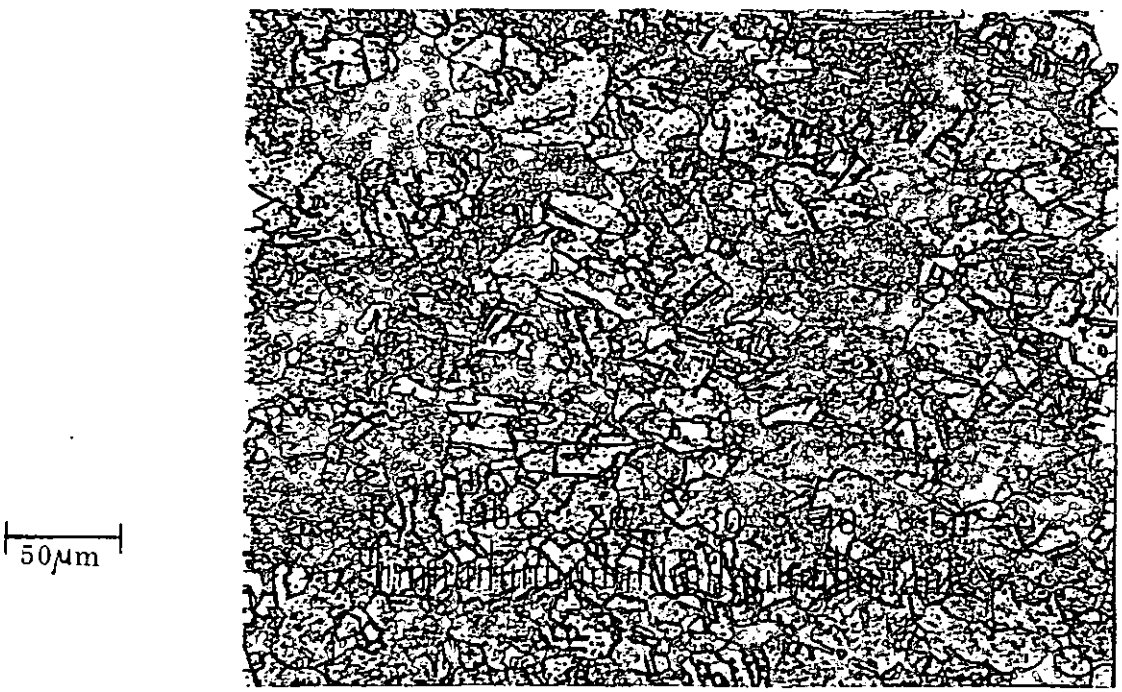

Figure 9.2 Unstrained Compressive Specimen - Annealing Temperature 400°C

Figure 9.3 Unstrained Compressive Specimen - Annealing Temperature 500°C

Figure 9.4 Unstrained Compressive Specimen - Annealing Temperature 600°C

Figure 9.5 Unstrained Compressive Specimen - Annealing Temperature 600°C

Figure 9.6 Unstrained Compressive Specimen - Annealing Temperature 800°C

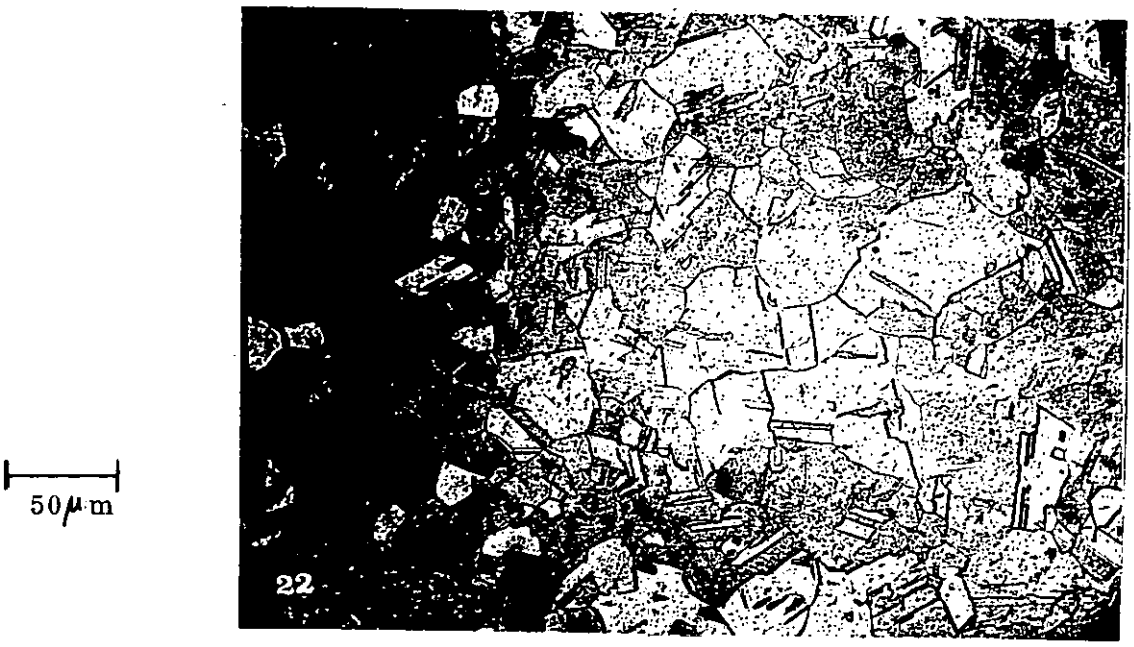

Figure 9.7 Unstrained Tensile Specimen - Annealing Temperature 310°C

Figure 9.8 Unstrained Tensile Specimen - Annealing Temperature 400°C

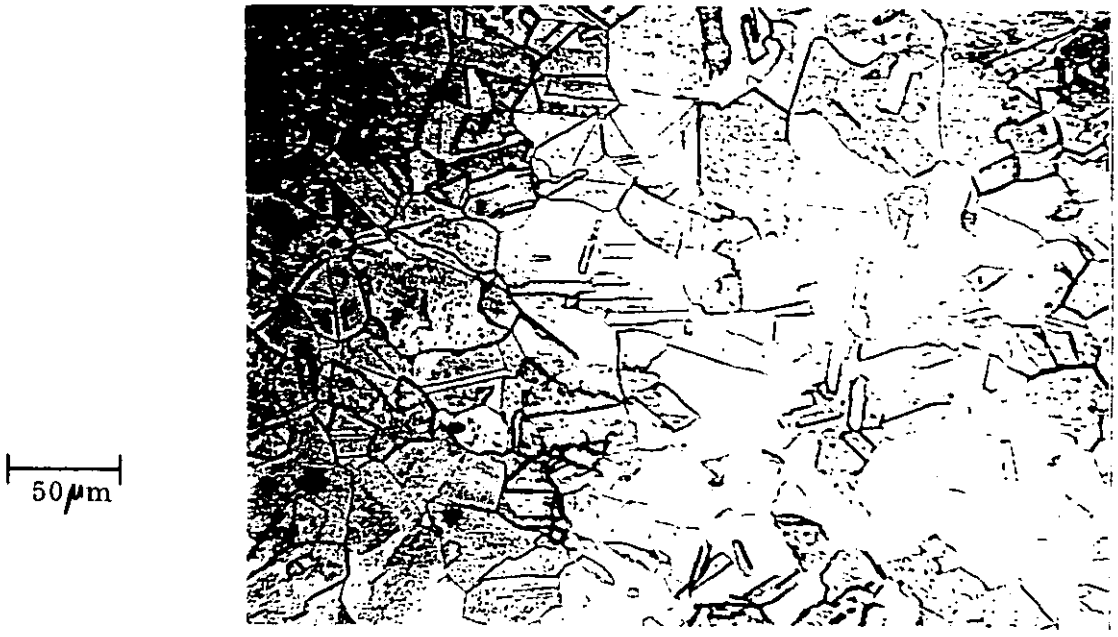

Figure 9.9 Unstrained Tensile Specimen - Annealing Temperature 500°C

Figure 9.10 Unstrained Tensile Specimen - Annealing Temperature 600°C

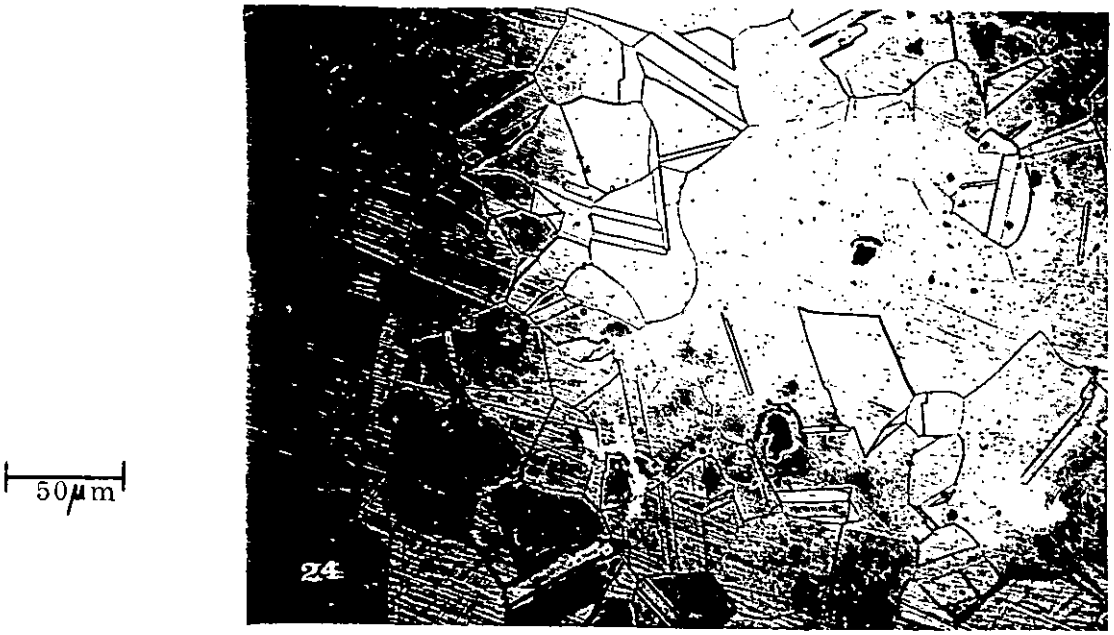

Figure 9.11 Unstrained Tensile Specimen - Annealing Temperature 800°C

Figure 9.12 Compressive Specimen - Annealing Temperature 600°C
- Tested at Strain Rate of 140s^{-1}
and Temperature of 20°C

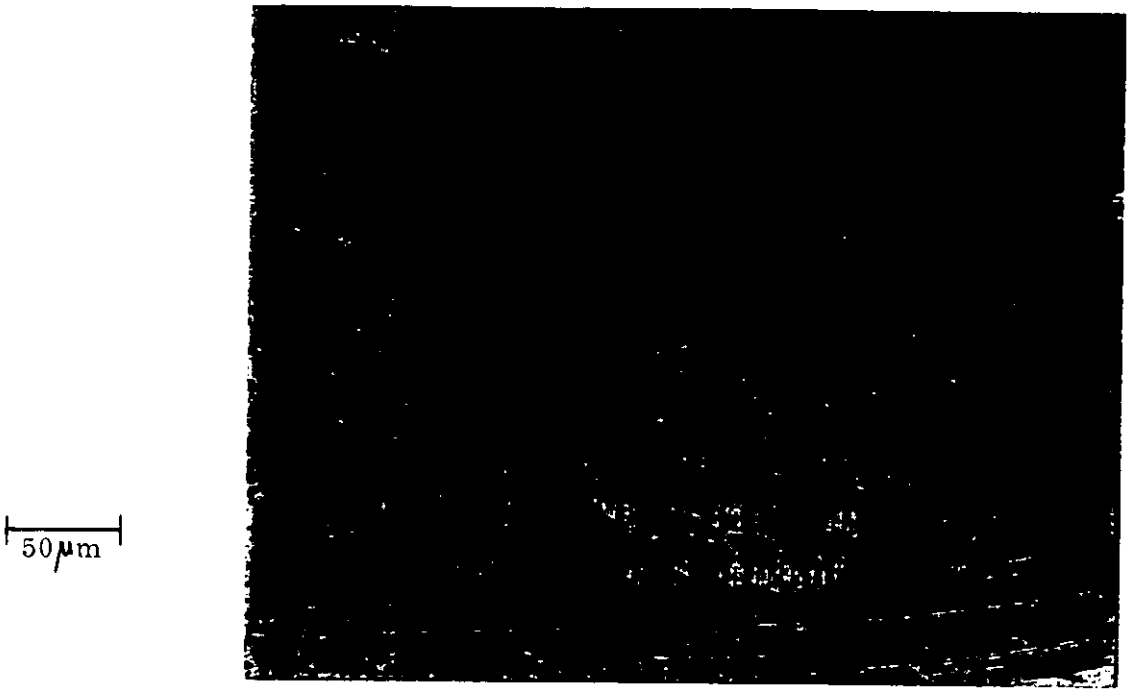

Figure 9.13 Compressive Specimen
- Annealing Temperature 600°C
- Tested at Strain Rate of $1600s^{-1}$ and Temperature of 20°C

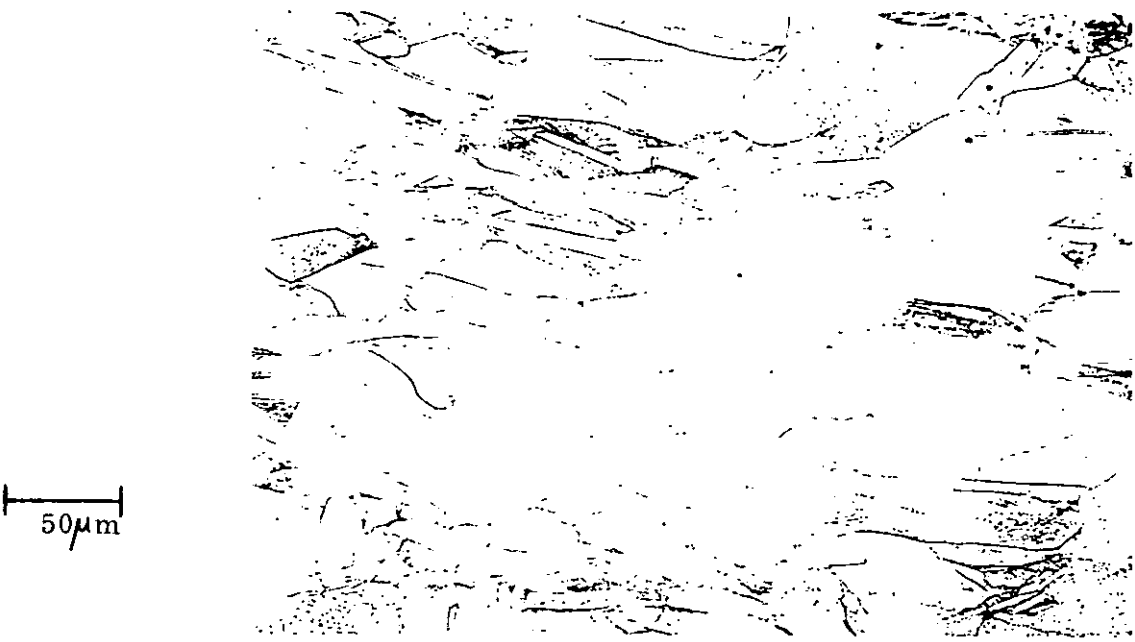

Figure 9.14 Compressive Specimen
- Annealing Temperature 800°C
- Tested at Strain Rate of $2 \times 10^{-3}s^{-1}$ and Temperature of 20°C

Figure 9.15 Compressive Specimen
- Annealing Temperature 800°C
- Tested at Strain Rate of 6400s^{-1} and Temperature of 20°C

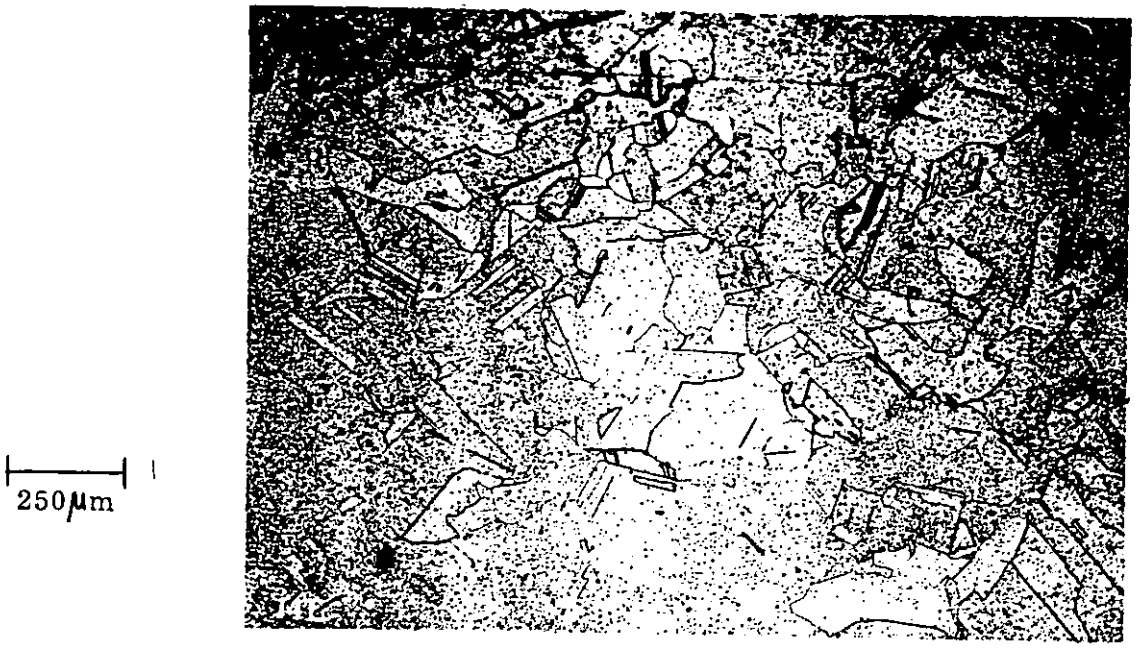

Figure 9.16 Compressive Specimen
- Annealing Temperature 800°C
- Tested at Strain Rate of 2 x $10^{-3}s^{-1}$ and Temperature of 600°C

Figure 9.17 Compressive Specimen
- Annealing Temperature 800°C
- Tested at Strain Rate of 4900s^{-1} and Temperature of 600°C

Figure 9.18 Tensile Specimen
- Annealing Temperature 800°C
- Tested at Strain Rate of 1200s^{-1} and Temperature of 20°C

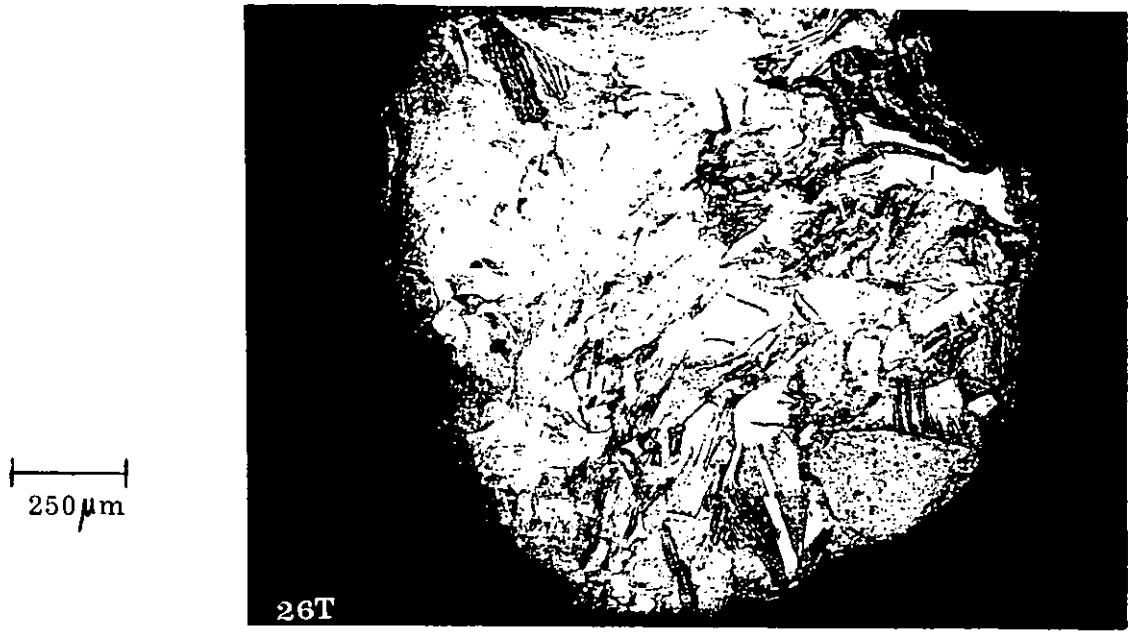

Figure 9.19 Tensile Specimen (transverse section)
- Annealing Temperature 800°C
- Tested at Strain Rate of 1200s^{-1} and Temperature of 20°C

Figure 9.20 Tensile Specimen
- Annealing Temperature 800°C
- Tested at Strain Rate of $10^{-3}s^{-1}$ and Temperature of 600°C

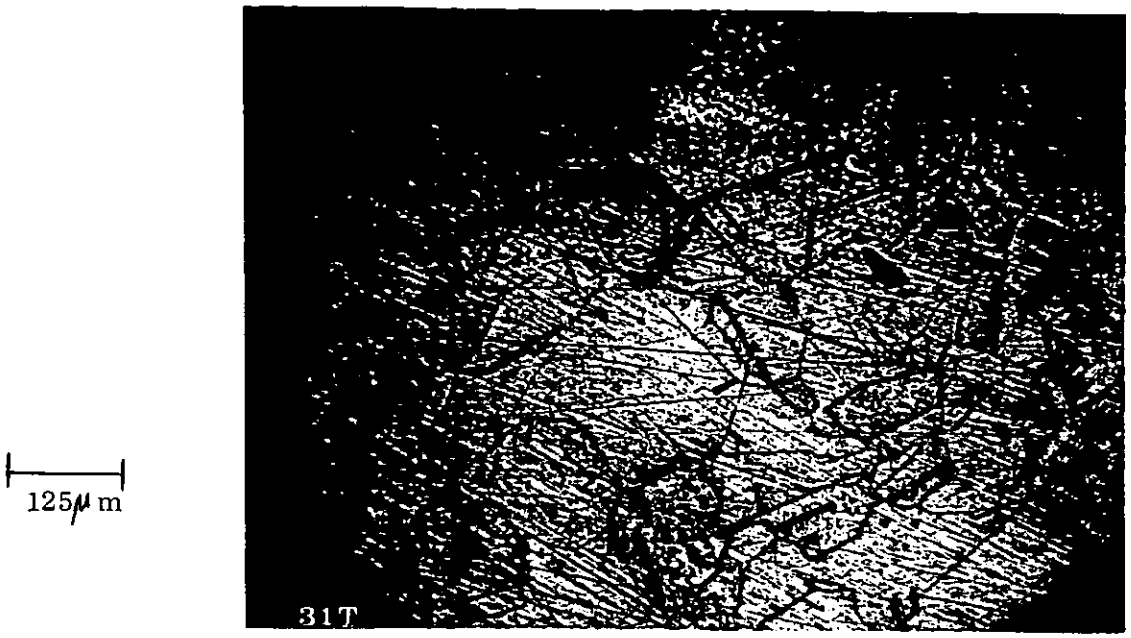

Figure 9.21 Tensile Specimen (transverse section)
- Annealing Temperature 800°C
- Tested at Strain Rate of $10^{-3}s^{-1}$ and Temperature of 600°C

Figure 9.22 Tensile Specimen
- Annealing Temperature 800°C
- Tested at Strain Rate of $1200s^{-1}$ and Temperature of 600°C

Figure 9.23 Tensile Specimen (transverse section)
- Annealing Temperature 800°C
- Tested at Strain Rate of 1200s^{-1} and Temperature of 600°C

are, respectively, 23μm, 26μm, 31μm, 53μm, 34μm and 240μm. These are different from those given in Table 7.1, because each grain size in the latter table is the mean from photomicrographs of several specimens each annealed at the same temperature.

Photomicrographs of representative unstrained tensile specimens at the 5 annealing temperatures are included in Figures 9.7 to 9.11. The average grain sizes are 36μm, 35μm, 35μm, 220μm and 290μm, respectively.

The remaining photomicrographs (Figures 9.12 to 9.23) represent specimens deformed under a variety of test conditions, i.e. compressive or tensile, quasi-static or dynamic strain rate, at room temperature or elevated temperature. The quasi-static compressive specimens had been strained to 30% and the quasi-static tensile specimens had all fractured, with a fracture strain varying between 60% and 85%. The maximum strain levels (%) of the specimens involved in dynamic compressive tests can be calculated, approximately, by dividing the strain rate by 100. The tensile specimens subjected to multiple dynamic loading fractured at a strain of about 70%.

It is interesting to compare Figures 9.14 to 9.17, all of which resulted from specimens suffering very large deformations. In the cases of the specimens tested at the elevated temperature of 600°C (Figures 9.16 and 9.17), the resultant microstructures are still equi-axed, in both cases, despite the vastly different strain rates ($2 \times 10^{-3} s^{-1}$ and $4900 s^{-1}$). There is an obvious difference,

however, between these two figures. The resultant grain size of the quasi-statically deformed specimen is a factor 2 larger than the dynamically deformed specimen, 240μm and 106μm, respectively.

Figures 9.14 and 9.15 resulting from room temperature tests at $2 \times 10^{-3} s^{-1}$ and $6400 s^{-1}$, respectively, indicate greatly distorted grain structures, the grains being elongated at right angles to the direction of stress application. A similar phenomenon can be observed in the photomicrograph of the tensile specimen in Figure 9.18.

Finally, it is worth mentioning that in some specimens there was a tremendous variation in grain sizes. This is evident in Figure 9.12, resulting from a compressive specimen which has only been slightly strained at a low dynamic strain rate at room temperature.

9.5 Hardness Tests

The variation of hardness with annealing temperature was determined for unstrained and quasi-statically strained compressive specimens using a Vickers Pyramid Hardness Testing Machine. The operational principles of the latter are as follows:

A hydraulic mechanism applies a load (chosen by the operator) to a diamond indentor, initially arranged to be touching the surface of the test material with its tip. The diamond pyramid has a square base and its opposite faces make an angle of 136° with one another. The use of a

large angle helps to minimise frictional effects. Upon lowering a small hand lever, the pyramid slowly indents the specimen for a fixed period of time. The specimen is then placed under the attached microscope and the lengths of the two diagonals of the indentation are measured using the micrometer controlled table supporting the specimen. The Vickers Hardness Number (VHN) is then determined corresponding to the size of the indentation and the applied load.

A hardness measurement was made at three positions on the longitudinally sectioned and polished face of each specimen. The positions lay on a straight line, one at the centre of the face (C), one approximately 2mm from the left hand edge (L) and one approximately 2mm from the right hand edge (R).

In general, apart from a couple of anomalies, the hardness of the unstrained specimens decreased as the annealing temperature was increased. Note that the Vickers Hardness Numbers in Table 9.1 are for individual specimens and so variations in the grain size within a specimen could affect these results, particularly since the depth and surface area of the indentation are very small. In almost all cases the unstrained specimens were found to be harder at the edges than in the centre (except for the right edge of the specimen annealed at $600^{o}C$). This variation in hardness and decrease in grain size may have resulted from work hardening during the machining of the specimens. If so, then this would reduce the plastic deformation during a compressive test.

Table 9.1

Vickers Hardness Tests - 5kg load

(a) Unstrained Specimens

Annealing Temperature (°C)	VHN at L	VHN at C	VHN at R
310	76.1	57.1	72.0
400	70.4	55.4	75.3
500	96.3	63.9	71.2
600	56.5	52.6	52.3

(b) Quasi-Statically Strained Specimens

Annealing Temperature (°C)	VHN at L	VHN at C	VHN at R
310	105	105	105
400	107	105	107
500	97.1	98.4	96.5
600	109	107	117

The quasi-statically strained specimens (Table 9.1(b)) were each strained to 20% except for the 600^{o}C specimen which was inadvertently strained to 36%. As expected, compressing the specimens resulted in higher VHN readings. There is also less variation in VHN from the centre to the edges of the specimens.

CHAPTER 10

CONCLUSIONS AND RECOMMENDATIONS

10.1 Introduction

Mechanical tests have been performed in compression and in tension on 99.98% pure oxygen-free high conductivity copper at strain rates between $10^{-3}s^{-1}$ and $6.25 \times 10^{3}s^{-1}$. The tests were carried out at temperatures of 20, 200, 400 and 600°C on specimens with grain sizes of 20, 29, 32, 124 and 240 microns.

10.2 Testing Techniques

Quasi-static tests were performed with an Instron machine. A split Hopkinson pressure bar was used for all dynamic tests. Various modifications were made to both the compressive and tensile versions of the SHPB in order to improve the accuracy, repeatability and validity of tests.

10.2.1 Dynamic Compressive Tests

(a) Constant Strain Rate Tests

The common practice of declaring the average strain rate for a test in which the strain rate is varying considerably is unsatisfactory, because no account is taken of the effects of strain rate history. To overcome this limitation, constant strain rate tests were attempted throughout the current work, using the modified SHPB apparatus developed by ELLWOOD et al (1982a), in which the

loading pulse is shaped.

The semi-empirical choice of a 'dummy' specimen or 'pulse shaper' yielded fairly constant strain rates from about $10s^{-1}$ to $1500s^{-1}$. Pulse shaping was not required at higher strain rates because reasonably constant strain rates were produced by the conventional SHPB technique.

(b) Tests at Various Temperatures

Room temperature tests were performed with either the 431 martensitic stainless steel pressure bars or the higher strength maraging steel bars. At elevated temperatures only the 431 bars were used because the maraging steel bars were plastically deformed above $400^{o}C$.

A small electrical furnace supplied the heat to the specimens, the temperature of the specimens being measured by a chromel/alumel thermocouple. The strain gauges, attached to the pressure bars, were far enough from the furnace that they remained at room temperature, even at the highest test temperature, and hence no change in their gauge factor resulted. It was shown that any variation of mechanical properties due to a possible alteration of the grain size of a specimen, when heating it to the test temperature, is so small as to be undetectable by the SHPB technique.

Lubricants were used to reduce the frictional effects between the faces of a specimen and those of the adjacent pressure bars. At room temperature lubricating oil was satisfactory, whereas at elevated temperatures, graphite

(from a 4B pencil lead) produced the best results.

10.2.2 Dynamic Tensile Tests

The dynamnic tensile technique of ELLWOOD et al (1982b) for stainless steels was modified and adapted for use in testing copper specimens. Dynamic tests were performed between strain rates of $300s^{-1}$ and $1300s^{-1}$.

(a) Sources of Error and Modifications

At strain rates in excess of $700s^{-1}$ the specimens were work hardened by the initial compressive pulse passing through the specimen/collar combination. By increasing the outer diameter of the protective steel collar from 12.7 to 25.4mm, tests were possible at strain rates up to $1300s^{-1}$ without strain hardening the specimen in compression.

Due to the narrow central diameter of the copper tensile specimen, the transmitted pulse is extremely small (approximately 0.005%). Consequently, spurious pulses which are insignificant in the compressive technique, introduced unacceptably large errors in the tensile technique. Causes of the spurious pulses were identified as flexural waves generated by imperfect alignment at impact, reflections from misaligned bars/collar, reflections from bar supports and slackness between the screw threads of the specimen and those of the pressure bars. These pulses were eliminated or diminished by the careful selection of the lengths of the pressure bars and the positions of the bar supports, and by packing the threads with plasticine at room temperature and with an

epoxy (Isopon) at elevated temperatures.

(b) Elevated Temperature Tests

Specimen heating was provided by a blow lamp because the external diameter of the protective collar was greater than the internal diameter of the available electrical furnace. The time taken to heat the tensile specimens to the required testing temperatures was approximately the same as the furance took for the compressive specimens.

Increasing the test temperature above room temperature reduced the small transmitted tensile pulse, and hence the interference of spurious pulses produced proportionately larger errors.

10.2.3 Calibration of the SHPB System

A new method of calibrating the strain gauge outputs of the SHPB apparatus was devised using an opto-electronic device to accurately measure the impact velocity of the projectile. This velocity is related to the strain in the pressure bars and hence can be used to calibrate the strain gauges.

10.3 Data Analysis

The data transfer, analysis and graphical presentation capabilities of the laboratory were considerably enhanced by the design and development of a suite of computer programs. Instead of hours of tedious calculations and manually plotting graphs, the researcher is now able to record and analyse data, list results, and obtain graphs

from a digital plotter in approximately fifteen minutes. Thus a greater number and variety of tests can be performed than was previously possible. The software packages are very flexible. For example, data analysis can be completely performed by the computer or operator interaction can be incorporated to override an erroneous computer interpretation of strain gauge data.

10.4 Discussion of Results

10.4.1 Compressive Tests

(a) Variation of Flow Stress with Strain Rate

At room temperature the flow stress always increases with strain, irrespective of the strain rate. In general, for any chosen strain level and grain size, the form of the flow stress-strain rate relation is an exponential increase of flow stress with strain rate from $2 \times 10^{-3}s^{-1}$ to $1500s^{-1}$, followed by a plateau region upto $3000s^{-1}$, with a further exponential increase in flow stress upto a maximum strain rate in excess of $4500s^{-1}$ (see, for example, Figure 7.7). One major exception to the general behaviour occurs at low strains (<5%) where, in the low strain rate region ($2 \times 10^{-3}s^{-1}$ to $1500s^{-1}$), flow stress is constant with strain rate.

Individual stress-strain rate results which differed from the general trends above were:

(i) 20μm grain size, strain 3% and strain rate $<3000s^{-1}$,

(ii) 20μm grain size, strain 4% and strain rate $<3000s^{-1}$,

(iii) 20μm grain size, strain 5% and strain rate $<3000s^{-1}$,

(iv) 240μm grain size, 10% strain and strain rates from $1150s^{-1}$ to $6150s^{-1}$.

In these cases, a linear increase in the stress versus strain rate relation was exhibited.

In the elevated temperature tests it was not possible from the restricted data to deduce a general form for the stress-strain rate behaviour. However, as the test temperature increases so the flow stress decreases. At $200^{o}C$, there is a much greater reduction of stress in quasi-static tests than in dynamic tests. A more general reduction of flow stress for all strain rates occurs at $400^{o}C$. Also at this temperature, due to additional data, it was observed that at 240μm grain size and at strains of 3%, 4% and 5%, a linear increase of stress with strain rate occurred from $650s^{-1}$ to $4050s^{-1}$. At $600^{o}C$, the most dramatic change involves the quasi-static test data where the stress-strain curves oscillate slightly about a mean value slightly in excess of 50MPa, before exhibiting a negative strain hardening exponent as the strain increases. The oscillatory behaviour is caused by dynamic recrystallisation, c.f. BLAZ et al (1983).

(b) Variation of Flow Stress with Grain Size

Flow stress decreases with increasing grain size for a given strain rate and strain level. This decrease is

almost independent of strain.

At a particular strain level the difference between the flow stress at a given grain size and that at 240μm was found and plotted as a function of strain. At room temperature and 2 x $10^{-3}s^{-1}$, two different linear relations were observed (Figure 7.26) with stress difference initially increasing with strain and then decreasing, the transition strain lying between 5% and 7%. A similar trend occurred for the dynamic tests at 2 x $10^{3}s^{-1}$ except that in the majority of cases the stress difference remains constant from 5% to 20% or 25% (Figure 7.27). At elevated temperatures two linear relations were again discernible. Both gradients were positive at 200°C and less than or equal to zero at 400°C.

(c) Strain Rate Sensitivity (λ)

At room temperature the results are consistent with many other investigators (e.g. KUMAR and KUMBLE (1969), DOWLING et al (1970) and REGAZZONI and MONTHEILLET (1984)) in that below $10^{3}s^{-1}$ the strain rate sensitivity of copper is low but increases rapidly at high strain rates (Figure 7.28(a)). In the low strain rate sensitivity region there is a linear relation between λ and log strain rate for a given strain. Below a strain of 5%, λ is zero but above 5% it increases with strain. λ decreases with increasing grain size. From the rather limited amount of data at elevated temperatures, it was shown that λ behaves in a similar manner to the room temperature tests. λ increases with test temperature.

(d) Work Hardening Exponent

From each plot of log stress against log strain (Figure 7.30), two linear regions can be identified, intersecting at a strain between 15 and 20%. The work hardening exponent (n) is always higher in the lower strain region and, with one exception, it falls between 0.18 and 0.6 for all strain rates, temperatures and grain sizes. At a particular temperature and grain size there is only a slight variation of n with strain rate.

Regazzoni and Montheillet (1984) determined the dependence of the work hardening exponent on strain and strain rate. They also found that two linear regions (intersecting at a strain between 11 and 14%) were evident in graphs of log stress versus log strain. Their tests on OFHC copper with a 25μm grain size at room temperature indicated that n is independent of strain rate for rates between 10^{-4} and $10^{3}s^{-1}$. Their values of n for the lower and upper strain regions were 0.55 and 0.36, respectively. These compare well with the current investigation. For example, in the lower strain region at room temperature, n varies from 0.39 to 0.51 over the three strain rates investigated, with a mean value of 0.44, for the 20μm grain size, and from 0.4 to 0.53, with a mean value of 0.47, for the 32μm grain size. In the upper strain region, n varies from 0.3 to 0.39, and from 0.33 to 0.36, for these two grain sizes, respectively, with a mean value of 0.35 in each case.

(e) Variation of the Dynamic to Quasi-static Flow Stress Rate (σ_D/σ_S) with Homologous Temperature

There is a linear increase of σ_D/σ_S with homologous

temperature when the latter is below 0.5, and the rate of change is small.

Above 0.5, σ_D/σ_S rapidly increases due to dynamic recrystallisation. σ_D/σ_S was determined for a strain of 15%. A similar observation was made by HAWKYARD et al (1968) who plotted the variation of the ratio of dynamic to static mean yield stress with homologous temperature. Above an homologous temperature of 0.5 the ratio rose rapidly. However, below 0.5 there was a slight linear decrease in σ_D/σ_S.

10.4.2 Tensile Tests

Due to all the modifications required to remove the many sources of error and because even then the results were far less consistent than the compressive tests, the range of tensile tests was far less comprehensive than that of the compressive tests. Where direct comparisons were possible, there was excellent correlation between the two modes of testing.

In the dynamic tests, all the specimens fractured at a strain rate of about $1300s^{-1}$, due to multiple dynamic loading. In the quasi-static tests, the 32 μm grain size had the largest elongation at fracture at room temperature and showed the least variation in elongation as the temperature increased (Figure 7.43). In general, the elongations at fracture at room temperature for the dynamic tests were approximately 1mm greater than their quasi-static counterparts. At elevated temperatures, the

dynamically fractured specimens were again extended further, except at 600°C because of dynamic recrystallisation.

As stated in section 4.5, the tensile SHPB technique is capable of testing materials of higher strengths than its compressive counterpart, strain rate is naturally constant and there are no frictional constraints. The results of the dynamic tensile tests have shown the additional advantage that the copper specimens can be strained to fracture at high strain rates. Examinations of the fracture surfaces revealed different fracture mechanisms depending on strain rate, grain size and temperatue. Three kinds of fracture surface were revealed, viz 'cup and cone', cleavage and very sharp points (see section 7.7.2(d)).

10.5 Constitutive Equations and Micromechanisms of Plastic Flow

10.5.1 Thermally Activated Mechanism

Below a strain rate of about $10^3 s^{-1}$, the stress-strain rate results are consistent with a thermally activated deformation mechanism where flow stress is linearly related to the logarithm of strain rate, i.e. (from equation (8.4))

$$\sigma = K_1 + K_2 \log \dot{\varepsilon} \qquad (10.1)$$

The activation volume V*, derived from the constant K2, varies at room temperature from $8.7 \times 10^{-28} m^3$ at a strain of 30% to infinity at a strain of 4%. (c.f. KLEPACZKO

(1974): $V^* = 2.06 \times 10^{-28} m^3$ at a strain of 15%).

10.5.2 Viscous Drag Mechanism

As indicated in section 10.4.1, above $10^3 s^{-1}$ there are a few instances where a linear relation exists between stress and strain rate, i.e.

$$\sigma = \hat{\sigma} + \beta \dot{\varepsilon} \qquad (10.2)$$

where $\hat{\sigma}$ is the internal back stress or threshold stress and β is inversely proportional to the mobile dislocation density, ρ_m.

This linear relation is due to the predominance of a viscous drag mechanism. ρ_m was found to vary between 1.9×10^{11} and $5.5 \times 10^{11} m^{-2}$ over a wide range of temperatures, grain sizes, strains and strain rates.

10.5.3 Combined Thermally Activated and Viscous Drag Mechanisms

Above $10^3 s^{-1}$, the majority of stress-strain rate curves exhibit a plateau region or inflexion. This behaviour, which has not been reported previously in the literature, was predicted theoretically by FOLLANSBEE et al (1984) and attributed to the simultaneous influences of both the thermal activation and viscous drag mechanism. The constitutive equation which describes the combined actions of the mechanisms is:

$$\dot{\varepsilon} = \frac{\hat{\dot{\varepsilon}}(\sigma/\hat{\sigma})}{1 + \psi(\sigma/\hat{\sigma}) \exp(\Delta G/kT)} \qquad (10.3)$$

(see section 8.2.3 for the definitions of the above symbols).

Equation (10.3) correlates excellently with the experimental data in the current investigation.

The threshold stress, $\hat{\sigma}$, varies considerably with strain and grain size, e.g. at 5% strain and 240 microns grain size, $\hat{\sigma}$ = 130MPa, whereas at 20% strain and 20 microns grains size, $\hat{\sigma}$ = 522MPa.

10.5.4 Relation between Stress and Grain Size

In the quasi-static compressive tests, the Hall-Petch relation, i.e.

$$\sigma = \sigma_o + KD^{-1/2}, \qquad (10.4)$$

was obeyed for all strains at temperatures of 673 and 873K (Figures 8.6 and 8.7). At room temperature (293K), the relation was valid for strains of 1, 10 and 20% (Figure 8.4). At $10^3 s^{-1}$, a Hall-Petch relation was found for all strains at room temperature (Figure 8.8). In addition, this linear relation was exhibited at $3500s^{-1}$ for a temperature of 473K and a strain of 30% (Figure 8.13), and at $4000s^{-1}$ for a temperature of 673K and a strain of 10% (Figure 8.14). Several combinations of strain rate,

temperature and strain indicate a dual linear relation between σ and $D^{-1/2}$, intersecting at a grain size of 32 microns.

The only tensile results showing an approximate Hall-Petch relation occurred at 1% (Figures 8.16 and 8.17).

In several cases, σ_o, the flow stress at infinite grain size or the single crystal flow stress, was found to be related to the strain ε by the work hardening equation

$$\sigma_o = C\varepsilon^n \qquad (10.5)$$

where C and n are constants

The values of this work hardening exponent n are almost identical to the values of the work hardening exponent for for the 240 microns grain size in the lower strain region (see Table 8.4).

10.6 Recommendations for Further Work

It is suggested that the following additions and improvements to this research project would be beneficial.

10.6.1 Improved Resolution of Mechanical Characteristics in the Plateau Region

Additional dynamic tests are required to more accurately define the extent of the plateau region in the

stress-strain rate curves which was evident in the room temperature compressive tests. This would yield more precise information on the characteristics of the deformation mechanisms in this region. Further tests at elevated temperatures and in tension, at a greater variety of high strain rates, are needed to ascertain if the plateau region is confined solely to dynamic compressive deformation at room temperature. It would also be beneficial to acquire data at intermediate strain rates, e.g. $1s^{-1}$ or $10s^{-1}$, using a test machine capable of producing substantial strains at these strain rates, such as an hydraulic actuator. This supplementary information would clarify the stress-strain rate relation of OFHC copper between $10^{-3}s^{-1}$ and $10^{2}s^{-1}$.

10.6.2 Specimen Preparation

In the current investigation the test material was annealed at atmospheric pressure prior to machining into compressive and tensile specimens. This second stage of specimen preparation, i.e. machining, may have caused the work hardening in the near surface regions of the specimens, detected by hardness tests and metallographic examinations. The work hardening is likely to be detrimental in mechanical tests, particularly in the case of the tensile specimen because of its narrow cross-section. If the order of specimen preparation were to be reversed, i.e. machining the specimens from the block of raw material and then annealing the specimens (in a vacuum to prevent surface oxidation), the specimens should then be free from work hardening.

10.6.3 Increased Strain to Strain Rate Ratio

One of the major disadvantages of the split Hopkinson pressure bar technique is the dependence of the ultimate specimen strain on the applied strain rate. Consequently, in the current investigation, at a strain rate of $3000s^{-1}$ the specimen strain was approximately 30% whereas at $1500s^{-1}$ the strain was only 15%. Hence direct comparisons between tests at these rates of strain can only be achieved for strains upto 15%. Now, the total strain is also proportional to the length of the impacting projectile. Thus one method of increasing the strain to strain rate ratio would be to use a longer projectile. In order to produce the same final specimen strain when reducing the strain rate by 50% it would be necessary to double the length of the projectile (assuming that the projectile impact velocity remains the same). This modification, however, would require twice the separation between the specimen and the pair of strain gauges which record the incident and reflected pulses, to prevent these pulses from overlapping. This extra separation may be unacceptable if the attenuation per unit distance of the stress pulses in the pressure bars is too large.

REFERENCES

ALBERTINI, C. and MONTAGNANI, M., 1979, Mechanical Properties at High Rates of Strain, ed. J. Harding, p.25 (The Institute of Physics, Bristol, London).

ARMSTRONG, R.W., CODD, I., DOUTHWAITE, R.M. and PETCH, N.J., 1962, Phil. Mag., 7, 45.

BAUER, D.P. and BLESS, S.J., 1979, Strain Rate Effects on Ultimate Strain of Copper, Dayton University (NTIS AD-AO72175).

BHUSHAN, B. and JAHSMAN, W.E., 1978, J. Solids Structures, 14, 739

BITANS, K. and WHITTON, P.W., 1970-71, Proc. Inst. Mech. Eng., 185, 1149.

BITANS, K. and WHITTON, P.W., 1972, Int. Metallurgical Reviews, 17, 66

BLAZ, L., SAKAI, T. and JONAS, J.J., 1983, Metal Science, 17, 609.

CAMPBELL, J.D. and DOWLING, A.R., 1970, J. Mech. Phys. Solids, 18, 43.

CAMPBELL, J.D., ELEICHE, A.M. and TSAO, M.C.C., 1977, Fundamental Aspects of Structural Alloy Design, eds. R.I. Jaffee & B.A. Wilcox, p.545 (Plenum Press, New York, London).

CHALUPNIK, J.D. and RIPPERGER, E.A., 1966, Exp. Mech., 6, 547

CHIU, S.S. and NEUBERT, V.H., 1967, J. Mech. Phys. Solids, 15, 177

CHREE, C., 1889, Trans. Camb. Phil. Soc., 14, 250

CHRISTMAN, D.R., ISBELL, W.M., BABCOCK, S.G., McMILLAN, A.R. and GREEN, S.J., 1971, Final Report under Contract DASA01-68-C-0114, Report No. DASA 2501-2, MSL 70-23, Vol.II.

CLYENS, S. and CAMPBELL, J.D., 1974, Mechanical Properties at High Rates of Strain, ed. J. Harding, p.62 (The Institute of Physics, London, Bristol).

CONN, A.F., 1965, J. Mech. Phys. Solids, 13, 311

DAVIES, E.D.H. and HUNTER, S.C., 1963, J. Mech. Phys. Solids, 11, 155

DAVIES, R.M.,1948, Phil. Trans. A., 240, 375

DORMEVAL, R., STELLY, M. and CAPUT, M., 1976, ICSMA 4 proceedings, Nancy, France, 3, 1141 (in French).

DORMEVAL, R. and STELLY, M., 1979, Mechanical Properties at High Rates of Strain, ed. J. Harding, p.154 (The Institute of Physics, Bristol, London).

DORN, J.E. and HAUSER, F.E., 1963, Proc. Symp. on Structural Dynamics under High Impulse Loading ASD-TDR-63-140, p.173

DOWLING, A.R., HARDING, J. and CAMPBELL, J.D., 1970, J. Inst. Metals, 98, 215.

EDINGTON, J.W., 1969, Phil. Mag., 19, 1189.

EDINGTON, J.W., 1969, Trans. Met. Soc. Aime, 245, 1653.

ELEICHE, A.M. and CAMPBELL, J.D., 1974, Oxford University, Report No. 1106174.

ELLWOOD, S., GRIFFITHS, L.J. and PARRY, D.J., 1982a, J. Phys. E: Sci. Inst., 15, 280

ELLWOOD, S., GRIFFITHS, L.J. and PARRY, D.J., 1982b, J. Phys. E: Sci. Inst., 15, 1169

ELLWOOD, S., 1983, "Dynamic Mechanical Properties of Austenitic Stainless Steels", Ph.D. Dissertation, Department of Physics, Loughborough University of Technology.

ELLWOOD, S., GRIFFITHS, L.J. and PARRY, D.J., 1984, Mechanical Properties at High Rates of Strain, ed. J. Harding, p.55 (The Institute of Physics, Bristol, London).

FOLLANSBEE, P.S. and FRANTZ, C., 1983, J. Eng. Mat. and Tech., 105, 61

FOLLANSBEE, P.S., REGAZZONI, G. and KOCKS, U.F., 1984, Mechanical Properties at High Rates of Strain, J. Harding, p.71 (The Institute of Physics, Bristol, London).

FRANTZ, R.A., Jr. and DUFFY, J., 1972, J. Appl. Mech., 39, 939.

FROST, H.J., and ASHBY, M.F.,1982, "Deformation-Mechanism Maps", (Pergamon Press)

FYFE, I.M., 1976, 2nd Int. Conf. on Mech. Behaviour of Materials, ASM, Metals Park, Ohio, p.1458

FYFE, I.M.,and RAJENDRAN, A.M. 1979, J. Mech. Phys. Solids, 28, 17.

GLENN, T. and BRADLEY, W., 1973, Metallurgical Trans. 4, 2343

GOLDSMITH, W., 1960, "Impact" (Arnold).

GUILLERY, M., 1906, Engineering, 49.

HALL, E.O., 1951, Proc. Phys. Soc., Ser. B. 64, 747

HARDING, J., WOOD, E.O. and CAMPBELL, J.D., 1960, J. Mech. Eng. Sci., 2, 88.

HARDING, J., 1971, Acta Metallurgica, 19, 1177

HASHMI, M.S.J. and HAQUE, M.M., 1986, Proc. of the Int. Symp. on Intense Dynamic Loading and its Effects, Beijing, China, p.637.

HAUSER, F.E., 1966, Exp. Mech., 6, 395

HAUSER, F.E., SIMMONS, J.A. and DORN, J.E., 1960, Response of Metals to High Velocity Deformation, ed. P.G. Shewmon and V.F. Zackay, p.93 (Interscience, New York).

HAWKYARD, J.B., EATON, D. and JOHNSON, W., 1968, Int. J. Mech. Sci., 10, 929

HOPKINSON, B., 1914, Phil. Trans. of the Royal Society, Series A, 213, 437

HOPKINSON J., 1872, "Collected Scientific Papers", Vol.ii, 316.

ISOZAKI, T. and OBA, T., 1979, Nuclear Engineering and Design, 55, 375.

JAHSMAN, W.E., 1971, J. Appl. Mech., 38, 75

JOHNSON, W., 1972, "Impact Strength of Materials", (Arnold).

KARNES, C.H. and RIPPERGER, E.A., 1966, J. Mech. Phys. Solids, 14, 75.

KAWATA, K., HASHIMOTO, S., KUROKAWA, K. and KANAYAMA, N., 1979, Mechanical Properties of Materials at High Rates of Strain, ed. J. Harding, p.71 (The Institute of Physics, Bristol, London).

KISHIDA, K. and SENDA, K., 1972, Bulletin of the JSME, 15, 25.

KLAHN, D., MUKHERJEE, A.K. and DORN, J.E., 1970, 2nd Int. Conf. on Strength of Metals & Alloys, p.951

KLEPACZKO, J.P., 1975, Mat. Sci. and Eng., 18, 121

KLEPACZKO, J.P. and CHIEM, C.Y., 1986, Proc. of the Int. Symp. on Intense Dynamic Loading and its Effects, Beijing, China, p.679.

KOLSKY, H., 1949, Proc. Phys. Soc. B., 62, 676

KOLSKY, H., 1963, "Stress Waves in Solids", (Dover).

KUMAR, A., 1970, 2nd Int. Conf. on the Strength of Metals and Alloys, ASM, Metals Park, 3, 1001.

KUMAR, A. and KUMBLE, R.G., 1969, J. Appl. Phys., 40, 3475.

LINDHOLM, U.S., 1964, J. Mech. Phys. Solids, 12, 317.

LINDHOLM, U.S., 1978, High Velocity Deformation of Solids Proc. Conf., Tokyo, Japan, Aug.1977, p.26

LINDHOLM, U.S. NAGY, A., JOHNSON, G.R. and HOEGFELDT, J.M., 1980, Trans. ASME. J. Eng. Mat. Tech., 102, 376.

LINDHOLM, U.S. and YEAKLEY, L.M., 1968, Ex. Mech., 8, 1

LIPKIN, J., CAMPBELL, J.D.and SWEARENGEN, J.C., 1978, J. Mech. Phys. Solids, 26, 251.

MALVERN, L.E., 1951, Trans. ASME. 73, Series E, J. Appl. Mech, 18, 203.

NICHOLAS, T., 1981, Experimental Mechanics, 21, 177

OHMORI, M., YOSHINAGA, Y. and MANIWA, H., 1968, Proc. 12th Japanese Congress on Materials Research, Kyoto, Japan, p.100

OROWAN, E., 1940, Proc. Phys. Soc., 52, 8.

OROWAN, E., 1950, "The Cam Plastometer", BISRA Rep. (WM/F/22/50).

PETCH, N.J., 1953, J. Iron & Steel Institute, 174, 25

POCHHAMMER, L., 1876, J. reine angew. Math., 81, 324

RAND, J.L., 1967, U.S. Naval Ordnance Laboratory Report NOLTR67-156.

REGAZZONI, G., MONTHEILLET, F., DORMEVAL, R. and STELLY, M., 1981, Deformation of Polycrystals: Mechanisms & Microstructures, ed. N. Hansen, A. Horsewell et al, p.343 (Riso National Lab, Roskilde).

REGAZZONI, G. and MONTHEILLET, F., 1984, Mechanical Properties at High Rates of Strain, ed. J. Harding, p.63 (The Institute of Physics, Bristol, London).

SAMANTA, S.K., 1969, Int. J. Mech. Sci., 11, 433.

SAMANTA, S.K., 1971, J. Mech. Phys. Solids, 19, 117.

SEEGER, A., 1954a, Z. Naturforsch, 9a, 758.

SEEGER, A., 1954c, Z. Naturforsch, 9a, 870.

SEEGER, A., 1955d, Phil. Mag., 46, 1194.

SEEGER, A., 1956a, "Deformation and Flow of Solids", p.90 (Springer-Verlag, Berlin).

SENSENY, P.E., RICHMAN, M.H. and DUFFY, J., 1975, J. Appl. Mech., 42, 245.

SENSENY, P.E., DUFFY, J. and HAWLEY, R.H., 1978, J. Appl. Mech., 45, 60.

SHIORI, J., SATOH, K. and NISHIMURA, K., 1978, High Velocity Deformation of Solids Proc. Conf., Tokyo, Japan, Aug. 1977, p.50.

SIEBEL, E., 1923, Stahl u. Eisen, Dusseldorf, 43, 1295.

STELLY, M. and DORMEVAL, R., 1978, High Velocity Deformation of Solids Proc. Conf. Tokyo, Japan, Aug. 1977, p.82.

STURGES, J.L., PARSONS, B. and COLE, B.N., 1979, Mechanical Properties at High Rates of Strain, ed. J. Harding, p.35 (The Institute of Physics, Bristol, London).

STURGES, J.L., PARSONS, B., COLE, B.N.and KAY, A.E., 1984, Mechanical Properties at High Rates of Strain, ed. J. Harding, p.159.

WALKER, A.G., 1982, Report "Literature Review of the Behaviour of Copper at High Rates of Strain", Department of Physics, Loughborough University of Technology.

WATSON, H., Jr. and RIPPERGER, E.A., 1969, Exp. Mech., 9, 289.

WILKINS, R.A. and BUNN, E.S., 1943, "Copper and Copper Base Alloys", p.23 (McGraw-Hill Book Company, New York).

WULF, G.L., 1974, Mechanical Properties of Materials at High Rates of Strain, ed. J. Harding, p.48 (The Institute of Physics, London, Bristol).

YEW, C.H. and RICHARDSON, H.A., Jr., 1969, Exp. Mech., 9, 366.

APPENDIX A

HOPK-BAR Software

```
10 REM HOPK-BAR VERSION 23-09-84 14.45
20 IF ZX=1 GOTO 89
25 INPUT"□NO OF DATA PTS FROM TRANS REC(1024,2048,3072,4096)";NT
26 IF NT<>1024 AND NT<>2048 AND NT<>3072 AND NT<>4096 THEN 25
27 N2=NT/1024
30 DIMA%(1024*N2)
40 PRINT"■SWITCH ON ALL PERIPHERALS CONNECTED TO PET"
41 PRINT"EXCEPT GRAPH PLOTTER"
42 GOSUB 12000
60 DIM SS(130),ES(130)
61 DIM ST(130),ET(130)
62 DIM TR(130),P(15)
63 PRINT"■IF RECORD LED ON,MOVE 'ARM/HOLD' SWITCH ON TRANS REC TO 'HOLD'"
64 GOSUB 12000
65 PRINT"■INITIALISING TRANS REC SOFTWARE"
66 ZX=1:MK%=4:N1=2
67 LOAD"TR-AUTO-CTRL",8
71 PRINT"■INITIALISING VARIABLES"
72 MK%=1:A=0:TP=0:ND=0:DE=0:EE=0:ES=0:F=0
73 I=0:J=0:K=0:JJ=0:SL=0:EL=0:L=0
74 DN=0:PN=130:NN=0:LP=0:SR=0:BR=0:FR=0:MR=0
75 VS=0:T=0:BT=0:FT=0:PU=0:N1=0:V1=0:G1=0
76 F1=0:G1=0:F2=0:K1=0:KK=0:K2=0:N3=0:CS=0:FY=0
77 VI=0:S1=0:S2=0:EB=0:DB=12.7:PP=0:C0=0:MI=0:PD=0:PC=0
78 A$="0":C$="0":CC$="0":D$="0":DD$="0":F$="0":FF$="0":F1$="0":F2$="0"
79 F3$="0":RF$="0":NF$="0":N$="0":MM$="0":TM$="0":AN$="0":PR$="0":AT$="0"
80 DT$="0":PV$="0":Z$="0":T1$="0":CH$="0":IL$="0"
89 ON MK% GOTO 90,1110,1310,71
90 PRINT"□■■■■■HOPKINSON BAR DATA CONTROL AND ANALYSIS"
91 PRINT"■■■■■■■■■■■■■■■■■SOFTWARE"
92 PRINT"■■THIS PROGRAM CAN BE USED TO ANALYSE DATA FROM BOTH COMPRESSION AND"
93 PRINT"■■■■■■■■■■■■■■■■■■■■■■■■■■■■TENSILE TESTS"
94 PRINT"■CHANNEL 1 DATA REFERS TO STRAIN DATA FROM BAR NEARER TO GAS GUN"
96 PRINT"■■COMPRESSION TESTS: CH1 FOR INCID & REFL PULSES - CH2 FOR TRANS PULSE"
98 PRINT"■■TENSILE TESTS: CH1 FOR TRANS PULSE - CH1 FOR INCID & REFL PULSES"
100 GOSUB 12000
102 INPUT"□HOPK BAR(431 OR MARAGING)";A$
103 IF A$<>"431" AND A$<>"MARAGING" THEN 102
104 IF A$="431" THEN 106
105 EB=187:C0=4818:MI=38.78*1016:GOTO 108
106 EB=212:C0=5240:MI=40.87*1016
108 PRINT"□□HOPKINSON BAR DIRECTORY"
109 PRINT"■■1. TRANSFER DATA FROM T.R.TO PET"
110 PRINT"2. HOPK BAR DATA ANALYSIS"
115 PRINT"3. INSTRON DATA INPUT & ANALYSIS
120 PRINT"4. LIST DATA"
130 PRINT"5. LIST RESULTS"
140 PRINT"6. DRAW GRAPHS"
150 PRINT"7. PARAMETERS ENTERED FROM KEYBOARD"
160 PRINT"8. BAR STRAIN & IMPACT VELOCITY"
170 PRINT"9. EXECUTE T.R. OPERATIONAL SOFTWARE"
175 PRINT"10.AVERAGE OF RESULTS FILES"
177 PRINT"11.FINISH
190 PRINT"■■SELECT CODE"
200 INPUT N1
```

```
210 IF N1<1 OR N1>11 THEN 190
250 ON N1 GOSUB 1000,3000,18000,2000,5000,6000,7000,8000,14000,15000,20000
260 GOTO 108
312 ) APPEARS
1000 PRINT"■■■■■DATA TRANSFER FROM T.R. TO PET"
1001 DA%=0
1002 PRINT"■■DATA WILL ALSO BE TRANSFERRED TO DISK"
1003 INPUT"■■MATERIAL TESTED";MM$
1004 INPUT"COMPRESSION OR TENSILE";CC$
1005 INPUT"TEST TEMP(E.G. 020)";TM$
1006 INPUT"ANNEALING TEMP(E.G. 310)";AN$
1007 INPUT"PROJECTILE TIME(1 TO 2)";T1
1008 INPUT"PROJECTILE TIME(2 TO 3)";T2
1009 S1=100.5/T1:S2=100/T2
1010 VI=S2-(S1-S2)*0.72
1011 TP=INT(VI):IF VI-INT(VI)>=0.5 THEN TP=INT(VI)+1
1012 PV$=STR$(TP):PV$=RIGHT$(PV$,2)
1013 INPUT"STEEL OR DURALUMIN PROJECTILE(S OR D)";PR$
1014 IF PR$<>"S" AND PR$<>"D" THEN 1013
1016 INPUT"IDENTITY LETTER(E.G. A)";IL$
1017 M$=LEFT$(MM$,2)
1018 CC$=LEFT$(CC$,1)
1019 F$=M$+CC$+TM$+AN$+PV$+PR$+IL$
1020 INPUT"PULSE SHAPER USED(Y OR N)";A$
1021 IF A$<>"Y" AND A$<>"N" THEN 1020
1022 IF A$="N" THEN 1030
1023 INPUT"ANNEALING TEMP(0=UNANNEALED)";AT$
1024 AT$=LEFT$(AT$,1)
1025 F$=F$+"P"+AT$
1030 INPUT"DISK DRIVE FOR DATA STOREAGE(0 OR 1)";DD$
1031 IF DD$<>"0" AND DD$<>"1" THEN 1030
1032 PRINT"■CHANNEL 1 DATA:"
1033 PRINT"■■SELECT RANGE OF DATA PTS TO BE STORED"
1034 PRINT"ALLOWING AT LEAST 10 PTS BEFORE START"
1035 PRINT"OF INCIDENT PULSE (IN TENSILE TESTS IGNORE COMP PULSE  FROM IMPACT)
1036 PRINT"■■START ADDRESS ( 1 - "N2*1024")";
1037 INPUT J
1038 PRINT"END ADDRESS OF DATA("J+1" - "N2*1024")"
1039 INPUT K
1040 F1$=DD$+":"+F$+CHR$(49)
1045 PRINT"■■DATA PTS "J" TO "K" WILL BE STORED"
1046 PRINT"IN DATA FILE #"F$ ,
1047 PRINT"   - STARTING AT ADDRESS 1"
1048 PRINT"       AND ENDING AT ADDRESS "K-J+1
1065 PRINT"■■SET 'MEMORY SELECT SWITCH' ON T.R. TO 1"
1075 GOSUB 12000
1090 Z%=1
1095 N1=2
1097 MK%=2
1098 PRINT"■LOADING TRANSIENT RECORDER SOFTWARE"
1100 LOAD"TR-AUTO-CTRL",8
1110 WF$=F1$+",SEQ,WRITE"
1120 OPEN8,8,8,WF$
1150 GOSUB 9000
```

```
1200 PRINT"■■■■■DATA TRANSFER FROM T.R. TO PET"
1205 PRINT"■CHANNEL 2 DATA:"
1215 F2$=DD$+":"+F$+CHR$(50)
1217 PRINT"■DATA PTS "J" TO "K" WILL BE"
1218 PRINT"STORED IN DATA FILE ■"F$
1219 PRINT"    - STARTING AT ADDRESS 1"
1220 PRINT"       AND ENDING AT ADDRESS "K-J+1
1221 PRINT"■N.B. CHANNEL 1 DATA IS ACTUALLY STORED"
1222 PRINT"IN FILE ■"F$+CHR$(49)"■ AND CHANNEL 2 DATA IN FILE ■"F$+CHR$(50)
1223 PRINT"HOWEVER DO NOT USE SUBSCRIPTS ■1■ OR ■2■"
1224 PRINT"WHEN SELECTING A FILENAME IN THIS"
1225 PRINT"PROGRAM"
1226 PRINT"■■SET 'MEMORY SELECT SWITCH' ON T.R. TO 2"
1235 GOSUB 12000
1290 N1=2
1295 MK%=3
1297 PRINT"■LOADING TRANSIENT RECORDER SOFTWARE"
1300 LOAD"TR-AUTO-CTRL",8
1310 WF$=F2$+",SEQ,WRITE"
1315 OPEN8,8,8,WF$
1320 GOSUB 9000
1330 MK%=1
1333 PRINT"■"
1336 SR=1:LP=25:V1=.5:V2=.5:G1=5.04:G2=5.04
1340 F=2.10:EM=117
1342 PRINT"WAVE VELOCITY IN BARS = "C0"MPS
1343 PRINT"ELASTIC MOD OF BARS = "EB"GPA
1344 PRINT"DIAMETER OF BARS = "DB"MM"
1346 PRINT"PROJECTILE LENGTH = "LP"CMS"
1347 PRINT"STRAIN GAUGE FACTOR = "F
1383 INPUT"VOLTS FULL SCALE,CH1";V1
1386 INPUT"VOLTS FULL SCALE,CH2";V2
1387 INPUT"GAIN OF SG1 AMPLIFIER";G1
1388 INPUT"GAIN OF SG2 AMPLIFIER";G2
1390 INPUT"ELASTIC MOD OF SPECIMEN(GPA)";EM
1391 INPUT"DATE";DT$
1393 INPUT"TIME";TM$
1394 INPUT"SAMPLE LENGTH(MM)";LS
1395 INPUT"SAMPLE DIAMETER(MM)";DS
1396 INPUT"POWER SUPPLY VOLTAGE";E
1397 INPUT"VOLTS ACROSS SG1";VA
1398 INPUT"VOLTS ACROSS SG2";VB
1399 INPUT"TIME DELAY BETWEEN TRANS & REFL PULSES(MICROSECS)";DE
1400 F3$=DD$+":"+F$+CHR$(51)
1405 WF$=F3$+",SEQ,WRITE"
1410 OPEN8,8,8,WF$
1415 PRINT"■TRANSFERRING PARAMETERS TO DISK"
1417 SR=1
1420 P(1)=SR:P(2)=LP:P(3)=V1:P(4)=V2
1425 P(5)=G1:P(6)=G2:P(7)=F:P(8)=LS
1430 P(9)=DS:P(10)=E:P(11)=VA:P(12)=VB
1435 P(13)=DE:P(14)=EM:P(15)=V1:P$(1)=DT$:P$(2)=TM$
1436 CS=0
```

```
1437 FOR J=1 TO 15:CS=CS+P(J):NEXT
1438 PRINT#8,CS;CHR$(13);
1440 FOR J=1 TO 15
1445 PRINT#8,P(J);CHR$(13);
1450 NEXT
1455 FOR J=1 TO 2
1460 PRINT#8,P$(J);CHR$(13);
1465 NEXT
1470 CLOSE8
1500 GOTO 108
2000 INPUT"□NAME OF FILE HOLDING DATA";F$
2130 INPUT"DISK DRIVE(0 OR 1)";DD$
2132 INPUT"HOPK-BAR OR INSTRON DATA(H OR I)";A$
2133 IF A$="H" THEN 2140
2134 IF A$<>"I" THEN 2132
2135 GOTO 2157
2140 INPUT"CH1 OR CH2 DATA(1 OR 2)";C$
2145 IF C$="1" OR C$="2" THEN 2150
2147 GOTO 2140
2150 RF$=DD$+":"+F$+C$
2155 GOTO 2160
2157 RF$=DD$+":"+F$
2160 A$=RF$+",SEQ,READ"
2170 OPEN 8,8,8,A$
2175 INPUT#8,CS
2180 INPUT#8,ND
2185 CLOSE 8
2187 PRINT"▲THERE ARE "ND" DATA PTS IN THIS FILE"
2190 INPUT"DATA TO BE LISTED FROM DATA PT NO";J
2200 INPUT"                    TO DATA PT NO";I
2201 PRINT"□▷▷▷▷LIST DATA ON - "
2210 PRINT"▲▲▲1. SCREEN"
2220 PRINT"2. LINE PRINTER"
2250 PRINT"▲▲"
2260 INPUT"□SELECT CODE■";N3
2270 IF N3<1 OR N3>2 THEN 2060
2300 DN=N3+2
2344 OPEN DN+2,DN,2
2345 IF DN=3 THEN 2350
2346 PRINT#DN+2,"999999"
2350 OPEN DN,DN,1
2352 IF C$="1" AND CC$="C" OR C$="2" AND CC$="T" THEN Z$="INCIDENT"
2353 IF C$="1" AND CC$="T" OR C$="2" AND CC$="C" THEN Z$="TRANSMITTER"
2354 IF CC$<>"0" THEN 2360
2355 INPUT"▲COMPRESSION OR TENSILE DATA(C OR T)";CC$
2356 IF CC$="C" OR CC$="T" THEN 2352
2357 GOTO 2355
2360 IF DN<>3 THEN PRINT#DN,CHR$(160)"          "Z$" BAR DATA PTS "J" TO"I;
2361 PRINT#DN,CHR$(160)"    "F$
2362 PRINT#DN
2365 IF DN=3 THEN PRINT"□DATA PT NO     DATA VALUES"
2366 IF DN=3 THEN 2375
2367 PRINT#DN,CHR$(160)"DATA PT NO                          DATA VALUES"
```

```
2375 GOSUB 10000
2380 CLOSEDN+2
2390 RETURN
3000 REM DATA ANALYSIS SECTION
3005 DA%=1
3006 GOSUB 3010
3007 GOTO 3095
3010 INPUT"■■■NAME OF FILE HOLDING DATA";F$
3020 INPUT"DISK DRIVE(0 OR 1)";DD$
3021 IF DD$<>"0" AND DD$<>"1" THEN 3020
3030 RF$=DD$+":"+F$+CHR$(51)
3040 A$=RF$+",SEQ,READ"
3050 OPEN8,8,8,A$
3055 INPUT#8,CS
3070 INPUT#8,SR,LP,V1,V2,G1,G2,F,LS
3080 INPUT#8,DS,E,VA,VB,DE,EM,VI,DT$,TM$
3090 CLOSE8
3092 RETURN
3095 TP=SR+LP+V1+V2+G1+G2+F+LS+DS+E+VA+VB+DE+EM
3140 DN=3:GOSUB 7030
3150 INPUT"DOES SG1 AMP INVERT SIGNAL(Y OR N)";A$
3152 IF A$="Y" THEN A1=-1
3153 IF A$="N" THEN A1=1
3154 IF A$<>"Y" AND A$<>"N" THEN 3150
3160 INPUT"DOES SG2 AMP INVERT SIGNAL(Y OR N)";A$
3162 IF A$="Y" THEN A2=-1
3163 IF A$="N" THEN A2=1
3170 IF A$<>"Y" AND A$<>"N" THEN 3160
3200 REM CALIBRATION FACTORS CALC -F1 &F2
3210 N=(E-VA)/VA
3215 INPUT"CH1 SG FACTOR";F
3220 F1=(N+1)↑2/(N*F*G1)
3230 N=(E-VB)/VB
3235 INPUT"CH2 SG FACTOR";F
3240 F2=(N+1)↑2/(N*F*G2)
3250 K1=(F1*V1)/(E*255)
3260 K2=(F2*V2)/(E*255)
3799 CC$=MID$(F$,3,1)
3800 Z$="2":IF CC$="T" THEN Z$="1"
3801 PRINT"■■■■■CHANNEL "Z$" DATA - TRANSMITTED PULSE"
3802 PP=1:IF CC$="T" THEN PP=-1
3803 IF A1=-1 AND CC$="T" THEN PP=1
3804 IF A2=-1 AND CC$="C" THEN PP=-1
3805 RF$=DD$+":"+F$+Z$
3806 A$=RF$+",SEQ,READ"
3807 OPEN8,8,8,A$
3808 INPUT#8,CS
3809 INPUT#8,ND
3810 CLOSE 8
3811 CH$="TRANS"
3812 PRINT"■■THERE ARE "ND" DATA PTS IN ■"F$
3814 J=1:I=ND
```

```
3820 GOSUB 11000
4020 PRINT"&SEARCHING FOR START OF TRANS PULSE"
4022 B=20
4025 GOSUB 14030
4100 BT=B:FT=BT+PN
4110 PRINT"REMOVING LARGE VARIATIONS IN TRANS PULSE"
4115 FOR J=BT-20 TO FT+20
4117 IF J=0 THEN 4125
4120 IF A%(J)=0 OR A%(J)=255 THEN A%(J)=A%(J-1)
4125 NEXT
4130 FOR J=BT-20 TO FT+20
4132 IF J=0 THEN 4140
4135 IF ABS(A%(J)-A%(J-1))>5 THEN A%(J)=(A%(J+1)+A%(J-1))/2
4140 NEXT
4142 GOTO 4290
4143 L2=A%(BT-22)
4144 L1=A%(BT-21)
4145 FOR J=BT-20 TO FT+20
4150 L0=A%(J)
4155 A%(J)=(L2+L1+A%(J)+A%(J+1)+A%(J+2))/5
4160 L2=L1
4161 L1=L0
4165 NEXT
4290 BT=B:FT=BT+PN
4295 PRINT"DATA PTS "BT" TO "FT" WILL BE ANALYSED"
4297 REM AVG OF 15 DATA PTS BEFORE TRANS PULSE
4300 REM THIS WILL BE ZERO PT OF DATA
4305 PRINT"&FINDING BASELINE OF TRANS PULSE"
4310 TP=0
4315 FOR J=BT-15 TO BT-1
4320 TP=TP+A%(J)
4325 NEXT
4330 TP=TP/15
4335 IF TP-INT(TP)>=0.5 THEN TP=INT(TP)+1
4340 TP=INT(TP)
4345 PRINT"&BASELINE FOR CHANNEL "Z$" DATA IS "TP
4346 INPUT"ALTER BASELINE(Y OR N)";A$
4347 IF A$="N" THEN 4350
4348 IF A$<>"Y" THEN 4346
4349 INPUT"NEW BASELINE VALUE";TP
4350 FOR J=BT-20 TO FT+20
4355 A%(J)=A%(J)-TP
4360 NEXT
4370 PRINT"&ANALYSING TRANSMITTED PULSE DATA"
4371 KK=K2:IF CC$="T" THEN KK=K1
4372 TP=EB*10↑9*DB12/(DS12)
4373 FOR J=BT TO FT
4374 JJ=J-BT
4388 A=A%(J)*KK
4389 SS(JJ)=A*TP*PP
4393 NEXT J
4394 PRINT"&ANALYSIS COMPLETED"
4395 GOSUB 12000
```

```
4397 Z$="1":IF CC$="T" THEN Z$="2"
4400 PRINT"□RCHANNEL "Z$" DATA■Q■■■■■■■■■■■INCIDENT & REFLECTED PULSES"
4410 RF$=DD$+":"+F$+Z$
4420 A$=RF$+",SEQ,READ"
4425 J=1:I=ND
4426 GOSUB 11000
4427 PRINT"□FINDING START OF INCID PULSE"
4428 CH$="INCID":PP=1:B=20
4429 IF CC$="T" THEN PP=-1
4430 IF A2=-1 AND CC$="T" THEN PP=1
4431 IF A1=-1 AND CC$="C" THEN PP=-1
4432 GOSUB 14030
4433 CH$="REFL":PP=-1:B=B+PN+20
4434 IF CC$="T" THEN PP=1
4435 IF A2=-1 AND CC$="T" THEN PP=-1
4436 IF A1=-1 AND CC$="C" THEN PP=1
4439 PRINT"□FINDING START OF REFL PULSE"
4440 GOSUB 14030
4441 BR=B:FR=BR+PN
4442 AS=0
4444 REM FIND AVG OF 20 PTS AT END OF REFL PULSE
4445 FOR J=FR TO FR+19
4446 AS=AS+A%(J)
4448 NEXT
4450 AS=AS/20
4454 IF AS-INT(AS)>=0.5 THEN AS=INT(AS)+1
4455 AS=INT(AS)
4456 PRINT"□BASELINE FOR CHANNEL "Z$" DATA IS "AS
4457 INPUT"ALTER BASELINE(Y OR N)";A$
4458 IF A$="N" THEN 4470
4459 IF A$<>"Y" THEN 4457
4460 INPUT"NEW BASELINE VALUE";AS
4470 ED=BR-BT
4475 PRINT"□REFLECTED PULSE STARTS "ED "MICROSECS AFTER TRANS PULSE"
4480 IF DE<=ED THEN 4556
4485 PRINT"□THIS DELAY SHOULD BE "DE" MICROSECS"
4487 INPUT"□DO YOU WANT TO MODIFY START OF REFL PULSE(Y OR N)";A$
4488 IF A$="N" THEN 4556
4489 IF A$<>"Y" THEN 4487
4490 PRINT"□MODIFYING START OF REFLECTED PULSE"
4492 JJ=0
4493 TP=DE-ED
4495 FOR J=BR TO FR
4500 IF A%(J)>A%(J+TP) THEN 4507
4505 J=FR:GOTO 4510
4507 JJ=JJ+1
4510 NEXT
4512 FOR J=BR+JJ-1 TO BR STEP -1
4513 A%(J+TP)=A%(J)
4514 NEXT
4520 BR=BR+TP:FR=FR+TP
4525 PRINT"□REFL PULSE NOW STARTS AT "BR
4530 PRINT"□    I.E."DE "MICROSECS AFTER TRANS PULSE"
```

```
4535 INPUT"DO YOU WANT TO SEE MODIFIED REFL PULSE(Y OR N)";A$
4536 IF A$="N" THEN 4557
4537 IF A$<>"Y" THEN 4535
4538 RB=BR
4540 FOR J=BR TO FR
4542 PRINT A%(J)
4544 JJ=J-RB
4546 IF JJ<20 THEN 4555
4548 RB=J
4550 INPUT"MORE(Y OR N)";A$
4551 IF A$="Y" THEN 4555
4552 IF A$<>"N" THEN 4550
4553 J=FR
4554 GOTO 4557
4555 NEXT
4556 GOSUB 17000
4557 FOR J=BR-20 TO FR+20
4558 A%(J)=A%(J)-AS
4559 NEXT
4561 PRINT"START CORRECTION OF REFL PULSE = "A%(BR)
4562 PRINT"END CORRECTION OF REFL PULSE ="A%(FR)
4563 INPUT"DO YOU WANT TO CHANGE THESE VALUES(Y OR N)";A$
4564 IF A$="N" THEN 4569
4565 IF A$<>"Y" THEN 4563
4566 INPUT"START CORRECTION";ES
4567 INPUT"END CORRECTION";EE
4568 GOTO 4572
4569 ES=A%(BR)
4570 EE=A%(FR)
4572 PRINT"CORRECTING REFL PULSE BASELINE"
4573 FOR JJ=BR TO FR
4576 J=JJ-BR
4577 A%(J)=A%(JJ)-(((ES-EE)*(PN+BR-JJ)/PN)+EE)
4579 NEXT
4589 PRINT"ANALYSING REFLECTED PULSE DATA"
4590 REM CALCULATE STRAIN IN SAMPLE
4600 TP=0
4620 MR=SR*1E-6
4625 J=1:I=ND
4630 FY=2*C0*1000/LS
4635 KK=K1:IF CC$="T" THEN KK=K2
4640 FOR JJ=BR TO FR
4641 J=JJ-BR
4650 A=A%(J)*KK
4660 TP=TP+A*MR
4680 ES(J)=TP*FY*PP
4700 NEXT JJ
4703 PRINT"ANALYSIS COMPLETED"
4704 GOSUB 12000
4910 REM CALC TRUE STRESS,STRAIN,STRAIN RATE
4915 PP=-1:IF CC$="T" THEN PP=1
4920 PRINT"CALCULATING TRUE STRESSES & STRAINS"
4921 FOR J=0 TO 130:ET(J)=0:ST(J)=0:NEXT
```

```
4922 FOR J=0 TO PN
4930 ET(J)=PP*LOG(1+PP*ES(J))
4940 ST(J)=SS(J)*(1+PP*ES(J))
4950 IF J=0 OR N1=3 THEN 4960
4955 TR(J)=(ET(J)-ET(J-1))/MR
4960 NEXT
4962 PRINT"CALCULATIONS COMPLETED"
4965 GOSUB 12000
4970 INPUT"DO YOU WANT TO STORE TRUE STRESS/STRAIN RESULTS ON DISK(Y OR N)";A$
4972 IF A$="N" THEN 108
4974 IF A$<>"Y" THEN 4970
4975 PRINT"ANY PREVIOUS RESULTS FROM DATA FILE "F$" WILL BE ERASED"
4976 INPUT"CONTINUE WITH TRANSFER TO DISK(Y OR N)";A$
4977 IF A$="N" THEN 108
4978 IF A$<>"Y" THEN 4976
4979 WF$="@"+DD$+":"+F$+CHR$(52)+",SEQ,WRITE"
4980 OPEN8,8,8,WF$
4985 PRINT"SWITCH OFF GRAPH PLOTTER"
4986 GOSUB 12000
4987 PRINT"TRANSFERRING RESULTS TO DISK"
4988 FOR J=0 TO PN
4989 PRINT#8,ST(J);CHR$(13);
4990 PRINT#8,ET(J);CHR$(13);
4991 PRINT#8,TR(J);CHR$(13);
4992 NEXT
4995 CLOSE8
4997 PN=130
4998 GOSUB 12000
4999 GOTO 108
5000 REM RESULTS
5010 PRINT"RESULTS"
5020 PRINT"1. TRUE STRESS/STRAIN"
5030 PRINT"2. ENGINEERING STRESS/STRAIN"
5037 PRINT"3. RETURN TO HOPK BAR MENU"
5040 INPUT"SELECT CODE";N1
5041 IF N1<1 OR N1>3 THEN 5010
5042 IF N1=3 THEN RETURN
5045 IF N1=1 THEN GOSUB 5500
5046 IF DA%=1 THEN 5050
5047 PRINT"ERROR - DATA NOT YET ANALYSED"
5048 GOSUB 12000
5049 RETURN
5050 PRINT"TRANSFER RESULTS TO :-"
5060 PRINT"1. SCREEN"
5070 PRINT"2. LINE PRINTER"
5090 INPUT"SELECT CODE";DN
5092 IF DN<1 OR DN>2 THEN 5050
5095 DN=DN+2
5097 L=1:R$=RIGHT$(F$,2):R$=LEFT$(R$,1)
5098 IF R$="2" OR RIGHT$(F$,1)="5" OR RIGHT$(F$,1)="6" THEN 5120
5100 INPUT"ENTER MICROSEC INTERVAL FOR RESULTS TABLE";L
5120 OPEN DN+2,DN,2
5130 FF$="9999.99   999999.999-  999.999-   99999.999-"
```

```
5140 PRINT#DN+2,FF$
5300 OPEN DN,DN,1
5301 PRINT#DN,CHR$(160)"FILENAME = "F$
5302 PRINT#DN:PRINT#DN:PRINT#DN
5305 IF N1=1 THENT1$="□      TRUE STRESS/STRAIN RESULTS"
5315 IF N1=2 THEN T1$="□      ENGINEERING STRESS/STRAIN RESULTS"
5322 PRINT#DN,T1$
5324 PRINT#DN
5325 IF N1=1 THEN 5335
5327 PRINT#DN,CHR$(160)"  TIME       STRESS      STRAIN"
5329 PRINT#DN,CHR$(160)"   -6"
5331 PRINT#DN,CHR$(160)"(10  SEC)   (MPA)          (%)"
5333 GOTO 5345
5335 PRINT#DN,CHR$(160)"  TIME       STRESS      STRAIN   STRAIN RATE"
5337 PRINT#DN,CHR$(160)"   -6"
5340 PRINT#DN,CHR$(160)"(10  SEC)   (MPA)          (%)      (/SEC)"
5345 PRINT#DN
5347 T=0
5350 FOR J=0 TO PN STEP L
5352 IF J>0 AND ST(J)=0 AND ET(J)=0 THEN 5365
5355 IF N1=1 THEN PRINT#DN,T,ST(J)/1E6,ET(J)*100,TR(J)
5362 IF N1=2 THEN PRINT#DN,T,SS(J)/1E6,ES(J)*100
5365 IF R$="%" THEN 5368
5367 T=T+L
5368 NEXT
5370 IF DN=4 THEN 5390
5375 GOSUB 12000
5390 CLOSE DN
5392 CLOSEDN+2
5395 GOTO 5010
5500 INPUT"DO YOU WANT RESULTS FROM DISK FILE(Y OR N)";A$
5510 IF A$="N" THEN RETURN
5520 IF A$<>"Y" THEN 5500
5523 PRINT"□SWITCH OFF GRAPH PLOTTER"
5524 GOSUB 12000
5525 DA%=1
5530 INPUT"FILENAME";F$
5540 INPUT"DISK DRIVE(0 OR 1)";DD$
5550 IF DD$<>"0" AND DD$<>"1" THEN 5540
5551 FT$=CHR$(52)
5552 INPUT"SMOOTHED RESULTS(Y OR N)";A$
5553 IF A$="Y" THEN FT$=CHR$(53)
5554 INPUT"AVERAGED RESULTS(Y OR N)";A$
5555 IF A$="Y" THEN FT$=CHR$(54)
5560 RF$=DD$+":"+F$+FT$+",SEQ,READ"
5570 OPEN8,8,8,RF$
5580 FOR J=0 TO PN
5590 INPUT#8,ST(J),ET(J),TR(J)
5600 NEXT
5610 CLOSE8
5620 RETURN
6000 Z%=1
6050 PRINT"□LOADING GRAPH PLOTTING PROGRAM"
```

```
6100 LOAD"GRAPHS",8
7000 REM LIST OF PARAMETERS ENTERED FROM THE KEYBOARD
7022 PRINT"□□PARAMETERS ENTERED FROM KEYBOARD"
7023 INPUT"□□LIST PARAMETERS ON SCREEN OR PRINTER    (S OR P)";A$
7024 IF A$="S" THEN DN=3
7025 IF A$="P" THEN DN=4
7026 IF A$="S" OR A$="P" THEN 7028
7027 GOTO 7003
7028 GOSUB 3010
7030 OPEN DN,DN
7110 PRINT#DN,"□PARAMETERS ENTERED FROM KEYBOARD"
7120 PRINT#DN,"----------------------------------------"
7127 PRINT#DN,"DATE                        = "DT$
7128 PRINT#DN,"TIME                        = "TM$
7129 PRINT#DN,"FILENAME                    = "F$
7130 PRINT#DN,"SAMPLING RATE               = "SR" MICROSECS"
7140 PRINT#DN,"PROJECTILE LENGTH           = "LP" CM"
7150 PRINT#DN,"VOLTS FULL SCALE,CH1        = "V1
7160 PRINT#DN,"VOLTS FULL SCALE,CH2        = "V2
7170 PRINT#DN,"GAIN OF SG1 AMPLIFIER       = "G1
7180 PRINT#DN,"GAIN OF SG2 AMPLIFIER       = "G2
7190 PRINT#DN,"STRAIN GAUGE FACTOR         = "F
7200 PRINT#DN,"SAMPLE LENGTH               = "LS" MM"
7210 PRINT#DN,"SAMPLE DIAMETER             = "DS" MM"
7220 PRINT#DN,"POWER SUPPLY VOLTAGE        = "E
7230 PRINT#DN,"VOLTS ACROSS SG1            = "VA
7240 PRINT#DN,"VOLTS ACROSS SG2            = "VB
7270 PRINT#DN,"ELASTIC MODULUS             = "EM" GPA"
7275 PRINT#DN,"DELAY BETWEEN PULSES        = "DE " MICROSECS"
7276 PRINT#DN,"VELOCITY OF IMPACT          = "VI" MPS"
7280 CLOSE DN
7285 IF DN=4 THEN RETURN
7290 GOSUB 12000
7300 RETURN
8000 REM COMPARE SG & PROJ VEL READINGS
8005 PRINT"□"
8006 INPUT"DO YOU KNOW DIGITAL SIZES OF BOTH CHANNELS 1 & 2 PULSES(Y OR N)";A$
8007 IF A$="Y" THEN 8020
8008 IF A$<>"N" THEN 8006
8009 PRINT"RETURN TO HOPK BAR DIRECTORY & LIST DATA"
8010 GOSUB 12000
8011 RETURN
8020 INPUT"POWER SUPPLY VOLTAGE";E
8030 INPUT"STRAIN GAUGE FACTOR";F
8040 INPUT"GAIN OF SG1 AMPLIFIER";G1
8045 INPUT"GAIN OF SG2 AMPLIFIER";G2
8050 INPUT"VOLTS ACROSS SG1";VA
8055 INPUT"VOLTS ACROSS SG2";VB
8060 INPUT"VOLTS FULL SCALE,CH1";V1
8065 INPUT"VOLTS FULL SCALE,CH2";V2
8066 INPUT"PROJECTILE DENSITY(KG/CU M)";PD
8067 INPUT"PROJECTILE WAVE VELOCITY(M/S)";PC
```

```
8070 INPUT"DIGITAL SIZE OF SG1 PULSE";PA
8075 INPUT"DIGITAL SIZE OF SG2 PULSE";PB
8100 NA=(E-VA)/VA
8105 NB=(E-VB)/VB
8110 SA=(NA+1)*(NA+1)*V1*PA/(NA*F*E*G1*255)
8115 SB=(NB+1)*(NB+1)*V2*PB/(NB*F*E*G2*255)
8130 PRINT"STRAIN FROM STRAIN GAUGES 1 = "SA*100"%"
8132 PRINT"STRAIN FROM STRAIN GAUGES 2 = "SB*100"%"
8135 VS=SA*EB*10↑9*(1/MI+1/(PD*PC))
8140 PRINT"PROJECTILE VEL FROM STRAIN GAUGES 1 ="VS"METRES PER SEC"
8142 VS=SB*EB*10↑9*(1/MI+1/(PD*PC))
8145 PRINT"PROJECTILE VEL FROM STRAIN GAUGES 2 ="VS"METRES PER SEC"
8150 GOSUB 12000
8160 RETURN
9000 ND=K-J+1
9002 PRINT"␣SWITCH OFF GRAPH PLOTTER"
9003 GOSUB 12000
9005 PRINT"␣TRANSFERRING DATA FROM PET TO DISK"
9006 CS=0
9007 FOR I=J TO K:CS=CS+A%(I):NEXT
9008 PRINT#8,CS;CHR$(13);
9010 PRINT#8,ND;CHR$(13);
9020 FOR I=J TO K
9100 PRINT#8,A%(I);CHR$(13);
9200 NEXT
9300 CLOSE8
9310 PRINT"␣TRANSFER COMPLETED"
9320 GOSUB 12000
9400 RETURN
10000 GOSUB 11000
10600 NN=(DN-2)*5
10605 FOR K=J TO I STEP NN
10610 PRINT#DN,K;
10611 PRINT#DN,CHR$(160)"          ";
10615 FOR L=0 TO NN-2
10620 PRINT#DN,A%(K+L);
10625 NEXT L
10628 PRINT#DN,A%(K+L)
10630 NEXT K
10635 IF DN=4 THEN 10700
10640 GOSUB 12000
10700 CLOSE DN
10750 RETURN
11000 OPEN8,8,8,A$
11001 PRINT"␣SWITCH OFF GRAPH PLOTTER"
11002 GOSUB 12000
11004 IF N3=1 THEN 11010
11005 PRINT"␣TRANSFERRING DATA FROM DISK TO PET"
11010 INPUT#8,CS
11015 TP=0
11020 INPUT#8,ND
11050 FOR K=0 TO ND-1
11060 INPUT#8,A%(K)
11065 TP=TP+A%(K)
```

```
11070 NEXT
11080 CLOSE 8
11081 IF CS=TP THEN 11088
11082 PRINT"■■CHECKSUM ERROR■"CS,TP
11083 INPUT"DO YOU WANT TO READ DATA AGAIN";D$
11084 IF D$="Y" THEN 11000
11085 IF D$<>"N" THEN 11083
11086 PRINT"■CONTINUING WITH ERRONEOUS DATA"
11088 IF N3=1 THEN 11090
11089 PRINT"■TRANSFER COMPLETED"
11090 RETURN
12000 PRINT"■■■■■■■HIT SPACE BAR TO CONTINUE"
12010 GET C$:IF C$<>" " THEN 12010
12020 RETURN
14000 REM LOAD TRANSIENT RECORDER PROGRAM
14005 PRINT"LOADING TRANSIENT RECORDER SOFTWARE"
14007 MK%=1
14010 LOAD"TR-AUTO-CTRL",8
14030 REM FIND START OF PULSE
14031 TP=0:JJ=0
14032 FOR J=B TO I STEP 10
14034 IF (A%(J)-A%(J-1))*PP<1 THEN 14038
14036 B=J-20:J=I
14038 NEXT
14039 TP=0:JJ=0
14040 FOR J=B TO I
14045 IF A%(J)*PP>A%(J+1)*PP THEN 14100
14050 IF A%(J)=A%(J+1) AND TP=0 THEN 14100
14055 IF A%(J)=A%(J+1) THEN 14090
14060 TP=TP+1
14065 IF TP<4 THEN 14110
14075 B=J-3-JJ
14080 J=I:GOTO 14110
14090 JJ=JJ+1
14092 IF JJ>3 THEN 14100
14095 GOTO 14110
14100 TP=0:JJ=0
14110 NEXT
14120 REM MANUAL CHECK OF START OF PULSE
14130 PRINT"■"CH$" PULSE STARTS AT";B
14140 INPUT"■■DO YOU WANT TO CHECK(Y OR N)";A$
14150 IF A$="N"GOTO 14282
14160 IF A$<>"Y" GOTO 14140
14165 J=B:IF J<10 THEN 14200
14170 FOR J=B-10 TO B+10
14180 PRINT J,A%(J)
14190 NEXT J
14200 INPUT"DO YOU WANT TO CHANGE PREDICTED START VALUE(Y OR N)";A$
14210 IF A$="N" GOTO 14282
14220 IF A$<>"Y" GOTO 14200
14230 PRINT"APPROX START OF "CH$" PULSE";
14235 INPUT B
14240 FOR J=B-10 TO B+10
```

```
14250 PRINT J,AX(J)
14260 NEXT J
14265 INPUT"DO YOU WANT TO ENTER APPROX START AGAIN(Y OR N)";A$
14270 IF A$="Y" THEN 14230
14275 IF A$<>"N" THEN 14265
14280 INPUT"ENTER EXACT STARTING VALUE";B
14282 RETURN
15000 PRINT"■■■■■■■■■■AVERAGED RESULTS"
15010 PRINT"■■THIS ROUTINE CAN BE USED TO AVERAGE 2 OR MORE RESULTS FILES"
15030 PRINT"ALTERNATIVELY THE AVG OF RESULTS FILES CAN BE INPUT FROM KEYBOARD"
15035 PRINT"TO BE STORED ON DISK"
15037 DA%=1
15040 INPUT"■FROM KEYBOARD(Y OR N)";A$
15050 IF A$="Y" THEN 15500
15060 IF A$<>"N" THEN 15040
15100 PRINT"■■■■■■■AUTOMATIC RESULTS AVERAGING"
15110 PRINT"■NOT YET AVAILABLE"
15120 GOSUB 12000
15130 RETURN
15500 INPUT"RESULTS FILENAME";F$
15510 INPUT"DISK DRIVE(0 OR 1)";DD$
15520 NF$=DD$+":"+F$+CHR$(54)+",SEQ,WRITE"
15530 INPUT"HOW MANY DATA PTS(1-130)";ND
15540 IF ND>130 THEN 15530
15550 PRINT"ENTER COORDS OF STRESS(MPA) & STRAIN(%)"
15560 FOR J=1 TO ND
15565 PRINT"COORDS OF PT NO"J;
15570 INPUT ST(J),ET(J)
15580 ST(J)=ST(J)*1E6
15581 ET(J)=ET(J)/100
15582 TR(J)=0
15590 NEXT
15600 OPEN8,8,8,NF$
15605 PRINT"■SWITCH OFF GRAPH PLOTTER"
15606 GOSUB 12000
15610 PRINT"■TRANSFERRING RESULTS TO DISK"
15620 FOR J=1 TO ND
15630 PRINT#8,ST(J);CHR$(13);
15640 PRINT#8,ET(J);CHR$(13);
15650 PRINT#8,TR(J);CHR$(13);
15660 NEXT
15670 CLOSE8
15680 RETURN
16010 LOAD"ROUND-STR-RATES",8
17000 REM SMOOTHING REFL DATA
17005 PRINT"■REMOVING LARGE VARIATIONS IN REFLECTED PULSE"
17010 FOR J=BR-20 TO FR+20
17015 IF AX(J)=255 OR AX(J)=0 THEN AX(J)=AX(J-1)
17020 NEXT
17025 FOR J=BR-20 TO FR+20
17030 IF ABS(AX(J)-AX(J-1))>10 THEN AX(J)=(AX(J+1)+AX(J-1))/2
17035 NEXT
17040 RETURN
18000 REM INSTRON DATA INPUT & ANALYSIS
18002 FOR J=0TO130:SS(J)=0:ES(J)=0:NEXT
```

```
18005 DA%=1
18010 INPUT"□DATA FROM KEYBOARD OR DISK(K OR D)";KD$
18015 IF KD$="K" THEN 18035
18020 IF KD$<>"D" THEN 18010
18021 INPUT"DATA FILENAME";F$
18022 INPUT"DISK DRIVE(0 OR 1)";DD$
18023 IF DD$<>"0" AND DD$<>"1" THEN 18022
18024 RF$=DD$+":"+F$
18025 A$=RF$+",SEQ,READ"
18028 GOSUB 11000
18030 GOTO 18200
18035 INPUT"NO OF DATA PTS(1-130)";ND
18037 IF ND<=130 THEN 18040
18038 PRINT"TOO MANY DATA PTS"
18039 GOTO 18035
18040 PRINT"□ENTER X,YS,YMC IN MM (EG 100,80,10)
18041 PRINT" WHERE X = LOAD"
18042 PRINT"       YS = CHART DISPLACEMENT WHEN                SPECIMEN TESTED"
18043 PRINT"      YMC = CHART DISPLACEMENT FOR               MACHINE COMPLIANCE"
18044 PRINT"□□N.B. EACH SMALL DIVISION SHOULD BE CONSIDERED AS 2 MM"
18045 PRINT"HENCE MAX LOAD = 200 MM":PRINT
18046 FOR J=1 TO ND
18050 PRINT"COORDS OF PT NO"J;
18055 INPUT SS(J),ES(J),MC
18056 ES(J)=ES(J)-MC
18060 NEXT
18085 INPUT"STORE DATA ON DISK(Y OR N)";A$
18090 IF A$="N" THEN 18290
18095 IF A$<>"Y" THEN 18085
18100 INPUT"MATERIAL TESTED";MM$
18105 INPUT"COMPRESSIVE OR TENSILE";CC$
18110 INPUT"TEST TEMP(E.G. 020)";TM$
18115 INPUT"ANNEALING TEMP(E.G. 310)";AN$
18120 INPUT"APPROX MAX STRAIN(%)(E.G. 30)";MS$
18125 INPUT"IDENTITY LETTER(E.G. A)";IL$
18130 M$=LEFT$(MM$,2)
18135 CC$=LEFT$(CC$,1)
18140 F$=M$+CC$+TM$+AN$+"QS"+MS$+"%"+IL$
18142 C$="1"
18145 PRINT"□TEST DATA FILENAME IS "F$
18150 INPUT"□DISK DRIVE(0 OR 1)";DD$
18155 IF DD$<>"0" AND DD$<>"1" THEN 18150
18160 J=1
18165 FOR I=J TO ND
18170 AX(2*I-1)=SS(I)*10
18175 AX(2*I)=ES(I)*10
18177 NEXT
18180 K=ND*2
18181 WF$=DD$+":"+F$+",SEQ,WRITE"
18182 OPEN8,8,8,WF$
18185 GOSUB 9000
18190 GOTO 18290
```

```
18200 ND=ND/2
18202 FOR J=0 TO ND-1
18205 SS(J)=AX(2*J)/1P
18210 ES(J)=AX(2*J+1)/.0
18215 NEXT
18290 INPUT"@CROSS HEAD SPEED(MM/MIN)";SX
18295 INPUT"CHART SPEED(MM/MIN)";SC
18300 INPUT"FULL SCALE LOAD(KG)";LK
18305 LM=200
18310 INPUT"SAMPLE GAUGE LENGTH(MM)";LS
18315 INPUT"SAMPLE DIAMETER(MM)";DS
18320 C1=LK/LM:C2=SX/SC
18325 AR=(π*DS↑2)/4
18327 PRINT"@CALCULATING EXT(MM) V LOAD(KG) FOR SPECIMEN"
18330 FOR J=0 TO ND-1
18335 SS(J)=SS(J)*C1
18340 ES(J)=ES(J)*C2
18345 NEXT
18375 PRINT"@CALCULATING ENG. STRESS V STRAIN"
18380 FOR J=0 TO ND-1
18385 SS(J)=SS(J)*9.81*1016/AR
18390 ES(J)=ES(J)/LS
18395 NEXT
18400 IF KD$="K" THEN PN=ND/2
18405 CC$=MID$(F$,3,1)
18410 GOTO 4910
20000 REM END OF PROGRAM
```

APPENDIX B

GRAPHS Software

```
10 REM GRAPHS  - VERSION 24-08-84 15.00 20 REM MAX VALUES OF X&Y SUB 4000
20 REM MAX VALUES OF X&Y SUB 4000
30 REM CALC AXES LIMITS SUB 5000
40 REM DRAW & LABEL AXES SUB 6000
50 REM CONVERT X DATA    SUB 7000
60 REM CONVERT Y DATA    SUB 8000
70 REM DRAW GRAPH(S)     SUB 9000
80 REM READ SG DATA      SUB 10000
85 PN=130
90 IF ZX=1 THEN 100
95 DIM S$(130),E$(130),ST(130),ET(130),TR(130)
100 IF GX=1 THEN 200
130 DIM X(150),Y(150)
150 GX=1
160 S1$="STRESS":S2$="(MPA)"
161 E1$="STRAIN":E2$="(%)":E3$="STRAIN GAUGE DATA":E4$="STRAIN RATE"
162 E5$="(/SEC)"
163 T1$="TIME":T2$="(MICROSECS)"
200 SYS 9*4096
210 PRINT"□GRAPH PLOTTER ACTIVATED"
310 S=3:!SZ,S
320 R=1:!RO,R
330 X0=22:Y0=20
332 PRINT"ORIGIN AT X = "X0 "MM AND Y = "Y0" MM"
333 INPUT"CHANGE THESE COORDS(Y OR N)";A$
334 IF A$="N" THEN 400
335 IF A$<>"Y" THEN 333
336 INPUT"NEW ORIGIN COORDS(X,Y)";X0,Y0
400 PRINT"□■■■■■■■DIRECTORY OF GRAPHS"
450 PRINT"■■1. STRESS V. STRAIN"
500 PRINT"2. STRESS V. TIME"
550 PRINT"3. STRAIN V. TIME"
600 PRINT"4. STRAIN RATE V. TIME"
700 PRINT"5. STRAIN GAUGE DATA V. TIME"
710 PRINT"6. BAR STRAIN V. TIME"
800 PRINT"7. INCIDENT PULSE V. TIME"
810 PRINT"8. REFLECTED PULSE V. TIME"
820 PRINT"9. TRANSMITTED PULSE V. TIME"
930 PRINT"10. HOPK BAR MENU"
950 PRINT"■■■SELECT CODE"
960 INPUT NN%
970 IF NN%<1 OR NN%>10 THEN 950
985 LN%=NN%
999 ON NN% GOSUB 2200,2300,2400,2900,2252,2253,3000,3100,3200,25000
1000 IF NN%=5 OR NN%=6 THEN Y0=105
2000 IF Y0=105 THEN GOSUB 10000
2010 INPUT"DO YOU WANT TO DRAW AXES(Y OR N)";AX$
2011 IF AX$="Y" OR AX$="N" THEN 2013
2012 GOTO 2010
2013 INPUT"DO YOU WANT TO LABEL AXES(Y OR N)";LB$
2014 IF LB$="Y" OR LB$="N" THEN 2016
2015 GOTO 2013
2016 INPUT"DO YOU WANT TO PRINT TITLE(Y OR N)";PT$
```

```
2017 IF PT$="N" THEN 2100
2018 IF PT$<>"Y" THEN 2016
2019 INPUT"NTITLE";TT$
2100 GOSUB 4000
2110 GOSUB 5000
2130 GOSUB 7000
2140 GOSUB 8000
2165 GOSUB 6000
2166 GOSUB 6700
2168 GOSUB 6535
2170 GOSUB 9000
2171 IF Y0<>105 THEN 400
2172 Y0=20:GOSUB 10000
2173 GOTO 2100
2196 GOTO 400
2200 REM ENG STRESS V STRAIN
2209 GOSUB 12100
2210 IF A$="T" THEN 2600
2211 IF A$<>"E" THEN 2209
2212 IF DA%=0 THEN 13000
2213 GOSUB 11000
2214 IF A$="Y" OR A$="N" THEN 2216
2215 GOTO 2212
2216 FOR J=0 TO PN
2220 Y(J)=SS(J)/1E6
2225 IF A$="Y" THEN X(J)=EC(J)*100
2230 IF A$="N" THEN X(J)=ES(J)*100
2240 NEXT
2244 V1$=S1$
2246 V2$=S2$
2248 H1$=E1$
2250 H2$=E2$
2251 RETURN
2252 RETURN
2253 IF DA%=0 THEN 13000
2254 RETURN
2260 PRINT"■■■■■■■STRAIN PULSES IN SHPB"
2300 REM ENG STRESS V TIME
2301 GOSUB 12100
2302 IF A$="T" THEN 2700
2303 IF A$<>"E" THEN 2301
2304 IF DA%=0 THEN 13000
2310 FOR J=0 TO PN
2320 Y(J)=SS(J)/1E6
2330 X(J)=J
2340 NEXT
2344 V1$=S1$
2346 V2$=S2$
2348 H1$=T1$
2350 H2$=T2$
2352 RETURN
2400 REM ENG STRAIN V TIME
2401 GOSUB 12100
```

```
2402 IF A$="T" THEN 2800
2403 IF A$<>"E" THEN 2401
2404 IF DA%=0 THEN 13000
2406 GOSUB 11000
2408 IF A$="Y" OR A$="N" THEN 2415
2410 GOTO 2406
2415 FOR J=0 TO PN
2420 IF A$="Y" THEN Y(J)=EC(J)*100
2425 IF A$="N" THEN Y(J)=ES(J)*100
2430 X(J)=J
2440 NEXT
2444 V1$=E1$
2446 V2$=E2$
2448 H1$=T1$
2450 H2$=T2$
2452 RETURN
2600 REM TRUE STRESS V STRAIN
2601 GOSUB 11000
2602 IF A$="Y" THEN 2630
2603 IF A$<>"N" THEN 2601
2604 IF DA%=0 THEN 13000
2610 FOR J=0 TO PN
2615 Y(J)=ST(J)/1E6
2620 X(J)=ET(J)*100
2625 NEXT
2628 GOTO 2644
2630 GOSUB 15000:INPUT A$
2631 IF A$<>"Y" AND A$<>"N" THEN 2630
2632 IF A$="N" THEN 2634
2633 GOSUB 14000:GOTO 2637
2634 IF DA%=0 THEN 13000
2635 IF RF%=1 THEN PRINT"#PLOTTING RESULTS FROM R"F$
2637 FOR J=0 TO PN
2638 Y(J)=ST(J)/1E6
2639 X(J)=ET(J)*100
2640 NEXT
2644 V1$=S1$
2646 V2$=S2$
2648 H1$=E1$
2650 H2$=E2$
2652 RETURN
2700 REM TRUE STRESS V TIME
2701 GOSUB 11000
2702 IF A$="Y" OR A$="N" THEN 2704
2703 GOTO 2701
2704 IF A$="N" AND DA%=0 THEN 13000
2705 IF A$="N" THEN 2735
2706 GOSUB 15000:INPUT A$
2707 IF A$<>"Y" AND A$<>"N" THEN 2706
2708 IF A$="N" AND DA%=0 THEN 13000
2709 IF A$="N" AND DA%=0 THEN 2714
2710 IF A$="Y" THEN 2713
```

```
2711 PRINT"PLOTTING RESULTS FROM #"F$
2712 GOTO 2714
2713 GOSUB 14000
2714 FOR J=0 TO PN
2715 Y(J)=ST(J)/1E6
2720 X(J)=J
2725 NEXT
2730 GOTO 2744
2735 FOR J=0 TO PN
2740 Y(J)=ST(J)/1E6
2741 X(J)=J
2742 NEXT
2744 V1$=S1$
2746 V2$=S2$
2748 H1$=T1$
2750 H2$=T2$
2752 RETURN
2800 REM TRUE STRAIN V TIME
2801 GOSUB 11000
2802 IF A$="Y" OR A$="N" THEN 2804
2803 GOTO 2801
2804 IF A$="N" AND DA%=0 THEN 13000
2805 GOSUB 15000:INPUT A$
2806 IF A$<>"Y" AND A$<>"N" THEN 2805
2807 IF A$="N" AND DA%=0 THEN 13000
2808 IF A$="N" AND DA%=0 THEN 2835
2809 IF A$="Y" THEN 2811
2810 PRINT"PLOTTING RESULTS FROM #"F$:GOTO 2812
2811 GOSUB 14000
2812 FOR J=0 TO PN
2815 Y(J)=ET(J)*100
2820 X(J)=J
2825 NEXT
2830 GOTO 2844
2835 FOR J=0 TO PN
2840 Y(J)=ET(J)*100
2841 X(J)=J
2842 NEXT
2844 V1$=E1$
2846 V2$=E2$
2848 H1$=T1$
2850 H2$=T2$
2852 RETURN
2900 REM TRUE STRAIN RATE V TIME
2902 GOSUB 15000:INPUT A$
2903 IF A$<>"N" AND A$<>"Y" THEN 2902
2904 IF A$="N" AND DA%=0 THEN 13000
2905 IF A$="N" AND DA%=0 THEN 2910
2906 IF A$="Y" THEN 2909
2907 PRINT"PLOTTING RESULTS FROM #"F$
2908 GOTO 2910
2909 GOSUB 14000
2910 FOR J=0 TO PN
2920 Y(J)=TR(J)
```

```
2930 X(J)=J
2940 NEXT
2944 V1$=E4$
2946 V2$=E5$
2948 H1$=T1$
2950 H2$=T2$
2952 RETURN
3000 REM INCIDENT PULSE
3010 V1$="INCIDENT PULSE"
3020 V2$=E2$
3030 H1$=T1$
3040 H2$=T2$
3050 GOSUB 16000
3060 RETURN
3100 REM REFLECTED PULSE
3110 V1$="REFLECTED PULSE"
3120 V2$=E2$
3130 H1$=T1$
3140 H2$=T2$
3150 GOSUB 16000
3160 RETURN
3200 REM TRANSMITTED PULSE
3210 V1$="TRANSMITTED PULSE"
3220 V2$=E2$
3230 H1$=T1$
3240 H2$=T2$
3250 GOSUB 16000
3260 RETURN
4000 REM FIND MAXIMUM VALUES
4001 INPUT"MORE THAN 1 GRAPH USING SAME AXES(Y OR N)";PM$
4003 IF PM$="N" THEN 4010
4004 IF PM$="Y" THEN 4080
4005 GOTO 4001
4010 PRINT"&FINDING MAX VALUES"
4015 TY=Y(1):TX=X(1)
4020 FOR J=0 TO PN
4030 IF Y(J)>TY THEN TY=Y(J)
4040 IF X(J)>TX THEN TX=X(J)
4050 NEXT
4060 RETURN
4080 PRINT"MAX VALUE OF "V1$+V2$;
4090 INPUT TY
4100 PRINT"MAX VALUE OF "H1$+H2$;
4110 INPUT TX
4120 RETURN
5000 REM CALC AXES LIMITS
5003 INPUT"LENGTH OF Y AXIS(150 OR 200 MM)";AY%
5004 IF AY%<>150 AND AY%<>200 THEN 5003
5005 PRINT"&CALCULATING AXES LIMITS"
5010 REM Y AXIS
5020 ON NN% GOSUB 5100,5100,5150,5200,5250,5200,5150,5150,5150
5030 REM X AXIS
5040 ON NN% GOSUB 5300,5350,5350,5350,5400,5400,5350,5350,5350
5050 RETURN
```

```
5100 REM MAX VALUE OF STRESS ON Y AXIS
5105 IF TY>1500*AY%/150 THEN TY=15000*AY%/150
5110 IF TY>750*AY%/150 AND TY<=1500*AY%/150 THEN TY=1500*AY%/150
5120 IF TY>300*AY%/150 AND TY<=750*AY%/150 THEN TY=750*AY%/150
5125 IF TY>150*AY%/150 AND TY<=300*AY%/150 THEN TY=300*AY%/150
5127 IF TY>75*AY%/150 AND TY<=150*AY%/150 THEN TY=150*AY%/150
5128 IF TY<=75*AY%/150 THEN TY=75*AY%/150
5130 RETURN
5150 REM MAX VALUE OF STRAIN ON Y AXIS
5152 IF TY>75*AY%/150 THEN TY=150*AY%/150
5153 IF TY>30*AY%/150 AND TY<=75*AY%/150 THEN TY=75*AY%/150
5155 IF TY>15*AY%/150 AND TY<=30*AY%/150 THEN TY=30*AY%/150
5160 IF TY>7.5*AY%/150 AND TY<=15*AY%/150 THEN TY=15*AY%/150
5162 IF TY>3*AY%/150 AND TY<=7.5*AY%/150 THEN TY=7.5*AY%/150
5165 IF TY>1.5*AY%/150 AND TY<=3*AY%/150 THEN TY=3*AY%/150
5170 IF TY>0.75*AY%/150 AND TY<=1.5*AY%/150 THEN TY=1.5*AY%/150
5175 IF TY>0.3*AY%/150 AND TY<=0.75*AY%/150 THEN TY=0.75*AY%/150
5177 IF TY>0.15*AY%/150 AND TY<=0.3*AY%/150 THEN TY=0.3*AY%/150
5178 IF TY>0.075*AY%/150 AND TY<=0.15*AY%/150 THEN TY=0.15*AY%/150
5179 IF TY<=0.075*AY%/150 THEN TY=0.075*AY%/150
5180 RETURN
5200 REM MAX VALUE OF STRAIN RATE ON Y AXIS
5205 IF TY>3000*AY%/150 THEN TY=7500*AY%/150
5210 IF TY>1500*AY%/150 AND TY<=3000*AY%/150 THEN TY=3000*AY%/150
5220 IF TY>750*AY%/150 AND TY<=1500*AY%/150 THEN TY=1500*AY/150
5230 IF TY>300*AY%/150 AND TY<=750*AY%/150 THEN TY=750*AY%/150
5232 IF TY>150*AY%/150 AND TY<=300*AY%/150 THEN TY=300*AY%/150
5234 IF TY<=150*AY%/150 THEN TY=150*AY%/150
5240 RETURN
5250 REM STRAIN GAUGE DATA ON Y AXIS
5260 TY=300*AY%/150
5270 RETURN
5280 REM BAR STRAIN ON Y AXIS
5281 TY=.75*AY%/150
5282 RETURN
5300 REM MAX VALUE OF STRAIN ON X AXIS
5302 IF TX>75 THEN TX=150
5303 IF TX>30 AND TX<=75 THEN TX=75
5305 IF TX>15 AND TX<=30 THEN TX=30
5310 IF TX>7.5 AND TX<=15 THEN TX=15
5315 IF TX>3 AND TX<=7.5 THEN TX=7.5
5317 IF TX>1.5 AND TX<=3 THEN TX=3
5320 IF TX>0.75 AND TX<=1.5 THEN TX=1.5
5322 IF TX>0.3 AND TX<=0.75 THEN TX=0.75
5322 IF TX>0.15 AND TX<=0.3 THEN TX=0.3
5324 IF TX<=0.15 THEN TX=0.15
5330 RETURN
5350 REM TIME ON X AXIS WITH STRESS/STRAIN OR STRAIN RATE ON Y
5360 TX=150
5370 RETURN
5400 REM TIME ON X AXIS & S.G. DATA ON Y
5410 IF TX>3000 THEN TX=4500
5420 IF TX>1500 AND TX<=3000 THEN TX=3000
```

```
5430,IF TX>750 AND TX<=1500 THEN TX=1500
5435 IF TX<=750 THEN TX=750
5440 RETURN
6000 REM DRAW & LABEL AXES
6003 IF AX$="Y" THEN 6025
6005 PRINT"%PLACE PAPER WITH THE FOLLOWING AXES ON GRAPH PLOTTER"
6006 PRINT"%VERTICAL AXIS - "V1$"%%%%%MAX VALUE - "TY;V2$
6007 PRINT"%HORIZONTAL AXIS - "H1$"%%%%%MAX VALUE - "TX;H2$
6009 !MA,X0,Y0
6010 PRINT"%PEN NOW AT ORIGIN"
6011 PRINT"%MOVE 'SET ZERO' CONTROLS TO CORRESPOND"
6012 GOSUB 12000
6022 RETURN
6025 PRINT"%DRAWING AXES"
6026 REM SIZE OF Y AXIS = 150 MM
6027 REM SIZE OF X AXIS = 150 MM
6028 REM (0,0)= (X=25,Y=20)
6029 REM STEP SIZES
6031 DX=TX/15:DY=TY/15
6035 II=10
6036 IF NN%=5 OR NN%=6 THEN II=5
6040 !MA,X0,Y0
6060 XL=0:YL=2
6080 X=X0:Y=Y0
6085 REM X AXIS
6090 FOR J=1 TO 15
6100 !DA,X,Y
6105 !DR,XL,YL:!DA,X,Y
6180 X=X+10
6190 NEXT
6210 REM Y2 AXIS - AT END OF X AXIS
6220 XL=-2:YL=0
6230 FOR J=1 TO 15*AY%/150
6240 !DA,X,Y
6250 !DR,XL,YL
6255 !DA,X,Y
6260 Y=Y+II
6270 NEXT
6280 REM X2 AXIS - AT END OF Y AXIS
6300 XL=0:YL=-2
6310 FOR J=1 TO 15
6320 !DA,X,Y
6330 !DR,XL,YL
6335 !DA,X,Y
6340 X=X-10
6350 NEXT
6370 REM Y AXIS
6390 XL=2:YL=0
6410 FOR J=1 TO 15*AY%/150
6420 !DA,X,Y:!DR,XL,YL:!DA,X,Y
6500 Y=Y-II
6510 NEXT
6512 !DA,X0,Y0
```

```
6520 RETURN
6535 IF NN%>4 AND NN%<7 AND Z=2 THEN 6645
6536 IF PT$="N" THEN 6545
6538 X=X0+55-LEN(TT$)/2:Y=220
6539 !MA,X,Y:!PR,TT$
6545 IF PM$="Y" THEN 6565
6550 IF F$="" THEN INPUT"FILENAME";F$
6558 TE$=MID$(F$,4,3):TE$=TE$+" C"
6559 X=X0+28:Y=195:!MA,X,Y:!PR,TE$
6560 AN$=MID$(F$,7,3):AN$=AN$+" C"
6561 X=X0+42:Y=190:!MA,X,Y:!PR,AN$
6563 X=X0+29:Y=185:!MA,X,Y:!PR,F$
6565 IF LB$="N" AND NN%<7 THEN RETURN
6566 IF NN%=5 OR NN%=6 THEN 6645
6567 X=X0+5:Y=Y0+130*AY%/150
6568 IF NN%>6 AND LB$="N" THEN Y=Y0+135
6570 !MA,X,Y:!PR,V1$
6575 IF LB$="N" THEN RETURN
6580 Y=Y-5
6590 !MA,X,Y:!PR,V2$
6600 X=X0+105:Y=Y0+10
6610 !MA,X,Y:!PR,H1$
6620 Y=Y0+5
6630 !MA,X,Y:!PR,H2$
6632 IF NN%<5 THEN RETURN
6645 X=X0+5:Y=Y0+65:!MA,X,Y
6647 IF NN%=5 THEN 6655
6648 IF Z=1 THEN A$="INCIDENT BAR STRAIN"
6649 IF Z=2 THEN A$="TRANSMITTER BAR STRAIN"
6650 !PR,A$
6651 X=X0+5:Y=Y0+60
6652 A$=E2$
6653 !MA,X,Y:!PR,A$
6654 GOTO 6660
6655 !PR,E3$
6656 Y=Y0+60:!MA,X,Y
6657 IF Z=1 THEN A$="(INCIDENT BAR)"
6658 IF Z=2 THEN A$="(TRANSMITTER BAR)"
6659 !PR,A$
6660 X=X0+105:Y=Y0+10
6665 !MA,X,Y:!PR,T1$
6670 Y=Y0+5:!MA,X,Y:!PR,T2$
6680 RETURN
6700 REM LABELLING AXES
6701 IF LB$="N" THEN 6800
6702 X=X0+150:Y=Y0
6703 YC=-5
6704 !MA,X,Y
6706 FOR J=15 TO 1 STEP-2
6707 NO=J*TX%/15
6708 K=0
6709 I=NO
6711 IF I<10 THEN 6719
```

```
6713 K=K+1
6715 I=I/10
6717 GOTO 6711
6719 XC=-K-2
6720 !MR,XC,YC
6730 A$=STR$(NO)
6760 !PR,A$
6780 X=X-20
6785 !MA,X,Y
6790 NEXT
6791 X=X0:!MA,X,Y
6792 XC=-2:!MR,XC,YC
6795 NO=0:A$=STR$(NO):!PR,A$
6800 XC=-6:YC=-1.5
6802 II=10:IF NN%=5 OR NN%=6 THEN II=5
6805 X=X0:Y=Y0+150*AY%/150
6807 IF LB$="N" THEN RETURN
6808 IF NN%=5 OR NN%=6 THEN Y=Y0+75*AY%/150
6810 !MA,X,Y
6811 FOR J=15*AY%/150 TO 1 STEP -2
6815 NO=J*TY/(15*AY%/150)
6817 IF NN%=6 THEN NO=NO-TY*35/75
6820 IF NO=INT(NO) THEN 6827
6825 XX=-10:GOTO 6840
6827 K=0
6829 I=NO
6831 IF I<10 THEN 6839
6833 K=K+1
6835 I=I/10
6837 GOTO 6831
6839 XX=XC-2*K
6840 !MR,XX,YC
6860 A$=STR$(NO)
6890 !PR,A$
6891 IF J=1 THEN 6897
6892 Y=Y-II*2
6895 !MA,X,Y
6897 NEXT
6900 RETURN
7000 REM CONVERT X DATA
7005 PRINT"@CONVERTING X DATA"
7007 I=150
7008 IF NN%=5 OR NN%=6 THEN 7400
7100 FOR J=0 TO PN
7150 X(J)=X(J)*I/TX+X0
7200 NEXT
7300 RETURN
7400 FOR J=0 TO 150
7450 X(J)=X(J)*I/TX+X0
7500 NEXT
7550 RETURN
8000 REM CONVERT Y DATA
8005 PRINT"@CONVERTING Y DATA"
```

```
8006 IF NN%=5 OR NN%=6 THEN 8300
8007 I=150*AY%/150
8100 FOR J=0 TO PN
8200 Y(J)=Y(J)*I/TY+Y0
8250 NEXT
8260 RETURN
8300 I=75*AY%/150
8310 FOR J=0 TO 150
8320 Y(J)=Y(J)*I/TY+Y0
8330 NEXT
8600 IF NN%=5 THEN RETURN
8611 YS=0
8612 FOR J=1 TO 10
8613 YS=YS+Y(J)
8614 NEXT
8615 YS=YS/10
8620 DF=Y0+35-YS
8630 FOR J=0 TO 150
8640 Y(J)=Y(J)+DF
8650 NEXT
8700 RETURN
9000 REM DRAW GRAPHS
9001 INPUT"CONTINUOUS CURVE OR INDIVIDUAL PTS(C OR P)";A$
9002 IF A$="C" THEN 9005
9003 IF A$<>"P" THEN 9001
9004 GOTO 9700
9005 PRINT"SWITCH GRAPH PLOTTER ON"
9006 GOSUB 12000
9010 PRINT"PLOTTING GRAPH"
9100 !MA,X(0),Y(0)
9110 IF NN%=5 OR NN%=6 THEN 9620
9200 FOR J=1 TO PN
9300 IF X(J)=X0 AND Y(J)=Y0 THEN 9600
9350 IF X(J)>X0+150 OR Y(J)>Y0+200 THEN 9600
9375 IF Y(J)>0 THEN 9400
9380 Y(J)=0
9400 !DA,X(J),Y(J)
9600 NEXT
9610 GOTO 9900
9620 FOR J=1 TO 150
9630 !DA,X(J),Y(J)
9640 NEXT
9650 GOTO 9900
9700 PRINT"SWITCH GRAPH PLOTTER ON"
9701 GOSUB 12000
9705 PRINT"PLOTTING GRAPH"
9710 FOR J=0 TO PN
9720 IF X(J)>X0+150 OR Y(J)>Y0+200 THEN J=PN
9730 !MA,X(J),Y(J)
9740 !PD:!PU
9800 NEXT
9900 !PU
```

```
9902 FOR J=0TOPN
9905 X(J)=0:Y(J)=0:SS(J)=0:ES(J)=0
9906 ST(J)=0:ET(J)=0:TR(J)=0
9908 NEXT
9910 RETURN
10000 REM READ DATA ON DISK FILE(S)
10001 IF Y0=105 THEN Z=1
10002 IF Y0<>105 THEN Z=2
10003 IF Z<>1 THEN 10030
10005 PRINT"□"
10010 INPUT"FILENAME";F$
10020 INPUT"DISK DRIVE(0 OR 1)";DD$
10021 IF DD$<>"0"AND DD$<>"1" THEN 10020
10022 PRINT"■SWITCH OFF GRAPH PLOTTER"
10023 GOSUB 12000
10025 C$=DD$+":"+F$+CHR$(51)+",SEQ,READ"
10026 OPEN 8,8,8,C$
10027 INPUT#8,CS,SR,LP,V1,V2,G1,G2,F,LS
10028 INPUT#8,DS,E,VA,VB
10029 CLOSE8
10030 C$=DD$+":"+F$+CHR$(48+Z)+",SEQ,READ"
10035 PRINT"■TRANSFERRING S.G. DATA TO PET"
10040 OPEN 8,8,8,C$
10050 INPUT#8,CS,N
10060 K=INT(N/150)
10070 FOR J=0 TO 150
10080 FOR I=1 TO K
10090 INPUT#8,D%
10100 Y(J)=D%
10110 NEXT I
10120 NEXT J
10132 IF NNK<>6 THEN 10150
10133 IF K1>0 AND K2>0 THEN 10146
10134 N=(E-VA)/VA
10135 K1=(F1*V1)/(E*255)
10136 N=(E-VB)/VB
10137 K2=(F2*V2)/(E*255)
10146 FOR J=0 TO 150
10147 IF Z=1 THEN Y(J)=Y(J)*K1*100
10148 IF Z=2 THEN Y(J)=Y(J)*K2*100
10149 NEXT
10150 FOR J=0 TO 150
10160 X(J)=SR*J*K
10170 NEXT
10180 CLOSE8
10200 RETURN
11000 REM INPUT"ELASTIC MODULUS CORRECTED STRAIN VALUES(Y OR N)";A$
11050 A$="Y"
11100 RETURN
12000 PRINT"■■■■■■HIT SPACE BAR TO CONTINUE"
12010 GET C$:IF C$<>" " THEN 12010
12020 RETURN
12100 INPUT"TRUE OR ENGINEERING STRESS/STRAIN(T OR E)";A$
12110 RETURN
13000 PRINT"■ERROR - DATA NOT ANALYSED"
13010 GOSUB 12000
13020 GOTO 400
```

```
14000 REM INPUT RESULTS FROM DISK
14010 INPUT"FILENAME";F$
14011 FT$=CHR$(52)
14012 INPUT"FILTERED RESULT(Y OR N)";A$
14013 IF A$="Y" THEN FT$=CHR$(53)
14014 IF A$<>"Y" AND A$<>"N" THEN 14012
14015 INPUT"AVERAGE OF RESULTS(Y OR N)";A$
14016 IF A$="Y" THEN FT$=CHR$(54)
14017 IF A$<>"Y" AND A$<>"N" THEN 14015
14020 INPUT"DISK DRIVE(0 OR 1)";DD$
14030 IF DD$<>"0" AND DD$<>"1" THEN 14020
14040 RF$=DD$+":"+F$+FT$+",SEQ,READ"
14050 OPEN8,8,8,RF$
14060 FOR J=0 TO PN
14070 INPUT#8,ST(J),ET(J),TR(J)
14080 NEXT
14085 RF%=1
14090 CLOSE8
14100 RETURN
15000 PRINT"DO YOU WANT TO TRANSFER RESULTS FROM DISK FILE TO PET";
15001 RETURN
16000 REM DATA TO PLOT INCID,REFL OR TRANS PULSE
16010 INPUT"□FILENAME";F$
16020 INPUT"□DISK DRIVE(0 OR 1)";DD$
16030 IF DD$<>"0" AND DD$<>"1" THEN 16020
16040 RF$=DD$+":"+F$+CHR$(51)+",SEQ,READ"
16050 OPEN8,8,8,RF$
16060 INPUT#8,CS,SR,LP,V1,V2,G1,G2,F,LS
16070 INPUT#8,DS,E,VA,VB
16075 CLOSE8
16080 N=(E-VA)/VA
16090 F1=(N+1)↑2/(N*F*G1)
16100 N=(E-VB)/VB
16110 F2=(N+1)↑2/(N*F*G2)
16120 K1=(F1*V1)/(E*255)
16130 K2=(F2*V2)/(E*255)
16140 I=1:IF NN%=9 THEN I=2
16150 RF$=DD$+":"+F$+CHR$(48+I)+",SEQ,READ"
16160 OPEN8,8,8,RF$
16162 IF PM$="N" THEN 16170
16164 BI=0:BR=0:BT=0
16170 IF NN%=7 THEN INPUT"START ADDRESS OF INCID PULSE";BI
16180 IF NN%=8 THEN INPUT"START ADDRESS OF REFL PULSE";BR
16190 IF NN%=9 THEN INPUT"START ADDRESS OF TRANS PULSE";BT
16192 IF NN%=7 THEN B=BI
16193 IF NN%=8 THEN B=BR
16194 IF NN%=9 THEN B=BT
16196 PRINT"□□SWITCH OFF GRAPH PLOTTER"
16197 GOSUB 12000
16200 PRINT"□TRANSFERRING DATA TO PET"
16210 INPUT#8,CS,N
16220 FOR J=0 TO B-1
16230 INPUT#8,D%
16240 NEXT
```

```
16250 FOR J=B TO B+PN
16255 JJ=J-B
16260 INPUT#8,D%
16270 Y(JJ)=D%
16271 IF JJ=0 THEN YF=Y(JJ)
16272 Y(JJ)=Y(JJ)-YF
16275 IF NN%=7 THEN Y(JJ)=Y(JJ)*K1*100
16276 IF NN%=9 THEN Y(JJ)=Y(JJ)*K2*100
16277 IF NN%=8 THEN Y(JJ)=-Y(JJ)*K1*100
16280 NEXT
16290 CLOSE8
16300 FOR J=0 TO PN
16310 X(J)=J
16320 NEXT
16330 RETURN
25000 REM END OF GRAPH PLOTTING ROUTINE
25100 !KI
25150 PRINT"@LOADING HOPK BAR PROGRAM"
25200 LOAD"HOPK-BAR",8
```

APPENDIX C

TR-AUTO-CTRL Software

```
50 REM TRANSIENT RECORDER CONTROL SOFTWARE
100 IF ZX=1 GOTO 140
110 DIMA%(4096)
130 N2=4
140 Q=1024*N2
150 F=1
160 GOSUB 630
170 A=10
175 IF ZX=1 AND N1=2 GOTO 290
177 ZX=0
180 REM***DISP. MENU & SELECTED CODE ***
190 GOSUB 2410
200 REM************************
210 REM* TAKE RECORD    2650 *
220 REM* TRANSFER DATA  2740 *
230 REM* STATIC PLOT    2850 *
240 REM* ROLLING PLOT    310 *
250 REM* RE.+T'FER DATA 2840 *
260 REM* DEVICE CLEAR    820 *
270 REM* HOPKINSON BAR 25000 *
280 REM************************
290 ON N1 GOSUB 2650,2740,2850 ,310,2840,820,3195,8000
300 GOTO 190
310 REM*****ROLLING PLOT*****
320 Q1=INT(Q/39):PRINT"□": PRINT"■ ROLLING PLOT ■"
330 PRINT:PRINT"COMPACTION FACTOR( 1 -";Q1;"):";
340 INPUT N5
350 IF N5<=0 OR N5>Q1 THEN 320
360 Y=Q-1
370 X=0
380 PRINT"□" : PRINT"■";TAB(39)
390 B1=0
400 FOR I=X TO  Y STEP N5
410 SYS(PEEK(53)*256+126)
420 B=INT((A%(I)*(200/255))+1/2)
430 GOSUB 560
440 GET A$:IF A$=" " THEN 460
450 NEXT I
460 GOTO 3140
470 IF B1>B2 THEN 520
480 FOR J=1 TO B2-B1
490 PRINT"■ ■";
500 NEXT J
510 RETURN
520 FOR J=1 TO B1-B2
530 PRINT"□ ■";
540 NEXT J
550 RETURN
560 IF B>199 THEN B=199
570 PRINT"■";: B2=24-INT(B/8)
580 IF B1<> B2 THEN GOSUB 470
590 PRINT MID$(L$,(7ANDB)+1,1);
600 REM  PRINT LEFT$(CR$,24-INT(B/8));MID$(L$,(7ANDB)+1,1);
610 B1=B2
```

```
620 RETURN
630 S=63:IF PEEK(53)>64 THEN S=127
640 POKE 53,S
650 POKE 52,56
660 CR$="QQQQQQQQQQQQQQQQQQQQQQQQ":L$="________"
670 A%(0)=0
680 RESTORE
690 FORI=826TO1020
700 READA
710 POKEI,A
720 NEXTI
730 FORI=PEEK(53)*256+56 TO PEEK(53)*256+208
740 READA
750 POKEI,A
760 NEXTI
770 POKE59456,255
780 POKE59425,60
790 POKE59427,60
800 POKE59409,60
810 RETURN
820 GOSUB1060:GOSUB1230:GOSUB1120:GOSUB1090
830 RETURN
840 REM****************************
850 REM*    MAIN GP-IB ROUTINES    *
860 REM*                           *
870 REM* SOURCE HANDSHAKE     1490 *
880 REM* ACCEPTOR HANDSHAKE   1520 *
890 REM* ADDRESS TO TALK      1030 *
900 REM* ADDRESS TO LISTEN    1060 *
910 REM* UNTALK               1090 *
920 REM* UNLISTEN             1120 *
930 REM* G E T                1150 *
940 REM* D C L                1200 *
950 REM* S D C                1230 *
960 REM* G T L                1280 *
970 REM* SERIAL POLL          1550 *
980 REM* P P E & P P C        1670 *
990 REM* PARALLEL POLL        1750 *
1000 REM* BUFFER OUT          1330 *
1010 REM* BUFFER IN           1360 *
1020 REM***************************
1030 POKE826,A+64
1040 SYS964
1050 RETURN
1060 POKE826,A+32
1070 SYS994
1080 RETURN
1090 POKE826,95
1100 SYS994
1110 RETURN
1120 POKE826,63
1130 SYS994
1140 RETURN
```

```
1150 GOSUB1060
1160 POKE826,8
1170 SYS994
1180 GOSUB1120
1190 RETURN
1200 POKE826,20
1210 SYS994
1220 RETURN
1230 GOSUB1060
1240 POKE826,4
1250 SYS994
1260 GOSUB1120
1270 RETURN
1280 GOSUB1060
1290 POKE826,1
1300 SYS994
1310 GOSUB1120
1320 RETURN
1330 GOSUB1390
1340 SYS PEEK(53)*256+56
1350 RETURN
1360 GOSUB 1390
1370 SYS PEEK(53)*256+90
1380 RETURN
1390 REM
1400 B=PEEK(44)+256*PEEK(45)+7·
1410 POKE1,255ANDB
1420 POKE2,INT(B/256)
1430 B=0 :REM  NO. BYTES TO BE TRANSFERRED
1440 S=255 AND B:B=INT(B/256)
1450 IF S<>0 THEN B=B+1
1460 POKE 254,S
1470 POKE 255,B
1480 RETURN
1490 POKE 826,B
1500 SYS 827
1510 RETURN
1520 SYS 883
1530 B=PEEK(826)
1540 RETURN
1550 POKE 826,63
1560 SYS 943
1570 POKE 826,24
1580 SYS 943
1590 POKE 826,A+64
1600 SYS 964
1610 SYS 883
1620 S=PEEK(826)
1630 POKE 826,25
1640 SYS 943
1650 GOSUB 1090
1660 RETURN
1670 POKE 826,A+32
```

```
1680 SYS 943
1690 POKE 826,5
1700 SYS 943
1710 POKE 826,104+S
1720 SYS 943
1730 GOSUB 1120
1740 RETURN
1750 POKE 59409,52
1760 SS=PEEK(59456)
1770 POKE 59456,250
1780 S=255-PEEK(59424)
1790 POKE 59409,60
1800 POKE 59456,255 AND SS
1810 RETURN
1820 DATA 0, 160, 128, 173, 64, 232
1830 DATA 41, 65, 201, 65, 240, 42
1840 DATA 173, 58, 3, 73, 255, 141
1850 DATA 34, 232, 32, 232, 3, 44
1860 DATA 64, 232, 80, 248, 169, 52
1870 DATA 141, 35, 232, 32, 232, 3
1880 DATA 173, 64, 232, 74, 144, 247
1890 DATA 169, 60, 141, 35, 232, 169
1900 DATA 255, 141, 34, 232, 160, 0
1910 DATA 132, 150, 96, 173, 64, 232
1920 DATA 9, 2, 141, 64, 232, 32
1930 DATA 232, 3, 44, 64, 232, 48
1940 DATA 248, 173, 64, 232, 41, 253
1950 DATA 141, 64, 232, 173, 32, 232
1960 DATA 73, 255, 141, 58, 3, 173
1970 DATA 16, 232, 41, 64, 73, 64
1980 DATA 133, 150, 169, 60, 141, 33
1990 DATA 232, 32, 232, 3, 44, 64
2000 DATA 232, 16, 248, 169, 52, 141
2010 DATA 33, 232, 96, 173, 64, 232
2020 DATA 41, 251, 141, 64, 232, 9
2030 DATA 2, 141, 64, 232, 169, 60
2040 DATA 141, 33, 232, 76, 59, 3
2050 DATA 32, 175, 3, 169, 52, 141
2060 DATA 33, 232, 173, 64, 232, 41
2070 DATA 253, 141, 64, 232, 169, 255
2080 DATA 141, 34, 232, 173, 64, 232
2090 DATA 9, 4, 141, 64, 232, 96
2100 DATA 32, 175, 3, 76, 217, 3
2110 DATA 173, 18, 232, 201, 239, 208
2120 DATA 6, 104, 104, 169, 2, 133
2130 DATA 150, 96,230,1 ,208,2
2140 DATA 230,2,96
2150 DATA 120,160,0,152,145,1,32,246,3
2160 DATA 32,115,3,173,58,3,145,1
2170 DATA 32,246,3,198,254,208,233,198
2180 DATA 255,208,229,88,96,0,0,0
2190 DATA 0
2200 DATA 32,246,3,160,0,177,1,141
```

```
2210 DATA 58,3,32,59,3,32,246,3
2220 DATA 198,254,208,236,198,255,208
2230 DATA 232,96,0 ,0,00,0,00,0
2240 DATA 0,0,0,0,0
2250 DATA 169,128,133,002,169
2260 DATA 000,133,001,162,032
2270 DATA 160,039,177,001,072
2280 DATA 138,145,001,104,170
2290 DATA 136,016,245,169,040
2300 DATA 024,101,001,133,001
2310 DATA 144,002,230,002,169
2320 DATA 232,197,001,208,224,096
2330 DATA 169,128,133,002,169
2340 DATA 000,133,001
2350 DATA 160,038,177,001,200
2360 DATA 145,001,136,136,016
2370 DATA 247,200,169,032,145,001,169,040
2380 DATA 024,101,001,133,001
2390 DATA 144,002,230,002,169
2400 DATA 232,197,001,208,223,096
2410 PRINT"□"
2420 PRINT TAB(10);"■ DL910 SERIES ■"
2430 PRINT TAB(14);"■ MENU ■":PRINT
2440 GOSUB 2510
2450 GOSUB 2530:GOSUB 2550
2460 GOSUB 2570:GOSUB 2590:GOSUB2610:GOSUB 2630
2470 PRINT:PRINT "■ SELECT CODE ■"
2480 PRINT
2485 IF Z%=1 GOTO 2490
2487 INPUT N1
2490 IFN1<0 ORN1>8 THEN 2410
2500 RETURN
2510 PRINT:PRINT"1" TAB(2)"TAKE RECORDING"
2520 RETURN
2530 PRINT"2" TAB(2)"TRANSFER DATA TO PET"
2540 RETURN
2550 PRINT "3"TAB(2)"STATIC PLOT"
2560 RETURN
2570 PRINT "4"TAB(2)"ROLLING PLOT"
2580 RETURN
2590 PRINT "5"TAB(2)"RECORD+TRANSFER DATA"
2600 RETURN
2610 PRINT "6"TAB(2)"DEVICE CLEAR"
2620 RETURN
2630 PRINT "7"TAB(2)"HOPK BAR COMPRESSION TEST PROG"
2640 RETURN
2650 PRINT"□"
2660 GOSUB 2510
2670 PRINT"*****************"
2680 GOSUB 1230:  GOSUB 1150
2690 PRINT:PRINT "RECORDER ARMED"
2700 GOSUB 1550:IF(S AND 64)=0 THEN 2700
2710 PRINT:PRINT "END OF RECORDING"
```

```
2720 FOR I=1 TO 1000 :NEXT I
2730 RETURN
2740 PRINT"□"
2745 IF Z%=1 THEN 2770
2750 GOSUB 2530
2760 PRINT"**********************"
2770 IF Z%=1 THEN GOSUB 3120
2773 IF Z%=0 THEN GOSUB 3080
2776 GOSUB 1030
2780 GOSUB 1330
2790 GOSUB 1520
2800 GOSUB 1090
2810 PRINT"TRANSFER COMPLETED"
2820 FOR I=1 TO 1000 :NEXT I
2830 GOSUB 1230
2833 IF Z%=0 GOTO 2837
2834 PRINT"LOADING HOPKINSON BAR SOFTWARE"
2835 LOAD"HOPK-BAR",8
2837 RETURN
2840 GOSUB 2650:GOTO 2740
2850 PRINT"□": PRINT" STATIC  PLOT "
2860 PRINT:PRINT
2870 PRINT "STARTING ADDRESS(0 -";Q;"):";
2880 INPUT N4
2890 IF N4< 0 OR N4>Q THEN 2850
2900 Q1=INT(Q/39): PRINT:PRINT "COMPACTION FACTOR(1-";Q1;"):";
2910 INPUT N5
2920 IF N5<=0 OR N5>Q1 THEN 2900
2930 PRINT"□"
2940 N6=N4:PRINT"";TAB(39);:B1=0
2950 FOR I=1 TO 40
2960 SYS(PEEK(53)*256+126)
2970 IF N4>=Q THEN 3000
2980 B=INT((A%(N4)*(200/255))+1/2)
2990 GOSUB 560 : N4=N4+N5
3000 NEXT I
3010 PRINT"FIRST ADDRESS";N6;" LAST ADDRESS";N4-N5
3020 GOSUB 3140
3030 RETURN
3040 PRINT"□"
3050 GOSUB 2550
3060 PRINT "*********************"
3070 RETURN
3080 PRINT:PRINT
3090 PRINT"SELECT MEMORY 1 OR 2 ":PRINT:PRINT
3100 PRINT"        HIT SPACE BAR TO CONTINUE        "
3110 GET T$: IF T$<>" " THEN 3110
3120 PRINT"TRANSFERRING DATA FROM TRANS REC TO PET"
3130 PRINT:RETURN
3140 PRINT"":PRINTTAB(39);
T[illegible]";
3160 PRINT"E[illegible]";
3170 GETT$:IF T$<>" " THEN  3170
```

```
3180 RETURN
3190 REM*HOPKINSON BAR PROGRAM*
3195 Z%=1
3197 PRINT"{CLR}LOADING HOPKINSON BAR SOFTWARE"
3200 LOAD"HOPK-BAR",8
8000 GOSUB 1060
8100 GOSUB 1360
8200 GOSUB 1490
8300 GOSUB 1120
8400 FOR I=1 TO 1000:NEXT I
8500 GOSUB 1230
8600 RETURN
```